Stony Brook University

The Macro- and Micro-Anatomy of Primate Volar Surfaces

A Dissertation Presented

by

Amanda Kathryn Kingston

to

The Graduate School

in Partial Fulfillment of the

Requirements

for the Degree of

Doctor of Philosophy

in

Anthropology

(Physical Anthropology)

Stony Brook University

May 2016

Stony Brook University

The Graduate School

Amanda K. Kingston

We, the dissertation committee for the above candidate for the

Doctor of Philosophy degree, hereby recommend

acceptance of this dissertation.

Susan G. Larson, Ph.D. – Dissertation Advisor
Professor, Department of Anatomical Sciences

Randall L. Susman, Ph. D. – Chairperson of Defense
Professor, Department of Anatomical Sciences

Brigitte Demes, Ph.D. – Member
Professor, Department of Anatomical Sciences

Nathan J. Kley, Ph.D. – External Member
Associate Professor, Department of Anatomical Sciences
Stony Brook Univeristy

Magdalena N. Muchlinski, Ph.D. – External Member
Assistant Professor, Department of Anatomy and Neurobiology
University of Kentucky

This dissertation is accepted by the Graduate School

Charles Taber
Dean of the Graduate School

Abstract of the Dissertation

The Macro- and Micro-Anatomy of Primate Volar Surfaces

by

Amanda K. Kingston

Doctor of Philosophy

in

Anthropology

(Physical Anthropology)

Stony Brook University

2016

The soft tissues of the volar surfaces of primate hands and feet are the primary point of interaction between an individual animal and its environment and, as such, are likely to be under strong functional selection. These tissues serve three major functions: 1) force attenuation – the volar fat pads assist in attenuating reaction forces generated during grasping locomotion; 2) friction enhancement – the volar fat pads also act as viscoelastic surfaces that increase the coefficient of friction between the pads and substrate at low body weights; in addition, the ridged volar skin interlocks with and thus increases friction with the substrate; and 3) tactile sensation – the tactile organs located in the volar skin receive and transmit information about the environment to the brain. The size and shape of the volar pads and skin have been shown previously to influence their ability to attenuate forces and produce friction at different body sizes and the morphology of the volar skin has been linked to differences in tactile acuity. Despite this clear, intuitive link between the morphology of the volar surfaces and locomotor and sensory adaptations, there has been relatively little formal analysis describing the nature of these relationships. The overarching goal of this dissertation research is, therefore, to describe and quantify the morphology of the volar pads and skin in strepsirrhine primates. Proposed relationships of the volar morphology to dietary preferences, locomotor regimes, substrate use, body size, and bony morphology are explored. Adaptations related to friction grasping at different body sizes and utilizing different modes of locomotion account for most of the variation present in both the volar pads and skin; variation relating to different force attenuation regimes is not evident in this sample. Some evidence is found for a link between tactile acuity, diet, and morphological adaptation of the volar skin, but this is preliminary and requires additional work.

For my family.

Thank you for your years of love, support, and encouragement.

Table of Contents

List of Tables

List of Figures

Chapter 6

Acknowledgements

Many, many thanks go to my dissertation advisor, Susan Larson, who not only allowed me to pursue interests far outside her own realm of expertise, but supported me throughout the process. Between the jars of mice and random mammal feet turning up under the fume hood, I can't imagine I was an easy student to put up with—thank you for your endless patience!

Many thanks also go to my committee; their comments and criticisms were instrumental in shaping this work and have given me the tools and confidence to finally call myself a scientist. I would have been absolutely lost without the guidance of Nathan Kley, who opened his laboratory to me and instructed me in the twin arts of histology and voodoo dancing, and Magdalena Muchlinski, who so graciously provided the majority of the skin samples examined herein from her personal research collection. I cannot thank them enough.

Beyond the faculty involved, this dissertation was further improved through countless discussions, arguments, and late-night coffees shared with my fellow IDPAS students. Stephanie Maiolino and Julia Winchester in particular were instrumental in keeping me both sane and engaged in the research process. I owe a debt of gratitude to Biren Patel and Douglas Boyer for introducing me to what would eventually become the topic of my thesis and guiding me through my early (and often painful) days of digital modeling.

Of course, I could not have come this far without the support of my family. My parents, Mark and Mary Dobratz, have always encouraged me in scholarly pursuits and indulged some of my weirder "experiments." They have worked hard to ensure I always had access to education and have given me the means to take advantage of it. Thank you, mom and dad; I know this pales in comparison to everything you've given me, but I am grateful all the same.

To my wonderful husband Thomas—these past ten years have flown by too quickly, but I can't even begin to imagine this journey without you. You've been my best friend, my sugar daddy, and are now the best daddy imaginable for our little rugrat. Calvin, you may have slowed me down a little bit, but you made me more determined than ever to finish. I love you both more than words.

Financial support for this dissertation was provided by the National Science Foundation through a Doctoral Dissertation Improvement Grant (1097438).

Chapter 1:
Introduction

1.1 Introduction

The volar integument and associated structures play an important role in environmental interactions for mammals. The ungulae – claws and hooves – provide support and protection for the digits during locomotion, the volar pads cushion the underlying bones, and the volar skin houses tactile organs used in exploration, food procurement and assessment, and object manipulation. In short, the integument provides the primary interface for many daily activities and essential interactions. As such, many of an animal's locomotor and tactile abilities are tightly correlated with the morphology of the volar integument; horses are able to run long distances over rocky terrain due in part to their thick, keratinous hooves, and a multitude of arboreal mammals are able to navigate the canopy thanks in large part to mediolaterally compressed falculae, or claws, which are used to interlock with vertical and inclined substrates.

The volar integument of primates is particularly interesting in its uniqueness among arboreal mammals. As an order, Primates is comprised predominantly of arboreal species, and all members (with the exception of *Homo sapiens*) engage in some amount of regular arboreal activity (Cartmill, 1979, 1985). The manner of this arboreal activity, however, is what sets primates apart from other arboreal species sharing the canopy; where the majority of arboreal species maintain clawed digits for interlocking with substrates, primates instead possess broad, flat apical phalanges that support correspondingly broad apical fat pads and flattened nails on most digits. The precise adaptive value of this configuration remains a topic of debate among investigators, but it appears to be closely associated with foraging in a terminal-branch niche. A secure connection to a substrate narrower than an animal's body is vital in such an environment, as it firmly anchors the limbs and allows them to produce torques to counter those created by the lateral deviation of the center of mass from the center of the substrate and thus maintain balance (Cartmill, 1985; Meldrum, 1991; Whitehead, 1993; Preuschoft et al., 1996). Among these fine terminal branches, apical claws are thought to be too large to interlock with the tiny substrates and would likely prevent an individual from maintaining a forceful grasp around the same (Cartmill, 1972, 1974, 1979, 1985, 1992; Sussman & Raven, 1978; Sussman, 1991; Hamrick, 1998; Lemelin, 1999; Bloch & Boyer, 2002; Silcox et al., 2007; Orkin & Pontzer, 2011; Shapiro et al., 2014; Maiolino et al., 2011, 2015). However, whereas flattened nails may prove advantageous in grasping fine terminal branches, they present a challenge in actually reaching them; species with clawed digits use these to interlock with large branches during climbing, whereas primates must rely solely on a friction grasp generated by a combination of muscular effort and characteristics of the volar surfaces to maintain contact (Cartmill, 1979, 1985; Hamrick, 1998; Soligo & Mueller, 1999). Although

many species are capable of utilizing friction grasps during food procurement, object manipulation, and the occasional locomotor bout, primates are unique among mammals in their absolute reliance upon them for all aspects of arboreal life.

With such heavy reliance on the volar surfaces to maintain a stable frictional bond with locomotor substrates, it is likely that the integumental structures comprising these surfaces—the volar fat pads and volar skin—are adapted to optimize their frictional characteristics to meet the differing mechanical demands produced by locomotor preferences, body size, and food procurement. Despite this intuitive link, however, both quantitative and functional studies of primate volar integument morphology remain sparse. The goal of this dissertation, then, is twofold: first, to quantify variation in the size and shape of the volar pads and skin structures in a representative sample of strepsirrhine primates, as this group comprises members with a six-fold range of body sizes and at least four different forms of habitual locomotion; and second, to determine if and how the physical demands of friction grasping may have shaped their morphology.

1.1.2 Anatomy of the Volar Pads

The volar pads are composed of adipose tissue surrounded by a fibrous sheath of collagen and elastin. This configuration produces a cushion that behaves mechanically as a semi-solid, viscoelastic material and therefore conforms to Fung's quasilinear viscoelastic tissue model (Bennet & Kerr, 1990; Ker, 1990; Aerts et al., 1995, 1996; Pawluk & Hower, 1999; Jindrich et al., 2003). Put simply, this means that the volar pads are not only able to deform when forces are applied, but also to return to their original shapes when these forces are removed.

In general, primates possess six volar pads on the palms of the hands and soles of the feet, which are separated by prominent flexion creases. Additional volar pads are found on the ventral surfaces of the free digits, however, these are not discussed here. Here, the term "volar pad" is used exclusively to refer to one of the six pads overlying the metapodial and carpal/tarsal bones. The thenar pad sits proximal to the hallux or pollex, the hypothenar pad sits proximal to the fifth digit, and four interdigital pads sit between the digits near the bases of the proximal phalanges. Moderate variation of pad number and shape within primates is well documented (Whipple, 1904; Midlo, 1934; Haines, 1955, 1958; Biegert, 1959, 1961). It is not uncommon to find species in which two volar pads have coalesced to become one surface—this is, in fact, a very *common* occurrence in strepsirrhines; in lemurids, the manual thenar and first interdigital pads are fused in all documented species (Figure 1.1). The reverse scenario, however, is not documented for any known species, though individuals may sporadically present what appear to be accessory pads closely aligned with the primary six (Biegert, 1959, 1961). The appearance of the volar pads is likewise varied; some species possess very distinct pads with sharp boundaries, while others appear to flow much more gently into one another.

1.1.3 Anatomy of the Volar Skin

The volar skin overlies the volar fat pads and comprises two regions: the superficial epidermis and deep-lying dermis. The epidermis comprises four avascular layers in the hairy skin that covers much of the body; from deep to superficial these are *stratum basale* or *stratum germinativum, stratum spinosum, stratum granulosum,* and *stratum corneum*. These layers are in constant flux, due in large part to the constant barrage of ultra violet light, oxygen, water, chemicals and friction the integument is subject to. A regular cycle of cell division in the *stratum germinativum* forces new cells superficially, where they fill with keratin as they move outward to provide a protective layer in the *stratum corneum* and are eventually shed (Montagna & Parakkal, 1974; Leeson et al., 1985; Fawcett, 1994; Williams, 1995).

The volar integument is further specialized with a fifth stratum sandwiched between the two outermost strata. By adding this extra *stratum lucidum* composed of half-keratinized cells, the volar epidermis increases not only its bulk, but also its strength, which allows the volar integument to maintain its integrity through a demanding repertoire of shearing, piercing, and stretching stresses.

The dermis is much more stable in its composition and houses the skin's vasculature. Its superficial papillary layer is named for its undulating surface, which butts up against the underside of the epidermis and is punctuated with superficial projections or papillae. These papillae increase the contact area between the dermis and epidermis and allow greater amounts of blood and nutrients to pass through the interstitial spaces and into the avascular epidermis. In the hairy skin, the waves created by this layer diminish as one travels superficially through the epidermis, until the surface of the skin contains no trace of their peaks and valleys. The volar skin, however, is notable for the patterned ridges that cover its surface. These epidermal ridges—also referred to as dermatoglyphics or friction ridges—align with the papillae in the dermis and together form a series of folds that extend through the entirety of the epidermis (Leeson et al., 1985; Okajima & Asai, 1985, Lemelin, 2000; Maiolino et al., in press). The dermal papillae interlock with the intermediate ridges – deep projections of the *stratum basale* of the epidermis – and the shallower limiting ridges (also projections of the *stratum basale*). Above the intermediate ridges, the overlying epidermal layers form into ridges with corresponding valleys sitting directly superior to the limiting ridges (Cauna, 1956; Leeson et al., 1985; Fawcett, 1994; Lemelin, 2000). These relationships are illustrated in Figure 1.2.

The development of the dermal papillae varies across mammals and appears to correlate with epidermal morphology. Primates possess relatively large, well-developed papillae, as do several species of rodents, scandentians, oppossums, and raccoons. The epidermis of these species is similarly punctuated with outwardly projecting structures; these take the form of folded ridges in primates, scandentians, oppossums, and several rodent species, and wart-like projections in raccoons (Munger & Pubols, 1972; Okajima & Asai, 1985; Haffner, 1998; Lemelin, 2000; Hamrick, 2001). Dermopterans and chiropterans, by contrast, have relatively

smooth junctions between the dermis and epidermis and correspondingly smooth epidermal surfaces (Lemelin, 2000).

The dermal papillae are also known to house tactile receptors. Meissner corpuscles are rapidly adapting encapsulated tactile receptors that respond to textures and dynamic changes as the volar skin moves across a surface. These sit superficially in the dermis and are specifically associated with the dermal papillae in primates (Cauna, 1954, 1956; Winkelmann, 1963, 1964, Martin, 1990).

1.1.4 Roles of the Volar Surfaces

The volar surfaces provide the primary interface between a primate and its environment. They are the point of contact between the limbs and substrates during locomotion and provide a link between the nervous system and the outside world during tactile exploration. It follows therefore, that both of these roles have been featured prominently in hypotheses and explanations concerning their morphology.

The volar pads play important roles in locomotion and postural behaviors. The pads are well known to provide impact damping, which shields underlying tissues from forces generated during walking, running, and leaping activities (Bennett & Ker, 1990; Ker, 1990; Aerts et al., 1995, 1996; Pawluk & Howe, 1999; Jindrich et al., 2003; Spears & Miller-Young, 2006). In addition, the pads also provide a friction-generating surface and thus prevent slippage during locomotion (Cartmill, 1979, 1985; Ker, 1990; Buck & Baer, 1993; Tomlinson et al., 2007; Derler et al., 2009a, 2009b). Variation in volar pad morphology has been described by several authors; however, despite these clear functional demands on the volar pads, it presently remains unknown how each of these roles may contribute to their morphology (Whipple, 1904; Biegert, 1959, 1961).

The role of the volar skin is slightly more complicated. Like the volar pads, the skin is involved in friction generation during postural and locomotor behaviors. The skin also houses nerve endings and is well known as a tactile organ. Both of these roles are likely to influence its morphology, though precisely how is still a matter of some debate. A review of evidence and proposed functional hypotheses are detailed in the following sections.

1.2 Predictions: Morphology of the Volar Surfaces

1.2.1 Morphological Correlates of Phylogeny

Phylogenetic non-independence of trait variables is a well-known phenomenon among evolutionary biologists; closely related species are more likely to share traits than distantly related species and it becomes difficult to determine which traits are tied to this pattern of

inheritance and which may be functional adaptations (Felsenstein, 1985; Harvey & Pagel, 1991; Nunn, 2011). Here, phylogenetic signal within primate volar pad and skin traits is examined as a means of understanding patterns of variation and accounted for by utilizing phylogenetic comparative approaches where appropriate.

1.2.2 Morphological Correlates of Body Size

Body size is among the most fundamental factors in producing morphological and behavioral variation among closely related species. There are few aspects of biology that are untouched by its influence; bone and muscle must scale to accommodate mechanical stressors at various sizes, the metabolism slows or races to accommodate energy requirements, the quantity and quality of food choices vary to provide adequate nutrition and in turn affect behavioral patterns such as group size, ranging areas, and activity patterns (Clutton-Brock, 1985; Fleagle, 1985; Jungers, 1985; Larson, 1985; Martin et al., 1985; Biewener, 1989, 2005; Jungers et al., 1995; Nunn & Barton, 2000). Understanding the influence of body size on specific morphologies, then, becomes paramount to understanding variation therein; only once variation due to biological necessities at various sizes is accounted for can meaningful associations between form and function be made across groups.

Body size variation is well-documented in primates, as are many morphological scaling relationships (Jungers, 1985; Smith & Jungers, 1997; Fleagle, 1999; Ankel-Simons, 2007). The scaling relationships of the volar pads and skin within primates, however, remain relatively unknown. This study first explores the scaling relationships of the volar pads and skin alongside a sample of metapodial bones to better understand their correlation with body size and provide a baseline for further morphological comparisons.

1.2.3 *Morphological Correlates of Friction Mechanics*

It is instructive to consider friction between solid surfaces as a starting point, as this type of friction is relatively simple to describe mathematically and lends itself well to examples and preliminary predictions. It is described by the equation:

$$\mathbf{F = \mu L}$$

where F is the force required to break frictional bonds, L is the normal force exerted between the objects, and μ is the empirically determined coefficient of friction that describes the surface properties of the objects. Because the strength of the frictional bonds are dependent upon both the objects' surface characteristics and the normal force exerted between them, it is likely that primates, who rely to such a large extent on friction grasps, exhibit morphology adapted to

optimize both aspects. Adaptations that allow for powerful grasping are well known; primates possess relatively long digits and large digital flexor musculature that allow them to generate a powerful grasping force normal to the substrate in all directions (Cartmill, 1985; Gebo, 1985, 2014; Hamrick, 2001; Lemelin & Jungers, 2007; Kirk et al., 2008; Smith & Smith, 2013). Adaptations that enhance frictional characteristics of the volar surfaces are less straightforward, and as such, they are currently less well understood (Cartmill, 1979, 1985; Buck & Baer, 1993; Haffner, 1998, Hamrick, 1998; Smith & Smith, 2013).

Obvious candidates for friction adaptation include the volar pads and the volar skin, as both are in immediate and continuous contact with substrates during locomotion. The volar pads possess a particularly large potential to affect changes in friction mechanics (Cartmill, 1979, 1985; Aerts et al., 1995, 1996; Pawluk & Howe, 1999; Maiolino et al., in press). This has to do with the mechanical properties of the pads; although $F = \mu L$ accurately describes friction between two solid objects, the fatty volar pads do not behave as a solid and thus require a different frictional model. The pads behave mechanically as semisolid, viscoelastic materials, capable of deforming with applied forces and returning to their original shapes once the stimuli is removed (Ker, 1990; Bennet & Ker, 1990, Aerts, 1995, 1996; Pawluk & Howe, 1999, Jindrich et al., 2003). This allows for cycled impact damping, where some of the force generated when the hand or foot strikes the substrate is used to deform the pads and subsequently converted to heat energy and dissipated, which leaves a smaller amount to be transferred to the underlying tissues, but it has important implications for frictional mechanics as well. Shearing force applied to break frictional bonds between the volar surfaces and substrates is subjected to this damping as well; that is, some of the applied force will be dissipated by deforming the volar pads before it can affect frictional bonds at all. Because of this, the force needed to break frictional bonds between the volar surfaces and solid substrates is no longer directly proportional to the normal force and coefficient of friction, but is better described by the exponential equation:

$$\mathbf{F = KL^n}$$

where L remains the normal force, but K and n replace μ as the empirically determined coefficients. K describes the adhesive qualities of the volar surfaces, whereas n describes the force dissipated through pad deformation. Thus, as the pads are able to dissipate more force, the force required to break frictional bonds increases exponentially.

In this scenario K is not affected only by obvious surface asperities like the familiar friction ridges, which can "catch" against roughened portion of substrates, but also by surface area. This is an important distinction from solid friction mechanics, where the contact area of the objects has no effect on the force required to break frictional bonds, and it provides an additional means by which frictional properties of the volar surfaces may be optimized. Where adjusting the number of interlocking surface asperities or ridges will affect solid or semisolid friction, simply expanding the surface area will increase friction with a semisolid volar pad.

The anatomy of primate volar surfaces presents several clear mechanisms by which they may adapt to varying friction demands. In one scenario, the pads become thicker and more voluminous, which requires more force be applied to them before they deform fully; this would result in a higher value for n (Figure 1.3a). Mathematically, this option makes sense, and there is plenty of experimental evidence to corroborate that changing the deformability of volar pads influences frictional coefficients (Cartmill, 1979; Buck & Baer, 1993; Spears & Miller-Young, 2006; Derler et al., 2009a). However, there is also a limit to how large the pads can be and still remain mechanically and metabolically viable—extra tissue is expensive to maintain, and at some point the pads will simply become too large to function as grasping surfaces (Cartmill, 1979, 1984). Further, because the pads would need to increase exponentially in size to accommodate larger body masses, this limit would be reached quickly, making the mechanism useful only to small-bodied species. Cartmill (1979) demonstrated this difference in humans and infant lemurs; the infant lemur's mass did not fully compress its volar pads, and thus it was able to maintain frictional bonds with a board at steeper angles than the more massive human.

In a second scenario, the volar pads expand in area to provide a larger contact surface during grasping (Figure 1.3b). This expansion results in a larger K coefficient, which in turn increases the force needed to break frictional bonds at a liner rate. This mechanism is also limited by metabolic and mechanical constraints related to body size, but not nearly so much as in the first scenario. Surface area is linearly, rather than exponentially, related to friction in this scenario. In fact, Cartmill (1979, 1985) proposes that expanding the breadth of the pads is a likely mechanism to increase K in larger-bodied primates, whose mass precludes substantial changes in n.

A third scenario also involves expanding the contact area between the volar surface and substrate, but achieves this in a slightly different way. Instead of expanding the gross area of the volar pads (i.e., the amount of space taken up on the volar surface by the pad), the surface of the pad is expanded, then folded to fit on top of a smaller pad, similar to the gray matter of the brain (Figure 1.3c). This is precisely the configuration seen in the dermatoglyphic ridges, and there is some evidence to suggest that the folds may be an adaptation to enhance volar friction. A coarse volar surface is common among mammals, but ridging of the volar skin is something of a rarity. The species for which it is reported—primates, scandentians, and several species of possum—all use frictional grasping in arboreal environments (Whipple, 1904; Lemelin, 2000; Hamrick, 2001). Further, within these species, there is evidence that the degree to which the ridges are developed is linked to grasping repertoire; Hamrick (1998) demonstrated that ridge development was positively correlated with increased grasping—as opposed to vertical claw (tegulae) clinging—in callithrichid primates. Callithrichids, however, are highly specialized in their exudivory and vertical clinging behaviors, and the relationships between ridge development and additional factors such as body size or locomotor regime are still largely unknown.

It's important to note that none of these mechanisms are exclusive of the others and they are, in fact, likely to work in conjunction to some degree. The most important factor in determining which is most heavily utilized is likely to be body size (Cartmill, 1978, 1984).

Adaptations to maximize the n coefficient will provide the greatest frictional boost, but are strongly limited by body size and are therefore likely to be utilized predominantly by smaller species. Adaptations to maximize K provide a smaller frictional boost but are not as strongly constrained by body size and are likely to be utilized by larger species for whom maximizing n is not viable. A negative allometric relationship between n and body mass is therefore likely, as is a positive allometric relationship between K and body mass.

1.2.4 Morphological Correlates of Locomotor Mode

Primates engage in several different types of locomotor activities, including terrestrial quadrupedalism, arboreal quadrupedalism, climbing, and leaping, each of which produces different mechanical stresses and frictional demands. Experimental evidence has shown that terrestrial quadrupedalism produces greater ground reaction forces than arboreal quadrupedalism, due in large part to complaint gaits – produced by crouched posture, substantial limb yield, increased step length, and prolonged contact time with the substrate – utilized by primates on arboreal substrates (Demes et al., 1994; Schmitt & Larson, 1995; Larson, 1998, Schmitt, 1999; Larson et al., 2001 Larney & Larson, 2004). Leaping produces greater impact forces still, especially during landing (Demes et al., 1995, 1999). It is expected that species engaging in particular locomotor regimes will share volar pad traits that provide mechanical support for habitual activities. These traits are expected to reflect differences in biomechanical stresses unique to each locomotor group; vertically clinging and leaping taxa are expected to have larger first and second interdigital volar pads with higher relief than other groups to cushion and support the grasping complex; arboreal quadrupedal taxa are expected to have larger hypothenar and fourth interdigital pads to assist in providing consistent contact for the ulnar portion of their cheiridia in an inverted position on arboreal substrates; slow climbing taxa are expected to have overall shorter, wider volar pads than other groups that correlate with their highly derived, hyper-ectaxonic hands and feet. Semi-terrestrial and nail-clinging taxa are expected to closely resemble arboreal quadrupeds as both semit-terrestrial *Lemur catta* and nail-clinging *Eutoicus elegantulus* both engage in arboreal quadrupedalism in addition to their unique forms of locomotion.

1.2.5 Morphological Correlates of Impact Damping

The impact damping role of the volar pads is well-studied. As the hand or foot strikes down against the substrate, impact forces are applied initially to the volar pads. The viscoelastic behavior of the pads allows them to deform, the force used to produce this deformation is dissipated, and an overall reduced impact force is transmitted to the underlying tissues (Ker, 1990; Bennett & Ker, 1990; Aerts et al., 1995, 1996; Pawluk & Hower, 1999; Jindrich et al., 2006; Spears & Miller-Young, 2006). It has been demonstrated both experimentally and

theoretically that thicker calcaneal pads in humans result in greater impact damping, but it remains unclear if and how this relationship might drive morphological adaptation (Aerts et al., 1995, 1996; Spears & Miller-Young, 2006). Though the volar pads do indeed damp impact forces, this effect is only a partial reduction of the initial impact force, with the remainder provided by the leg or forearm. Additionally, the pads themselves are likely constrained by the physiological costs of maintaining tissue and functional demands of concurrent uses of the hands and feet such as grasping or manipulating objects. If the morphology of the volar pads is indeed influenced by the magnitude of impact forces experienced as part of a regular locomotor regime, it is expected that thicker pads will be found in semi-terrestrial species and those that engage regularly in leaping. In species that leap, it is further expected that the pads of the landing limb will be thicker than those of the non-landing limb.

1.2.6 Morphological Correlates of Arboreal Locomotion

As discussed previously, the surface area of the volar pads plays a large role in generating friction. A secure friction grasp is especially important during vertical climbing or clinging, when gravity and body mass both work actively to break frictional bonds, and while traveling quadrupedally over substrates that are narrower than the body, when torques must be produced by the limbs to counter those produced by lateral deviation of the center of mass over the center of the substrate. Some comparative evidence supports that this mechanism exists in viverrids; Veron (1999) found that the volar pads of arboreal species are significantly broader than those of their terrestrial counterparts. It is predicted here that the total surface area of the volar pads will increase with dependence on friction grasping during arboreal locomotion.

1.2.7 Fusion of Manual Thenar and First Interdigital Pads in Lemurids

There appears to be a morphological link between pad fusion (the creation of one pad from two of the six normally present on the primate hand) and digit reduction. The thenar and first interdigital pads are invariably fused on the hand of lemurids (Figure 1.1); this is correlated with a relative reduction in the first manual digital ray in these taxa and the smallest ratio of first to third digit length of examined strepsirrhine species (Biegert, 1959, 1961; Jouffroy et al., 1991). It remains unclear whether this is related strictly to reduction of the digit, or if it may reflect a concurrent shortening of the underlying metapodial bones.

1.4 Predictions: Morphology of the Dermatoglyphic Ridges

1.4.1 Morphological Correlates of Locomotor Mode

Several authors have noted an apparent link between locomotion and dimensions of the dermal papillae and dermatoglyphic ridges. Within primates, Hamrick (2001) described a morphocline in calltrichid primates where the intermediate ridges and corresponding dermal papillae become longer and better developed with decreased amounts of vertical tegulae (derived, medio-laterally compressed nails possessed by members of the *Callithrichidae*) clinging and increased use of small-diameter substrates. Similar morphology is seen rodents; climbing rodents, and especially those who use their hands and feet to grasp substrates, exhibit greater numbers of papillary ridges in their skin (Veron, 1999; Haffner, 1998). Further variation in the development of dermatoglyphic ridges of primates has been documented but remains to be quantified and assessed in a functional context (Lemelin, 2000).

Here, it is expected that the widths of the dermatoglyphic ridges will scale with negative allometry and the depth of the intermediate ridges will increase with dependence on friction grasping during arboreal locomotion. This scaling pattern would produce a relatively larger potential surface area in large bodied primates with a greater number of surface asperities available for interlocking with roughened substrates. Slow climbers and members of the vertical clinging and leaping group are therefore predicted to possess narrower ridges (and thus a greater number of ridges overall) and deeper ridges than arboreal quadrupeds. Small-substrate specialists are expected to have narrower and deeper ridges than large-branch specialists.

1.4.2 Morphological Correlates of Tactile Acuity and Diet

The association of nerve endings with features of the skin is well known for mammals. For several species, these relationships are thought to have functional correlates; in raccoons, the dermal papillae are surrounded by Merkel cells (slowly adapting type I tactile receptors, responsible for determining form and roughness of stimuli against the skin) such that movement of the dermal papillae will activate the Merkel cells (Munger & Pubols, 1972; Rice & Rassmussen, 2000). Similarly, the semi-aquatic water opossum (*Chironectes minimus*) is equipped with cone-shaped papillae that are well-suited for transmitting tactile information about changes in water flow from any direction to their associated Merkel cells (Hamrick, 1998, 2001).

In primates, the close association between the intermediate ridges of the epidermis and the Meissner corpuscles is thought to have a functional correlate as well; Cauna (1954, 1956) first described this association as a lever mechanism, in which the deep intermediate ridges are displaced by movement of or against the epidermis and function as levers, which press against the dermal papillae and activate the Meissner corpuscles. This relationship is illustrated in Figure 1.4. Martin (1990) further suggested that the intermediate ridges not only activate the Meissner

corpuscles by pressing into the dermal papillae, but also act to magnify external forces and heighten tactile sensation.

To date, no work has been done connecting intermediate ridge length directly to tactile acuity, but several hypotheses have been offered regarding their morphological connection. First, because Meissner corpuscles sit in the dermal papillae, which in turn sit between the dermatoglyphic ridges (Figure 1.4), narrower ridges have been hypothesized to result in a greater number of Meissner corpuscles per unit area and greater tactile acuity (Hoffmann et al., 2004). Lengthening the intermediate ridges would likewise increase tactile acuity by providing a larger lever arm through which to activate the Meissner corpuscles (Cauna, 1954, 1956; Martin, 1990).

Greater tactile acuity has been proposed to correlate with frugivory in primates; the hand is the primary cheiridium used in foraging and both strepsirrhine and haplorrhine primates have been observed to palpate and assess their food manually before ingestion (Charles-Dominique & Bearder, 1979; Wrangham, 1977; Dominy, 2004; Hoffman et al., 2004). It is predicted therefore that frugivorous primates will possess narrower dermatoglyphic ridges with deeper intermediate ridges than their folivorous, faunivorous, or omnivorous counterparts. It is further predicted that the volar skin of the hand will possess narrower dermatoglyphic ridges with deeper intermediate ridges than the volar skin of the foot for all groups.

1.5 Summary of the Dissertation

The overarching goal of this dissertation is to quantify and document variation present in the volar pads and skin of strepsirrhine primates. This variation is then evaluated in a functional context by examining the associated effects and constraints of each of the above described roles using a representative sample of strepsirrhine primates and the methods outlined in Chapter Two. Prior to undertaking this research, a feasibility study was conducted to ensure preservation of the volar surfaces in museum specimens did not significantly alter their morphology; the results of this study are presented in Chapter Three. Chapter Four explores the relationship between body size and scaling of the various volar structures. Chapter Five assesses the scaling patterns in relation to specific hypotheses regarding friction mechanics and body size. Chapter Six further identifies shared morphological traits of the volar pads among taxa engaging in similar locomotor repertoires and evaluates specific hypotheses relating to the role of the volar pads in arboreal locomotion and impact damping. Chapter Seven assesses the gross morphology of the volar skin ridges in relation to hypotheses regarding specific forms of locomotion and adaptations for tactile acuity. Throughout the dissertation, relationships of the volar pads to the underlying bony morphology and broader aspects of primate locomotion are discussed. Conclusions are presented in Chapter Eight.

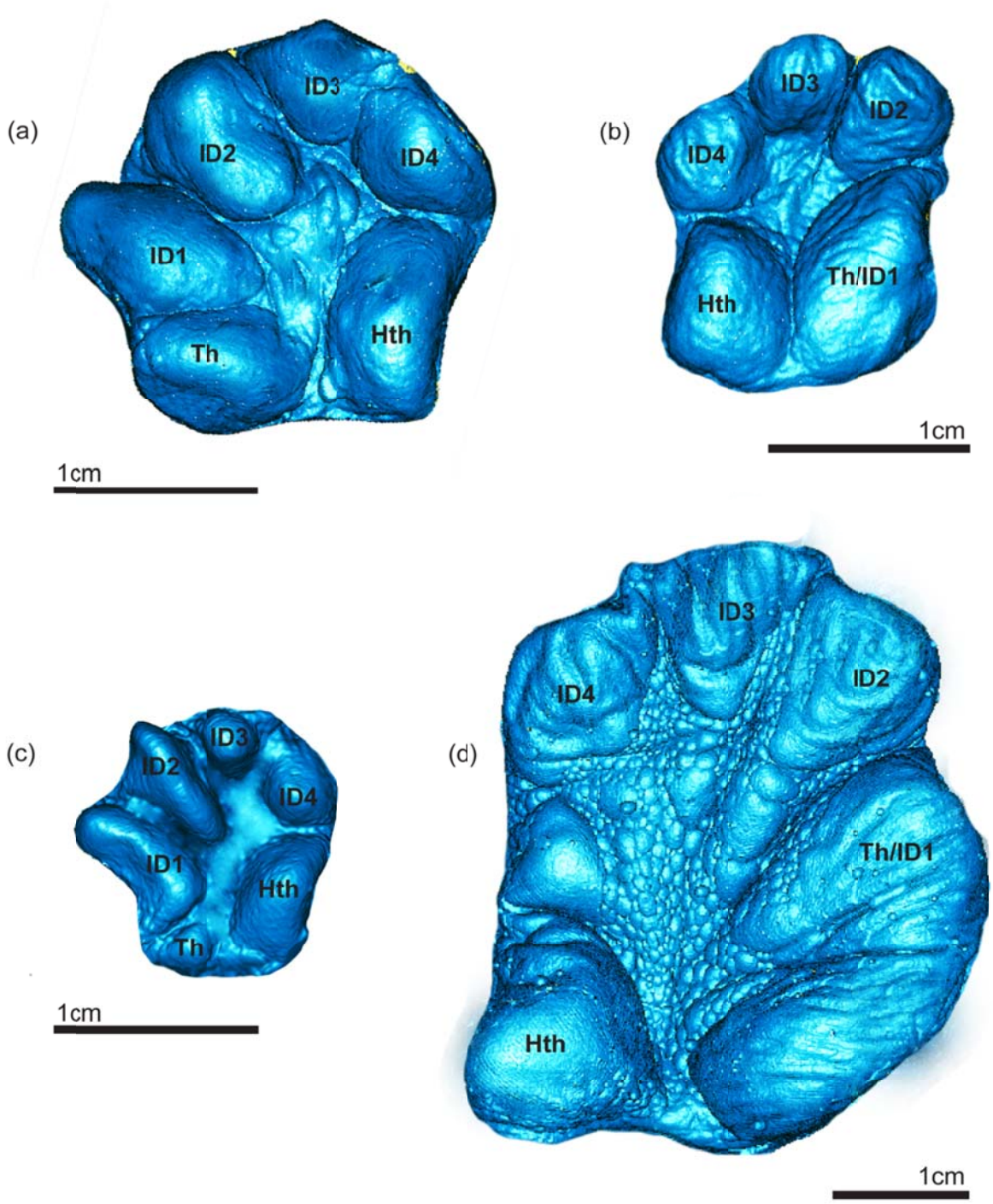

Figure 1.1. Illustration of variation in volar surface morphology. (a) Left hand of *Eutoicus elegantulus*. (b) Right hand of *Mirza coquereli*. (c) Left hand of *Galago senegalensis*. (d) Right hand of *Varecia variegata variegata*..Pictured volar pads are: thenar (Th), combination thenar and ID1 (Th/ID1), hypothenar (Hth), first interdigital (ID1), second interdigital (ID2), third interdigital (ID3), and fourth interdigital (ID4).

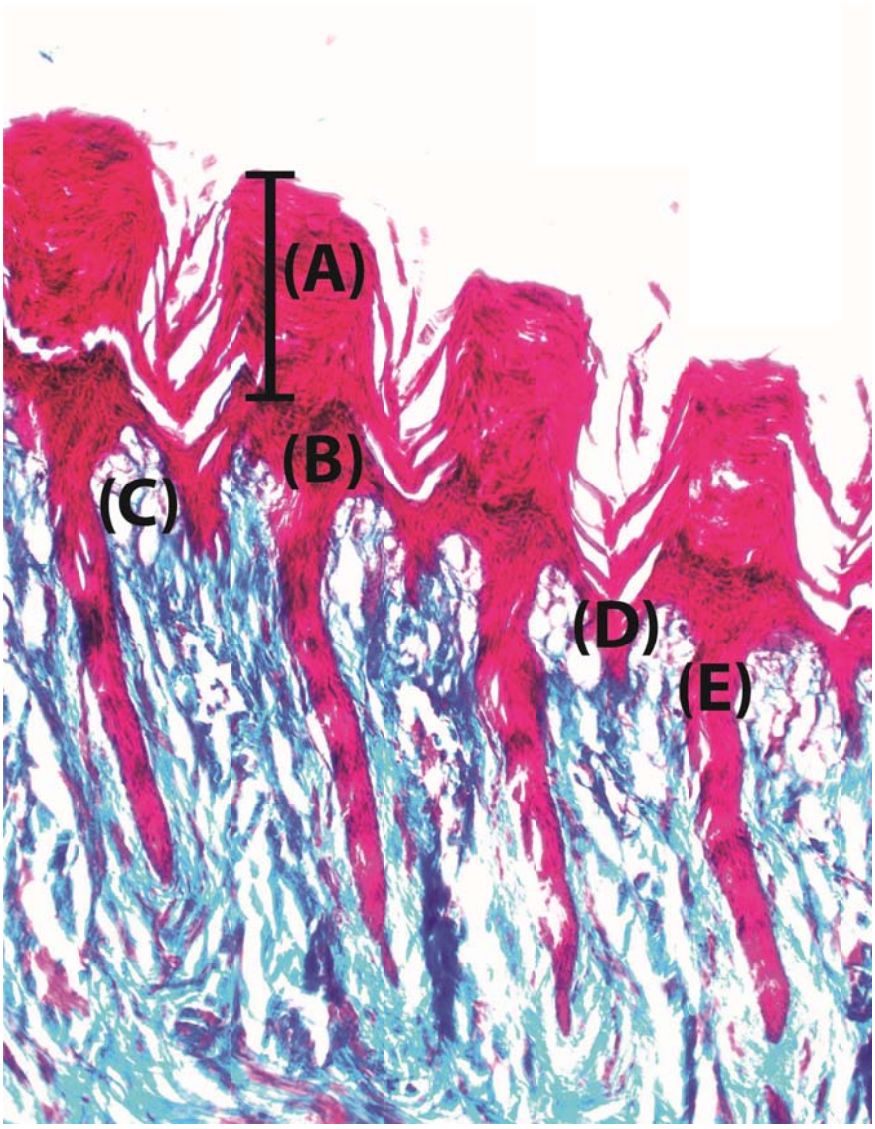

Figure 1.2. Illustration of dermatoglyphic ridge features. Features of the epidermis are stained red, features of the dermis are blue. The epidermis is visibly separated into two distinct sections; (A) denotes the superficial *strata spinosum* through *corneum*, where the epidermal cells have begun the process of keratinization, (B) denotes the stratum germinativum, which comprises live, unkeratinized cells. (C) denotes a dermal papilla, which is flanked on either side by folds of the *stratum germinativum*. These folds are classified by depth; (D) indicates a shallow limiting ridge and (E) indicates a deep intermediate ridge.

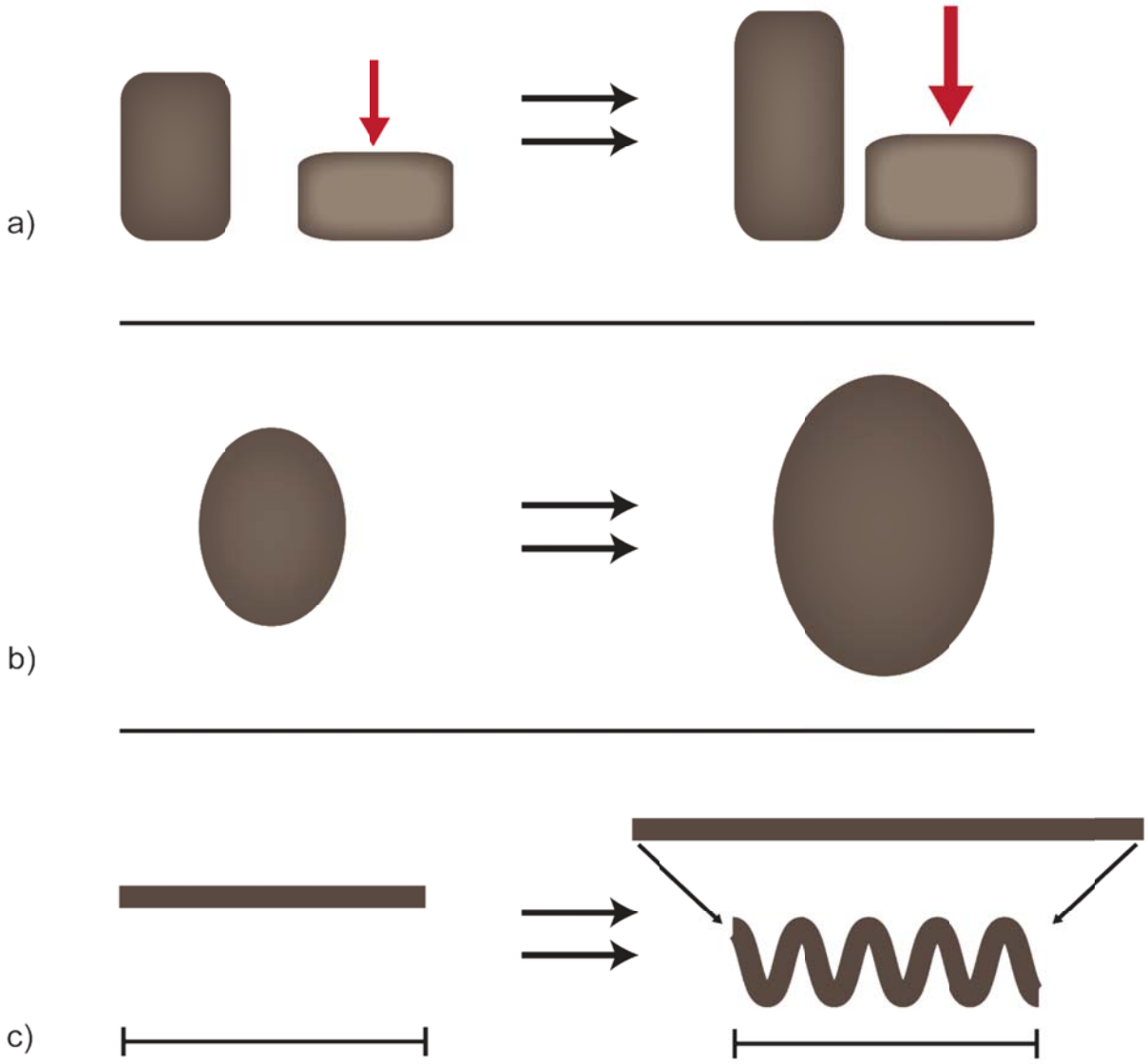

Figure 1.3. Illustration of predicted friction adaptations. (a) Volar pads become thicker and more protuberant; more force is required to fully deform the pads and the "n" component describing friction mechanics is increased.. (b) Volar pads expand surface area, which increases the "K" component describing friction mechanics. (c) Volar skin is folded to form ridges, which provides greater surface contact on irregular substrates and also increases the "K" component.

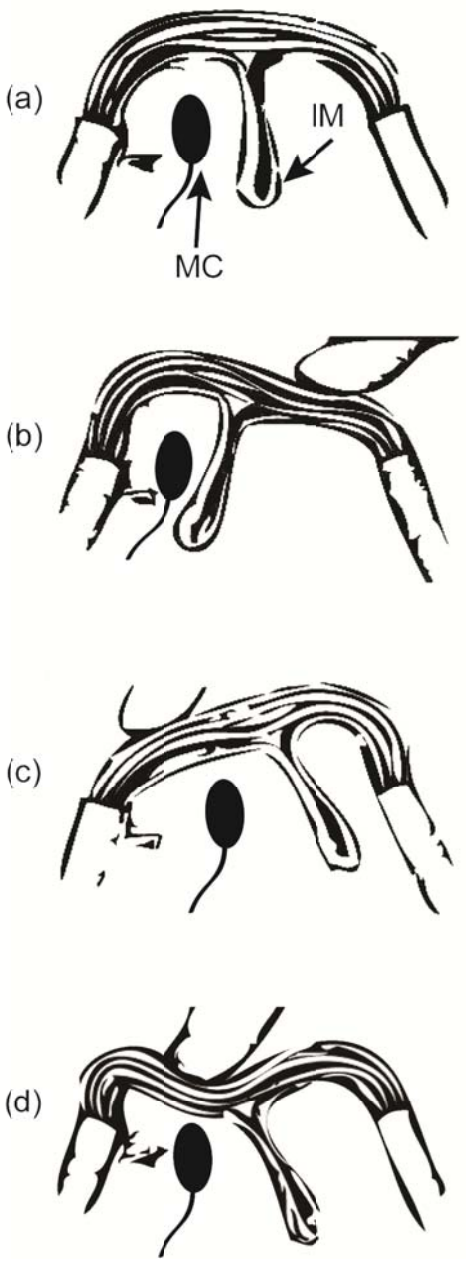

Figure 1.4. Illustration of the anatomical relationship between the intermediate ridges of the epidermis (IM) and the Meissner corpuscles (MC). (a) Shows both structures absent stimulus. (b) Stimulus is applied from the right. The intermediate ridge is forced left, deforming and activating the Meissner corpuscle. (c) Stimulus moves to left. The intermediate ridge is forced right, deactivating the Meissner corpuscle. (d) Stimulus is applied centrally. Meissner corpuscle is deformed by compression. Adapted from Cauna (1954).

Chapter 2:
Methodology

2.1 Study Sample

This study examined a representative sample of strepsirrhine primates. This clade contains members with varied locomotor preferences and a near sixty-fold span of body sizes, ranging from 60g to 3500g, making it ideal to examine the effects of both on morphology. Three sample pools of primates were utilized to accommodate differences in preservation and to avoid damaging rare museum specimens. Overlap between individuals of these groups was limited; in several cases the volar pads and skin of the same individuals were examined, but these were exceptions rather than the rule.

The first pool comprised molded impressions of the manual and pedal volar surfaces of 19 species of primates compiled from individuals stored in the fluid collections of the American Museum of Natural History (AMNH) and the National Museum of Natural History (NMNH). Taxa, sample sizes, and physical and behavioral descriptions of this sample pool are detailed in Table 2.1. The volar pads of this group were measured and compared to identify gross morphological differences.

The second pool comprised the same species included in the first, but was drawn from the skeletal collections of the AMNH and NMNH. Sample sizes for this pool are detailed in Table 2.1 alongside species descriptions.

The third pool consisted of manual skin samples purchased through Duke Lemur Center either directly or through Dr. Magdalena Muchlinski, who kindly provided many samples from her personal collection. These samples were utilized for histological investigation and are detailed in Table 2.2.

2.2 Data Collection

2.2.1 Volar Pad Morphology

Impressions of the manual and pedal volar surfaces were created by applying Coltene President light body dental molding compound (a low-viscosity polyvinylsiloxane) to the target surface and allowing it to harden. Once solidified, the molds peeled easily and completely away from the surfaces and left no residue. The physical molds were then digitized using the VivaCT75 microCT scanner housed in the Division of Laboratory Animal Resources (DLAR)

facilities in the Stony Brook University Health Sciences Center. Power parameters were set at 70 kVp and 114 μA, and specimens were scanned at a resolution of 30μm with an integration time of 100 ms. Image files were stacked and converted to three-dimensional digital objects in Amira® and imported into Raindrop Geomagic Studio 10® for measurement.

Digital measurements of the length, width, and surface area of each volar pad were taken in Geomagic Studio®. Length was defined as the longest proximo-distal dimension; width was defined as the longest medio-lateral dimension perpendicular to the measured length. Surface area was defined as the entire surface of the volar pad, including all contours; projected area was defined as the two-dimensional area of the palm or sole covered by the volar pad. Projected area was measured by aligning the volar surface and a digitally generated scale orthogonal to the screen in Geomagic Studio® and captured as a TIFF image. That image was subsequently outlined in Adobe Photoshop® and the included area measured. Relief index was calculated by dividing the surface area measurement by the projected area measurement. A shape index was calculated by dividing the length of the pad by the width of the pad. These measurements, except for relief index, are illustrated in Figure 2.1.

2.2.2 Metapodial Bone Morphology

Measurements of metapodial bones were collected using a digital caliper. These included the length of the metapodial and the widths of its articular base and head.

2.2.3 Volar Skin Morphology

Skin samples from the thenar and hypothenar pads were sliced free from the manual and pedal volar surfaces and prepared for histological examination following paraffin embedding procedures outlined in Humason (1997). Prepared samples were sectioned perpendicular to the dermatoglyphic ridges and mounted to slides. These slides were then stained using Masson's trichrome method, which produced red keratin and muscle fibers, blue collagen and bone, and black nuclei. Additionally, this stain produced a stark contrast between the collagen-rich papillary layer of the dermis and the keratinous stratum germinativum of the epidermis (Figure 2.2).

The width and depth of the dermatoglyphic ridges were measured photomicroscopically. Photographs of magnified sections were collected using ToupView® software, then measured using Piximétre 5.9 (Henriot, 2016). The distance between the intermediate ridges of the stratum germinativum were measured as a proxy for dermatoglyphic ridge width, as the epidermis was shed and lost during processing in several instances. (The intermediate ridges sit immediately deep to the epidermal ridges and share similar dimensions; see Figure 2.2). Ridge widths and depths were sampled opportunistically at 30 locations across each sample.

2.3 Feasibility Study

To ensure post-mortem changes related to ethanol storage did not significantly alter the morphology of the volar pads, a feasibility study was carried out. Post-mortem changes in the volar pads of rats were examined and compared across different stages of preservation. This is presented as a stand-alone study in Chapter Three.

2.4 Phylogenetic Non-independence of Variables

Phylogenetic non-independence of trait variables is a well-known phenomenon among evolutionary biologists; closely related species are more likely to share traits than distantly related species and it becomes difficult to determine which traits are tied to this pattern of inheritance and which may be functional adaptations (Felsenstein, 1985; Harvey & Pagel, 1991; Nunn, 2011). To assess possible phylogenetic correlation of traits that could potentially confound further statistical analysis, two methods were employed. Phylogenetic consensus trees containing the sampled species were downloaded from the 10k Trees Project (Version 3; Arnold et al., 2010). These trees were then paired with species means of collected measurements in R and maximum likelihood estimates of Blomberg's K and Pagel's λ statistics calculated for each measurement type (Pagel, 1999; Blomberg et al., 2003). These statistics both produce a coefficient ranging from 0 (no phylogenetic correlation) to 1 (significant phylogenetic correlation), but measure phylogenetic correlation by different means. Blomberg's K calculates the ratio of variance among species to the variance produced by independent contrasts between them, then scales this by a similar, hypothetical ratio predicted by a Brownian motion model of evolution. A maximum likelihood estimate of K was generated using the APE and PICANTE packages in R, then compared to 100 values of K generated by assigning random phylogenetic relationships to the data (Paradis et al., 2004; Kembel et al., 2010). Signal was determined to be significant when these random iterations failed to approximate the original value of K. Pagel's λ scales the off-diagonal elements of the phylogenetic covariance matrix. A maximum likelihood value for λ was also generated using the APE and CAPER packages and compared to zero by a single-sample t-test to determine statistical significance (Paradis et al., 2004; Orme et al., 2013). Both statistics were developed for use with a Brownian motion model of evolution; however, recent analysis suggests that they are useful for determining phylogenetic correlation under differing models and when the specific model of evolution is unknown (Diniz-Filho et al., 2012). Concurrence of the measures was taken as strong evidence of phylogenetic signal. It is important to note that these values are only estimates for individual traits—they do not indicate phylogenetic correlation of trait interactions (for example, although the projected areas of the majority of volar pads exhibit phylogenetic correlation, the relationship between body size and

the same projected areas are not, i.e.: $\lambda = 0$). Therefore, λ was calculated independently for each analysis and was reported with the results.

The primate phylogeny used here was a 50% majority-rule consensus tree compiled by the *10kTrees* website, a free resource that samples 11 mitochondrial and six autosomal genes from GenBank (Benson et al., 2005; Arnold et al., 2010). The consensus tree was downloaded in NEXUS format and read into R to perform phylogenetically informed analyses. An illustration of the phylogeny is provided in Figure 2.3.

The majority of raw variables showed significant phylogenetic signal. Blomberg's K and Pagel's λ statistics are provided in Table 2.3. Importantly, body size was significantly correlated with phylogeny ($K = 0.74$, $p < 0.01$; $\lambda = 1.00$, $p < 0.01$). As all variable measurements are also correlated with body size (see Chapter Five), it was deemed necessary to examine the phylogenetic signal present in the variables without the confounding effects of body size. Statistics for scaled variables are provided in Table 2.4. With the effects of body size removed, many variables show no significant phylogenetic signal.

2.5 Body Size and Scaling of Variables

2.5.1 Body Size Surrogates

Body size surrogates were constructed for skeletal samples by calculating the geometric mean of anteroposterior and mediolateral midshaft diameters from each associated humerus and femur, as these measures have been shown to correlate strongly with body mass in strepsirrhine primates and provide a suitable proxy when individual masses are not available (Demes et al., 1991; Lemelin & Jungers, 2007). Midshaft diameters were not available for fluid preserved specimens, and as such a body size surrogate was constructed by calculating the geometric mean of the species mean body mass as reported by Smith & Jungers (1997) and body length as measured from rostrum to the base of the tail. This scales the average reported masses by an individual factor that is unrelated to the functional demands of the traits being investigated (Coleman, 2008). No individual size data were available for the volar skin samples, so the masses reported by Smith & Jungers (1997) were used as estimates.

2.5.2 Scaling of Variables

The relationships with body size of raw measurements taken of the volar pads, volar skin, and metapodial bones were examined via phylogenetic generalized least squares (PGLS) analyses. This least squares regression method accounts for phylogenetic non-independence of variables when examining the correlation of variables. Species means were computed from

measured values and body size surrogates. Analyses were carried out using the R software packages APE and CAPER (Paradis et al., 2004; Orme et al., 2013).

Examined variables included the projected area, surface area, length, width, and shape of the volar pads. Shape was calculated by dividing the length of each pad by the width; values larger than one indicate a long pad, values smaller than one indicate a wide pad. Scaling of the length, base width, and head width of the metapodial bones were examined, as were the width and depth of the dermatoglyphic ridges. The slopes of significantly correlated variables were then compared to a hypothetical slope value representing isometric scaling with body mass with a single-sample t-test. These included a slope of 0.33 for length and width, 0.66 for surface and projected areas. While no specific expectation for shape existed *a priori*, the resulting slopes were compared to a slope of 1 which indicated no change. Statistically significant deviation from these values was considered allometric scaling.

2.5.3 Standardization of Volar Pad Measurements

To facilitate comparisons of pad morphology across taxa that vary widely in body size, it was desirable to standardize raw measurements to account for both the effects of body size and shape changes due to allometric scaling. Collected volar pad measurements were transformed using the equation:

$$\mathbf{Y = X/Body\ Size^{b}}$$

where Y is the scaled measurement, X is the raw measurement, Body Size is a surrogate score defined above for each group of variables, and individual body length measured from rostrum to the base of the tail, and b is the slope of the correlation determined by PGLS analyses in Chapter Five.

2.6 Correlation of variables and dimension reduction

The measured dimensions of the volar pads were related geometrically and likely to be correlated to some degree, though the exact extent of this correlation was not predictable by simple geometry. Pad length and width variables were both expected to correlate with projected and surface areas, but because the volar pads are irregular in shape, it was unclear whether they could provide an accurate estimate of area or be restricted to variables denoting shape. Likewise, the projected and surface areas were likely to be correlated, but whether this correlation would prove isometric across taxa and body size remained unknown; certain taxa might possess more convex pads than others, which could alter the correlation coefficient or render it insignificant. The relationships of these variables to one another were therefore interesting in their own right.

Additionally, perfect or near-perfect correlation of two or more dependent variables provides no increase in statistical or analytical power, whereas combining or removing one variable provides the benefit of reducing the size of the dataset.

To detect correlation, species means were computed for each variable and PGLS regressions carried out. Correlations between the following variable pairs were examined: (1) pad projected area and surface area, (2) pad length and width, (3) pad length and surface area, and (4) pad width and surface area. Very strong correlation was identified between projected and surface area measurements (Table 2.5); as such, projected area was dropped from further analyses, except when contributing to the relief index of the pads. Surface area was retained as the "area" value, as it was demonstrated in the feasibility study (Chapter Three) to be a more precise measure of area and holds greater functional significance during friction grasping.

2.7 Morphological Correlates of Friction Mechanics in the Volar Surfaces

2.7.1 Volar Pad Relief

The relief of the volar pads was of interest due to its relationship to the "n" variable in the equation quantifying semi-solid friction. The n variable is proportional to the amount of force needed to deform the pads completely. The most direct way to alter this force, without changing the composition of the pads themselves, would be to increase the thickness of the pad. This would produce a more convex pad with a large ratio of surface area to projected area. Cartmill (1979) hypothesized that the volar pads of small-bodied primates would be optimized toward more convexity than those of large-bodied primates, as large-bodied primates would require exponentially larger pads to reap any benefit.

The relationship between projected area and surface area was examined in two ways. First, species means were computed for surface area and projected area measurements for each pad, then a phylogenetic generalized least squares analysis (PGLS) was conducted to examine correlation of the two measurements. Second, individual projected area and surface area measurements were combined into a relief index by dividing the surface area of the pad by its projected area. A species mean was calculated for this index, and a second PGLS analysis conducted to examine its correlation with body size. To test the null hypothesis that the relief index is correlated with body size, the resulting slopes of the PGLS regression lines were compared to a slope of one, representing isometry, via one-sample Student t-tests.

2.7.2 Volar Pad Surface Area

Volar pad surface area was of interest as it contributes directly to the "K" variable in the equation quantifying viscoelastic friction. Species means were computed for each manual and

pedal pad's surface area and a PGLS analysis was conducted to examine the correlation of these measurements with body size. To test the hypothesis that surface area is increased through allometric scaling of the pads, the resulting slopes of the PGLS regression lines were compared to an isometric scaling model (Area = 2/3 * Mass; slope = 0.66) using one-sample Student t-tests.

2.7.3 Dermatoglyphic Ridge Width

Ridge width measurements collected from each sample were averaged to form a composite score, and log transformed to meet the assumptions of parametric statistical tests. Species means of these composite scores were computed and the relationship between ridge width and body mass was examined using PGLS. The resulting slopes of the PGLS regression lines were compared to an isometric scaling model (Length = 1/3 * Mass; slope = 0.33) using one-sample Student t-tests to test the hypothesis that dermatoglyphic ridges scale with negative allometry with regards to body size and thus increase potential surface contact area.

2.8 Morphological Correlates of Function in the Volar Pads

2.8.1 Locomotor Groups

The primates in this study fell into five gross locomotor categories, several of which overlapped in specific activities. All strepsirrhine primates engage in some degree of arboreal locomotion, and all apart from lorisids engage in some amount of leaping. The locomotor categories used here therefore reflect a suite of behaviors shared by species, rather than singular activities in which an individual might engage. Table 2.6 provides a reference of these categories and the primate species comprising them. These categories were defined as: (1) Arboreal Quadruped: exclusive use of arboreal substrates, generalized quadrupedal leaping behaviors; (2) Vertical Clinging and Leaping: specialized leaping between two vertical substrates where the feet are responsible for both leveraging the jump and establishing contact with the landing substrate (Napier & Walker, 1967; Demes et al., 1995, 1996); (3) Slow Climbing: exclusive use of arboreal substrates, quadrupedal walking and climbing, no leaping behaviors; (4) Arboreal Nail-clinging: exclusive use of arboreal substrates, quadrupedal walking on horizontal substrates, use of specialized nails on apical phalanges to interlock with vertical substrates; (5) Semi-terrestrial Quadruped: quadrupedal walking on arboreal and terrestrial substrates, generalized leaping behaviors. The final two categories describe only one species each: *Euoticus elegantulus*—the needle-clawed galago—and *Lemur catta*, respectively. Although it seemed unlikely that either species on its own would possess the statistical power necessary to differentiate itself in the analysis, they were included to provide a fuller understanding of

morphological variation. To test the general hypothesis that pad morphology varies between locomotor groups, a discriminant function analysis was carried out. Directional hypotheses were then addressed by ANOVA.

2.8.2 Discriminant Function Analysis

Discriminant function analysis provided a means to perform an omnibus statistical test for differences between locomotor categories using the entirety of the volar surfaces (as opposed to individual pads), as well as determine the statistical validity of those groups as applied to categorizing volar morphology. Mathematically, this analysis was identical to ANOVA, but provided additional information as to which variables were most responsible for differences between locomotor groups and allowed for easy visualization of the results.

The locomotor categories described above were entered as group (predictor) variables for both hand and foot analyses. For the hand, the length, width, and surface area measurement for the hypothenar, second interdigital, third interdigital, and fourth interdigital pads were entered as discriminating variables. The thenar, first interdigital, and combination thenar/first interdigital pads were excluded from analysis as they are variably present in the study sample. For the foot, the length, width, and surface area of all pads were entered as variables.

Several authors have shown that phylogenetic non-independence of variables can produce type II errors in discriminant function analysis (Motani & Schmitz, 2011; Barr & Scott, 2014). It was therefore desirable to account for phylogenetic non-independence in the analysis while still allowing for within-group variation and cross-validation with individual specimens. Cross-validation, also called the "leave-one-out" method, is a technique used to test the robusticity of the discriminant functions generated by the entire dataset. The technique works by removing a single specimen, computing new discriminant functions, and attempting to classify the removed specimen based on the new functions; this is repeated for each specimen. Currently, phylogenetic comparative methods for FDA and ANOVA rely on computed species means to address phylogenetic correlation and do not account for within-species variation during cross-validation. A compromise was therefore made, and narrow phylogenetic comparisons were conducted in addition to an omnibus discriminant function. The discriminant function analysis included all species, and was conducted to identify shared morphology for locomotor groups across all examined taxa, regardless of phylogenetic history.

The "Arboreal Quadruped" and "Vertically Clinging and Leaping" locomotor groups comprise members of the both the superfamily *Lemuroidea* and family *Galagidae*. Shared phylogenetic history is known to result in shared, functionally-related features between closely related taxa that may be obscured when the greater group is examined; i.e., the vertically clinging and leaping galagos may have different adaptations to this form of locomotion than the vertically clinging and leaping lemurs. To address this, analysis of variance was conducted on measured volar pad dimensions between these groups. Utilization of both of these methods allowed

assessment of group morphology in cases where locomotor habits are tightly correlated with a single clade or taxa, as is the case for the lorises and *Euoticus elegantulus,* and in groups that span multiple clades.

The subsequent discriminant analyses were restricted to family groups. These were conducted to identify shared morphological features of locomotor groups within a narrow phylogenetic context. This allows shared morphology of locomotor groups unique to these clades to be identified and its functional significance assessed. The first of these was carried out between members of Galagidae, and the second between members of Lemuridae. All variables defined above were included, regardless of phylogenetic signal.

2.8.3 Correlates of Impact Damping

Relief index (computed by dividing the surface area of the pads by the projected area) was used here as a proxy for a pad's thickness. This was appropriate in this instance as measuring thickness of the pads is difficult to measure reliably on digital models where deep tissue cannot be compared. The volar pads are convex in form and their relief indices therefore provide an estimate of how far they project from the palm or sole. To determine if loading regime affects the thickness of the volar pads, two analyses were conducted. Relief index was not found to be significantly correlated with phylogeny for any pad and therefore standard analysis of variance was carried out in SPSS comparing the corresponding volar pads of different locomotor groups. All volar pads were included in the analysis; the variably present manual thenar, first interdigital, and combined thenar/first interdigital pads were compared where available. A second analysis compared the relief index of corresponding pads between the landing and non-landing limbs of individuals falling into the "vertical clinging and leaping" locomotor category via paired Student t-tests (Table 2.1).

2.8.4 Correlates of Arboreal Locomotion

It was hypothesized that pad surface area would increase with dependence on friction grasping in arboreal locomotion. Slow climbers and members of the vertical clinging and leaping group were expected to possess greater total volar surface area than their arboreal quadruped counterparts, and all three of these groups were expected to possess a greater total surface area than the semi-terrestrial *Lemur catta.* Surface area shows significant phylogenetic correlation in several pads, therefore phylogenetically informed analyses were used (Table 2.4). The total surface area for each volar surface was computed by summing the standardized surface areas of the individual pads. Species means were computed for these totals and compared with a phylogenetically informed ANOVA using the APE and GEIGER packages in R (Paradis et al., 2004; Harmon et al., 2008).

2.8.5 Fusion of Manual Thenar and First Interdigital Pads in Lemurids

It was hypothesized that fusion of the thenar and first interdigital pads in lemurids was due to a reduction in length in the first metacarpal. Because this pad configuration is clearly phylogenetically linked, both a phylogenetically informed analysis of variance and an unadjusted analysis were conducted to assess both relational and absolute differences between groups. Species means were computed for the scaled lengths of the first metacarpals and compared between species that possessed individual thenar and first interdigital pads or a combination pad using a phylogenetically informed ANOVA computed by the APE and GEIGER packages for R (Paradis et al., 2004; Harmon et al., 2008). Additionally, species means of the scaled surface areas of the combination thenar first interdigital pad were compared via a phylogenetically informed ANOVA to the summed surface area of individually held thenar and first interdigital pads to determine if perhaps fusion yielded greater surface area than individual pads.

2.9 Morphological Correlates of Function in the Dermatoglyphic Ridges

2.9.1 Morphological Correlates of Locomotion

The widths of the dermatoglyphic ridges were hypothesized to decrease and the depth of the intermediate ridges to increase with dependence on friction grasping during arboreal locomotion. Slow climbers and members of the vertical clinging and leaping group were therefore predicted to possess narrower ridges (and thus a greater number of ridges overall) than arboreal quadrupeds. Small-substrate specialists were expected to possess narrower and deeper ridges than large-substrate specialists. No significant correlation with phylogeny was found to be present in the measured widths of the dermatoglyphic ridges or the depths of the intermediate ridges (Table 2.4) and analysis of variance was carried out comparing standardized ridge width and intermediate ridge depth between the same locomotor categories described in section 2.8.1.

2.9.2 Morphological Correlates of Tactile Acuity and Diet

The widths of the dermatoglyphic ridges and depth of the intermediate ridges were further hypothesized to vary with diet categories, due to their close association with the Meissner corpuscle tactile receptors. Specifically, ridge widths were expected to decrease and intermediate ridge depth expected to increase with frugivory; faunivorous species were then predicted to have the widest ridges and shallowest intermediate ridges, and frugivorous species the narrowest

ridges and deepest intermediate ridges. A Kruskal-Wallis analysis of variance was carried out comparing standardized ridge width and depth between the diet categories listed in Table 2.2.

Table 2.1. Species included in volar pad and metapodial analyses with associated sample sizes, masses, and locomotor regimes. Species are ordered by clade: lemuroids, lorisids, galagids.

Taxon (n_{pads}; $n_{metapodials}$)	Mass (g)	Locomotor Regime
Daubentonia madagascariensis(1; 0)	2500	Arboreal quadruped [1]
Cheirogaleus major (4; 2)	400	Arboreal quadruped [1]
Eulemur fulvus collaris (5; 6)	2336	Arboreal quadruped [1]
Eulemur fulvus fulvus (5; 5)	2200	Arboreal quadruped [1]
Eulemur macaco macaco (9; 1)	1800	Arboreal quadruped [1]
Eulemur mongoz (2; 0)	1620	Arboreal quadruped, leaping (landing limb variable) [2]
Hapalemur griseus griseus (9; 7)	950	Vertical clinging and leaping (lands on hindlimbs) [2]
Lemur catta (6; 4)	2210	Terrestrial quadruped [1]
Lepilemur leucopus (2; 8)	617	Vertical clinging and leaping [1]
Microcebus murinus (11; 7)	115	Arboreal quadruped , leaping (lands on all limbs) [3]
Mirza coquereli (3; 0)	320	Arboreal quadruped [1]
Varecia variegata variegata (5; 4)	3600	Arboreal quadruped, some leaping (landing limb variable) [2]
Loris tardigradus (6; 4)	200	Arboreal quadruped, uses exclusively small diameter supports [4, 5]
Nycticebus coucang (8; 4)	650	Arboreal quadruped, favors large-diameter supports [6, 7]
Perodicticus potto (2; 5)	1200	Arboreal quadruped, no leaping, favors large-diameter supports [7, 8]
Euoticus elegantulus (2)	300	Arboreal quadruped, vertical climbing. [9]
Galagoides demidoff (10; 4)	60	Arboreal quadruped, leaping (lands on forelimbs), favors small diameter supports [9, 10]
Galago moholi (7; 5)	180	Vertical clinging and leaping (lands on hind limbs), favors small diameter supports [10, 11, 12]
Galago senegalensis (6; 5)	300	Vertical clinging and leaping (lands on hind limbs), favors small diameter supports [10, 11, 13]
Otolemur crassicaudatus (1; 4)	1200	Arboreal quadruped [12, 13]

References: [1] Fleagle, 1999; [2] Terranova, 1996; [3] Martin, 1972; [4] Subramonian, 1957; [5] Petter & Hladik, 1970; [6] McArdle, 1989; [7] Charles-Dominique, 1977; [8] Oates, 1984; [9] Charles-Dominique & Bearder, 1979; [10] Nash et al., 1989; [11] Harcourt & Bearder, 1989; [12] Crompton, 1984; [13] Bearder & Doyle, 1974

Table 2.2. Species included in histological analysis and their associated sample sizes, masses, and locomotor regimes and diets.

Taxon (n)	Mass (g)	Locomotor Regime and Diet
Cheirogaleus medius (3)	280	Arboreal quadruped, favors large supports, frugivores (occasional insects and small vertebrates) [1, 12]
Eulemur coronatus (2)	650	Arboreal quadruped, frugivores [1]
Eulemur fulvus (3)	2500	Arboreal quadruped, flexible folivore [1]
Eulemur macaco flavifrons (2)	1800	Arboreal quadruped, frugivore [1]
Eulemur mongoz (1)	1620	Arboreal quadruped, leaping (landing limb variable), frugivore [2, 3]
Hapalemur griseus griseus (2)	950	Vertical clinging and leaping (lands on hind limbs), bamboo [2]
Microcebus murinus (3)	115	Arboreal quadruped , leaping (lands on all limbs), omnivorous [4]
Mirza coquereli (3)	320	Arboreal quadruped, omnivorous [1]
Loris tardigradus (2)	200	Arboreal quadruped, uses exclusively small diameter supports, insects and small vertebrates [5,6]
Nycticebus coucang (1)	650	Arboreal quadruped, favors large-diameter supports, omnivore [7,8]
Galago moholi (2)	180	Vertical clinging and leaping (lands on hind limbs), favors small diameter supports, insects and exudates [9, 10, 11, 12]
Galago senegalensis (3)	300	Vertical clinging and leaping (lands on hind limbs), favors small diameter supports, omnivore [9, 11, 12]

References: [1] Fleagle, 1999; [2] Terranova, 1996; [3] Curtis 2004; [4] Martin, 1972; [5] Subramonian, 1957; [6] Peter & Hladik, 1970; [7] McArdle, 1989; [8] Charles-Dominique, 1977; [9] Nash et al., 1989; [10] Harcourt & Bearder, 1989; [11] Crompton, 1984; [12] Bearder & Doyle, 1974

Table 2.3. Measures of phylogenetic signal in raw variables.

Volar Pads	Projected Area		Surface Area		Length		Width	
	K	λ	K	λ	K	λ	K	λ
Forelimb								
Thenar	0.35	0.00	0.38	0.00	0.37	0.00	0.26	0.00
Thenar/ID1	1.20**	1.00**	1.39**	1.00**	1.42**	1.00**	0.78*	1.00
Hypothenar	0.54**	0.96*	0.65**	1.00**	0.76**	0.99**	0.51**	0.96*
ID1	0.41	0.00	0.43	0.00	0.26	0.00	0.60*	0.00
ID2	0.51**	0.97*	0.51**	0.98	0.50**	0.97	0.60**	1.00*
ID3	0.57**	0.98*	0.57**	0.99*	0.64**	1.00**	0.37	0.58*
ID4	0.56**	0.95*	0.60**	0.99*	0.80**	1.00**	0.34	0.56
Hindlimb								
Thenar	0.75**	1.00**	0.67**	0.00	0.74**	0.99**	0.62**	0.99*
Hypothenar	0.82**	1.00**	0.86**	1.00**	1.24**	1.00**	0.86**	0.85
ID1	0.51**	0.92*	0.58**	0.93*	0.43*	0.87*	0.42*	1.00
ID2	0.61**	1.00**	0.63**	1.00**	0.73**	1.00**	0.33	0.51
ID3	0.73**	1.00**	0.74**	1.00**	0.60**	1.00*	0.78**	1.00**
ID4	0.65**	1.00**	0.60**	1.00**	0.35*	0.53	0.39*	0.50

Metapodials	Length		Head Width		Base Width	
	K	λ	K	λ	K	λ
Forelimb						
MC_1	0.63**	1.00	0.57**	1.00	0.71**	1.00*
MC_2	0.88**	1.00**	0.66**	1.00*	0.46*	0.00
MC_3	0.79**	1.00**	0.22	0.35	0.61**	1.00
MC_4	0.81**	1.00**	0.67**	1.00*	0.64**	1.00*
MC_5	0.76**	1.00*	0.64**	1.00	0.67**	1.00*
Hindlimb						
MT_1	0.83**	1.00**	0.67*	1.00	0.72**	1.00*
MT_2	0.97**	1.00**	0.66*	1.00	0.74**	1.00*
MT_3	0.92**	1.00**	0.65*	1.00	0.64**	0.99
MT_4	0.94**	1.00**	0.59*	0.99	0.59*	0.98
MT_5	0.94**	1.00**	0.70**	1.00*	0.67**	1.00*

Volar Skin	Ridge Width		Ridge Depth	
	K	λ	K	λ
Forelimb				
Thenar	0.77**	0.95**	0.83**	0.99*
Hypothenar	0.53*	0.87**	1.18**	1.00**
Hindlimb				
Thenar	0.86*	0.00	0.71	0.85
Hypothenar	0.44	0.94	1.35*	1.00

Body Size	K	Λ
	0.74**	1.00**

** $p < 0.01$

* $p < 0.05$

Table 2.4. Measures of phylogenetic signal in variables after standardization for body size.

Volar Pads	Projected Area		Surface Area		Length		Width		Relief	
	K	λ	K	λ	K	λ	K	Λ	K	λ
Forelimb										
Thenar	0.00	0.21	0.65	0.00	0.49	0.00	0.11	0.00	0.19	0.44
Thenar/ID1	0.62	0.31	0.79	0.00	0.77	0.00	0.26	0.00	0.20	0.40
Hypothenar	0.00	0.22	0.27	0.00	0.36	0.00	0.57	0.09	0.09	0.00
ID1	0.00	0.33	0.80	0.00	0.14	0.00	0.79	0.09	0.19	0.00
ID2	0.00	0.24	0.37	0.06	**0.95****	**1.00****	0.48	0.25	0.20	0.05
ID3	0.45	0.35	**0.66****	**1.00***	**0.63****	**1.00**	0.48	0.21	0.60	0.31
ID4	0.00	0.29	0.32	0.00	0.52	0.00	0.28	0.02	0.29	0.00
Hindlimb										
Thenar	0.35	0.00	0.46	0.00	0.40	0.00	**1.18****	**1.00****	0.18	0.54
Hypothenar	0.23	0.00	0.21	0.00	**0.79****	**1.00***	**0.78****	**1.00***	0.22	0.67
ID1	0.17	0.00	0.25	0.00	0.13	0.00	0.25	0.00	0.34	0.09
ID2	0.38	0.56	0.33	0.38	0.44	0.95	0.51	0.09	0.19	0.00
ID3	0.20	0.00	0.31	0.58	0.14	0.00	0.39	0.52	0.28	0.00
ID4	0.30	0.18	0.30	0.17	0.10	0.00	0.13	0.68	0.27	0.32

Metapodials	Length		Head Width		Base Width	
	K	λ	K	λ	K	λ
Forelimb						
MC_1	0.27	0.00	0.22	0.36	**0.49***	**0.75***
MC_2	0.41	0.38	0.34	0.00	0.34	0.31
MC_3	0.19	0.00	0.08	0.00	0.32	0.36
MC_4	0.26	0.00	**0.58****	**0.81***	0.25	0.00
MC_5	0.19	0.00	0.32	0.53	0.44	0.00
Hindlimb						
MT_1	0.32	0.00	0.41	0.36	0.48	0.00
MT_2	0.51	0.32	0.29	0.61	0.55	0.76
MT_3	0.36	0.00	0.18	0.24	0.33	0.00
MT_4	0.41	0.14	0.32	0.74	0.49	0.00
MT_5	0.39	0.00	0.18	0.41	0.34	0.00

Volar Skin	Ridge Width		Ridge Depth	
	K	λ	K	λ
Forelimb				
Thenar	0.39	0.00	0.22	0.00
Hypothenar	0.27	0.00	0.39	0.00
Hindlimb				
Thenar	0.24	0.00	0.45	0.00
Hypothenar	0.38	0.00	0.52	0.00

** $p < 0.01$

* $p < 0.05$

Table 2.5. Correlation statistics between variables. R^2 values are provided for correlations of individual pad dimensions.

		Length	Width	Projected Area
Forelimb				
Thenar	Length	1		
	Width	0.15	1	
	Project Area	**0.89****	**0.64****	1
	Surface Area	**0.91****	**0.63****	0.99**
Thenar/ID 1	Length	1		
	Width	**0.70****	1	
	Project Area	**0.87****	**0.92****	1
	Surface Area	**0.95****	**0.80****	**0.99****
Hypo-thenar	Length	1		
	Width	0.20	1	
	Project Area	**0.66****	**0.62****	1
	Surface Area	**0.70****	**0.51****	**0.99****
ID1	Length	1		
	Width	0.09	1	
	Project Area	**0.51***	**0.68****	1
	Surface Area	**0.70****	0.36	**0.99****
ID2	Length	1		
	Width	0.11	1	
	Project Area	**0.39****	**0.58****	1
	Surface Area	**0.48****	**0.48****	**0.97****
ID3	Length	1		
	Width	0.11	1	
	Project Area	**0.66****	**0.59****	1
	Surface Area	**0.66****	**0.54****	**0.99****
ID4	Length	1		
	Width	0.12	1	
	Project Area	**0.45****	**0.43****	1
	Surface Area	**0.49****	**0.38****	**0.99****

(cont'd)

		Length	Width	Projected Area
Hindlimb				
Thenar	Length	1		
	Width	0.11	1	
	Project Area	**0.84****	**0.67****	1
	Surface Area	**0.88****	**0.61****	**0.99****
Hypo-thenar	Length	1		
	Width	0.11	1	
	Project Area	**0.53****	**0.38***	1
	Surface Area	**0.54****	**0.25***	**0.99****
ID1	Length	1		
	Width	0.06	1	
	Project Area	**0.44****	**0.70****	1
	Surface Area	**0.44****		**0.97****
ID2	Length	1		
	Width	0.09	1	
	Project Area	**0.51****	0.08	1
	Surface Area	**0.55****	0.04	**0.99****
ID3	Length	1		
	Width	0.22	1	
	Project Area	**0.71****	**0.65****	1
	Surface Area	**0.72****	**0.60****	**0.99****
ID4	Length	1		
	Width	0.02	1	
	Project Area	**0.38***	**0.53****	1
	Surface Area	**0.38***	**0.58****	**0.99****

Table 2.6. Locomotor categories and associated species. Substrate preferences listed where present and known.

Locomotor Category	Taxon	Substrate
Arboreal Quadruped	*Daubentonia madagascariensis*	-
	Cheirogaleus major	Medium – Large[1]
	Eulemur fulvus collaris	-
	Eulemur fulvus fulvus	-
	Eulemur macaco macaco	-
	Eulemur mongoz	-
	Microcebus murinus	Small[1]
	Mirza coquereli	Small[1]
	Varecia variegata variegata	-
	Galagoides demidoff	Small[2]
	Otolemur crassicaudatus	-
Vertical Clinging and Leaping	*Hapalemur griseus griseus*	-
	Lepilemur leucopus	-
	Galago moholi	Small[3]
	Galago senegalensis	Small[3]
Slow Climbing	*Loris tardigradus*	Small[4]
	Nycticebus coucang	Large[5]
	Perodicticus potto	Large[6]
Nail Climbing	*Euoticus elegantulus*	-
Semi-terrestrial	*Lemur catta*	-

[1] Doyle, 1974; [2] Harcourt & Bearder, 1989; [3] Nash et al., 1989; [4] Nekaris, 2005; [5] Dykyj, 1980; [6] Oates, 1984;

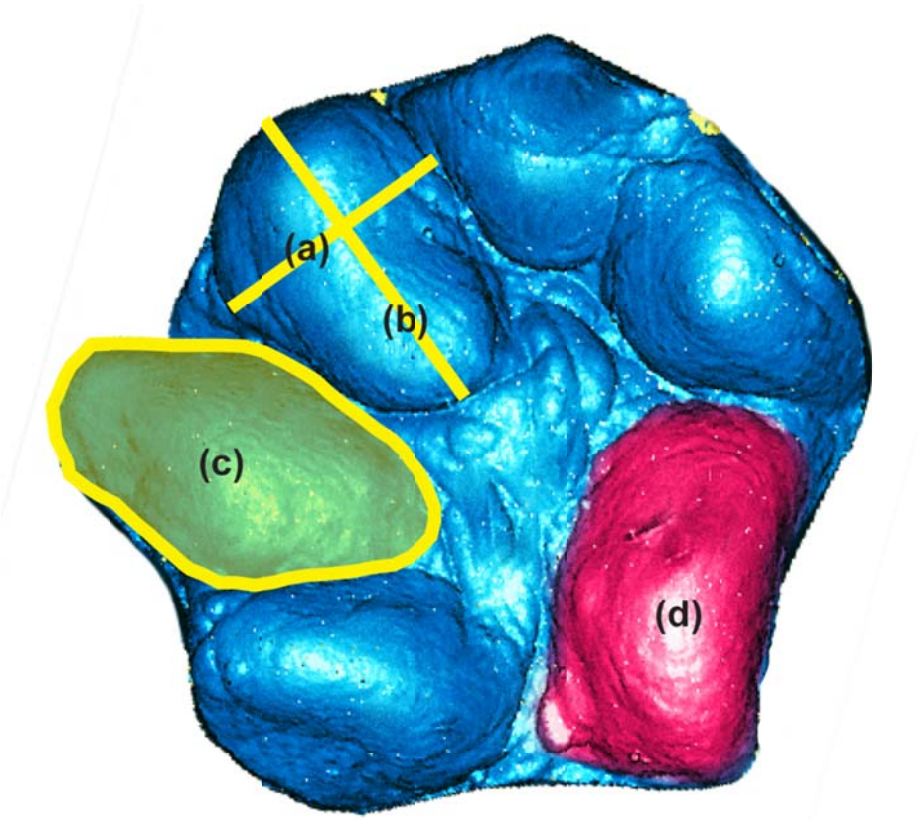

Figure 2.1. Illustration of volar pad measurements. (a) Width, (b) Length, (c) Projected Area (yellow), (d) Surface Area (red). Projected area is a two-dimensional measurement, while surface area includes all surface features and curvatures.

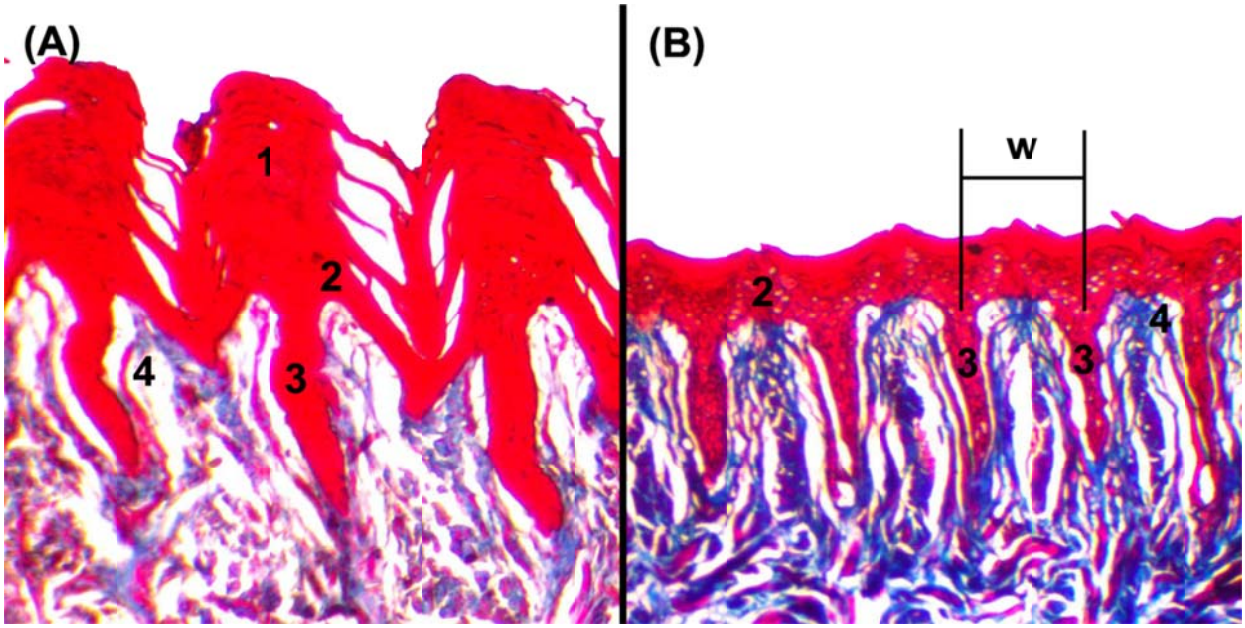

Figure 2.2. Illlustration of volar skin features. (A) Volar skin section from the hypothenar pad of *Eulemur fulvus* with intact epidermis. (B) Volar skin section from the thenar pad of *Cheirogaleus medius* missing stratum corneum of the epidermis. The stratum corneum of the epidermis (1), stratum germinativum of the epidermis (2), intermediate ridges (3), and dermal papillae (4) are also labeled. The widths of the dermatoglyphic ridges were measured as indicated by (w).

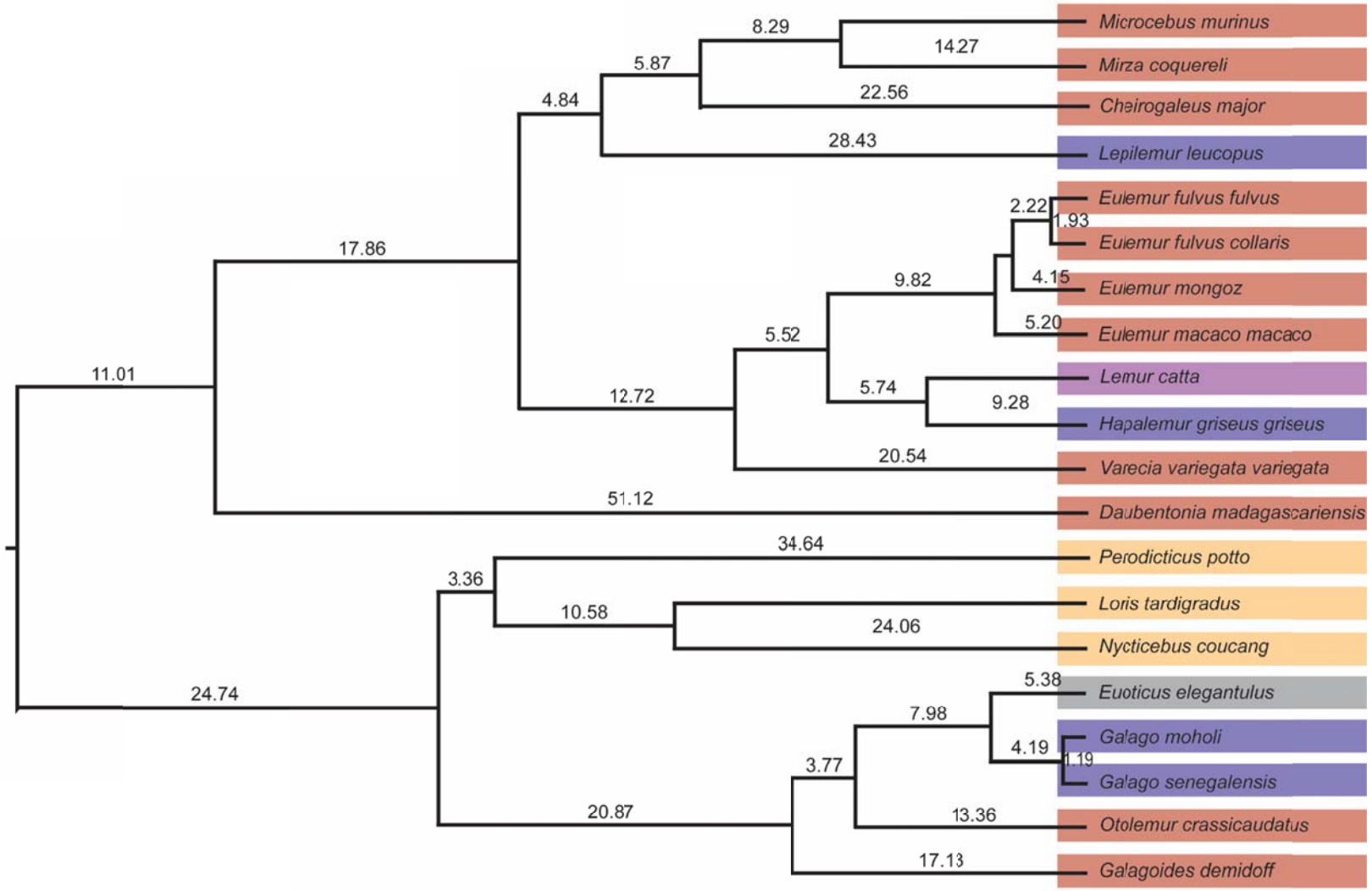

Figure 2.3. Fifty percent majority-ruleconsensus tree from the *10kTrees* website. Color blocks indicate locomotor groups. Red: arboreal quadrupedalism. Blue: vertical clinging and leaping. Purple: semi-terrestrialism. Yellow: slow climbing. Gray: nail-climbing.

Chapter 3:
Feasibility Study

3.1 Summary

A feasibility study was undertaken to ensure that significant changes to the volar pad dimensions did not occur during alcohol preservation. Measurements taken from a sample of rat (*Rattus norvegicus*) manual and pedal volar pads were compared at various stages of preservation. A small sample of frozen primate surfaces were also compared to alcohol-preserved specimens to identify any differences attributable to preservation method. No significant differences are found between preservation stages or preservation method. This is likely due to the anhydrous nature of the preserved tissues. It is determined that alcohol preserved volar pads are appropriate for morphometric study.

3.2 Introduction

Ideally, comparisons of soft-tissue morphology should be based on measurements taken on living individuals. However, for primatologists interested in species beyond the handful of taxa commonly used in laboratory research, access to living endangered, protected, and sparsely zoo-kept animals is very limited. Therefore, museum specimens often make up a majority of available study samples. This raises the issue as to whether preserved soft-tissue morphology can be taken as representative of living tissue, and if not, are the differences predictable such that it might be possible to correct for the effects of preservation. In this chapter I will first review what is currently known regarding the impact of preservation on the size and shape of soft-tissues. This is followed by descriptions of two feasibility studies undertaken to explore potential issues related to use of preserved specimens for the current study.

Alcohol-preserved museum specimens provide the richest sample of strepsirrhine species (the target group for this project) available for study. However, alcohol preservation is known to affect tissue morphology (Humason, 1997), though to what extent remains a topic of in-depth investigation by morphologists. A review of the literature reveals universal agreement that changes to specimen mass are inevitable during alcohol preservation and therefore mass cannot be accurately measured from preserved specimens. This is expected, as water—a primary component of most tissue—is forced out during preservation and replaced by alcohol with a different specific weight. Other size changes in the preserved tissue, however, are less intuitive. Different tissue types may expand or contract depending on their starting water content, and the varying tissue compositions of individual species may cause correspondingly unique shape and size changes. Studies quantifying changes in size and shape at different stages of preservation

bear these concerns out; specimens submersed in alcohol almost universally cycle through a process of dehydration wherein tissues change quickly in size and shape over a period of weeks and then settle into a stable configuration approximating their original states between three and six months (Billy, 1982; Moku et al., 2004; Neave et al., 2006; Vervust et al., 2009; Gaston et al., 2013). Tissues with high water content, such as eyes and muscle, tend to be more affected by size and shape changes than tissues with high fat or calcium content, and measurements taken across heterogeneous tissue samples tend to vary by species (Billy, 1982; Fey, 1999; Berbel-Filho et al., 2013; Gaston et al., 2013; Gomez et al., 2014).

Because these changes are consistently identifiable, investigators are cautioned to be mindful when using alcohol-preserved museum specimens, especially if their analysis hopes to detect fine differences in shape or size. Still, preserved specimens are often the only available resource for comparative morphological study. Luckily, preservation changes in size and shape do not render alcohol preserved specimens completely useless. Complex shape variables, like those used in geometric morphometric analysis, are the most affected as many small changes (for example, the slight retraction of the jaw or expansion of a fin) quickly add together to alter the overall shape (Bininda-Emonds & Russel 1993; Gaston et al., 2013.) However, changes to two-dimensional measurements are small and generally fall within 0.01 – 5.00% of the pre-preservation measurements, although up to 10% is reported for small marine larvae (Bininda-Emonds & Russel, 1993, 1994; Shields & Carlson, 1996; Neave et al., 2006; Gomez et al., 2014). Bony animals are less susceptible to warping than soft-bodied forms; marine larvae may experience up to 10% change in size, whereas no significant change is reported for lizard cheiridia (Neave et al., 2006; Vervust et al., 2009). Several authors report an overall size effect wherein larger individuals are less affected by preservation than their smaller counterparts (Fey, 1999; Edwards et al., 2009). Most importantly, however, it is consistently reported that intraspecific aspect ratios remain constant throughout preservation; that is, each individual of a species may undergo size and shape changes, but they do it in a predictable and consistent manner that allows for correction (Gaston et al., 2013).

It should be noted that the literature on preservation artifacts is rich with studies carried out on small fishes, reptiles, and soft-bodied marine life. The same, unfortunately, cannot be said for mammals, and especially for larger mammals. This is somewhat expected, as large collections of alcohol preserved mammals are a rarity due to the space required to house them. Although tissue types are likely to behave similarly in both mammals and reptiles, the dearth of comparative data is notable, since what little has been reported highlights the need for such studies. Bininda-Emonds & Russel (1993, 1994) report a pattern of post-preservation changes similar to those found in fishes for the wings of brown bats (*Myotis lucifugus*). Although they do not report percent changes, the t-values and measurements provided confirm that post-preservation measurements deviate consistently from live animals. These changes are small, however, and accurate measurements—statistically indistinguishable from live animals—are nonetheless obtainable when specimens are preserved with the joints of the target sampling area extended in 70 percent ethanol. Researchers should be cautious when considering pooling data

collected from live and preserved specimens, as subtle differences can unnecessarily complicate analyses.

Of interest to this particular study are the effects of fixation of primate volar skin and fat pads in 10% buffered formalin and subsequent preservation in 70% ethanol for extended periods of time. In isolation, it might be expected that the low percentage of water found in adipose tissue (10% per unit volume; Schmidt & Thews, 1983) might spare the volar pads from excessive warping during preservation. However, the fat pads are almost never preserved without the rest of the hand or foot, so the underlying tissues must also be taken into consideration. The hands and feet of primates are somewhat unique among bodily regions in that they are controlled largely by muscles whose bellies reside proximally in the arms and legs—well outside the immediate region. This leaves the cheiridia comprised mostly of bone and tendon, with smaller amounts of muscle and neurovascular tissue spaced between. It is possible that the preponderance of bone (22% water per unit volume; Schmidt & Thews, 1983) comprising the hands and feet might protect them from preservation warping, but as of yet no means exists to estimate *a priori* what counter effects the higher-water-content soft tissues might have.

With these possibilities in mind, two feasibility studies were undertaken to explore the effects of alcohol preservation and digital preparation on volar fat pads. First, the volar fat pads of rats were examined as a model species before and after preservation to provide an idea of how much warping one might expect in similarly structured primate cheiridia. Second, two sample groups of primate volar pads were examined—one freshly frozen after death and the other fixed in 10% buffered formalin and preserved in 70% ethanol—and their dimensions compared to determine whether significant differences exist due to preservation method.

In addition to shape changes caused by alcohol preservation, intra-observer measurement error is a known factor in morphological studies and is of special concern here as measurements are collected from digitally reconstructed impressions of volar pads (von Cramon-Taubadel et al., 2007; Muñoz-Muñoz & Perpiñan, 2010). Digital reconstruction provides a valuable tool to obtain measurements easily and accurately that would otherwise be impossible or unduly onerous to collect. In the case of this study, measurement of the surface areas of the volar pads would be next to impossible due to their irregular shapes and convex surfaces; digital imaging makes this measurement possible with a single mouse click. However, it is important that a significant amount of error not be introduced to the analysis through the added steps of digital scanning and reconstruction. Although use of a well-maintained and calibrated μCT scanner with adequate resolution eliminates most variation between repeated scans, there is still opportunity to introduce error during reconstruction and measurement (Maret et al., 2012; Wei et al., 2015). In addition, it is not feasible to scan the alcohol-preserved specimens themselves due to both size concerns (a μCT scanner is necessary to produce digital reconstructions with a high enough resolution to suit small primates, but the specimen compartment measures only 1650 x 1090 x 920 mm, or roughly the size of a mouse) and practical concerns (museums are often unwilling to loan out alcohol-preserved specimens and do not allow the disarticulation of the cheiridia from the limbs necessary to fit them into the scanning compartment). Measurements have therefore

been obtained by creating molded impressions of preserved specimens using high performance dental polyvinyl siloxane, then μCT scanning and reconstructing digital models of these in lieu of the actual specimen. To assess the extent of the error this process introduces to measurements the volar surfaces of rats were examined and compared to mold taken of the same surfaces before further comparisons were made.

3.3 Feasibility Study I: the Volar Pads of Rats

3.3.1 Sample and Procedure

The volar pads of ten lab rats (*Rattus norvegicus*) were examined before and after preservation. Newly euthanized rats were obtained from Stony Brook University's Division of Laboratory Animal Resources (DLAR), and a hand and foot were removed from each for observation. Within one hour post-mortem, molds were created of each rat's volar pads by applying Coltene President light body dental molding compound (low-viscosity polyvinylsiloxane) to the entire volar surface and allowing them to harden. Once solidified, the molds peeled easily away from volar surfaces and left behind no residue. These molds were then μCT scanned alongside the actual specimens to provide both a baseline measurement for comparison post-preservation and ensure that accurate measurements could be taken from a mold of the original specimen. The hands and feet were fixed in 10% buffered formalin for 24 hours, then placed separately into glass containers of 70% ethanol with joints extended and stored for 365 days. At the end of one year, the specimens were removed from the alcohol and molded once again. The resulting molds were μCT scanned and their dimensions compared to the initial measurements.

3.3.2 MicroCT Scanning

All scans were conducted using the VivaCT75 microCT scanner located in the main DLAR facility in Stony Brook University's Health Sciences Center. Specimens were scanned at a resolution of 30μm and integration time of 100 ms. Other parameters included an E of 70kVp and I of 114 μA.

3.3.3 Analysis

Image files were stacked and converted to three-dimensional digital objects in Amira® and imported into Raindrop Geomagic Studio 10®. Digital measurements were taken in Geomagic Studio for the thenar, hypothenar, and each of the four interdigital pads. Definitions of

measurements are as follows (see also Fig. 3.1). *Pad length:* the longest dimension of the pad in a plane radiating from the wrist joint toward the associated digits. *Pad width:* the longest dimension of the pad in a plane perpendicular to the length. *Pad surface area:* the entire area of the skin covering the pad, including all surface features. *Pad area:* the flat (or approximately so) area occupied on the volar surface by the pad, such that would be left bare were the pad to be cut away. To obtain this last measurement, the specimen was digitally rotated such that the edges of the pad aligned to a single approximate plane and captured via "screenshot." This image was then outlined and the two-dimensional included area measured in Photoshop.

To determine the accuracy of digital measurements taken from molded impressions, scans of the actual hands and feet were compared to the impressions taken shortly after the time of death. Additionally, the percentage error present in the calculations was calculated with the formula:

(Real – Mold)/Real * 100

The mean percent error was calculated for all measurements and a 95% confidence interval computed using the standard error of the mean. In addition, the mean percent error for each individual category of measurement (length, width, surface area, and area) was also calculated and a 95% confidence interval computed for each mean. These were calculated and examined due to the possibility of introducing observer error into the measurements of width, which relies by definition in this instance on the accuracy of the length measurement, and pad area, which requires the investigator to manually align the digital model before it can be calculated.

Once the percentage errors were established, comparisons were carried out between samples collected at the time of death and those collected after fixation and one year preservation in 70% ethanol. Measurements taken before and after preservation were analyzed using paired-sample t-tests in SPSS®. A pooled sample of all successive measurements was examined first to determine if any overall effect of preservation existed (i.e., all measurements shrunk or expanded predictably). To ensure that regional preservation changes were not masked by pooling the entire sample, further paired-sample t-tests were carried out for measurements taken on specific pads (for example, successive measured lengths of the thenar pad were compared). The null hypothesis of no difference between groups was rejected when $p < 0.01$ to help mitigate the possibility of false positives stemming from multiple comparisons.

3.3.4 Results: Accuracy of Impression Measurements

Mean percent error scores for measurement types are recorded in Table 3.1 along with a 95% confidence interval for each mean. The average percent error for all measurements combined was 2.99, with individual means not deviating much more than a percentage point therefrom. The largest percent error was found in the measurement of pad area, with an average

of 4.07. All 95% confidence intervals for the observed mean percent error fall below a 5% threshold. A paired sample t-test further revealed no significant differences in measurements between the flesh samples and impressions taken at the time of death ($t = 0.76$, $p = 0.45$). When specific measurements were compared between the actual specimens and perimortem molds, only the measurements taken from the third pedal interdigital pad yielded a significant result. The t-scores and *p* values for these comparisons are presented in Table 3.2.

3.3.5 Results: Comparisons of pre- and post-preservation samples

A paired sample t-test comparing successive measurements taken from impressions at time of death and after one year preservation found no significant differences ($t = -1.02$, $p = 0.33$), nor did a further comparison between measurements taken from scans of the flesh specimens and impressions taken after one year of preservation ($t = -0.97$, $p = 0.31$). Further comparisons of specific measurements for each pad revealed only two isolated incidences of significant difference (Table 3.2). For the third manual interdigital pad (ID3), comparisons of width measurements taken from the actual specimens and molds created after one year of preservation yielded significant results, as did comparisons of the area measurements taken from the perimortem molds and molds taken after one year. Because these are isolated and occur between either the one year impressions and the real specimens or the one year impressions, these cases are likely the result of type I statistical error, which would not be unexpected due to the sheer number (44) of t-tests conducted, or observer error.

3.4 Feasibility Study II: Differences in Preservation Techniques

3.4.1 Sample and procedure

Several samples of strepsirrhine cheiridia were obtained from the Duke Lemur Center to increase the sample size for species detailed in Table 3.3. These specimens had been frozen after death and thawed upon arrival at Stony Brook. Impression molds were made of the thawed volar surfaces utilizing the procedure detailed in the previous section and the samples were fixed in 10% buffered formalin and placed in 70% alcohol for long-term storage (following Humason, 1997, re-freezing of thawed biological tissue is not recommended). These molds were then μCT scanned using the same protocols and parameters discussed above.

3.4.2 Analysis

Image files were once again converted to three-dimensional digital objects in Amira®, and measurements of the thenar, hypothenar, and four interdigital pads collected in Raindrop Geomagic Studio 10®. These measurements were then grouped by preservation type and compared using two-sample t-tests in SPSS®, adjusted by the Welch-Satterthwaite procedures when variances between groups were determined to be unequal. Even with small sample sizes, two-sample t-tests have been shown to effectively discriminate differences between groups, especially when correlation between groups is high, as it is here (de Winter, 2013). The null hypothesis that no differences exist between groups was again rejected when p was found to equal 0.01 or less.

3.4.3 Results

Box and whiskers plots illustrating the means and ranges of measurements taken for each species and preparation are provided in Figure 3.2. Visually, there appears to be very little difference between measurements taken on differently preserved feet.

Results from independent samples t-tests are presented in Table 3.3 and support the initial visual appraisal of very few differences between the groups. Whereas the null hypothesis was rejected at $p < 0.01$, instances where $p < 0.05$ have been bolded as well to help identify any patterns of mismatch approaching significance. The only sample that produced significant differences in measurements was the single *Loris tardigradus* obtained from the Duke Lemur Center, which was found to have a significantly longer second interdigital pad than the alcohol preserved sample. This was part of a larger pattern of size differences between this sample and the alcohol preserved members of the same species, in which differences in all measurements taken on the first interdigital pad, the length of the thenar pad, and the area of the fourth interdigital pad approached significance ($p < 0.05$). Differences in the length of the hypothenar pad in *Microcebus murinus* and the width of the hypothenar pad of *Galago moholi* also approached significance, but unlike those found in *L. tardigradus,* these differences were singular and not clustered around a specific pad or species.

3.5 Discussion

3.5.1 Accuracy of measurements

A paired-sample t-test is unable to discriminate measurements taken from the original specimens and impressions taken shortly after time of death. Further examination of the error inherent in these measurements reveals that collecting digital measurements from these

impressions produces results that are both accurate and precise. The average mean error for all measurements falls well below the commonly accepted threshold of 5% at 2.99%, with a 95% confidence interval ranging from 2.72 – 3.26%. Pad width and pad area, the two measurements that posed the highest risk of observational error, both have percent errors which are larger than the 2.90% average (3.04% and 4.07%, respectively), but still fall below 5%, even within their 95% confidence intervals (Table 3.1).

The measurement error calculated in this study is consistent with those reported in other morphological studies (Suwa et al., 1994; Meeuwing & Bayer, 2005; von Cramon-Taubadel et al., 2007; Vervust et al., 2009; Munoz-Munoz & Peripinan, 2010; Davies et al., 2012). While there is no hard and fast rule, or even an agreed upon rejection threshold, insisting upon a percent error of less than five for measurements is consistent with using a 95% probability threshold to reject a null hypothesis of no difference between groups (i.e., $p < 0.05$). It is important to note here as well that the rats examined are smaller in size than all but one of the primate species examined. As body size in subjects increases, observed variation among individuals increases as well, which reduces the proportion of the group variance accounted for by measurement error (Muñoz-Muñoz & Peripiñan, 2010). Having verified the percent error inherent in the collection and measurement procedure in a smaller subject, it is likely that the actual percent error for measurement of the larger sample will be even smaller. Because the error values found in this instance do indeed fall below this 5% threshold and their corresponding confidence intervals span less than 1.5%, they are determined to be accurate and precise enough to justify use of volar impressions and digital imaging for further study.

3.5.2 Preservation effects

This study reveals no significant differences in the measured aspects of rat volar fat pads before and after fixation in 10% buffered formalin and long-term preservation in 70% alcohol, nor is it able to discriminate alcohol preserved primate volar pads from frozen samples. There are several possible reasons for these findings.

Firstly, it is important to note that hands and feet preserved in alcohol do indeed change in appearance. A side-by-side illustration of this is provided in Figure 3.3. As predicted by previous studies, as alcohol replaces water in the preserved tissues, the tissues shrink. The tissues most affected are those with the highest concentration of water, such as muscle, where water constitutes ~78% per unit volume (Schmidt & Thews, 1983). This is clearly evident in the position of the fingers and toes in this case; the digits have flexed as the tissue has shrunk and the volar surface has been pulled into a concave posture. The volar pads, however, are largely unaffected in size and shape. This is likely attributable to both their composition—adipose tissue comprises only 10% water per unit volume (Schmidt & Thews, 1983)—and their position. Movement of the metapodials in the palm and sole is limited; most of the change in shape comes from flexion of the digits and is limited to the distal ends of the volar surface. Further, movement

of the volar surfaces occurs at flexion creases, which run between the volar pads rather than crossing them, which helps to maintain their shape. In the rats examined here as well as small-bodied primates, the discrete nature of each pad allows for a small range of movement without a corresponding change in shape (for example, from colliding with a neighbor). Instead of bending and flexing with the rest of the volar surface, the fat pads are able to merely shift position. By way of contrast, many of the cases previously studied involved measurements taken across multiple joints, where muscles could shrink and alter the shape and size of the specimens in numerous ways (Bininda-Emons et al., 1993, 1994; Fey, 1999; Neave et al., 2006; Edwards et al., 2009; Vervust et al., 2009; Gaston, 2013). Here, the relative regional isolation of each pad likely spares them these changes.

Secondly, it is possible that the pads do shrink or expand during preservation, but that the error introduced during the collection procedure is large enough to mask them. If this is indeed the case, the changes are small enough to be statistically insignificant and unlikely to impact the greater study. Indeed, even in the larger primate species compared here—where the percent error in measurement is likely smaller—significant differences between frozen and alcohol preserved specimens were only found in *Loris tardigradus*, which appears to be an outlier. That the larger primate species show few effects of preservation is also consistent with published data; both Fey (1999) and Edwards et al. (2009) showed that larger individuals experienced lesser preservation effects in larval fishes and leeches.

Although a multitude of factors may influence why the single frozen *Loris* specimen was so drastically different from the alcohol preserved specimens, the most likely cause is an overall difference in body size. Even without precise body mass measurements, the specimen obtained from the Duke Lemur Center was obviously a much larger animal than those housed in the museum collections. Additionally, many of the inconsistencies between the preservation types clustered around the first interdigital pad, which may be significant in and of itself. In lorises, the first digit of the hand is rotated greater than 90 degrees from the subsequent digits, and the resulting first interdigital pad is relatively massive and not well supported by bony infrastructure, like the other volar pads. Thus, when the hand is preserved and the first metacarpal is adducted, the pad is compressed and its shape altered. No other primates included in this study possess digits that deviate as sharply as the lorises, but this brings to light an important complication nonetheless. Going forward, any first interdigital pads that appear compressed or warped will be removed from the analyses. The frozen *Loris tardigradus* specimen will be removed from further analyses as well, regardless of what factors underlie its differences with the alcohol-preserved museum specimens.

3.6 Conclusions

Impressions of volar surfaces created using high performance dental molding gel provide a good proxy for μCT scanning and digital measurement when the actual specimens are

unavailable for direct use. Digital measurements taken from these molds are accurate when compared to the same measurements taken from the same subject with a small range of error that falls below 5% in all cases examined here.

Alcohol preserved museum specimens provide a rich source of research material, but investigators must be mindful of the ways preservation may alter the specimens. In this case, the volar fat pads of rats and primates were not found to significantly differ before and after alcohol preservation. Their adipose composition and location on stable portions of the volar surfaces protect them from significant shrinkage or warping during preservation, and thus appropriate for morphological study. Despite this, caution should always be exercised when utilizing alcohol-preserved specimens and the effects of preservation on specific traits investigated beforehand.

Table 3.1. Average percent error scores for each type of measurement taken.

	N	Mean % Error	95% Conf. Int.
Length	92	2.84	2.36–3.26
Width	91	3.04	2.91–3.97
Surface Area	91	1.76	1.32–2.13
Area	86	4.07	3.41–4.73
Total	**372**	**2.99**	**2.72–3.26**

Table 3.2. T scores and corresponding values of *p* for paired comparisons of measurements taken from rat volar surfaces. Subscript numbers indicate comparisons between the following groups: (1) flesh specimens and perimortem impressions, (2) flesh speciments and impressions after one year preservation, (3) perimortem impressions and impressions after one year preservation. Scores for the Forelimb are provided above the thick median line; score for the hindlimb are below.

	Length	Width	Area	Surface Area
Forelimb				
Thenar	$t_1 = -0.40$, $p_1 = 0.71$	$t_1 = -1.31$, $p_1 = 0.24$	$t_1 = -0.02$, $p_1 = 0.99$	$t_1 = 1.04$, $p_1 = 0.34$
	$t_2 = 2.06$, $p_2 = 0.11$	$t_2 = -1.63$, $p_2 = 0.18$	$t_2 = 0.78$, $p_2 = 0.48$	$t_2 = 1.54$, $p_2 = 0.20$
	$t_3 = 3.50$, $p_3 = 0.02$	$t_3 = -1.40$, $p_3 = 0.21$	$t_3 = -1.06$, $p_3 = 0.33$	$t_3 = 0.43$, $p_3 = 0.68$
Hypothenar	$t_1 = 0.45$, $p_1 = 0.66$	$t_1 = 0.73$, $p_1 = 0.50$	$t_1 = -1.14$, $p_1 = 0.30$	$t_1 = 0.38$, $p_1 = 0.71$
	$t_2 = 0.27$, $p_2 = 0.80$	$t_2 = -0.72$, $p_2 = 0.51$	$t_2 = -1.90$, $p_2 = 0.13$	$t_2 = -0.67$, $p_2 = 0.54$
	$t_3 = -0.83$, $p_3 = 0.44$	$t_3 = -1.82$, $p_3 = 0.12$	$t_3 = 0.72$, $p_3 = 0.50$	$t_3 = 0.23$, $p_3 = 0.83$
ID2	$t_1 = -1.02$, $p_1 = 0.34$	$t_1 = -2.29$, $p_1 = 0.06$	$t_1 = -0.39$, $p_1 = 0.71$	$t_1 = -0.24$, $p_1 = 0.82$
	$t_2 = 1.82$, $p_2 = 0.13$	$t_2 = -3.05$, $p_2 = 0.03$	$t_2 = -1.57$, $p_2 = 0.18$	$t_2 = -0.01$, $p_2 = 0.99$
	$t_3 = 1.02$, $p_3 = 0.34$	$t_3 = -2.79$, $p_3 = 0.03$	$t_3 = -0.54$, $p_3 = 0.61$	$t_3 = 0.22$, $p_3 = 0.83$
ID3	$t_1 = 1.02$, $p_1 = 0.35$	$t_1 = -1.07$, $p_1 = 0.325$	$t_1 = 0.15$, $p_1 = 0.89$	$t_1 = 0.92$, $p_1 = 0.39$
	$t_2 = 2.04$, $p_2 = 0.11$	**$t_2 = -4.75$, $p_2 = 0.01$***	$t_2 = -1.47$, $p_2 = 0.22$	$t_2 = 1.07$, $p_2 = 0.35$
	$t_3 = 1.61$, $p_3 = 0.17$	$t_3 = -3.65$, $p_3 = 0.02$	**$t_3 = -4.10$, $p_3 = 0.01$***	$t_3 = -1.53$, $p_3 = 0.19$
ID4	$t_1 = -0.29$, $p_1 = 0.78$	$t_1 = -0.40$, $p_1 = 0.70$	$t_1 = 0.26$, $p_1 = 0.80$	$t_1 = 0.06$, $p_1 = 0.96$
	$t_2 = -0.89$, $p_2 = 0.42$	$t_2 = -0.46$, $p_2 = 0.67$	$t_2 = -1.25$, $p_2 = 0.27$	$t_2 = -0.61$, $p_2 = 0.57$
	$t_3 = -0.83$, $p_3 = 0.44$	$t_3 = -0.47$, $p_3 = 0.66$	$t_3 = -1.65$, $p_3 = 0.15$	$t_3 = -0.72$, $p_3 = 0.50$
Hindlimb				
Thenar	$t_1 = -0.65$, $p_1 = 0.54$	$t_1 = 1.30$, $p_1 = 0.24$	$t_1 = 2.97$, $p_1 = 0.02$	$t_1 = -0.04$, $p_1 = 0.97$
	$t_2 = 1.93$, $p_2 = 0.09$	$t_2 = 1.50$, $p_2 = 0.17$	$t_2 = 0.96$, $p_2 = 0.37$	$t_2 = 1.48$, $p_2 = 0.18$
	$t_3 = 2.24$, $p_3 = 0.06$	$t_3 = 0.26$, $p_3 = 0.80$	$t_3 = -0.80$, $p_3 = 0.45$	$t_3 = 1.28$, $p_3 = 0.24$
Hypothenar	$t_1 = 0.78$, $p_1 = 0.46$	$t_1 = -1.01$, $p_1 = 0.34$	$t_1 = -0.54$, $p_1 = 0.60$	$t_1 = 0.94$, $p_1 = 0.37$
	$t_2 = 2.54$, $p_2 = 0.03$	$t_2 = -1.15$, $p_2 = 0.28$	$t_2 = -0.93$, $p_2 = 0.38$	$t_2 = 2.15$, $p_2 = 0.06$
	$t_3 = 2.15$, $p_3 = 0.06$	$t_3 = 0.14$, $p_3 = 0.90$	$t_3 = -0.98$, $p_3 = 0.35$	$t_3 = 1.12$, $p_3 = 0.29$
ID1	$t_1 = 1.64$, $p_1 = 0.14$	$t_1 = -0.06$, $p_1 = 0.95$	$t_1 = -1.17$, $p_1 = 0.27$	$t_1 = -0.68$, $p_1 = 0.52$
	$t_2 = -1.72$, $p_2 = 0.10$	$t_2 = -2.54$, $p_2 = 0.03$	$t_2 = -2.55$, $p_2 = 0.03$	$t_2 = 0.84$, $p_2 = 0.43$
	$t_3 = 1.12$, $p_3 = 0.29$	$t_3 = -2.37$, $p_3 = 0.04$	$t_3 = -0.12$, $p_3 = 0.97$	$t_3 = 1.63$, $p_3 = 0.14$
ID2	$t_1 = 1.01$, $p_1 = 0.34$	$t_1 = -0.02$, $p_1 = 0.98$	$t_1 = -1.94$, $p_1 = 0.08$	$t_1 = 0.98$, $p_1 = 0.35$
	$t_2 = 2.16$, $p_2 = 0.06$	$t_2 = -1.16$, $p_2 = 0.26$	$t_2 = -1.78$, $p_2 = 0.11$	$t_2 = 1.36$, $p_2 = 0.21$
	$t_3 = 1.74$, $p_3 = 0.12$	$t_3 = -1.76$, $p_3 = 0.11$	$t_3 = -0.85$, $p_3 = 0.42$	$t_3 = 1.05$, $p_3 = 0.32$
ID3	$t_1 = 2.71$, $p_1 = 0.03$	$t_1 = -0.60$, $p_1 = 0.56$	**$t_1 = 3.73$, $p_1 < 0.01$***	$t_1 = 1.81$, $p_1 = 0.11$
	$t_2 = 1.98$, $p_2 = 0.08$	$t_2 = 0.26$, $p_2 = 0.80$	$t_2 = 0.11$, $p_2 = 0.91$	$t_2 = 1.79$, $p_2 = 0.10$
	$t_3 = 0.83$, $p_3 = 0.43$	$t_3 = 0.38$, $p_3 = 0.70$	$t_3 = -2.23$, $p_3 = 0.06$	$t_3 = 1.50$, $p_3 = 0.18$
ID4	$t_1 = 0.76$, $p_1 = 0.47$	$t_1 = 0.62$, $p_1 = 0.55$	$t_1 = -0.87$, $p_1 = 0.41$	$t_1 = 0.69$, $p_1 = 0.51$
	$t_2 = -0.32$, $p_2 = 0.76$	$t_2 = -1.15$, $p_2 = 0.28$	$t_2 = -0.34$, $p_2 = 0.74$	$t_2 = 1.51$, $p_2 = 0.16$
	$t_3 = -0.85$, $p_3 = 0.42$	$t_3 = -1.58$, $p_3 = 0.15$	$t_3 = -0.32$, $p_3 = 0.76$	$t_3 = 0.94$, $p_3 = 0.37$

Table 3.3. Two-sample t-tests statistics for comparisons of frozen and alcohol preserved hand specimens. Means are provided in millimeters.

	Eulemur fulvus collaris $n_1 = 2$ $n_2 = 2$	***Eulemur fulvus fulvus*** $n_1 = 2$ $n_2 = 3$	***Eulemur macaco macaco*** $n_1 = 5$ $n_2 = 3$	***Galago moholi*** $n_1 = 4$ $n_2 = 2$	***Hapalemur griseus griseus*** $n_1 = 2$ $n_2 = 1$	***Loris tardigradus*** $n_1 = 5$ $n_2 = 1$	***Microcebus murinus*** $n_1 = 8$ $n_2 = 3$
Thenar							
Length	M_1 = 22.71 M_2 = 18.38 t = 7.05 *p = 0.06*	M_1 = 25.43 M_2 = 20.22 t = 1.84 *p = 0.16*	M_1 = 19.40 M_2 = 20.48 t = -0.64 *p = 0.55*	M_1 = 4.15 M_2 = 4.34 t = -0.32 *p = 0.76*	M_1 = 13.82 M_2 = 13.65 t = 1.51 *p = 0.37*	M_1 = 4.11 M_2 = 5.83 t = -4.10 ***p = 0.02****	M_1 = 6.06 M_2 = 6.08 t = -0.12 *p = 0.91*
Width	M_1 = 8.68 M_2 = 10.2 t = -1.193 *p = 0.37*	M_1 = 9.65 M_2 = 10.46 t = -1.20 *p = 0.32*	M_1 = 9.64 M_2 = 9.75 t = -0.12 *p = 0.91*	M_1 = 3.32 M_2 = 3.17 t = 0.49 *p = 0.65*	M_1 = 7.28 M_2 = 5.92 t = 6.58 *p = 0.10*	M_1 = 4.07 M_2 = 2.90 t = 1.03 *p = 0.36*	M_1 = 3.41 M_2 = 3.46 t = -0.23 *p = 0.82*
Projected Area	M_1=165.89 M_2=147.74 t = 0.77 *p = 0.58*	M_1=182.45 M_2=160.44 t = 0.98 *p = 0.40*	M_1=141.86 M_2=160.25 t = -0.70 *p = 0.51*	M_1 = 10.03 M_2 = 10.37 t = -0.25 *p = 0.82*	M_1 = 82.97 M_2 = 70.92 t = 1.59 *p = 0.36*	M_1 = 11.31 M_2 = 14.24 t = -1.50 *p = 0.21*	M_1 = 15.10 M_2 = 14.95 t = 0.20 *p = 0.85*
Surface Area	M_1=268.60 M_2=254.74 t = 0.51 *p = 0.693*	M_1=368.87 M_2=261.79 t = 2.17 *p = 0.12*	M_1=245.23 M_2=253.48 t = -0.21 *p = 0.85*	M_1 = 14.99 M_2 = 16.56 t = -0.51 *p = 0.64*	M_1=127.43 M_2=124.14 t = 0.15 *p = 0.91*	M_1 = 17.02 M_2 = 24.90 t = -2.02 *p = 0.11*	M_1 = 25.27 M_2 = 23.92 t = 0.50 *p = 0.63*
Hypothenar							
Length	M_1 = 22.87 M_2 = 20.17 t = 0.00 *p = 0.33*	M_1 = 24.10 M_2 = 20.55 t = 0.94 *p = 0.42*	M_1 = 18.99 M_2 = 17.30 t = 0.86 *p = 0.44*	M_1 = 5.90 M_2 = 5.96 t = -0.11 *p = 0.92*	M_1 = 14.27 M_2 = 10.31 t = 8.57 *p = 0.07*	M_1 = 6.194 M_2 = 6.54 t = -0.87 *p = 0.44*	M_1 = 4.68 M_2 = 3.91 t = 2.44 ***p = 0.04****
Width	M_1 = 9.43 M_2 = 9.47 t = -0.02 *p = 0.99*	M_1 = 9.12 M_2 = 10.96 t = -1.59 *p = 0.21*	M_1 = 9.24 M_2 = 10.34 t = -1.26 *p = 0.26*	M_1 = 3.62 M_2 = 4.73 t = -3.403 ***p = 0.03****	M_1 = 5.78 M_2 = 6.68 t = -2.67 *p = 0.23*	M_1 = 4.68 M_2 = 4.82 t = -0.47 *p = 0.66*	M_1 = 2.98 M_2 = 2.90 t = 0.38 *p = 0.71*
Projected Area	M_1=171.58 M_2=156.50 t = 0.53 *p = 0.66*	M_1=204.31 M_2=169.78 t = 1.17 *p = 0.33*	M_1=117.53 M_2=119.59 t = -0.10 *p = 0.93*	M_1 = 16.96 M_2 = 19.17 t = -0.70 *p = 0.52*	M_1 = 67.76 M_2 = 51.6 t = 1.43 *p = 0.39*	M_1 = 22.87 M_2 = 26.20 t = -0.92 *p = 0.41*	M_1 = 11.71 M_2 = 11.11 t = 0.43 *p = 0.67*
Surface Area	M_1=276.34 M_2=246.46 t = 5.07 *p = 0.09*	M_1=369.86 M_2=271.78 t = 1.79 *p = 0.17*	M_1=202.69 M_2=177.39 t = 0.55 *p = 0.60*	M_1 = 29.81 M_2 = 34.67 t = -0.80 *p = 0.47*	M_1=109.04 M_2 = 80.01 t = 2.78 *p = 0.22*	M_1 = 36.43 M_2 = 40.37 t = -0.87 *p = 0.44*	M_1 = 18.54 M_2 = 18.74 t = -0.07 *p = 0.95*

	Eulemur fulvus collaris	*Eulemur fulvus fulvus*	*Eulemur macaco macaco*	*Galago moholi*	*Hapalemur griseus griseus*	*Loris tardigradus*	*Microcebus murinus*
ID1							
Length	n/a	n/a	n/a	M_1 = 5.39 M_2 = 6.73 t = -2.04 *p = 0.11*	n/a	M_1 = 5.92 M_2 = 9.96 t = -2.84 ***p = 0.05****	n/a
Width	n/a	n/a	n/a	M_1 = 4.31 M_2 = 4.53 t = -0.68 *p = 0.54*	n/a	M_1 = 3.40 M_2 = 5.25 t = -3.17 ***p = 0.03****	n/a
Projected Area	n/a	n/a	n/a	M_1 = 15.18 M_2 = 19.42 t = -1.76 *p = 0.15*	n/a	M_1 = 13.98 M_2 = 22.02 t = -2.82 ***p = 0.05****	n/a
Surface Area	n/a	n/a	n/a	M_1 = 29.69 M_2 = 39.20 t = -2.18 *p = 0.10*	n/a	M_1 = 29.15 M_2 = 51.05 t = -3.67 ***p = 0.02****	n/a
ID2							
Length	M_1 = 11.03 M_2 = 11.34 t = -0.37 *p = 0.78*	M_1 = 12.15 M_2 = 9.81 t = 0.07 *p = 0.16*	M_1 = 10.06 M_2 = 10.95 t = -0.60 *p = .57*	M_1 = 5.83 M_2 = 6.11 t = -0.47 *p = 0.67*	M_1 = 8.34 M_2 = 7.65 t = 0.56 *p = 0.68*	M_1 = 5.30 M_2 = 8.91 t = -5.05 ***p = 0.01***	M_1 = 2.98 M_2 = 2.98 t = -0.02 *p = 0.99*
Width	M_1 = 10.11 M_2 = 8.00 t = 37.52 ***p = 0.02***	M_1 = 7.47 M_2 = 10.17 t = -2.19 *p = 0.12*	M_1 = 8.23 M_2 = 9.42 t = -0.90 *p = 0.46*	M_1 = 3.60 M_2 = 3.87 t = -0.54 *p = 0.62*	M_1 = 6.87 M_2 = 5.2 t = 1.79 *p = 0.33*	M_1 = 3.593 M_2 = 3.94 t = -0.71 *p = 0.67*	M_1 = 2.85 M_2 = 3.21 t = -1.17 *p = 0.38*
Area	M_1=83.88 M_2=67.66 t = 3.28 *p = 0.19*	M_1 = 79.04 M_2 = 63.75 t = 1.18 *p = 0.44*	M_1 = 62.87 M_2 = 73.76 t = -0.86 *p = 0.42*	M_1 = 11.94 M_2 = 15.35 t = -1.55 *p = 0.20*	M_1 = 36.34 M_2 = 29.51 t = 0.69 *p = 0.61*	M_1 = 13.21 M_2 = 20.22 t = -1.34 *p = 0.25*	M_1 = 6.91 M_2 = 7.1 t = -0.32 *p = 0.76*
Surface Area	M_1=196.54 M_2=118.21 t = 1.01 *p = 0.50*	M_1=138.36 M_2=114.23 t = 0.90 *p = 0.53*	M_1=100.80 M_2=116.91 t = -0.61 *p = 0.57*	M_1 = 21.57 M_2 = 37.07 t = -1.97 *p = 0.29*	M_1 = 59.88 M_2 = 56.3 t = 0.33 *p = 0.80*	M_1 = 22.73 M_2 = 25.37 t = -0.88 *p = 0.42*	M_1 = 12.91 M_2 = 11.75 t = 0.73 *p = 0.48*
ID3							
Length	M_1 =7.90 M_2 = 8.83 t = -1.25 *p = 0.43*	M_1 = 8.63 M_2 = 7.44 t = 0.68 *p = 0.54*	M_1 = 8.00 M_2 = 7.36 t = 0.59 *p = 0.57*	M_1 = 4.49 M_2 = 4.59 t = -0.19 *p = 0.86*	M_1 = 6.26 M_2 = 5.14 t = 1.70 *p = 0.34*	M_1 = 3.35 M_2 = 4.86 t = -1.42 *p = 0.23*	M_1 = 2.8 M_2 = 3.4 t = -2.54 *p = 0.03*
Width	M_1 = 8.39 M_2 = 8.35 t = 0.21 *p = 0.99*	M_1 = 8.13 M_2 = 7.81 t = 0.25 *p = 0.82*	M_1 = 6.95 M_2 = 7.05 t = -0.10 *p = 0.93*	M_1 = 2.42 M_2 = 3.19 t = -1.58 *p = 0.25*	M_1 = 5.79 M_2 = 3.97 t = 0.77 *p = 0.58*	M_1 = 2.07 M_2 = 2.93 t = -1.22 *p = 0.29*	M_1 = 2.93 M_2 = 3.11 t = -0.47 *p = 0.65*
Area	M_1 = 40.94 M_2 = 48.03 t = -6.49 *p = 0.10*	M_1 = 48.45 M_2 = 42.48 t = 0.47 *p = 0.57*	M_1 = 35.67 M_2 = 35.24 t = 0.06 *p = 0.95*	M_1 = 6.97 M_2 = 7.54 t = -1.25 *p = 0.06*	M_1 = 25.90 M_2 = 16.02 t = 2.30 *p = 0.26*	M_1 = 4.54 M_2 = 11.27 t = -1.55 *p = 0.20*	M_1 = 5.90 M_2 = 7.07 t = -1.00 *p = 0.42*
Surface Area	M_1 = 65.33 M_2 = 76.30 t = -3.18 *p = 0.19*	M_1 = 89.49 M_2 = 72.50 t = 0.99 *p = 0.40*	M_1 = 62.34 M_2 = 57.44 t = 0.43 *p = 0.69*	M_1 = 10.93 M_2 = 21.44 t = -4.34 *p = 0.11*	M_1 = 42.26 M_2 = 23.79 t = 3.86 *p = 0.16*	M_1 = 7.14 M_2 = 14.02 t = -1.26 *p = 0.28*	M_1 = 10.77 M_2 = 11.88 t = -1.15 *p = 0.28*

	Eulemur fulvus collaris	*Eulemur fulvus fulvus*	*Eulemur macaco macaco*	*Galago moholi*	*Hapalemur griseus griseus*	*Loris tardigradus*	*Microcebus murinus*
ID4							
Length	M_1 = 9.02 M_2 = 8.985 t = 0.03 *p = 0.98*	M_1 = 10.05 M_2 = 7.86 t = 1.52 *p = 0.23*	M_1 = 8.10 M_2 = 7.67 t = 0.38 *p = 0.72*	M_1 = 3.65 M_2 = 4.12 t = -0.49 *p = 0.65*	M_1 = 6.74 M_2 = 6.14 t = 0.40 *p = 0.76*	M_1 = 3.037 M_2 = 3.499 t = -0.95 *p = 0.40*	M_1 = 2.69 M_2 = 2.66 t = 0.10 *p = 0.93*
Width	M_1 = 9.64 M_2 = 8.52 t = 0.52 *p = 0.70*	M_1 = 10.59 M_2 = 7.86 t = 1.32 *p = 0.28*	M_1 = 6.87 M_2 = 7.85 t = -1.51 *p = 0.18*	M_1 = 3.50 M_2 = 3.37 t = 0.15 *p = 0.89*	M_1 = 6.33 M_2 = 6.08 t = 0.09 *p = 0.94*	M_1 = 3.86 M_2 = 5.07 t = -2.46 *p = 0.07*	M_1 = 2.83 M_2 = 3.4 t = -2.01 *p = 0.08*
Projected Area	M_1 = 61.56 M_2 = 54.21 t = 2.22 *p = 0.23*	M_1 = 83.85 M_2 = 56.88 t = 1.77 *p = 0.17*	M_1 = 46.79 M_2 = 49.35 t = -0.44 *p = 0.67*	M_1 = 7.67 M_2 = 10.02 t = -1.23 *p = 0.29*	M_1 = 34.91 M_2 = 33.72 t = 0.89 *p = 0.94*	M_1 = 11.69 M_2 = 16.02 t = -3.13 ***p = 0.04****	M_1 = 6.01 M_2 = 6.78 t = -1.33 *p = 0.22*
Surface Area	M_1=100.75 M_2=101.69 t = -0.39 *p = 0.76*	M_1=138.85 M_2=100.30 t = 2.59 *p = 0.08*	M_1 = 78.84 M_2 = 81.46 t = -0.17 *p = 0.87*	M_1 = 13.58 M_2 = 18.68 t = -1.91 *p = 0.13*	M_1 = 54.94 M_2 = 56.39 t = -0.07 *p = 0.96*	M_1 = 21.06 M_2 = 27.47 t = -1.93 *p = 0.13*	M_1 = 10.32 M_2 = 12.47 t = -2.29 *p = 0.05*

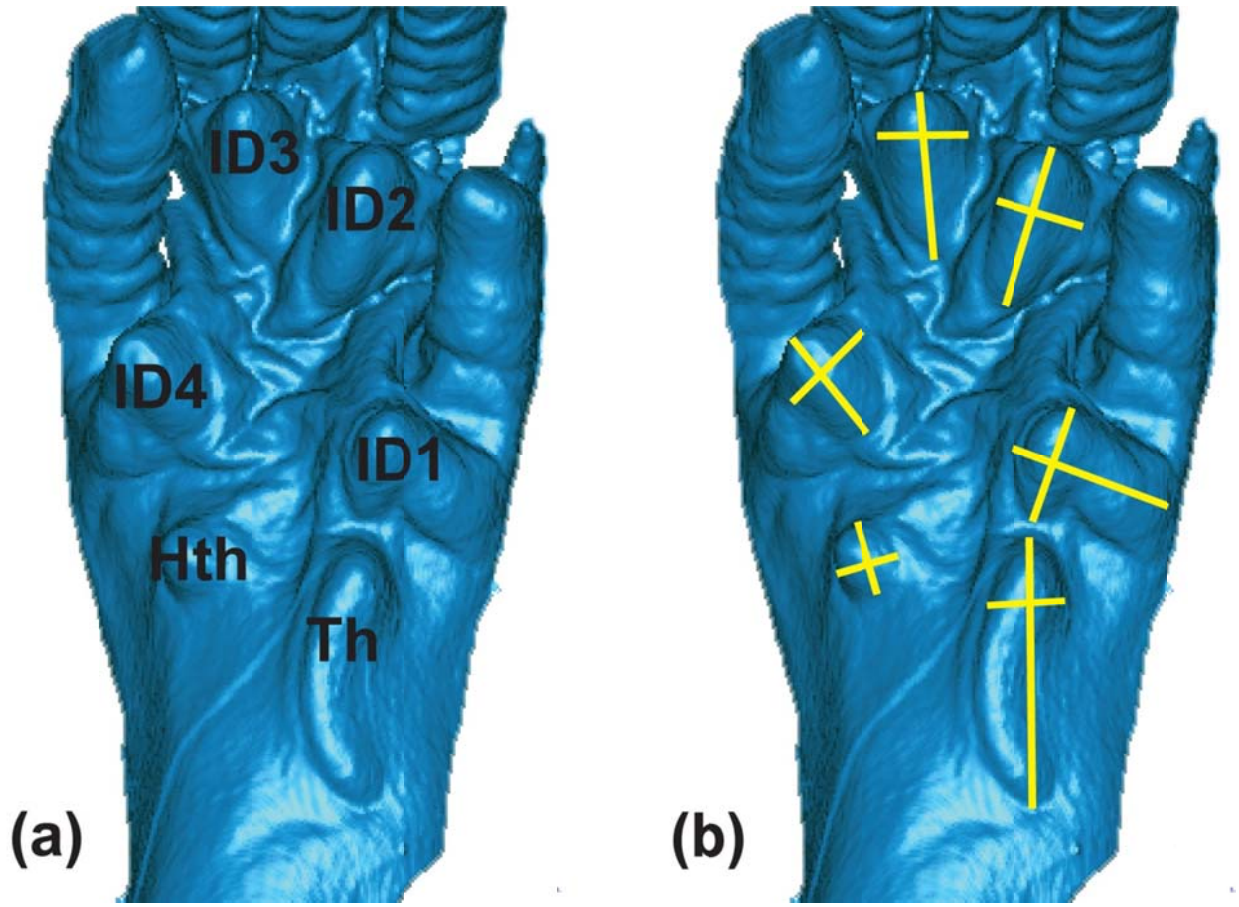

Figure 3.1. Illustration of the volar surfaces of *Rattus norvegicus*. (a) Indicates the positions of each volar pad; Th = Thenar, Hth = Hypothenar, ID1 = first interdigital, ID2 = second interdigital, ID3 = third interdigital, ID4 = fourth interdigital. (b) Illustrates an approximation of measurement axes for each pad. Length was defined as the longest proximo-distal distance across the pad; width was defined as the longest mediolateral distance perpendicular to the length.

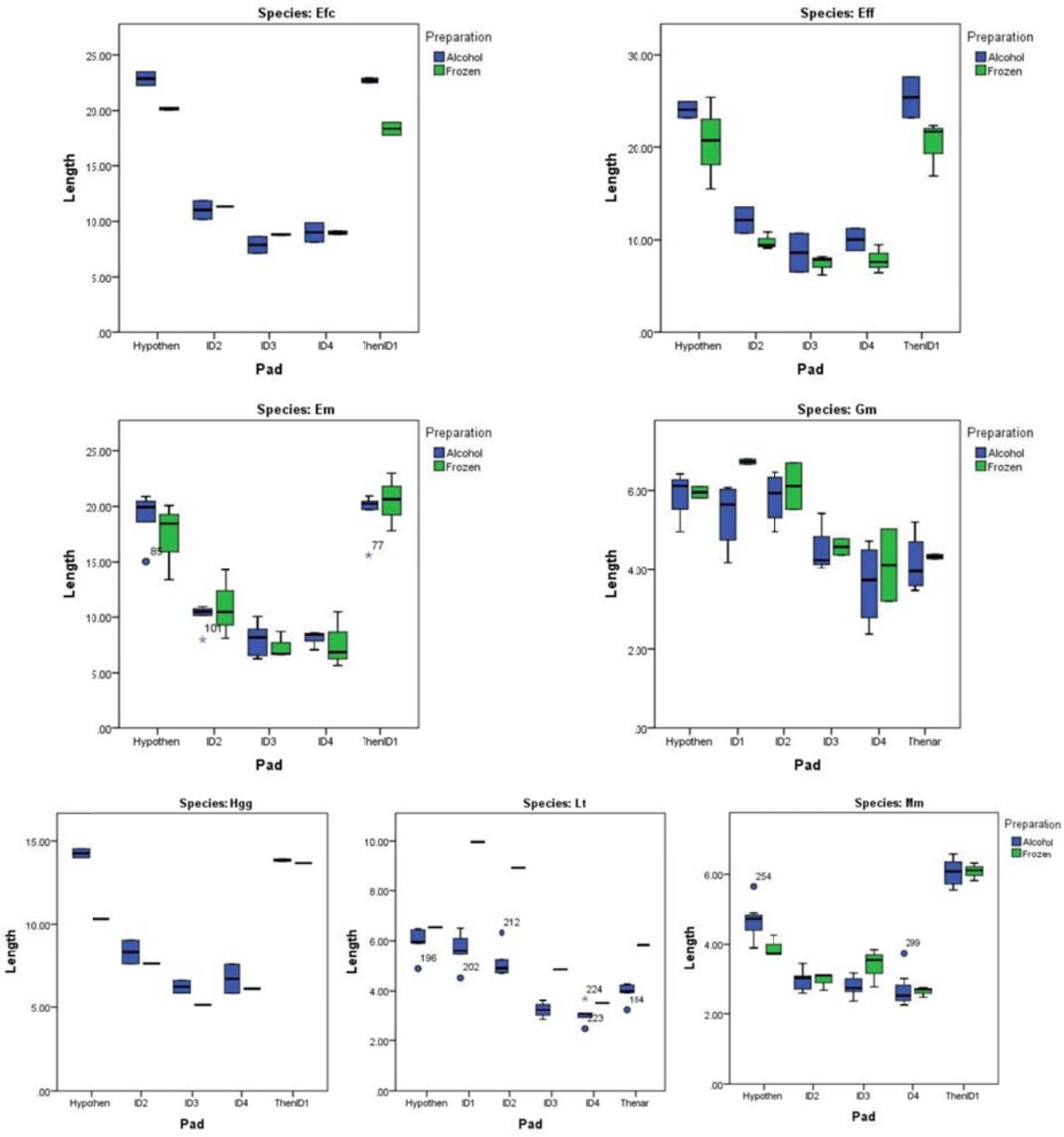

Figure 3.2a. Boxplot comparisons for means of the length of frozen and alcohol-preserved specimens. Significant differences between preservation types are not evident for most examined species; *Loris tardigradus* is the only examined taxa exhibiting significant differences. Species abbreviations are as follows; Efc: *Eulemur fulvus collaris*, Eff*: Eulemur fulvus fulvus*, Em: *Eulemur macaco*, Gm: *Galago moholi*, Hgg: *Hapalemur griseus griseus*, Lt: *Loris tardigradus*, Mm: *Microcebus murinus*.

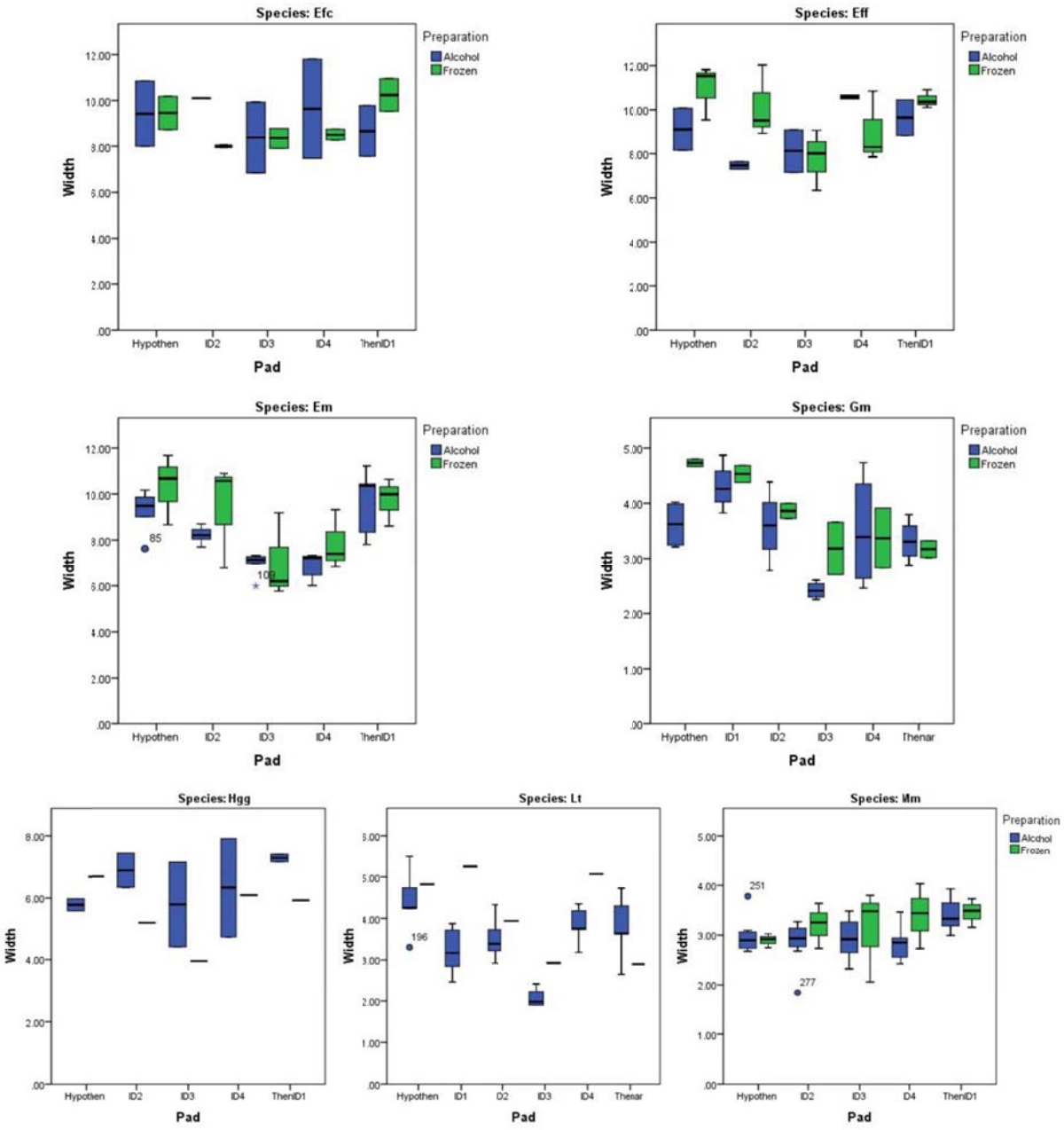

Figure 3.2b. Boxplot comparisons for means of the width of frozen and alcohol-preserved specimens. Significant differences between preservation types are not evident for most examined species; *Loris tardigradus* is the only examined taxa exhibiting significant differences. Species abbreviations are as follows; Efc: *Eulemur fulvus collaris*, Eff*: Eulemur fulvus fulvus*, Em: *Eulemur macaco*, Gm: *Galago moholi*, Hgg: *Hapalemur griseus griseus*, Lt: *Loris tardigradus*, Mm: *Microcebus murinus*.

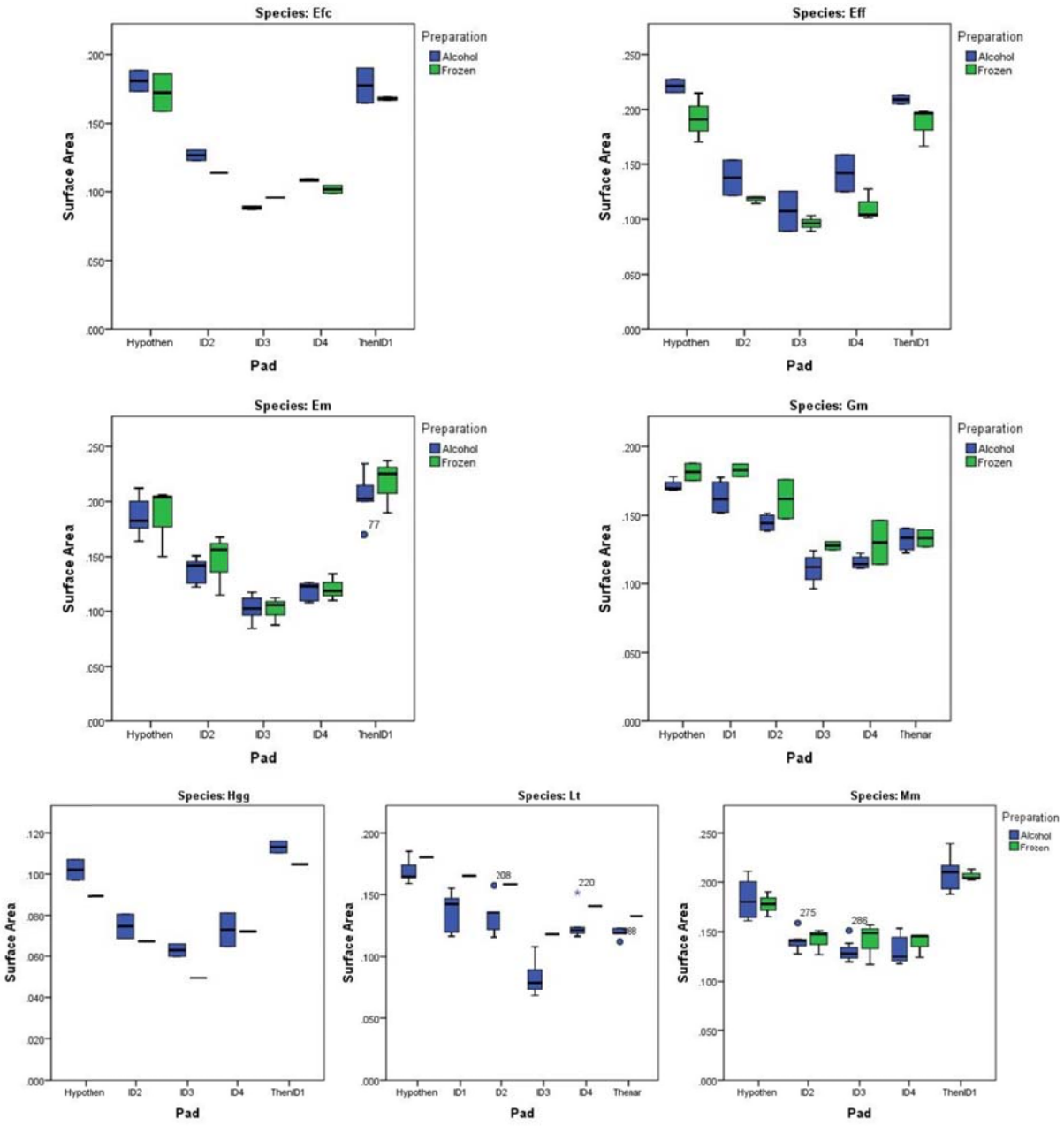

Figure 3.2c. Boxplot comparisons for means of the surface area of frozen and alcohol-preserved specimens. Significant differences between preservation types are not evident for most examined species; *Loris tardigradus* is the only examined taxa exhibiting significant differences. Species abbreviations are as follows; Efc: *Eulemur fulvus collaris*, Eff*: Eulemur fulvus fulvus*, Em: *Eulemur macaco*, Gm: *Galago moholi*, Hgg: *Hapalemur griseus griseus*, Lt: *Loris tardigradus*, Mm: *Microcebus murinus*.

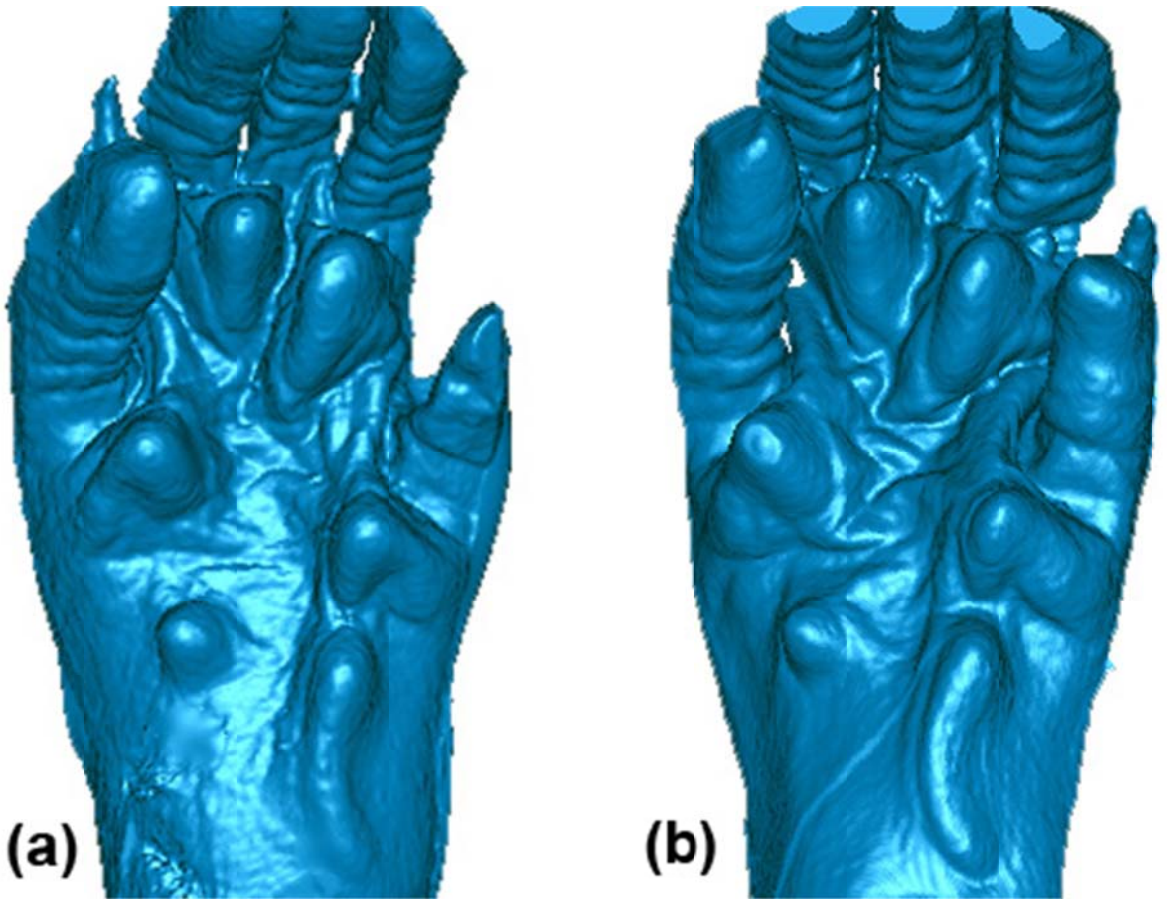

Figure 3.3. Illustration of pre- and post-preservation volar surfaces from the right foot of a single *Rattus norvegicus* specimen. (a) shows the foot at the time of death and (b) shows the foot after one year preserved in 70% alcohol. Subtle changes in the volar surfaces are evident in (b), though these did not prove statistically significant. (Note: the first digit in (a) was clipped during the digital reconstruction process.)

Chapter 4:
Body Size and Scaling of Volar Pads, Skin, and Metapodial Bones

4.1 Summary

Body size plays a well-recognized role in shaping morphological and behavioral adaptation. Body size is an important determinant of gravitational and shear forces experienced during arboreal locomotion, and the surface area and scaling of primate cheiridia play a large role in friction mechanics. Understanding the relationship between body size and volar surface size is therefore fundamental to understanding variations in pad morphology. In this chapter, the scaling relationships of the metapodial bones, volar pads, and dermatoglyphic skin ridges are examined using phylogenetic generalized least squares regressions. The lengths and base widths of the metapodial bones are found to scale with positive allometry, as do the volar pads. The proximal pads scale with greater positive allometry than the distal pads and the pedal pads scale with greater positive allometry than the manual pads. The widths of the dermatoglyphic ridges scale with negative allometry and their corresponding intermediate ridge depths scale isometrically. Descriptive statistics for the volar pad measurements are provided in Appendices A-C.

4.2 Results: Metapodial Scaling

4.2.1 Scaling of Metapodial Length with Body Size

The lengths of all metapodial bones are significantly correlated with body size. Correlation statistics are provided in Table 4.1 and illustrations of these relationships are provided in Figure 4.1. In the hand, Metacarpal$(MC)_2$-$MC_{5\ scale}$ with positive allometry, as do their counterparts, Metatarsal$(MT)_2$-$MT_{5,}$ in the foot. The first metatarsal scales isometrically with body size, and the first metacarpal scales with negative allometry. This indicates that large-bodied strepsirrhines possess relatively shorter halluces and pollices than smaller-bodied species and is consistent with previous findings (Jouffroy et al., 1991; Lemelin & Jungers, 2007).

4.2.2 Scaling of Metapodial Base Width with Body Size

The widths of all metapodial bases are significantly correlated with body size. Correlation statistics are provided in Table 4.2 and illustrated in Figure 4.2. With the exception of the first metacarpal, all widths scale with positive allometry relative to body size.

4.2.3 Scaling of Metapodial Head Width with Body Size

The widths of the metapodial heads are significantly correlated with body size and generally scale with slight positive allometry. Correlation statistics are provided in Table 4.3. This scaling relationship is not as consistent as that seen in the base widths, and several metapodial heads, including the second and fourth metacarpals and the second metatarsal, scale isometrically. This inconsistent scaling pattern is likely a result of several factors. First, most of the metapodial heads scale with very slight positive allometry, so there is very little difference between the actual scaling slopes. Second, where the metapodial bases articulate with other carpal and metacarpal bones on their proximal, medial, and lateral faces, the metapodial heads are much more mobile, with phalangeal articulations only at their distal end, and are flanked on either side by interosseous muscles. It is possible that the varying scaling relationships reflect different mechanical constraints on metapodial head than on the base.

4.3 Results: Volar Pad Scaling

4.3.1 Scaling of Volar Pad Projected Area with Body Size

The projected area of all volar pads is significantly correlated with body size. Correlation statistics for these relationships are provided in Table 4.4 and illustrations of the correlation and scaling relationships are provided in Figure 4.3. The volar areas of most pads scale with significant positive allometry to body size. Notable exceptions are the manual thenar and second interdigital pads and the pedal first interdigital pad, which scale isometrically, and the manual first interdigital pad, whose areas scale with significant negative allometry.

4.3.2 Scaling of Volar Pad Surface Area with Body Size

The surface area of the volar pads is likewise significantly correlated with body mass. Correlation and descriptive statistics are provided in Table 4.5 and the correlation and scaling relationships are illustrated in Figure 4.4. The surface areas of most pads scale with positive allometry, however, significant negative allometry is seen in the scaling of the manual first interdigital pad, and the manual thenar and pedal first interdigital pads scale isometrically. This mirrors the scaling pattern seen in the projected area of the volar pads.

4.3.3 Scaling of Volar Pad Relief with Body Size

Volar pad relief shows no correlation with body mass. Correlation statistics are provided for individual pads in Table 4.6.

4.3.4 Scaling of Volar Pad Length with Body Size

The length of all volar pads is significantly correlated with body mass. Correlation and descriptive statistics are provided in Table 4.7 and the correlation and scaling relationships are illustrated in Figure 4.5. In the Forelimb, most lengths scale with positive allometry; the first interdigital pad is again the exception. In the hindlimb, the thenar, hypothenar and second interdigital pad scale with positive allometry, whereas the first and fourth interdigital pads scale with negative allometry and the third interdigital pad scales isometrically.

4.3.5 Scaling of Pad Width with Body Size

The width of all volar pads is significantly correlated with body mass. Correlation and descriptive statistics are provided in Table 4.8 and the correlation and scaling relationships are illustrated in Figure 4.6. In the forelimb, the widths of the thenar, first, and fourth interdigital pads scale with negative allometry; the second and third interdigital pads scale isometrically; and the hypothenar and combination thenar/first interdigital pad scale with positive allometry. In the hindlimb, width scales with positive allometry for all pads except the first interdigital, which scales isometrically.

4.3.6 Relationship of Pad Shape to Body Size

No significant relationship exists between the shape of the volar pads and body mass. Correlation and descriptive statistics are provided in Table 4.9.

4.4 Results: Dermatoglyphic Ridge Scaling

Correlation statistics are provided in Table 4.10 for both ridge width and depth, and illustrations of their scaling relationships are provided in Figure 4.7. Both measures are significantly correlated with body size for all samples, but each measure scales differently. Dermatoglyphic ridge width scales with negative allometry in both areas sampled on the hand and foot. Ridge depth, however, scales isometrically with body size in the hand and thenar region of the foot, but scales with positive allometry in the hypothenar region of the foot.

4.5 Discussion

In general, both the hands and feet of the strepsirrhine primates examined here can be said to scale with positive allometry. With the exception of the first metacarpal and first metatarsal, the length of the metapodial bones and the width of their bases scale with positive allometry, which produces a relatively longer and wider bony support structure for the hands and feet in larger primates. These findings agree well with previous work by Lemelin & Jungers (2007), who reported allometric scaling of digital ray lengths in strepsirrhine primates of similar magnitudes.

Three patterns of scaling are evident in the volar pads. The first involves differential scaling in two- and three-dimensions. As the metapodial bones expand to provide relatively broader palms and soles, the lengths and widths (and correspondingly, the projected areas) of the volar pads likewise expand allometrically across their surfaces. At the same time, however, the relative convexity or protuberance of the volar pads, estimated here by the ratio of surface area to projected area, exhibits no relationship with body size (Table 4.6). The ratio of surface area to projected area remains constant across body sizes, and the two measures are tightly correlated for all pads ($R^2 = 0.99$, $p < 0.01$). This indicates that the volar pads become relatively broader in larger species, but not relatively thicker, and is different from the scaling pattern suggested by Cartmill (1979) and predicted here This has important implications for primates' ability to generate friction via their volar surfaces and will be dealt with in more detail in Chapter Five.

The second pattern in volar pad scaling concerns differential scaling of the proximal and distal portions of the palms and soles. The surface and projected areas of the distal volar pads—the second through fourth interdigital pads—scale with positive (and in most cases, statistically significant) allometry, but this relative increase in area is generally very small (slope = 0.71–0.73; Figures 4.3, 4.4). The proximal pads, by contrast, scale much more rapidly with body mass and provide a much larger relative surface area for larger-bodied species (slope = 0.66–1.02; Figures 4.3, 4.4). This pattern is not altogether surprising when the position of the pads is taken into consideration. The distal pads sit directly ventral to the metacarpo- or metatarsophalangeal joints and are thus subject to movement and deformation as the fingers or toes are flexed and extended; too great of an expansion in size would result in excessive bunching of the pad as the digits flex which in turn has the potential to impede the grasp rather than enhance it. Conversely, the proximal pads sit entirely on the metapodial bones and experience relatively little deformation as the surrounding joints move.

In addition to differences in the scaling of the proximal and distal pads, differences also exist between the scaling of manual and pedal pads. The projected and surface areas of the proximal pads of the foot scale at a much greater rate than those of the hand (Figures 4.3, 4.4). This increase in area is driven by relatively equal scaling of the lengths and widths of the individual pads (Tables 4.7, 4.8). Increases in pad area for the hand, however, are driven by

greater rates of positive allometric scaling in their lengths (Table 4.7). These differences are likely related to different roles of the hands and feet in locomotion and object manipulation and are discussed further in Chapter Five.

The first interdigital pad stands out as a bit of an anomaly. It is located neither fully in line with the proximal nor distal pads, but across the midline of the cheiridia, sandwiched between the first and second digits. It is the only pad supported internally by muscle rather than bone and is the only pad that protrudes distally from the palm or sole. In the hand, the surface and projected areas of this pad scale isometrically with body mass; in the foot, they scale with significant negative allometry (Figures 4.3, 4.4). It is unclear from this study what factors might be driving this, though its position and unique characteristics seem to be likely culprits. It is possible that the first interdigital pad might begin to impede, rather than aid, a friction grasp at a certain size threshold. This seems especially likely for the foot, where arboreal substrates are grasped between the first and second digits (Gebo, 1985; Gebo & Dagosto, 1988; Boyer et al., 2007; Kingston et al., 2010). It is also possible that the lack of bony support renders a large first interdigital pad too unwieldy to be useful. Future study of how the volar pads are specifically applied to substrates may elucidate this.

Although the majority of the volar structures scale with positive allometry to body size, the dermatoglyphic ridges are an exception to this rule. The depth of the intermediate ridges scale with isometry or slight positive allometry, but the widths of the ridges scale with negative allometry to body size. Large bodied primates therefore possess an absolutely and relatively greater number of ridges on each volar surface than their small-bodied relatives. There are several reasons why this may be. First, fitting a greater number ridges onto the volar surface provides a greater potential surface area for contact and may represent an adaptaion to increase fricitonal bonding; this hypothesis is explored further in Chapter Five (Buck & Baer, 1993; Hamrick, 1998; Derler et al., 2009a,b; Adams et al., 2013). Second, the ridge widths may be constrained by their relationship with the Meissner corpuscle tactile endings. These tactile organs sit within the dermal papillae – between the limiting and intermediate ridges of the dermatoglyphics – and a relatively greater number of ridges could theoretically accommodate a greater number of tactile organs. Additionally, the ridge widths may be constrained by Meissner corpuscle size; if the ridges become substantially wider than the corpsucles, they may not effectively activate them (Cauna, 1954; Bowlanowski & Pawson, 2003). Both the width of the ridges and the depth of the intermediate ridges exhibited some of the lowest overall correlations with body size while still retaining statistical significance (Table 4.10; Figure 4.7). This may reflect a strong influence of other factors, such as locomotor regime, on their morphology and will be explored further in coming chapters.

4.6 Conclusions

The hands and feet of strepsirrhine primates scale allometrically with body size in two dimensions. This results in large-bodied species with relatively broader and longer volar surfaces than their smaller-bodied counterparts. Both groups, however, retain a similar relief to their pads; the pads expand allometrically in length and width but not in depth. As the metapodial bones and volar pads expand to provide a relatively greater volar surface area with increasing body mass, the ridges of the volar skin scale at a much slower rate. This produces volar surfaces with greater numbers of ridges and has the overall effect of expanding potential surface contact area.

Table 4.1. Correlation statistics for metapodial length and mass. Coefficients for PGLS models are provided with corresponding maximum likelihood values for lambda transformations. Metacarpals are abbreviated as MC, metatarsals as MT.

	R^2	Intercept	Slope	Std. Dev.	λ
Forelimb					
MC_1	**0.81****	0.22	**0.26****	0.04	0.00
MC_2	**0.78****	0.04	**0.36***	0.04	0.27
MC_3	**0.92****	0.04	**0.39****	0.03	0.00
MC_4	**0.93****	-0.03	**0.40****	0.03	0.00
MC_5	**0.89****	-0.08	**0.41****	0.04	0.00
Hindlimb					
MT_1	**0.89****	0.26	**0.34**	0.04	0.00
MT_2	**0.85****	0.15	**0.37****	0.05	0.21
MT_3	**0.89****	0.09	**0.40****	0.04	0.00
MT_4	**0.89****	0.07	**0.41****	0.04	0.14
MT_5	**0.91****	-0.04	**0.44****	0.04	0.00

* $p < 0.05$

** $p < 0.01$

Table 4.2. Correlation statistics for metapodial base width and mass. Coefficients for PGLS models are provided with corresponding maximum likelihood values for lambda transformations. Metacarpals are abbreviated as MC, metatarsals as MT.

	R^2	Intercept	Slope	Std. Dev.	λ
Forelimb					
MC_1	**0.76****	-0.42	0.33	0.05	**0.76****
MC_2	**0.81****	-0.64	**0.37****	0.05	0.34
MC_3	**0.88****	-0.74	**0.39****	0.04	0.38
MC_4	**0.91****	-0.72	**0.37****	0.03	0.00
MC_5	**0.89****	-0.73	**0.36****	0.04	0.00
Hindlimb					
MT_1	**0.87****	-0.31	**0.36****	0.04	0.00
MT_2	**0.87****	-0.56	**0.36****	0.04	0.98
MT_3	**0.88****	-0.68	**0.39****	0.04	0.00
MT_4	**0.94****	-0.77	**0.41****	0.03	0.00
MT_5	**0.92****	-0.64	**0.40****	0.03	0.00

* $p < 0.05$

** $p < 0.01$

Table 4.3. Correlation statistics for metapodial head width and mass. Coefficients for PGLS models are provided with corresponding maximum likelihood values for lambda transformations. Metacarpals are abbreviated as MC, metatarsals as MT.

	R^2	Intercept	Slope	Std. Dev.	λ
Forelimb					
MC_1	**0.82****	-0.55	**0.36****	0.05	0.40
MC_2	**0.87****	-0.47	0.31	0.03	0.00
MC_3	**0.68****	-0.58	**0.37****	0.07	0.00
MC_4	**0.89****	-0.45	0.32	0.03	0.97
MC_5	**0.92****	-0.61	**0.36****	0.03	**0.61***
Hindlimb					
MT_1	**0.91****	-0.46	**0.39****	0.04	0.29
MT_2	**0.88****	-0.52	0.34	0.04	0.44
MT_3	**0.88****	-0.59	**0.36****	0.04	0.25
MT_4	**0.92****	-0.61	**0.37****	0.03	0.80
MT_5	**0.90****	-0.65	**0.38****	0.04	0.45

* $p < 0.05$

** $p < 0.01$

Table 4.4. Correlation statistics for volar pad projected area and mass. Coefficients for PGLS models are provided with corresponding maximum likelihood values for lambda transformations.

	R^2	Intercept	Slope	Std. Dev.	λ
Forelimb					
Thenar	**0.88****	-0.42	0.67	0.10	0.00
Then/ID1	**0.84****	-0.74	**0.92****	0.11	0.96
Hypothenar	**0.95****	-0.53	**0.81****	0.05	0.00
ID1	**0.79****	0.04	**0.53****	0.11	0.00
ID2	**0.89****	-0.37	0.68	0.06	0.00
ID3	**0.88****	-0.62	**0.69***	0.06	0.00
ID4	**0.92****	-0.64	**0.74****	0.05	0.00
Hindlimb					
Thenar	**0.93****	-0.79	**0.88****	0.07	0.00
Hypothenar	**0.93****	-1.17	**1.02****	0.07	0.81
ID1	**0.85****	0.17	0.63	0.07	0.00
ID2	**0.92****	-0.26	**0.70***	0.06	0.08
ID3	**0.91****	-0.67	**0.71****	0.06	0.00
ID4	**0.87****	-0.51	**0.73****	0.08	0.88

* $p < 0.05$
** $p < 0.01$

Table 4.5. Correlation statistics for volar pad surface area and mass. Coefficients for PGLS models are provided with corresponding maximum likelihood values for lambda transformations.

	R^2	Intercept	Slope	Std. Dev.	λ
Forelimb					
Thenar	**0.83****	-0.19	0.66	0.11	0.00
Then/ID1	**0.89****	-0.47	**0.89****	0.11	0.82
Hypothenar	**0.96****	-0.37	**0.83****	0.04	0.00
ID1	**0.79****	0.32	**0.52****	0.10	0.00
ID2	**0.88****	-0.24	**0.71****	0.06	0.36
ID3	**0.82****	-0.49	**0.72****	0.08	0.70
ID4	**0.93****	-0.37	**0.73****	0.05	0.00
Hindlimb					
Thenar	**0.91****	-0.75	**0.90****	0.08	0.22
Hypothenar	**0.91****	-1.02	**1.02****	0.08	0.87
ID1	**0.89****	0.42	0.65	0.06	0.00
ID2	**0.93****	-0.01	**0.70***	0.05	0.02
ID3	**0.91****	-0.47	**0.71****	0.06	0.00
ID4	**0.91****	-0.32	**0.73****	0.06	0.40

* $p < 0.05$

** $p < 0.01$

Table 4.6. Correlation statistics for relief index and mass. Coefficients for PGLS models are provided with corresponding maximum likelihood values for lambda transformations.

	R^2	Intercept	Slope	Std. Dev.	λ
Forelimb					
Thenar	0.06	0.26	-0.01	0.01	0.00
Then/ID1	0.01	0.21	0.00	0.02	0.38
Hypothenar	0.08	0.17	0.01	0.01	0.00
ID1	0.00	0.32	0.00	0.02	0.00
ID2	0.07	0.37	-0.02	0.01	0.00
ID3	0.01	0.21	0.00	0.01	0.94
ID4	0.07	0.31	-0.01	0.01	0.00
Hindlimb					
Thenar	0.00	0.12	0.00	0.01	0.57
Hypothenar	0.01	0.10	0.01	0.01	0.57
ID1	0.01	0.37	0.00	0.02	0.14
ID2	0.00	0.26	0.00	0.01	0.00
ID3	0.00	0.24	0.00	0.01	0.00
ID4	0.14	0.18	0.01	0.01	0.00

* $p < 0.05$

** $p < 0.01$

Table 4.7. Correlation statistics for volar pad length and mass. Coefficients for PGLS models are provided with corresponding maximum likelihood values for lambda transformations.

	R^2	Intercept	Slope	Std. Dev.	λ
Forelimb					
Thenar	**0.83****	-0.16	**0.37***	0.06	0.00
Then/ID1	**0.89****	-0.48	**0.48****	0.05	0.86
Hypothenar	**0.95****	-0.30	**0.48****	0.03	0.00
ID1	**0.83****	0.10	**0.31***	0.05	0.00
ID2	**0.84****	-0.33	**0.44****	0.05	1.00
ID3	**0.78****	-0.32	**0.40****	0.05	0.89
ID4	**0.82****	-0.32	**0.40****	0.05	0.91
Hindlimb					
Thenar	**0.88****	-0.26	**0.46****	0.05	0.00
Hypothenar	**0.81****	-0.35	**0.48****	0.06	0.97
ID1	**0.86****	0.31	**0.30****	0.03	0.00
ID2	**0.84****	-0.03	**0.38****	0.05	0.00
ID3	**0.85****	-0.09	0.32	0.04	0.00
ID4	**0.84****	-0.07	**0.31***	0.04	0.00

* $p < 0.05$
** $p < 0.01$

Table 4.8. Correlation statistics for width and mass. Coefficients for PGLS models are provided with corresponding maximum likelihood values for lambda transformations.

	R^2	Intercept	Slope	Std. Dev.	λ
Forelimb					
Thenar	**0.82****	-0.04	**0.27****	0.05	0.00
Then/ID1	**0.72****	-0.34	**0.42****	0.09	0.67
Hypothenar	**0.93****	-0.23	**0.38****	0.02	0.06
ID1	**0.47***	0.09	**0.22****	0.09	0.00
ID2	**0.91****	-0.18	0.34	0.03	0.00
ID3	**0.80****	-0.22	0.34	0.04	0.00
ID4	**0.83****	-0.06	**0.30****	0.03	0.00
Hindlimb					
Thenar	**0.89****	-0.64	**0.50****	0.05	0.64
Hypothenar	**0.91****	-0.61	**0.49****	0.04	0.93
ID1	**0.79****	0.06	0.32	0.05	0.00
ID2	**0.84****	-0.17	**0.37****	0.05	0.29
ID3	**0.85****	-0.36	**0.36****	0.04	0.82
ID4	**0.81****	-0.28	**0.39****	0.05	0.31

* $p < 0.05$
** $p < 0.01$

Table 4.9. Correlation statistics for volar pad shape index and mass. Coefficients for PGLS models are provided with corresponding maximum likelihood values for lambda transformations.

	R^2	Intercept	Slope	Std. Dev.	λ
Forelimb					
Thenar	0.23	-0.23	-0.09	0.06	0.00
Then/ID1	0.13	0.20	0.06	0.05	0.54
Hypothenar	0.05	0.27	0.03	0.03	0.92
ID1	0.12	0.03	0.09	0.09	0.00
ID2	0.10	-0.10	0.07	0.05	0.81
ID3	0.08	-0.17	0.07	0.05	0.45
ID4	0.12	-0.51	0.09	0.06	0.68
Hindlimb					
Thenar	0.05	1.05	-0.06	0.08	1.00
Hypothenar	0.03	0.83	-0.05	0.08	0.99
ID1	0.02	0.61	-0.03	0.05	0.00
ID2	0.02	0.58	-0.03	0.07	1.00
ID3	0.12	0.70	-0.05	0.04	0.00
ID4	0.06	0.32	-0.06	0.06	0.00

* $p < 0.05$
** $p < 0.01$

Table 4.10. Correlation statistics for dermatoglyphic ridge dimensions and mass. Coefficients for PGLS models are provided with corresponding maximum likelihood value for lambda transformations.

		R^2	Intercept	Slope	SD Slope	λ
Forelimb	**Ridge Width**					
	Thenar	0.84**	1.73	0.21**	0.03	0.00
	Hypothenar	0.52**	1.69	0.19**	0.06	0.00
	Ridge Depth					
	Thenar	0.68**	1.18	0.35	0.08	0.00
	Hypothenar	0.71**	1.16	0.35	0.07	0.00
		R^2	Intercept	Slope	SD Slope	λ
Hindlimb	**Ridge Width**					
	Thenar	0.45*	1.61	0.24**	0.10	0.00
	Hypothenar	0.68**	1.47	0.30*	0.09	0.00
	Ridge Depth					
	Thenar	0.66**	1.02	0.39	0.11	0.00
	Hypothenar	0.68**	0.43	0.43**	0.11	0.00

* $p < 0.05$

** $p < 0.01$

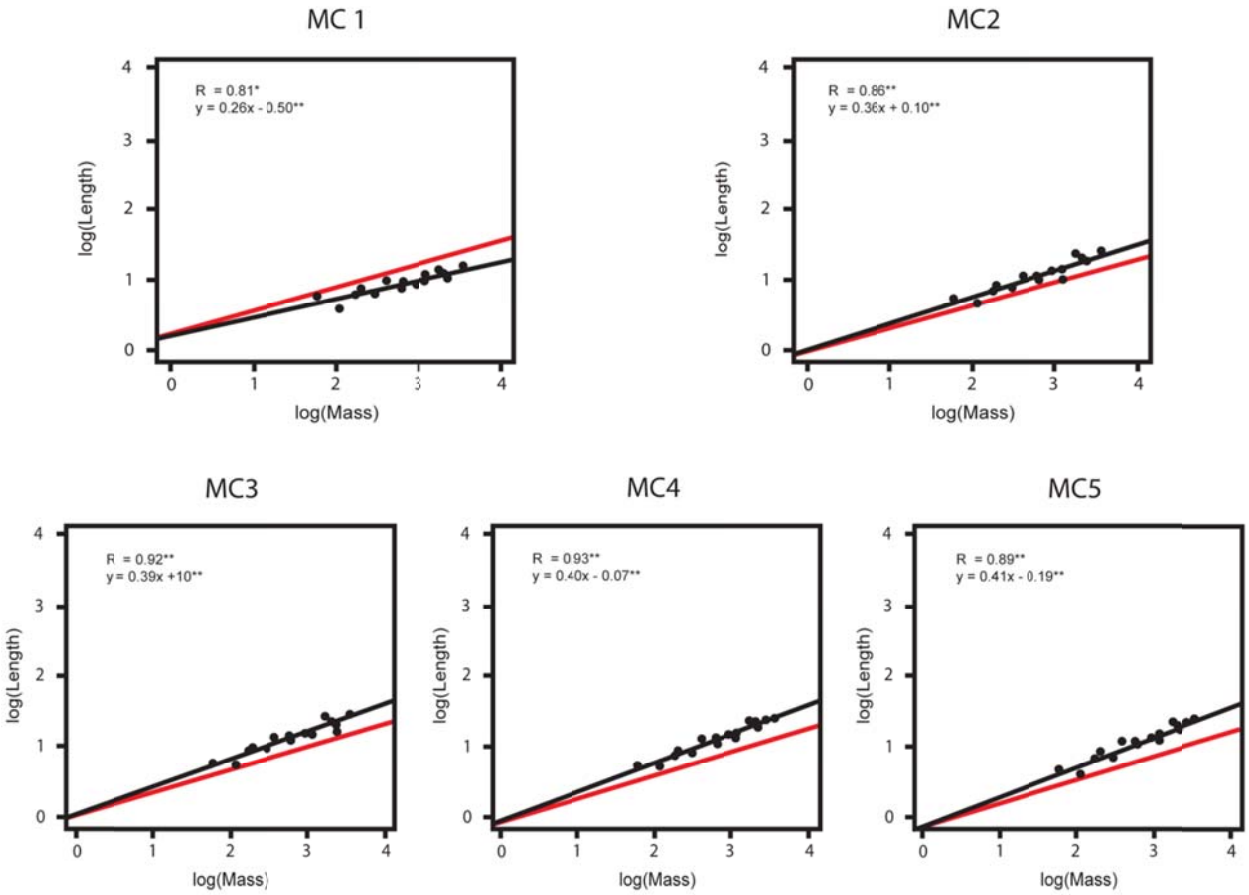

Figure 4.1a. PGLS regressions of metacarpal length on mass for forelimb. Isometric scaling represented by red line. The length of metacarpals 2–5 scale with positive allometry; the first metacarpal is the only one to scale with negative allometry.

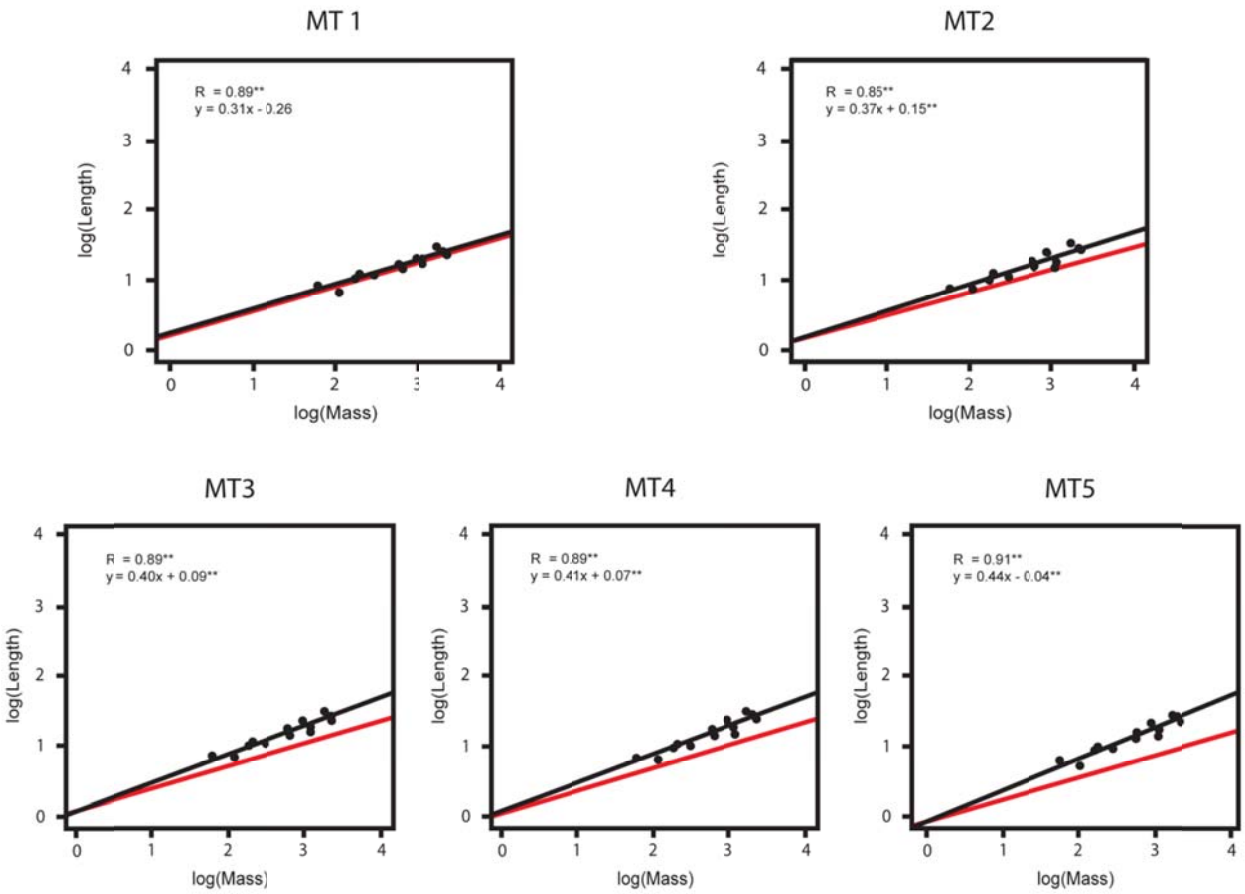

Figure 4.1b. PGLS regressions of metatarsal length on mass for hindlimb. Isometric scaling represented by red line. All metatarsals scale with positive allometry.

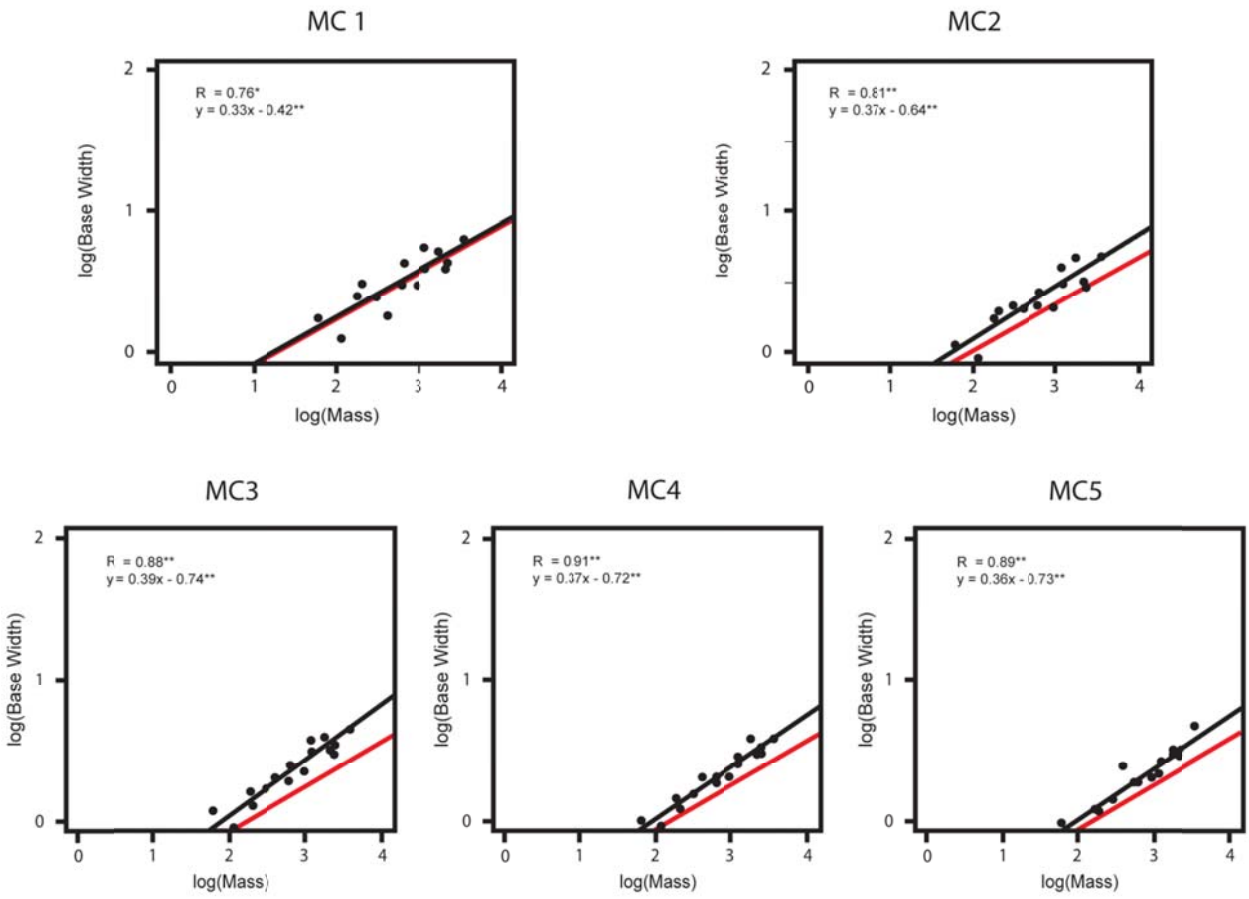

Figure 4.2a. PGLS regressions of metatarsal base width on mass for forelimb. Isometric scaling represented by red line. The width of the metacarpal bases scale with positive allometry except for the first metacarpal, which scale isometrically.

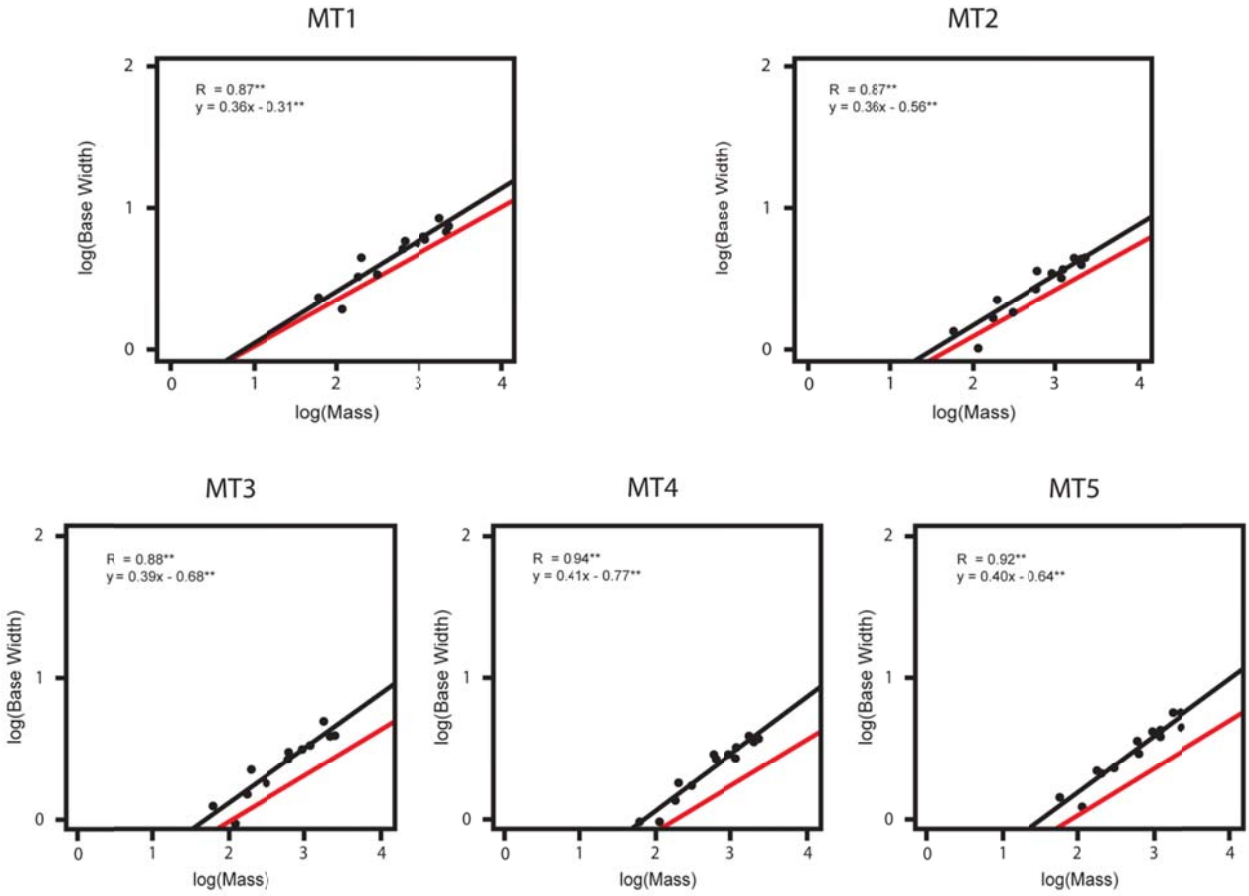

Figure 4.2b. PGLS regressions of metatarsal base width on mass for hindlimb. Isometric scaling represented by red line. The widths of all metacarpal bases scale with positive allometry.

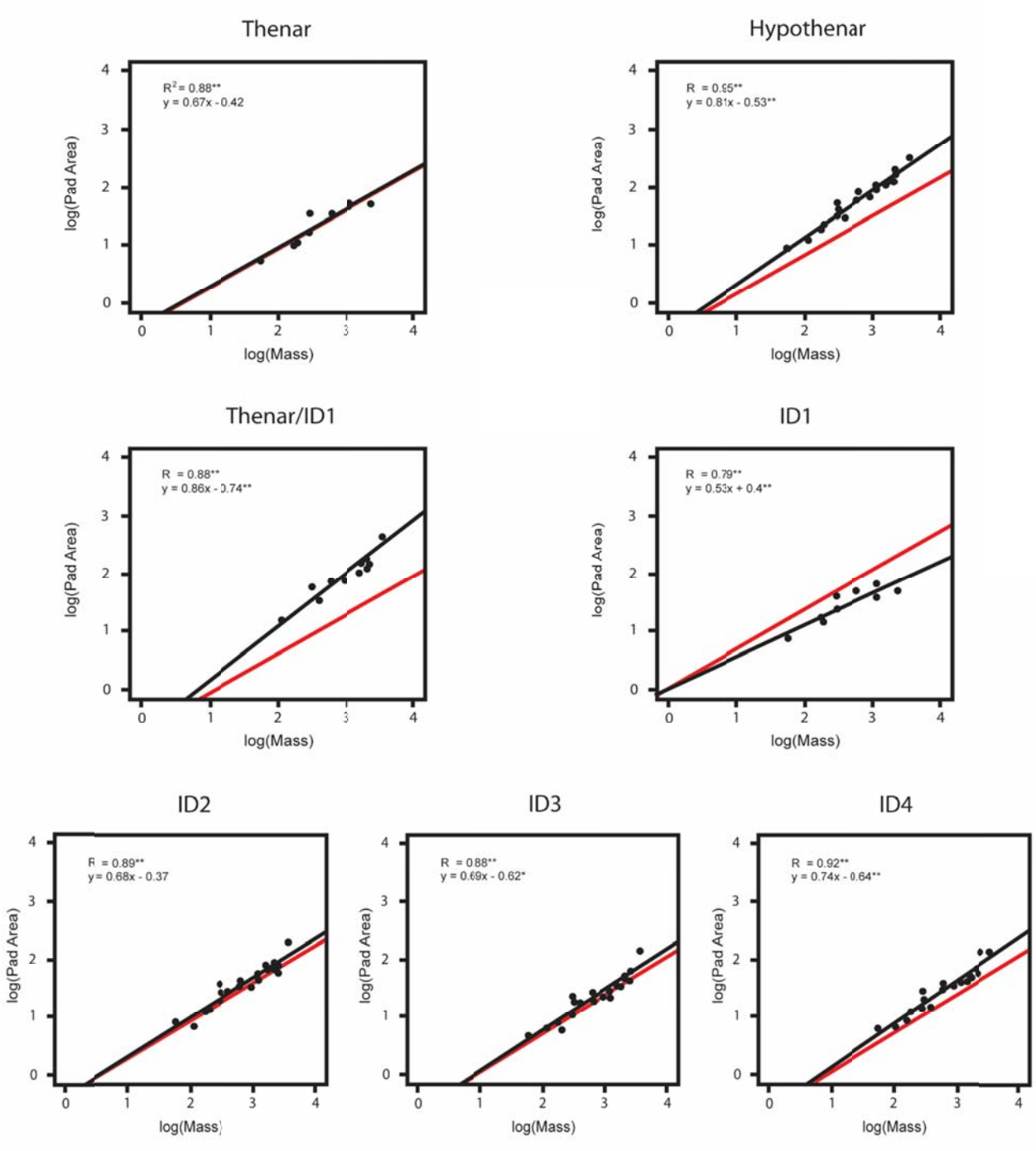

Figure 4.3a. PGLS regressions of volar pad projected area on mass for forelimb pads. Isometric scaling represented by red line. The distal volar pads scale with slight positive allometry; the proximal pads scale at a much greater rate with the exception of the thenar pad.

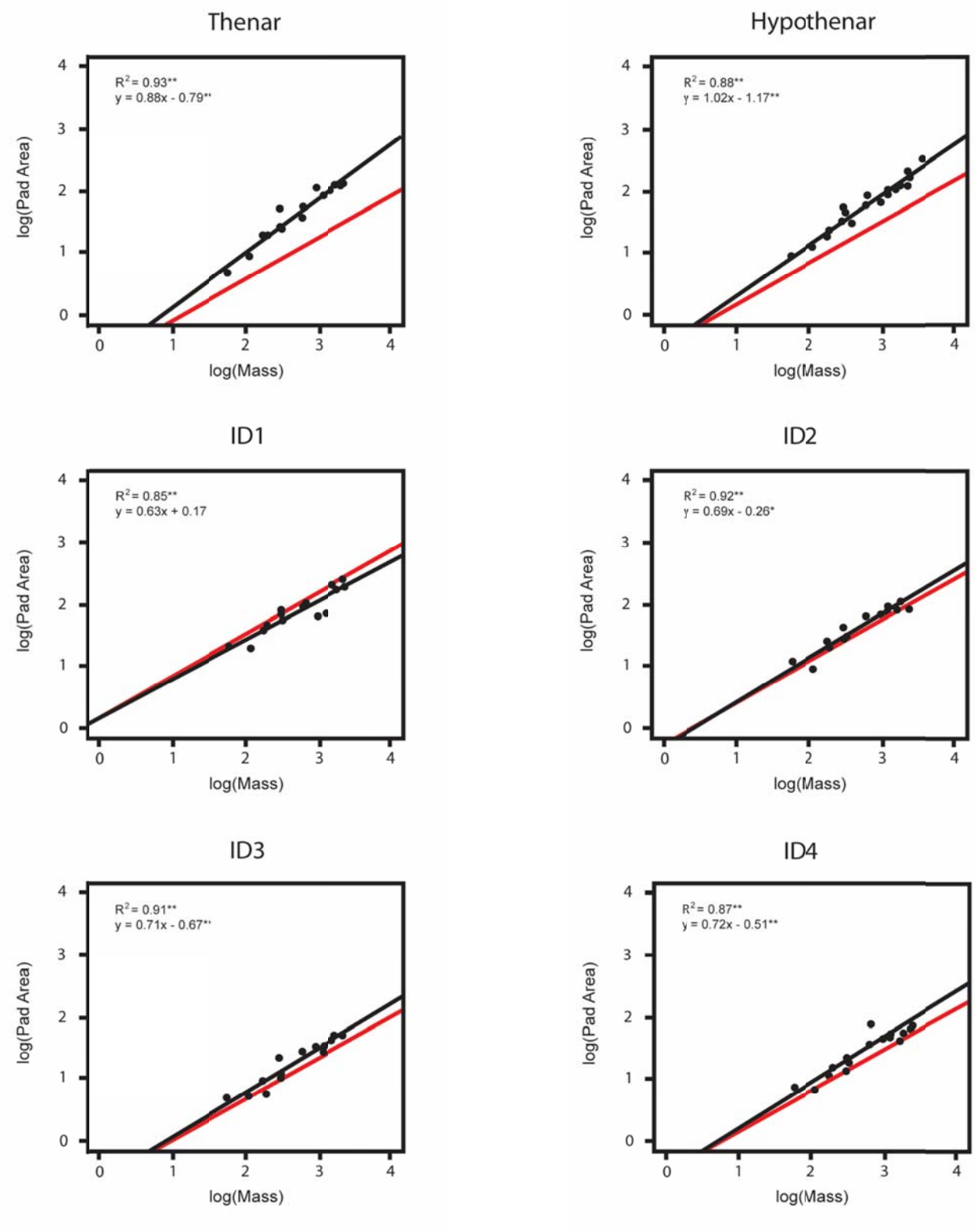

Figure 4.3b. PGLS regressions of volar pad projected area on mass for hindlimb pads. Isometric scaling represented by red line. The distal volar pads scale with slight positive allometry; the proximal volar pads scale at a much greater positive rate.

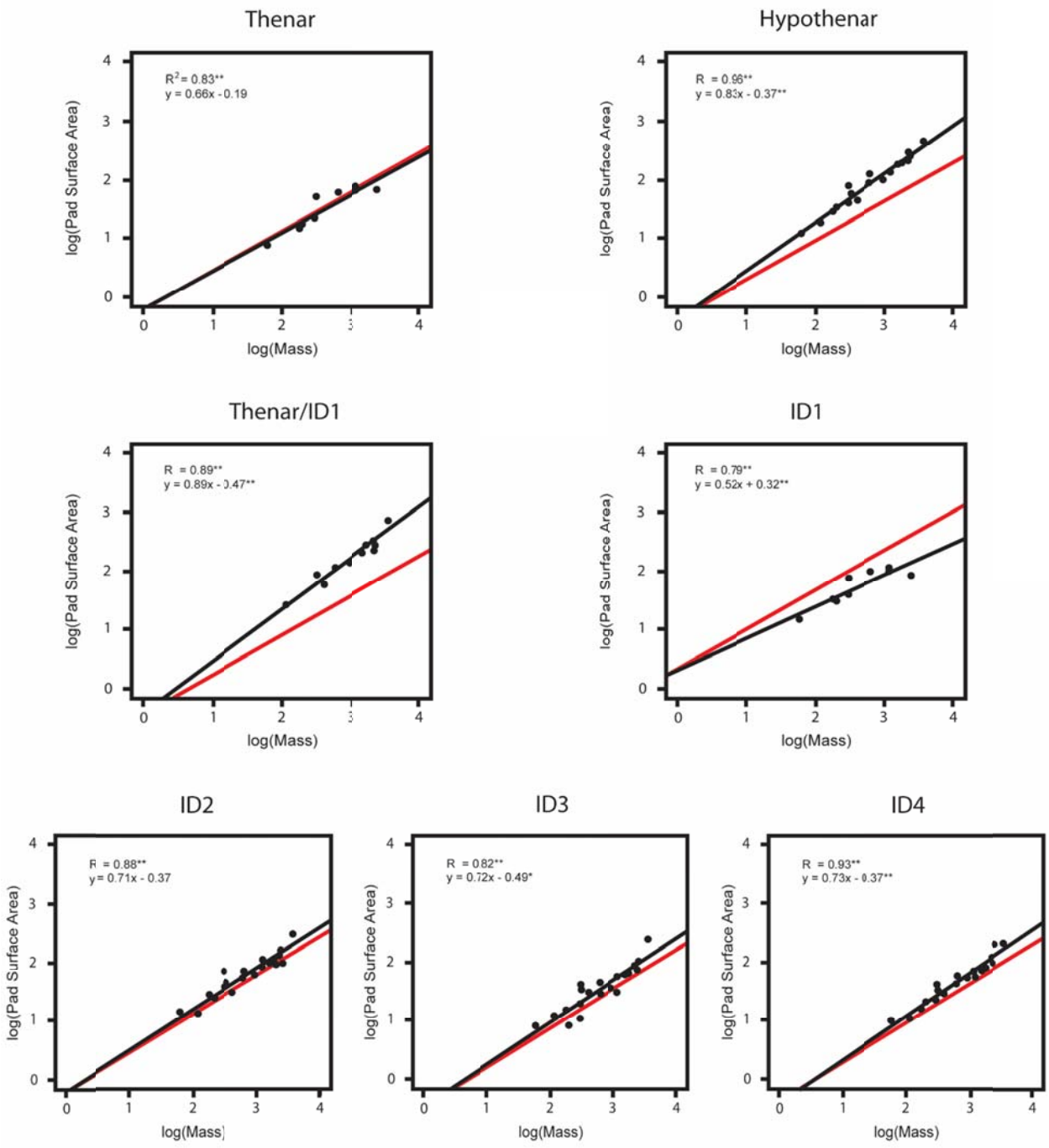

Figure 4.4a. PGLS regressions of volar pad surface area on mass for forelimb pads. Isometric scaling represented by red line. Scaling patterns for surface area mirror those for projected area.

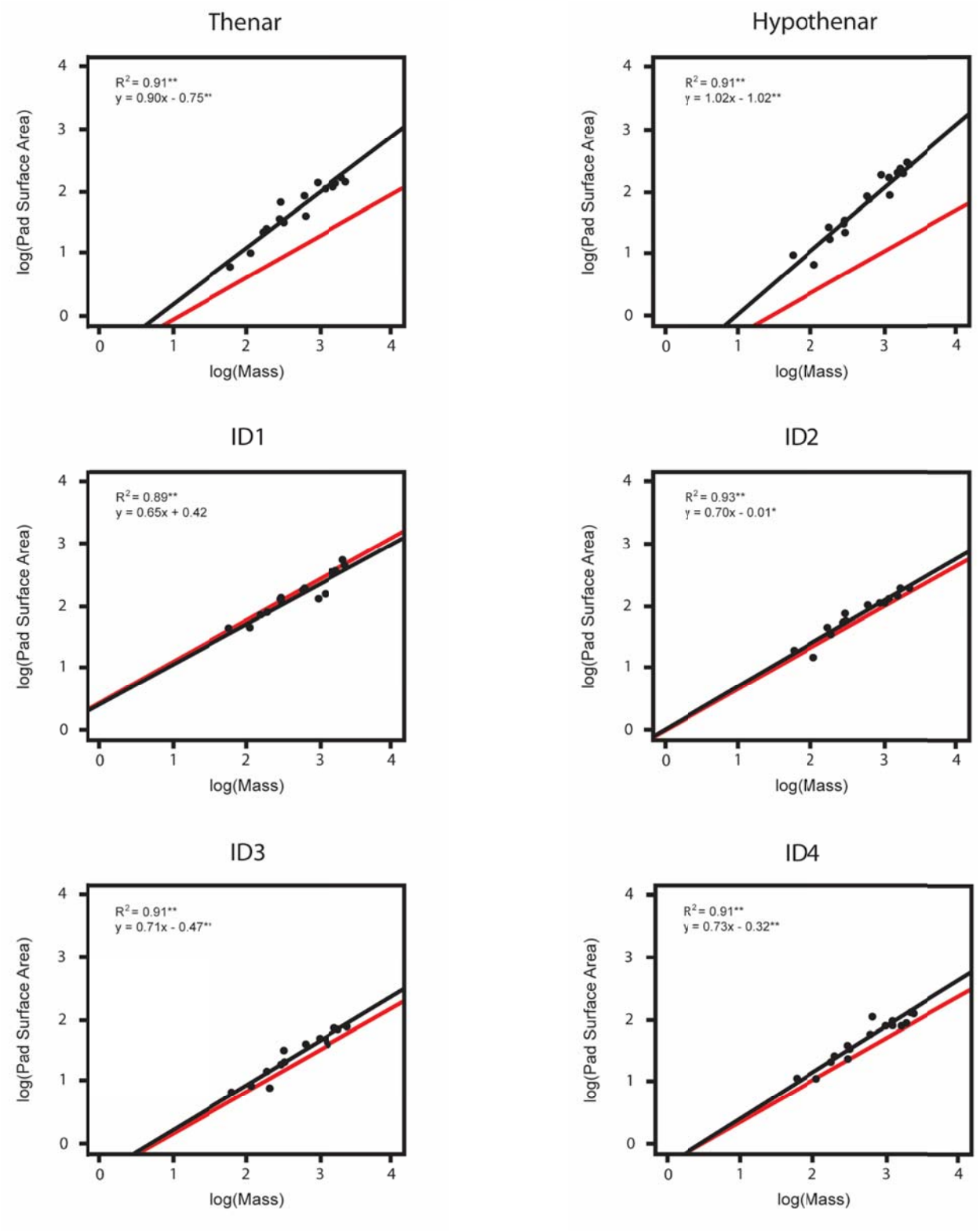

Figure 4.4b. PGLS regressions of volar pad surface area on mass for hindlimb pads. Isometric scaling represented by red line. Scaling patterns for surface area mirror those for projected area.

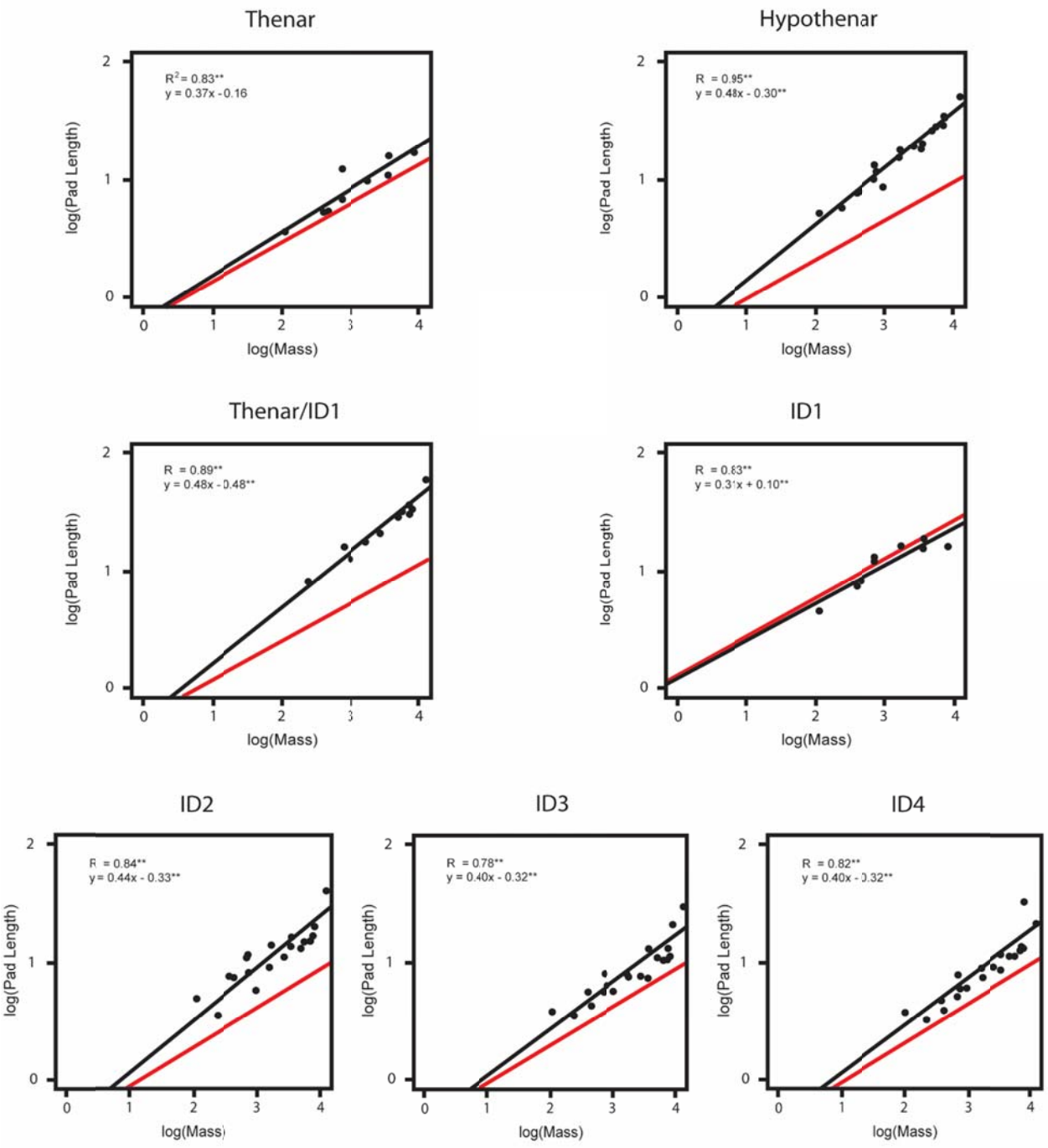

Figure 4.5a. PGLS regressions of volar pad length on mass for forelimb pads. Isometric scaling represented by red line. The lengths of all pads scale with positive allometry.

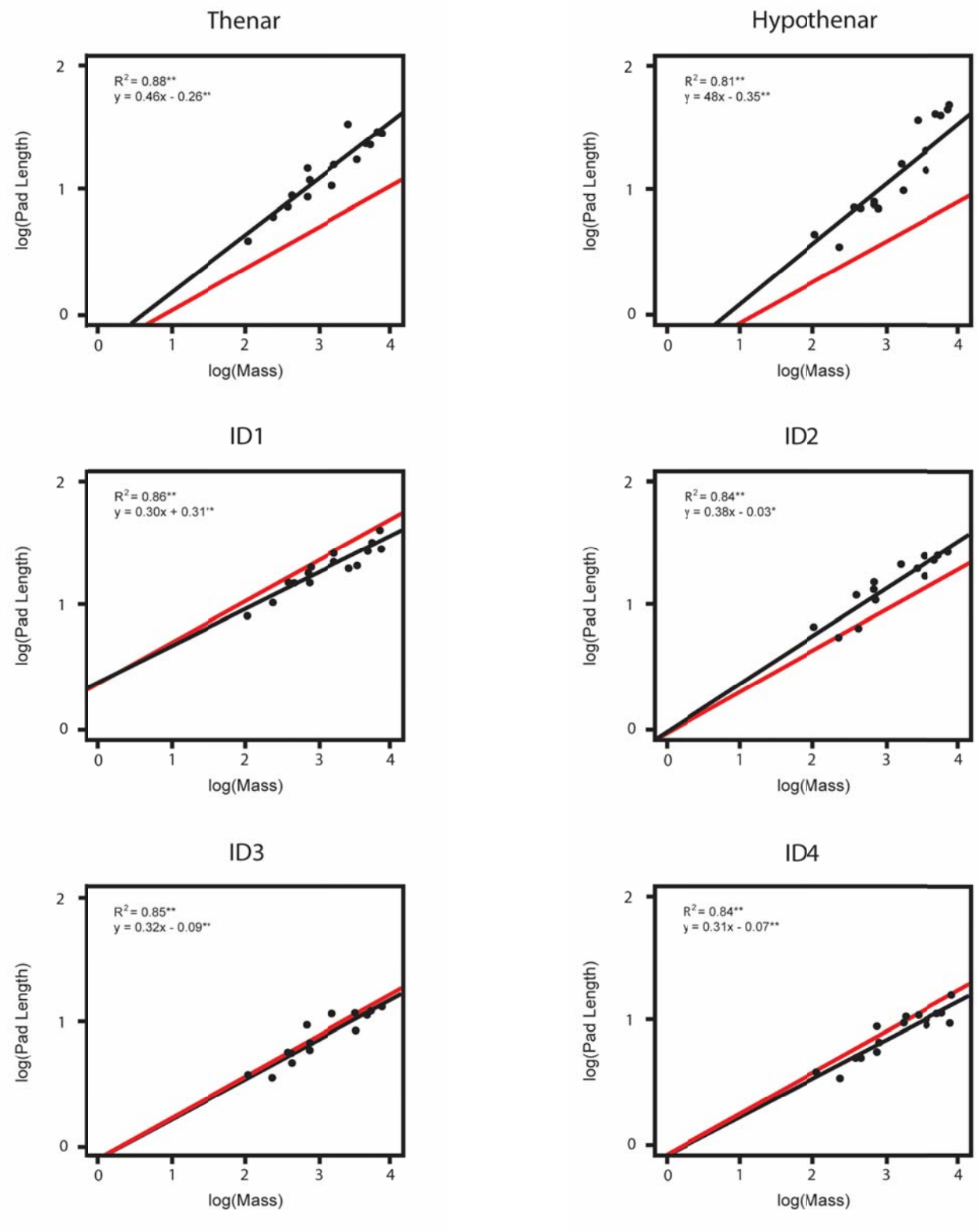

Figure 4.5b. PGLS regressions of volar pad length on mass for hindlimb pads. Isometric scaling represented by red line. The widths of all pads scale with positive allometry. This is most pronounced in the proximal pads.

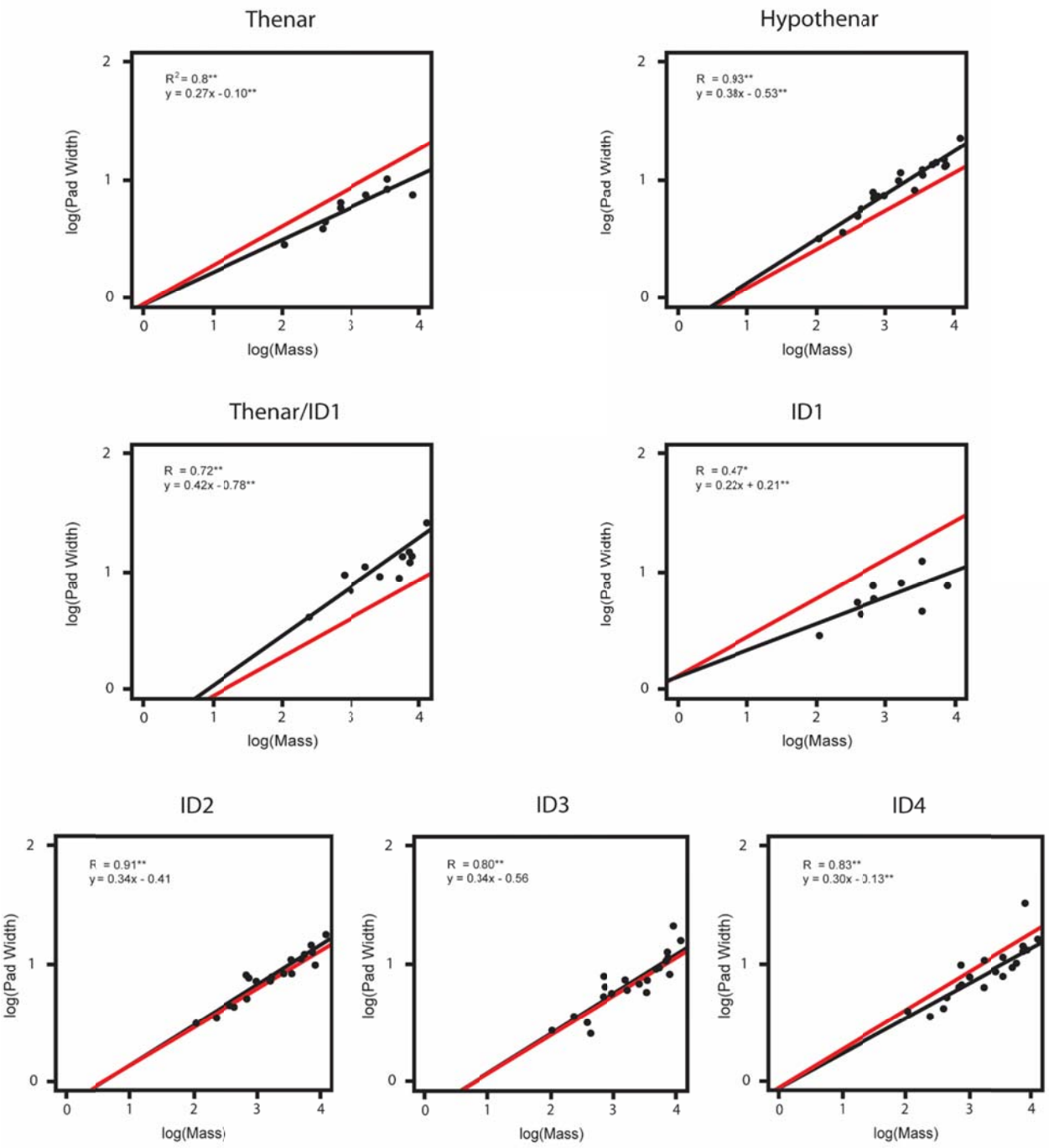

Figure 4.6a. PGLS regressions of volar pad width on mass for forelimb pads. Isometric scaling represented by red line. The widths of most pads scale with positive allometry; the widths of the thenar and first interdigital pads scale with negative allometry.

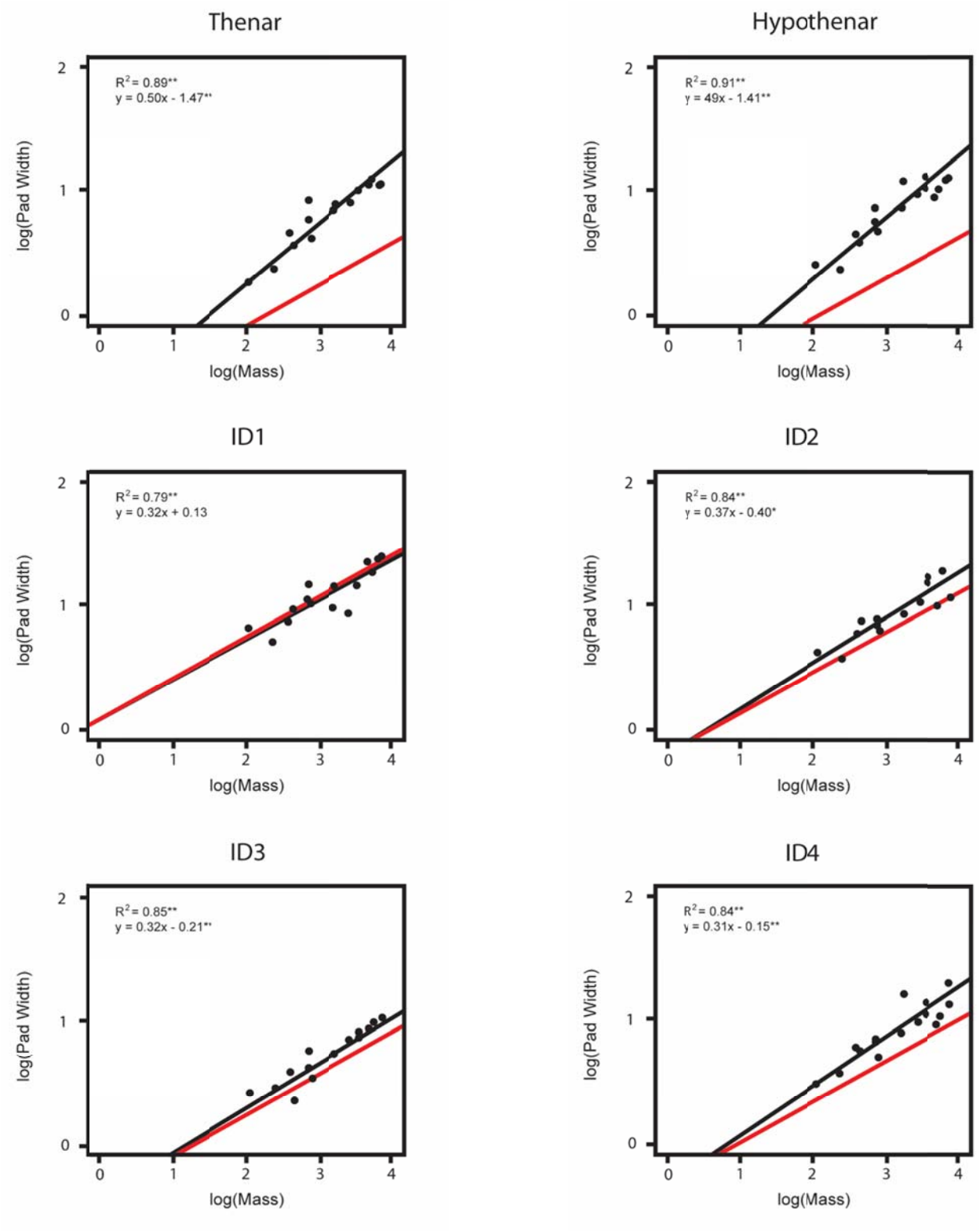

Figure 4.6b. PGLS regressions of volar pad width on mass for hindlimb pads. Isometric scaling represented by red line. The widths of all pads scale with positive allometry. This is most pronounced in the proximal pads.

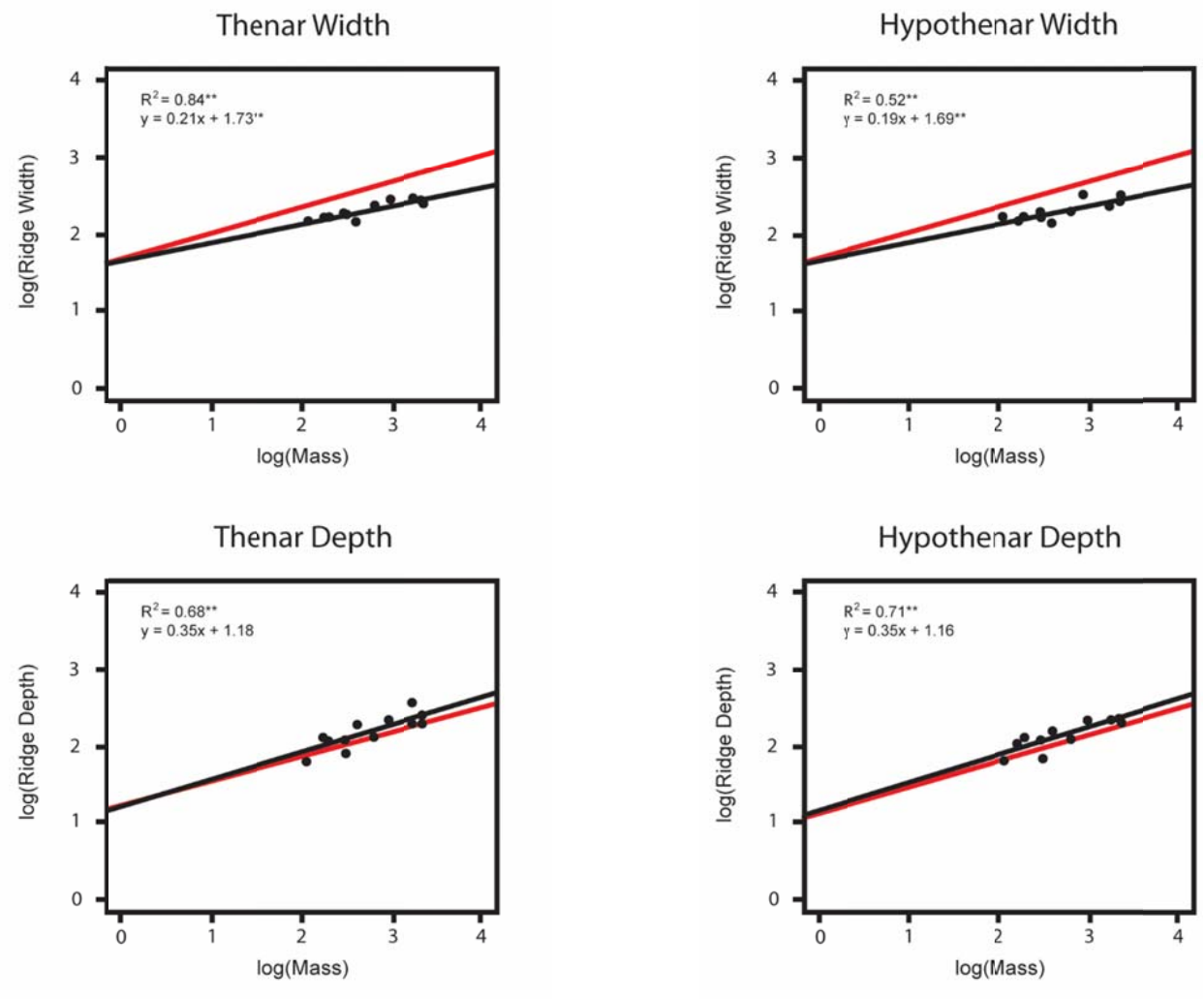

Figure 4.7a. PGLS regressions of dermatoglyphic ridge width and depth on body size for skin clipped from the forelimb thenar and hypothenar pads. Isometric scaling represented by red line. The widths of the dermatoglyphic ridges scale with positive allometry. The depths of the intermediate ridges scale isometrically.

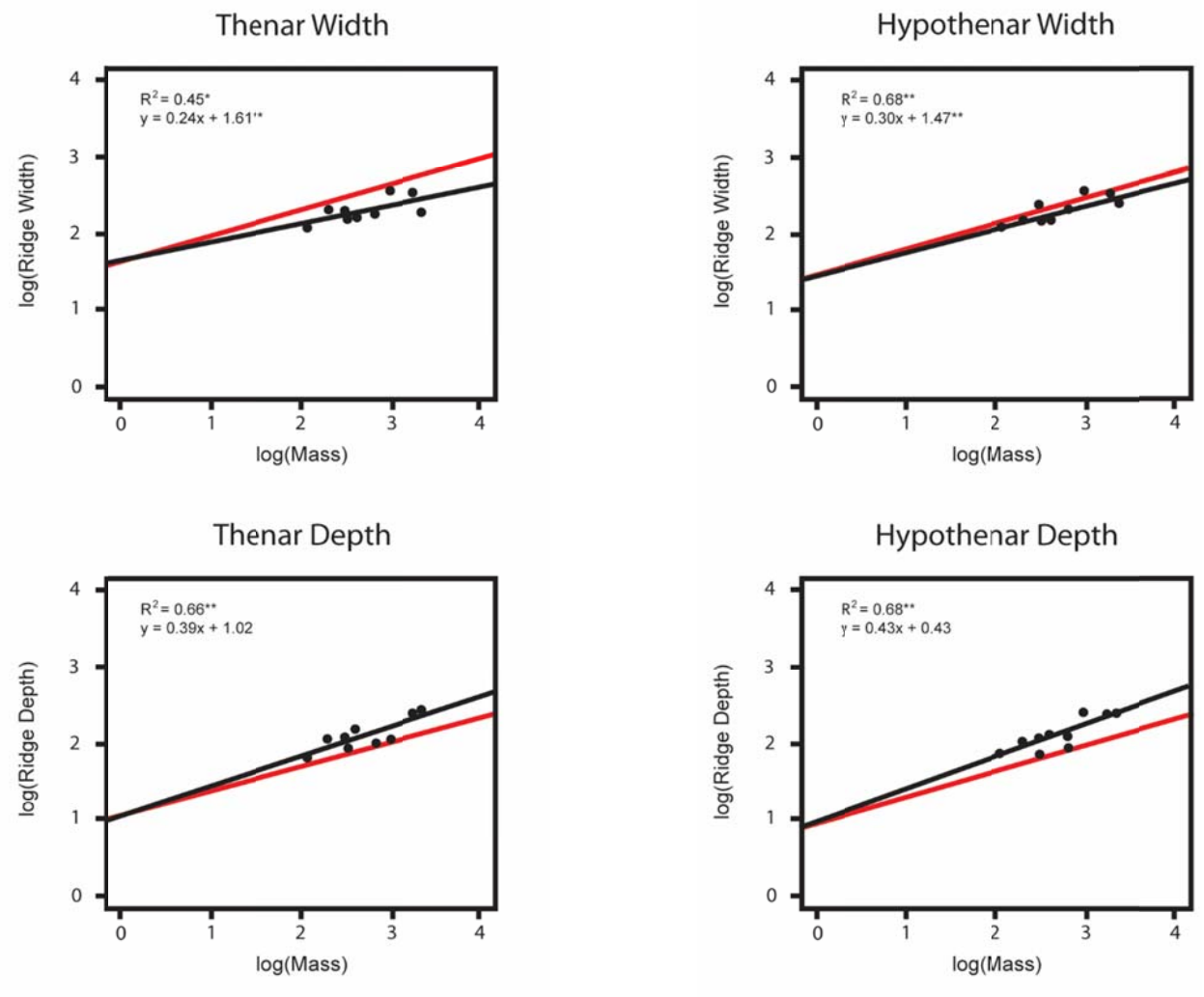

Figure 4.7b. PGLS regressions of dermatoglyphic ridge width and depth on body size for skin clipped from the hindlimb thenar and hypothenar pads. Isometric scaling represented by red line. The widths of the dermatoglyphic ridges scale with positive allometry. The depths of the intermediate ridges scale isometrically.

Chapter 5:
Friction Adaptations

5.1 Summary

In the previous chapter, positive allometric scaling relationships were established for the dimensions of the volar pads. Here, phylogenetic generalized least squares analyses are used to test specific hypotheses to determine if these scaling relationships are consistent with those predicted by friction mechanics. The relief of the volar pads is hypothesized to scale with negative allometry, providing smaller-bodied species with more protuberant pads and optimizing the "n" component of the equation describing viscoelastic friction. The surface areas of the volar pads and skin are hypothesized to scale with positive allometry, which would provide a relatively greater contact area for large-bodied species and therefore optimize the "K" component of the equation describing viscoelastic friction. These hypotheses are partially supported by findings here. The volar surface area is expanded both through positive allometric scaling of the volar pads and negative allometric scaling of the dermatoglyphic ridge widths. Pad relief, however, is consistent across body sizes. It remains likely that small-bodied species make use of the "n" component of viscoelastic friction to enhance frictional bonding, but this mechanism does not appear to strongly affect volar pad dimensions. Rather, adaptation for friction grasping at different body sizes revolves around optimizing the "K" component of the equation describing viscoelastic friction, as exemplified by a strong correlation between volar surface area and body size.

5.2 Results: Volar Pad Relief

The surface area and projected area of the volar pads are strongly correlated for all pads. Table 5.1 provides correlation statistics and Figure 5.1 illustrates the relationship for each pad. Coefficients of determination ($R^{2)}$ are very high and range from 0.97–0.99 ($p < 0.01$). Slopes of the best-fit lines hover around one (though several differ significantly, these are identified in Table 5.1), indicating that these variables scale isometrically with one another.

As demonstrated in Chapter Four, the relief indices of the volar pads show no correlation with body mass in either the fore- or hindlimbs (see Table 4.6). This lack of relationship is further illustrated in Figure 5.2.

5.3 Results: Volar Pad Surface Area

The surface area of the volar pads is significantly correlated with body mass. As demonstrated in Chapter Four, the majority of the volar pads scale with positive allometry to body mass (see Table 4.5; Figure 4.4). Notable exceptions are the first interdigital pad of the hand, which scales with significant negative allometry and the first interdigital pad of the foot, which scales isometrically.

5.4 Results: Dermatoglyphic Ridge Widths

The widths of the dermatoglyphic ridges found on the thenar and hypothenar regions of the hands and feet are significantly correlated with body mass for the skin of both proximal volar pads and the apical pad of digit five as reported in Chapter Four. Ridge width for digit two is positively associated with body mass, but this correlation is not significant (see Table 4.10; Figure 4.7). In all cases, the width of the ridges exhibits negative allometry with body mass.

5.5 Discussion

The results of this study indicate that changes in volar pad surface area are the primary friction-enhancing adaptation in strepsirrhine primates. There is a strong correlation between body mass and surface area for all volar pads, and most pads scale with significant positive allometry, which provides a relatively larger surface area for larger-bodied species. This allometric relationship is most pronounced in the proximal pads—the thenar, hypothenar, and combination thenar/first interdigital pads—for both limbs. The volar skin is likewise adapted to provide a relatively larger surface area; in this case, the widths of the dermatoglyphic ridges scale with negative allometry, which has the effect of fitting a larger number of ridges onto the volar surfaces of larger-bodied species. Surprisingly, there appears to be no difference in the absolute or relative relief of the volar pads between large- and small- bodied strepsirrhines.

Significant differences exist between the scaling of manual and pedal pads. The proximal pads of the foot scale at a much greater rate than those of the hand (see Chapter four, Table 4.5 and Figure 4.4). This is likely related to different roles of the hands and feet in locomotion and object manipulation, as discussed in Chapter Four. Although strepsirrhines may lack some of the finer coordination and range of motion found in higher primates, behavioral evidence indicates that the hand is still the primary extremity used in food procurement and exploration (Charles-Dominique, 1974, 1977; Yamashita, 2003; Nekaris & Rassmussen, 2003; Nekaris, 2005; Siemers et al., 2007; Lhota et al., 2009; Scheumann et al., 2011). The hind limb is used primarily in locomotion and postural behaviors and plays a dominant role in these; the hind limb supports a greater percentage of the body's weight than the forelimb during locomotion, it produces the

majority of propulsive forces to move the body forward, and it is the last to relinquish contact with the substrate during leaping behaviors (Demes et al., 1995, 1994b, 1996, 1999; Schmitt & Hanna, 2004; Hanna et al., 2006; Larson & Demes, 2011; Young, 2012; Johnson et al., 2015; Patel et al., 2015). It follows logically, then, that the cheiridium responsible for maintaining a secure grasp amidst inundation by more frequent and greater acting forces would possess adaptations to counteract these. Adaptations of this kind are already known from comparisons of the primate hand and foot: the foot possesses a relatively more massive grasping musculature and greater divergence and differentiation of the grasping hallux from the lateral digits (Gebo, 1985, 2014; Napier, 1993; Demes et al., 1998; Ankel-Simons, 2007). The relatively greater surface area provided by the proximal volar pads in the foot complements these adaptations by passively enhancing frictional bonds with the substrate (Cartmill, 1979, 1985).

Like the volar pads, the surface area of the volar skin also scales with positive allometry relative to body mass (see Chapter Four, Figure 4.7). In this case, the width of the dermatoglyphic ridges scales at a much slower rate than mass, such that larger species have relatively narrower ridges, and therefore a greater number of them fit onto the volar surface of a large-bodied primate. Although a greater number of ridges increase the absolute surface area of the volar skin, some have argued that they reduce the effective surface area. Warman & Ennos (2009) showed that this is indeed the case when the volar skin is applied to a smooth, unblemished surface; however, smooth surfaces, such as the acrylic glass used in their study, are rarely found in nature. Texturized surfaces are far more common and ridged volar skin allows for interlocking and greater surface contact with these, as demonstrated by a number of investigators (Buck & Baer, 1993; Derler et al., 2009a,b; Adams et al, 2013)

It is important to note that while fitting a relatively large number of dermatoglyphic ridges onto the volar skin likely enhances its frictional properties, other factors have been hypothesized to influence this morphology as well. The skin receives tactile information through Meissner corpuscles, tactile end organs that inhabit the dermal papillae deep to the dermatoglyphic ridges and may influence their spacing (Cauna, 1954; Bolanowski & Pawson, 2003). The folded structure may strengthen the epidermis, protecting underlying tissues. The furrows between the ridges may provide channels for moisture, so that contact between the skin and substrate remains uninterrupted. These relationships are beyond the scope of the current study, but are not necessarily mutually exclusive of the findings here.

Surprisingly, the volar pads are not more protuberant in smaller species. More protuberant pads have been hypothesized to maximize the “n” component of viscoelastic friction in smaller-bodied primates, and a cursory visual inspection of the pads themselves seems to confirm this (Cartmill, 1979; 1985). However, this hypothesis, and indeed description, seems to stem from an optical illusion. The pads of smaller species are not more protuberant than those of larger species at all; surface area scales isometrically with projected area and the ratio of these measurements remains remarkably consistent across all body sizes (see Chapter Four, Figures 4.4, 4.7). Instead, as body size increases, both the projected and surface areas expand, which

gives the appearance of the pads becoming flatter, though in reality they retain their convexity while becoming broader.

This doesn't mean that small-bodied strepsirrhines do not benefit from their volar pads deforming incompletely from the application of body weight alone; that they do is still clearly indicated by the mathematics and this has been demonstrated physically by Cartmill (1979). What is indicated, however, and corroborated by the presence of narrow volar pads separated by ample space in small-bodied, non-grasping mammals is that this configuration is likely a retention of the primitive mammalian state rather than an adaptation or even optimization of this state that enhances the frictional properties of small primates' volar surfaces (Whipple, 1904; Haines, 1955, 1958; Biegert, 1959, 1961; Haffner, 1998; Hamrick, 2001; Sargis, 2001; Lemelin & Jungers, 2007; Lemelin & Schmitt, 2007).

5.6 Conclusions

Expansion of surface area is the primary means of friction adaptation for the volar surfaces as body mass increases in strepsirrhine primates, and changes in the morphology of both the pads and overlying skin that accomplish this are present. Most of the increase in surface area occurs on the proximal volar pads, which sit entirely upon the metapodial bones and are relatively unaffected by movement of the digits and proximal joints. The pads of the foot increase in size at a much faster rate than those of the hand, which likely reflects the differing roles of each cheiridium. The ridges of the volar skin become relatively narrower with increasing body size and provide a greater absolute surface area for large-bodied primates. The pattern of allometry in the volar pads agrees well with osteological features reported in the literature and should be considered when examining size and scaling of manual and pedal proportions.

Table 5.1. Correlation statistics for surface area and projected area. Coefficients for PGLS models are provided with corresponding maximum likelihood values for lambda transformations. Slopes compared to isometric model (1.00).

	R^2	Intercept	Slope	Std. Dev.	λ
Forelimb					
Thenar	0.99**	-0.39	1.00	0.04	0.00
Then/ID1	0.99**	-0.57	1.02	0.04	0.62
Hypothenar	0.99**	-0.41	1.00	0.02	0.00
ID1	0.97**	-0.59	0.99	0.07	0.00
ID2	0.97**	-0.64	**1.03****	0.04	0.00
ID3	0.99**	-0.40	**0.98***	0.03	0.91
ID4	0.99**	-0.61	**1.02****	0.02	0.00
Hindlimb					
Thenar	0.99**	-0.23	0.99	0.02	0.55
Hypothenar	0.99**	-0.21	0.97**	0.02	0.00
ID1	0.97**	-0.63	0.99	0.05	0.08
ID2	0.99**	-0.53	1.00	0.03	0.00
ID3	0.99**	-0.43	1.00	0.03	0.00
ID4	0.99**	-0.44	0.99*	0.02	0.09

** $p < 0.01$

* $p < 0.05$

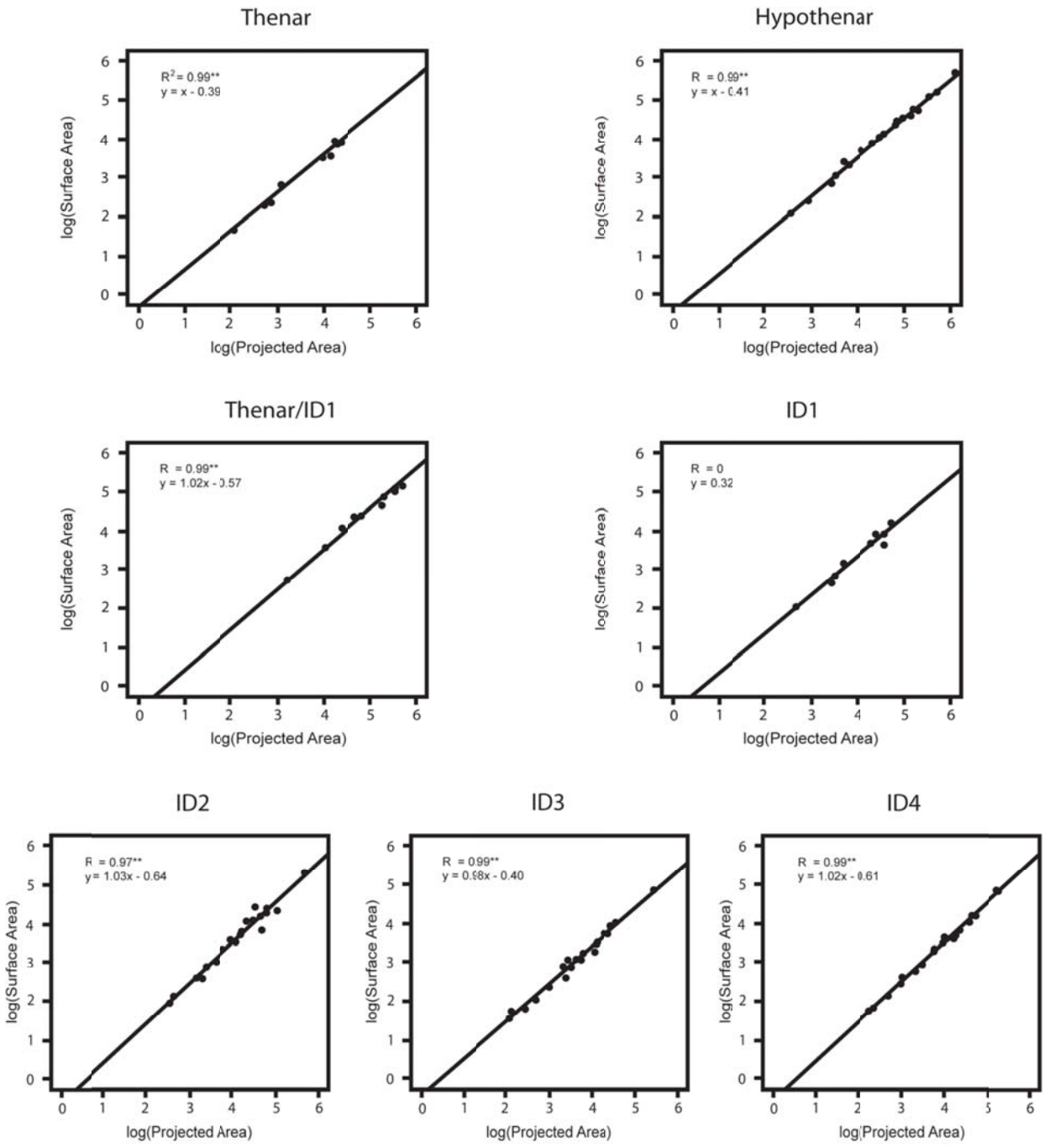

Figure 5.1a. PGLS regressions of surface area on projected area for forelimb volar pads. Correlation coefficients indicate a near perfect correlation between these variables for all manual volar pads.

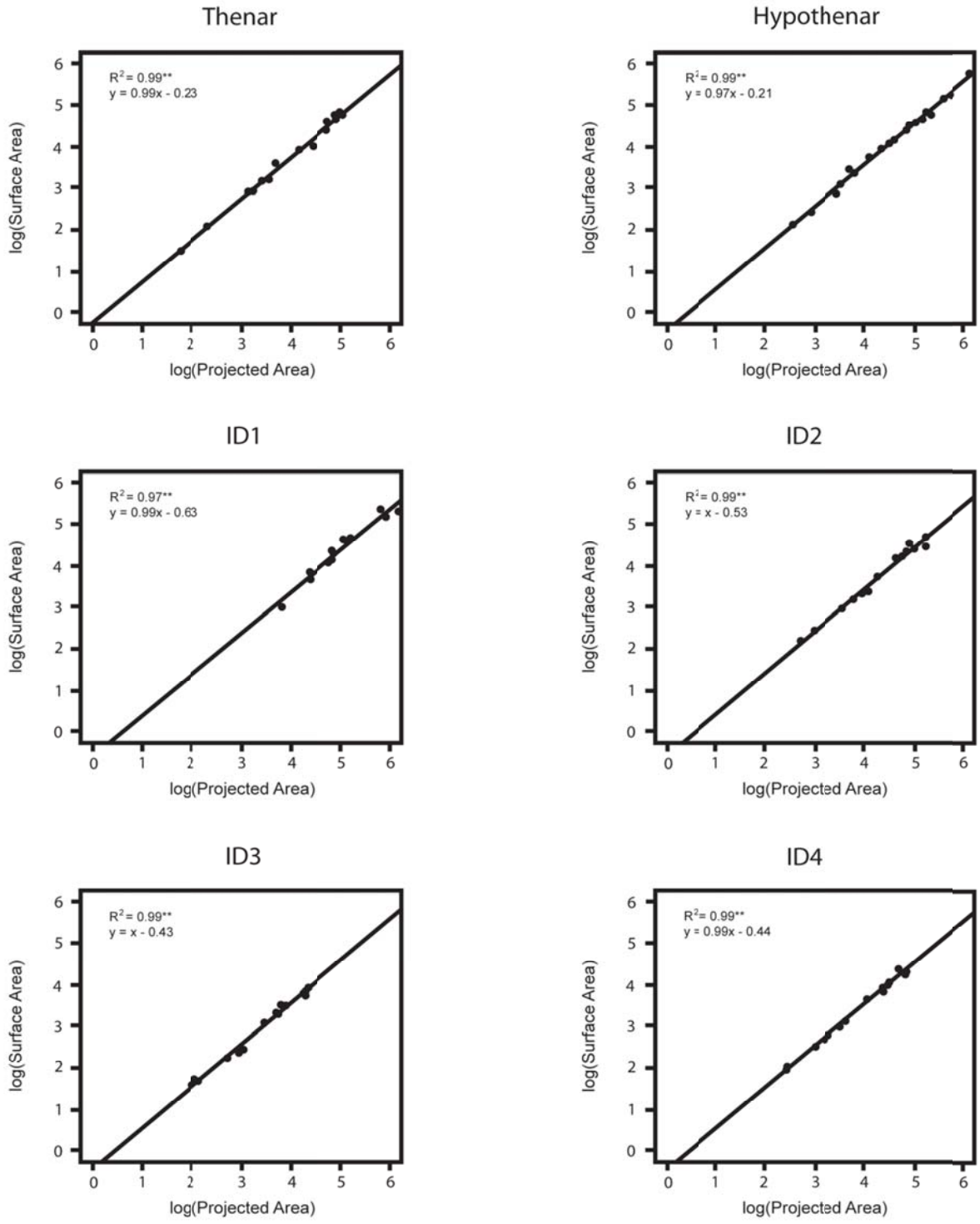

Figure 5.1b. PGLS regressions of surface area on projected area for hindlimb volar pads. Correlation coefficients indicate a near perfect correlation between these variables for all pedal volar pads.

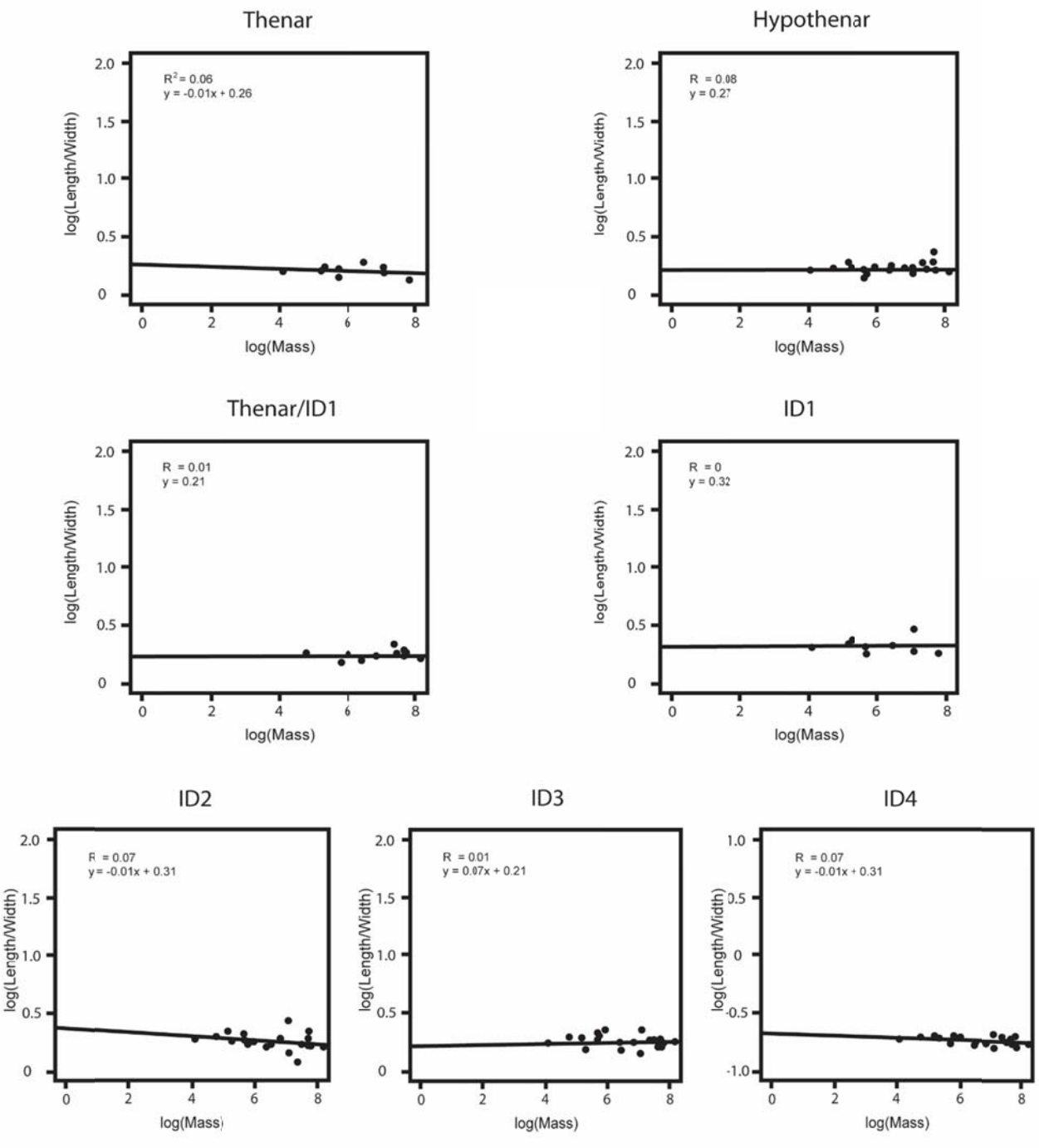

Figure 5.2a. PGLS regressions of relief index on body size for volar pads of the forelimb. Correlation coefficients indicate no relationship between relief index and body size for any of the manual volar pads.

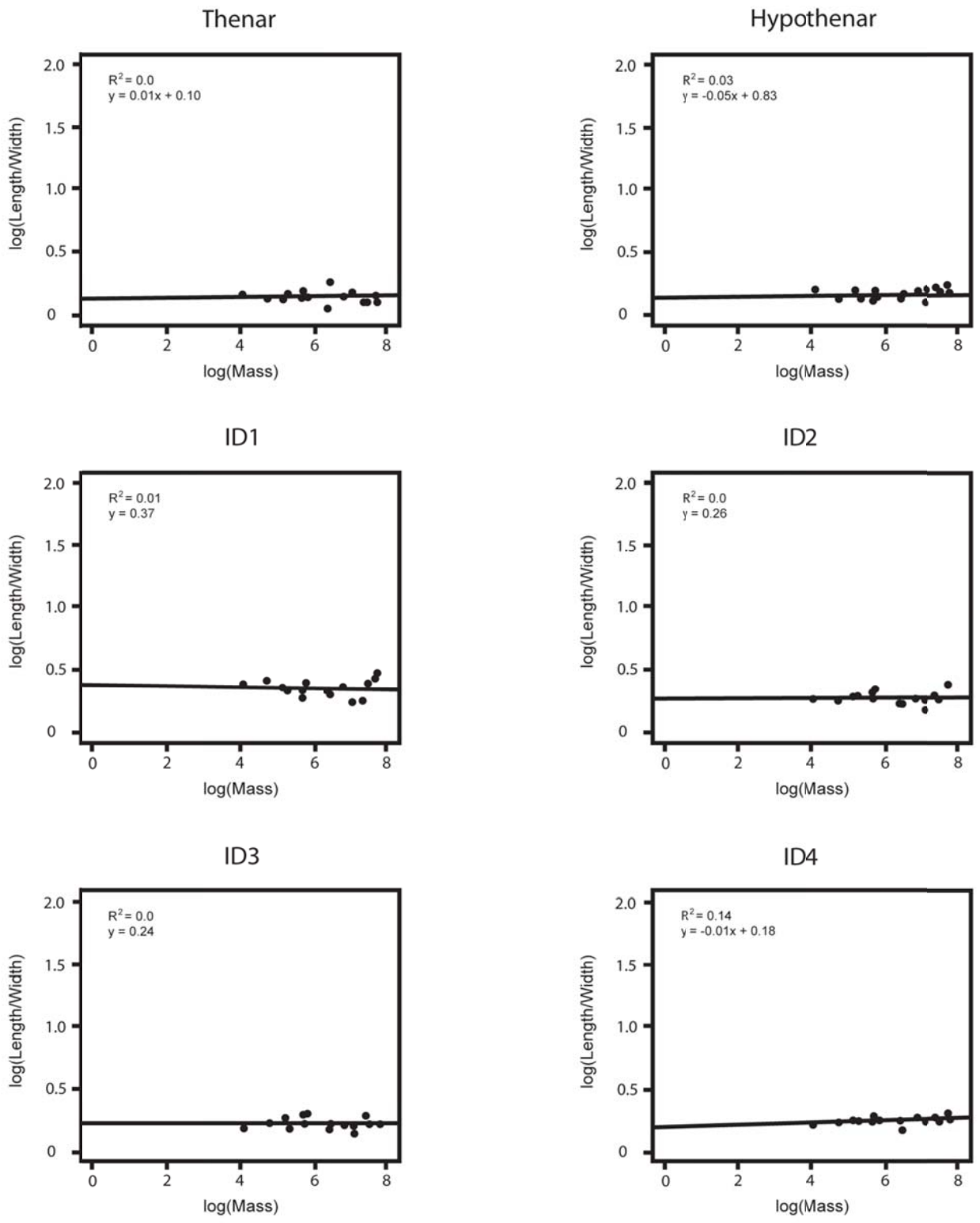

Figure 5.2b. PGLS regressions of relief index on mass for volar pads of the hindlimb. Correlation coefficients indicate no relationship between relief index and body size for any of the pedal volar pads.

Chapter 6:

Morphological Correlates of Locomotor Preference and Ecology in the Volar Pad

6.1 Summary

Discriminant analyses and post-hoc comparisons of the manual and pedal volar pad dimensions are carried out to test the hypothesis that different locomotor modes are associated with different pad morphologies. Manual thenar, first interdigital, and combined thenar/first interdigital pads are excluded from analysis as they are variably present. Significant differences in morphology are found between locomotor groups for both the manual and pedal pads; for cheirogaleid and lemurid taxa, these differences are heavily concentrated in the pedal pads whereas differences in the manual pads are found for galago and loris species. *Euoticus elegantulus*, the needle-clawed galago, exhibits unique volar morphology with significantly larger volar pads than those of other examined taxa. Lorises, in general, are characterized by short, wide pads along the margins of their volar surfaces and extremely reduced third interdigital pads. Large lemurid vertical clinging and leaping taxa exhibit distinct volar pad morphology from smaller galagid leapers that is likely attributable to their differently derived leaping mechanics and pedal morphology.

A major role of the volar pads in locomotion is presumed to be impact damping, and it is hypothesized that the relief of the pads should increase with impact forces experienced by locomotor groups, i.e., semi-terrestrial and leaping species would possess pads with greater relief than arboreal quadrupeds or slow climbers. This is not supported by the analysis; differences in volar pad relief are found to be related to mediolateral over-hang of the thenar and first interdigital pads in lorises.

The surface area of the volar pads is expected to be tightly correlated with the degree of frictional bonding the volar surfaces are capable of generating. It is therefore predicted that taxa experiencing greater shear forces during vertical locomotor behavior will possess greater total pad surface area in the hands and feet. That is, slow-climbing taxa and vertical clinging and leaping taxa should have the greatest total pad surface area. This prediction is partially supported; differences exist in pad surface area in the hand, but not in the foot. This is likely due to different, known roles of the hands and feet in primate locomotion.

The morphology of the volar pads is expected to be closely associated with the underlying bony morphology. In lemurid and cheirogaleid taxa with fused manual thenar and

first interdigital pads, the first metacarpal is correspondingly reduced. The short, wide pads possessed by lorises correlate with their hyper-ectaxonic hands and feet, relatively short metapodial bones, and reduced second digits. Differences in the volar pad morphology of large- and small-bodied vertical clinging and leaping taxa are also aligned with different pedal articulations and adaptions for leaping.

6.2 Results: Discriminant Function Analysis of the Forelimb Volar Pads

6.2.1 Discriminant Function Analysis.

It was predicted that members of each of the five defined locomotor categories would exhibit shared morphologies. Descriptive statistics for each of these locomotor categories are provided in Table 6.1. Discriminant analysis produced four functions that, together, significantly differentiate the five locomotor categories present in the study sample (Table 6.2). The eigenvalues associated with these functions are provided in Table 6.2 along with the percentage of the total variance accounted for by each function, the discriminant loading coefficients for each function, and multivariate test statistics for discriminatory ability. In all, these four functions were able to discriminate the input samples into their associated locomotor categories correctly 82.6% of the time; cross-validation brought this down to 62.8% (Table 6.3). The most commonly misidentified locomotor category is "Vertical Clinging and Leaping" with only 68.8% of individuals successfully classified in the analysis and 50% successfully classified during cross-validation. "Arboreal Quadrupeds" fared slightly better as a category with 84.8% of individuals correctly classified during analysis and 63% correctly assigned during cross-validation. These categories were most often misidentified as belonging to one another (Table 6.3), and substantial overlap between the groups is visually confirmed in Figure 6.1.

The eigenvalues for the discriminant functions are in general very low; only the first function has a value greater than one. This first function accounts for the majority of discriminating ability of the four functions (65.40%) and relies heavily on the widths of the hypothenar and third interdigital pads to discriminate between the slow climbing lorises and other species (Figure 6.1). *Lemur catta*, the only species that regularly engages in both arboreal and terrestrial locomotion, is partially separated from the remainder of the species by this function as well. Function two separates the nail-climbing needle-clawed galago, *Euoticus elegantulus,* from the rest of the sampled species and appears to discriminate on the widths and surface areas of the pads; the widths of all pads and the surface areas of the interdigital pads load significantly and positively on this function (Figure 6.1; Table 6.2.). Functions three and four possess very little discriminatory power and do not successfully isolate any of the locomotor groups.

6.2.2 Post-hoc comparisons

Discriminant function analysis is an extension of standard analysis of variance (ANOVA) and as such assesses groups for significant differences in a mathematically identical manner. The results of the ANOVA performed as part of the discriminant function analysis are provided in Table 6.4. Significant differences are present in all pads for one or more dimensions. Post-hoc comparisons were performed where indicated to assess differences between specific groups; these results are also provided in Table 6.4. By and large, these results mirror the discriminant function analysis. *Euoticus elegantulus*, the needle-clawed galago and single member of the nail-climbing group, shows significant differences for every examined pad; all of its pads are significantly wider and have significantly larger surface area than those of the other groups. The slow-climbing lorises are likewise quite distinct in their manual pad morphology; this group is largely defined by a narrow third interdigital pad with reduced surface area. Very few differences are found between arboreal quadrupeds and vertically clinging and leaping species, but vertical clinging and leaping species possess significantly longer second interdigital pads than arboreal quadrupeds. Semi-terrestrial species are characterized by narrow second interdigital pads. Examples of volar morphology for each locomotor group are illustrated in Figure 6.2.

6.3 Results: Discriminant Function Analysis of the Hindlimb Volar Pads

6.3.1 Discriminant Function Analysis

For the hindlimb volar surfaces, discriminant function analysis produced three functions that significantly differentiate the four locomotor groups represented in the sample. (No pedal samples of *Lemur catta* were available for analysis, thus the category "Semi-terrestrial Quadruped" was dropped.) Descriptive statistics for these groups are reported in Table 6.5. The eigenvalues associated with these functions are provided in Table 6.6 along with the percentage of the total variance accounted for by each function, the discriminant loading coefficients for each function, and multivariate test statistics for discriminatory ability. Classification and cross-validation percentages are provided in Table 6.7. The functions for the hindlimb volar surfaces were much more successful at discriminating between locomotor categories than those for the forelimb; overall, 98.3% of cases were correctly classified in the analysis and 78.8% were correctly classified during cross-validation. In the initial analysis, only one case was misclassified; this was an arboreal quadruped placed into the vertically clinging and leaping category. During cross validation, "Vertical Clinging and Leaping" was the most commonly misclassified group with 68.8% classified correctly; "Nail-Climbing" was correctly classified 100% of the time in both the initial analysis and cross-validation.

All eigenvalues for the discriminant functions are greater than one, and Wilks' lambda statistics confirm that each of the functions has significant discriminating ability (Table 6.6). The

first function isolates the slow climbing lorises from the remainder of the cases and discriminates primarily on the length of the hypothenar pad and the width and surface area of the third interdigital pad (Figure 6.3; Table 6.6). The second function isolates the arboreal quadrupeds from the vertical clinging and leaping taxa using the width and surface area of the thenar pad and the length of the second interdigital pad (Figure 6.3; Table 6.6). The third function isolates the nail climbing *Euoticus elegantulus* from the remainder of the group and partially separates the arboreal quadrupeds from the vertical clinging and leaping group. This function relies primarily on the width of the first interdigital pad and the length and surface area of the third interdigital pad to discriminate (Table 6.6).

6.3.2 Post-hoc Comparisons

Post-hoc comparisons were conducted where indicated by the ANOVA associated with the discriminant function analysis. The results of this ANOVA are provided in Table 6.8 along with the results of post-hoc comparisons. *Euoticus elegantulus* once again displays a unique pad morphology; all pedal volar pads have significantly greater surface areas than those of the other groups. The thenar and first interdigital pads are relatively wide in this taxon, whereas the third and fourth interdigital pads are long. Like in the hand, the slow-climbing lorises are again unique in their narrow, reduced third interdigital pads. The pedal hypothenar pad in this group is significantly wider and shorter than that of other locomotor groups, and the fourth interdigital pad has a significantly larger surface area. Arboreal quadrupeds and vertically clinging and leaping taxa are again very similar in their volar pad morphology; a long second interdigital pad separates the vertically clinging and leaping taxa. Examples of volar morphology for each locomotor group are illustrated in Figure 6.4.

6.4 Narrow Phylogenetic Comparisons

The “Arboreal Quadruped” and “Vertically Clinging and Leaping” locomotor groups comprise members of the both the superfamily Lemuroidea and family Galagidae. Shared phylogenetic history is known to result in shared, functionally-related features between closely related taxa that may be obscured when the greater group is examined; i.e., the vertically clinging and leaping galagos may have different adaptations to this form of locomotion than the vertically clinging and leaping lemurs. To address this, analysis of variance was conducted on body size standardized volar pad dimensions between these groups. Narrow phylogenetic comparisons reveal a greater number of differences in both the manual and pedal volar pads than the long second interdigital pad seen in the omnibus analysis.

6.4.1 Galagid Comparisons

Results of the analysis of variance for this clade are provided in Table 6.9 and examples of different morphologies are illustrated in Figure 6.5. In the hand, vertically clinging and leaping galagos are found to have a significantly larger first interdigital pad in all dimensions than arboreal quadrupeds. The length of the second interdigital pad is greater in the vertically clinging and leaping taxa as suggested by the previous analysis. The hypothenar and third and fourth interdigital pads are larger in arboreal quadrupeds and the fourth interdigital pad has a correspondingly larger surface area in these taxa.

In the foot, the second interdigital pad of vertical clinging and leaping galagos is indeed longer than the arboreal quadrupedal taxa, as indicated by the discriminant function analysis. The first interdigital pad is likewise long and the thenar pad is significantly wider in this group with a correspondingly large surface area. The hypothenar and fourth interdigital pads are significantly longer and possess larger surface areas in the arboreal quadruped group.

6.4.2 Lemuroid Comparisons

Results of the analysis of variance for this group are provided in Table 6.10 and examples of different morphologies are illustrated in Figure 6.6. No significant differences in manual volar pad dimensions are seen between the "Vertically Clinging and Leaping" and "Arboreal Quadruped" groups within Lemuroidea, suggesting the previous finding of a long pad in vertical clinging and leaping taxa as a whole was driven largely by galago morphology. In the foot, the thenar and hypothenar pads are significantly longer and have correspondingly greater surface area among the vertically clinging and leaping taxa. The second interdigital pad is also significantly longer in this group. The first interdigital pad, however, is significantly wider in arboreal quadruped taxa and has a greater surface area as well.

6.5 Results: Morphological Correlates of Impact Damping

An analysis of variance comparing the relief indices of corresponding volar pads across different locomotor groups was carried out. It was expected that groups experiencing higher impact forces would possess pads with greater relief to damp them with; specifically, the semi-terrestrial *Lemur catta* should possess pads with greater relief than members of the arboreal quadruped group, and the vertical clinging and leaping group should similarly possess pads with greater relief than arboreal quadrupeds. Pad relief was calculated by dividing the surface area of each pad by its projected area to produce a relief index; a larger index indicates greater pad relief. Results of the analysis of variance and post-hoc comparisons are provided in Table 6.11. Significant differences in the relief of the manual and pedal thenar and manual third interdigital pads and are found between the slow climbing lorises and the arboreal quadruped and vertical

clinging and leaping groups. Lorises possess a thenar pad with much greater relief than the other groups, and a third interdigital pad with significantly lower relief.

An analysis of variance comparing the relief indices of corresponding volar pads was similarly carried out for the hindlimb. Results of this analysis and post-hoc comparisons are provided in Table 6.12. Here, significant differences are found in the relief of the thenar and first interdigital pads. These are again attributable to differences between slow-climbing lorises and the arboreal quadruped and vertical clinging and leaping groups. Lorises again possess a thenar pad with high relief, but their first interdigital pad has significantly lower relief than that of the arboreal quadruped and vertical clinging and leaping groups. No significant differences in relief were found for pads of other locomotor groups.

The relief indices of the manual volar pads were compared via paired t-tests to those of the corresponding pedal pads in members of the vertical clinging and leaping locomotor group to test the hypothesis that differential loading regimes of the hand and foot are mitigated by a thicker pad in the foot, which bears the brunt of impact force during landing. Results of this analysis of variance are provided in Table 6.13. Significant differences were found between the manual and pedal indices of the thenar, hypothenar, and first interdigital pads. Of these, only the first interdigital pad shows higher relief in the foot; the other pads have greater relief in the hand.

6.6 Results: Surface Area and Arboreal Locomotion

The results of an analysis of variance comparing total pad surface area (the summed surface area of all volar pads) of the hand and foot between locomotor groups is presented in Table 6.14. Significant differences in total pad surface area were found in the hand, but not in the foot. In the hand, *Euoticus elegantulus* possesses a greater total surface area than all other taxa. The slow climbing lorises have the second greatest surface area, vertical clinging and leaping taxa the third, and arboreal quadrupedal and semi-terrestrial taxa the least.

6.7 Results: Fusion of Thenar and First Interdigital Pads in Lemuroids

It was hypothesized that the fusion of the thenar and first interdigital pads in the hand of lemurs was related to reduction of the first metacarpals. Taxa with fused pads were predicted to have a correspondingly shorter first metacarpals, which in turn was expected to make the surface area of the combined pad equal to that of the combined total surface area of the individual thenar and first interdigital pads of other taxa. The results of two analyses of variance testing both of these hypotheses are provided in Table 6.15. The first metatarsals of taxa with combined pads are significantly shorter than those with separate pads, but the surface area of the combined pad is significantly less than the combined surface areas of separate thenar and first interdigital pads.

6.8 Discussion

The manual volar surfaces of strepsirrhine primates are remarkably similar across Malagasy strepsirrhines, but differences are more apparent in their African relatives. The lorises and *Euoticus elegantulus* stand out as the most unique in the discriminant analysis—lorises in possessing relatively short, wide pads and *Euoticus* in having very large pads for its body size (Figures 6.2, 6.3). Vertically clinging and leaping galagos have large first interdigital pads, whereas arboreal quadrupedal taxa have longer and larger ulnar pads—the hypothenar and third and fourth interdigital pads are proximo-distally expanded (Figure 6.5). This configuration likely maximizes surface contact between the lateral part of the hand and the substrate during arboreal quadrupedalism. In quadrupedal galagos, the substrate is grasped between the first and third digits of the hand during locomotion with the second digit hyper-extended at the metacarpophalangeal joint, and several member of this group have been observed to grasp with a greater angle between the first and fourth digits than vertically clinging and leaping taxa (Bishop, 1964). Vertically clinging and leaping galagos use a similar grasp, but employ smaller angles between their first and fourth digits (Bishop, 1964; Lemelin & Schmitt, 2007). A smaller grasp angle "pinches" the substrate between the first and third digits; a wider grasp angle allows opposing forces to be generated by the fourth and fifth digits as well (Bishop, 1964; Gebo, 1985). The greater development of the volar pads along the hypothenar margin of the hand in quadrupedal galagos may reflect a larger role for these digits.

Lemurids and cheirogaleids have been observed to use grasping angles similar to those exhibited by vertically clinging and leaping galagos (Bishop, 1964). It is further likely that the similarity in the dimensions of the manual volar surface across locomotor groups in lemur taxa reflects a relatively unspecialized role for the hand in locomotion in this group. The decoupling of upper and hindlimb roles in primate locomotion has long been known, and has been observed in lemurs directly; the hind limb bears a significantly larger proportion of body weight during both terrestrial and arboreal locomotion and produces much of the necessary force to propel the body forward during quadrupedal walking, and upward during vertical climbing (Demes et. al., 1994; Larson, 1998; Schmitt, 1999; Schmitt & Hanna, 2004; Hanna et al., 2006; Hanna & Schmitt, 2011; Patel et al., 2015). Though this pattern applies to both terrestrial and arboreal primates, it is exaggerated during arboreal locomotion, where hind limb dominance is thought to facilitate exploration, testing of substrates, and foraging by the hands (Wood Jones, 1916; Napier, 1967; Cartmill, 1972; Sussman, 1991; Cartmill et al., 2002; Patel et al., 2015).

Quadrupedal locomotor mechanics are known for only some of the African strepsirrhine taxa, but may help to elucidate why this group shows significant differences in manual pad morphology between locomotor groups. Lorises are somewhat unusual in their quadrupedal walking mechanics and support a greater proportion of their weight on their forelimbs; this pattern is shared by *Callithrix jacchus*, a gummivorous platryrrhine with similar nail-clinging adaptations to those seen in *Euoticus elegantulus* (Schmitt & Lemelin, 2004). Gait mechanics of

Otolemur and *Galagoides* are unknown at present; further study may reveal additional specializations of the African group as well.

The foot of primates is highly specialized for grasping. The hallux is strongly divergent from the lateral digits and equipped with powerful flexor musculature that enables the grasp to anchor the body securely to arboreal substrates (Gebo, 1985, 2004; Boyer et al., 2007; Kingston et al., 2010). Experimental studies confirm this role; not only does the hind limb support a disproportionate amount of the body's mass in walking and climbing, electromyographical study has shown that the hind limb flexor muscles are more strongly recruited for a greater proportion of the step cycle than their fore limb counterparts in *Varecia variegata variegata*, and a recent analysis of forces has revealed that a greater proportion of normal force is applied to vertical substrates by the feet during clinging behaviors, which in turn supports a greater proportion of body mass against the pull of gravity (Patel et al., 2015; Johnson et al., 2014).

The pedal volar pads of strepsirrhine primates also show several specializations for grasping behaviors during locomotoion. Notable among these are a relatively long second interdigital pads among all vertical clinging and leaping species (Figure 6.7). Species included in this group engage in a specialized form of leaping between vertical supports wherein the feet are the last aspect of the body to lose contact with the substrate after take-off and the trunk is rotated during flight to bring them into position to be the first aspect to contact the landing support (Demes et al., 1996). The first and second interdigital pads surround the interval between the first and second pedal digits, where substrates are grasped during takeoff and landing. A longer second interdigital pad maximizes contact with the axis of a grasped substrate, which in turn increases frictional bonding, which is vital for maintaining a secure grasp amidst the mechanical forces involved in take-off and landing, and may also serve to buffer the second metatarsophalangeal joint while landing.

Specialization of the pads surrounding the cleft between the first and second toe is further seen in galagid vertical clinging and leaping taxa. The first interdigital pad is correspondingly long to form a grasp complex between the first and second digits and the thenar pad is large and wide (Table 6.7; Figure 6.5). Conversely, in quadrupedal galago taxa, it is the hypothenar and fourth interdigital pads that expand in size; the hypothenar and fourth interdigital pads are significantly longer and larger in this group, much like in the hand (Figure 6.5).

In lemurs, the thenar and hypothenar pads expand significantly in length and surface area in vertical clinging and leaping taxa (Figure 6.6). This difference between African and Malagasy taxa is likely related to differences in both the bony morphology of the foot and adaptations for leaping. Gebo (1985) describes two distinct tarsal articulations (Figure 6.7). A I-V grasp is found in African strepsirrhine taxa and cheirogaleids and is characterized by two distinct articular surfaces between the metatarsals and the cuboid and entocuneiform bones; this produces a relatively flat foot, where the first digit lies in the same plane as the opposing digits. A I-II grasp is found in lemurids and indriids and is characterized by a single articular surface spanning the cuboid, entocuneiform, and second metatarsal. This configuration is additionally associated with an oblique orientation of the first digit relative to the opposing digits, which brings the proximal

portion of the foot—where the thenar and hypothenar pads are located—into closer contact with a grasped substrate. The vertically clinging and leaping lemurs that utilize this grasp also possess derived hip and femoral morphologies that enables powerful leaping propelled by the thigh musculature, whereas adaptations for leaping in the smaller African taxa are found in the elongated tarsals (Oxnard et al., 1981a,b; Demes et al., 1995; Runestad Connour et al., 2000). Unlike the lemur taxa, where propulsive forces are generated at the hip and knee, and the foot plays little to no role, the galagid species use their elongated hind feet as a fulcrum to propel themselves (Demes et al., 1995, 1996). This leaves the forefoot to maintain a friction grasp until the leap is executed and may explain the expansion of the first and second interdigital pads in these taxa.

The pedal volar pads of the needle-clawed galago, *Euoticus elegantulus,* are exceptional among the examined taxa in their relatively large size (Table 6.8). Figure 6.4 shows the foot of *E. elegantulus* alongside *Nycticebus coucang,* which has a mass roughly twice that of *E. elegantulus* (Smith & Jungers, 1997). Previous work has acknowledged the uniqueness of this species' manual volar pads, and also found their projected area to be greater than average among galago species (Anderson, 1999). Here, the total size-standardized volar surface area for this species was found to be the largest among all compared groups (Table 6.14). Although this difference was found to be insignificant once phylogenetic history was accounted for, the pads provide a physically greater surface area for the body size of *Euoticus elegantulus* than those found in other groups and thus provide greater contact area during grasping and presumably improve frictional bonding. This is somewhat curious, considering the needle-clawed galago's unique locomotor repertoire, which includes using its keeled nails to interlock with the trunks of gum trees during feeding (Nash, 1986; Nash et al., 1989; Stephenson et al., 2010). It is worth noting that these keeled nails are not true claws and their precise role in clinging and climbing remains uninvestigated (Maiolino et al., in press). Although the keeled nails may provide additional security on supports that are too large to grasp, the expanded volar pads may also be a necessary adaptation to maintain frictional bonds.

The loris clade is similarly well-differentiated from the remainder of the examined taxa. Because these species are closely related, significant statistical results did not obtain from comparisons with more distantly related taxa utilizing phylogenetic comparative methods. In terms of absolute size comparisons, however, the pedal pads of lorises are quite distinctive (Table 6.6). They possess a thenar pad with a relatively large surface area and high relief, a wide first interdigital pad, and a drastically reduced and flattened third interdigital pad. These differences in volar pad morphology are almost certainly linked to the extreme derivation of their feet; all three species examined here possess an extremely ectaxonic, "pincer-like" foot with a markedly reduced second pedal digit, hyper-deviation of the hallux, and relatively short metatarsals for their body size (Grand, 1967; Gebo, 1985; Lemelin & Jungers, 2007). The wide first interdigital pad seen in these species correlates with the divergence of the first metatarsal, and the reduction of the third interdigital pad appears to be related to the reduction in metatarsal length forcing the second and fourth interdigital pads (which are not significantly different from

other groups examined here in size or shape) into the space it normally occupies. The high relief of the thenar pad appears to be linked to its position on the sole rather than to impact damping functions. In most species examined here, this pad is positioned proximally and slightly medial to the margin of the first metatarsal; in lorises, however, the first metatarsal is deviated to an extreme position, and the pad is positioned along its lateral margin, which produces substantial over-hang of the pad and a higher relief index. This relationship is illustrated in Figure 6.4 and likely serves to provide a greater contact surface for the deviated hallux to grip arboreal substrates.

That the relief index of the volar pads is not significantly different between groups or limbs experiencing different impact forces as part of their locomotor regime is surprising. The volar pads are capable of only partial impact damping, and additional shock attenuation has been documented as occurring in the bones and soft tissues of the leg and forearm (Paul et al., 1978; Aerts et al., 1995; Pain & Challis, 2001, 2006; Chi & Schmitt, 2005; Coventry et al., 2006). Further, specialized strepsirrhine leapers possess adaptations to lengthen the hindlimb and enable effective leaping without generation of the high take-off forces required by a generalist; this in turn reduces impact forces at landing that require attenuation (Demes et al., 1999). In light of these mechanisms, the role of the volar pads in impact damping remains important, but not untransmutable.

Slightly more surprising is the discrepancy in total volar pad surface area similarity between the hand and foot. Significant differences between locomotor groups are present in the manual volar pads, and these align well both with predictions of increased area correlating with reliance on friction grasping to counteract shear forces during locomotion and comparative studies of viverrid taxa (Cartmill, 1979, 1985; Veron, 1999). No significant differences are found in volar pad surface area in the foot, however. That no relationship between habitual locomotion and total volar surface area is evident here suggests that arboreal locomotion in and of itself may be the source of selection for pedal pad surface area, rather than any of its variations. As all non-human primates engage in some degree of arborealism for feeding, sleeping, or traveling, conservation of an adequate volar surface area to maintain frictional bonds is as vital for species that spend 10% of their day in the trees as it is for those who spend 100%.

Finally, the fusion of the manual thenar and first interdigital pads in cheirogaleid and lemuroid taxa is associated with significantly reduced length in the first metacarpals. It was hypothesized that this fusion might provide a greater pad surface area on this reduced bony platform than would be available from two separate pads. This may still be the case, but the overall surface area provided by the combined pads remains significantly smaller than that provided by individual thenar and first interdigital pads found in other taxa.

6.9 Conclusions

Several differences in volar morphology exist between locomotor groups. These differences are largely evident in the foot, which comports well with documented evidence of a larger role for the hind limb in primate locomotion. Nail-climbing *Euoticus elegantulus* possesses relatively large volar pads that may be related to its gummivorous dietary habits and the need to access gum flows on broad trunks. The volar morphology of lorises is highly derived and likely related to specializations of their overall pedal morphology. Differences between arboreal quadrupeds and vertical clinging and leaping species are few, but center around the first and second pedal interdigital pads where substrates are grasped. Despite these differences, an overall high level of conservatism is seen in the relief of the volar pads and the total volar surface areas for all groups.

Table 6.1. Descriptive statistics for manual volar pad dimensions. Group means have been calculated from body-size standardized measurements.

		N	Mean	SD	95% CI
Thenar					
Length	Arboreal Quadruped	9	0.67	0.01	0.59–0.76
	Vertical Clinging and Leaping	11	0.63	0.09	0.57–0.70
	Slow-climbing	16	0.63	0.10	0.57–0.69
	Nail-climbing	2	1.11	0.01	0.99–1.23
	Semi-terrestrial Quadruped	0	n/a	n/a	n/a
Width	Arboreal Quadruped	9	0.83	0.12	0.74–0.93
	Vertical Clinging and Leaping	11	0.90	0.15	0.80–1.00
	Slow-climbing	16	0.97	0.17	0.88–1.06
	Nail-climbing	2	1.12	0.17	-0.37–2.61
	Semi-terrestrial Quadruped	0	n/a	n/a	n/a
Surface Area	Arboreal Quadruped	9	0.53	0.14	0.43–0.64
	Vertical Clinging and Leaping	11	0.52	0.09	0.46–0.58
	Slow-climbing	16	0.71	0.23	0.59–0.83
	Nail-climbing	2	1.32	0.01	1.25–1.38
	Semi-terrestrial Quadruped	0	n/a	n/a	n/a
Relief	Arboreal Quadruped	9	1.21	0.05	1.17–1.25
	Vertical Clinging and Leaping	11	1.20	0.07	1.15–1.24
	Slow-climbing	16	1.29	0.08	1.24–1.33
	Nail-climbing	2	1.25	0.10	0.35–2.14
	Semi-terrestrial Quadruped	0	n/a	n/a	n/a
Th/ID1					
Length	Arboreal Quadruped	39	0.61	0.19	0.56–0.67
	Vertical Clinging and Leaping	5	0.53	0.02	0.50–0.55
	Slow-climbing	0	n/a	n/a	n/a
	Nail-climbing	0	n/a	n/a	n/a
	Semi-terrestrial Quadruped	6	0.47	0.06	0.41–0.54
Width	Arboreal Quadruped	39	0.48	0.13	0.43–0.52
	Vertical Clinging and Leaping	5	0.45	0.09	0.33–0.56
	Slow-climbing	0	n/a	n/a	n/a
	Nail-climbing	0	n/a	n/a	n/a
	Semi-terrestrial Quadruped	6	0.34	0.05	0.29–0.39
Surface Area	Arboreal Quadruped	39	0.41	0.18	0.35–0.47
	Vertical Clinging and Leaping	5	0.32	0.05	0.25–0.38
	Slow-climbing	0	n/a	n/a	n/a
	Nail-climbing	0	n/a	n/a	n/a
	Semi-terrestrial Quadruped	6	0.22	0.02	0.19–0.24
Relief	Arboreal Quadruped	39	1.29	0.08	1.26–1.31
	Vertical Clinging and Leaping	5	1.24	0.05	1.17–1.17
	Slow-climbing	0	n/a	n/a	n/a
	Nail-climbing	0	n/a	n/a	n/a
	Semi-terrestrial Quadruped	6	1.29	0.09	1.19–1.38

		N	Mean	SD	95% CI
Hypothenar					
Length	Arboreal Quadruped	47	0.52	0.13	0.49–0.56
	Vertical Clinging and Leaping	16	0.49	0.44	0.47–0.51
	Slow-climbing	16	0.51	0.06	0.48–0.54
	Nail-climbing	2	0.65	0.04	0.32–0.97
	Semi-terrestrial Quadruped	6	0.46	0.05	0.41–0.51
Width	Arboreal Quadruped	47	0.56	0.08	0.54–0.59
	Vertical Clinging and Leaping	16	0.56	0.09	0.51–0.61
	Slow-climbing	16	0.64	0.09	0.59–0.69
	Nail-climbing	2	0.70	0.02	0.55–0.85
	Semi-terrestrial Quadruped	6	0.49	0.05	0.44–0.54
Surface Area	Arboreal Quadruped	47	0.45	0.16	0.41–0.50
	Vertical Clinging and Leaping	16	0.40	0.07	0.35–0.44
	Slow-climbing	16	0.51	0.15	0.42–0.59
	Nail-climbing	2	0.73	0.03	0.44–1.03
	Semi-terrestrial Quadruped	6	0.34	0.08	0.26–0.43
Relief	Arboreal Quadruped	47	1.26	0.08	1.24–1.29
	Vertical Clinging and Leaping	16	1.26	0.09	1.21–1.31
	Slow-climbing	16	1.27	0.07	1.23–1.31
	Nail-climbing	2	1.24	0.07	0.59–1.89
	Semi-terrestrial Quadruped	6	1.23	0.06	1.16–1.31
ID1					
Length	Arboreal Quadruped	9	1.10	0.15	0.98–1.21
	Vertical Clinging and Leaping	11	1.30	0.22	1.15–1.45
	Slow-climbing	16	1.38	0.31	1.22–1.55
	Nail-climbing	2	1.65	0.15	0.30–2.99
	Semi-terrestrial Quadruped	0	n/a	n/a	n/a
Width	Arboreal Quadruped	9	0.97	0.10	0.88–1.05
	Vertical Clinging and Leaping	11	1.38	0.12	1.30–1.46
	Slow-climbing	16	1.39	0.36	1.19–1.58
	Nail-climbing	2	1.69	0.25	-0.58–3.95
	Semi-terrestrial Quadruped	0	n/a	n/a	n/a
Surface Area	Arboreal Quadruped	9	1.74	0.33	1.48–2.00
	Vertical Clinging and Leaping	11	2.16	0.41	1.88–2.44
	Slow-climbing	16	2.78	0.96	2.26–3.29
	Nail-climbing	2	3.95	0.10	3.01–4.89
	Semi-terrestrial Quadruped	0	n/a	n/a	n/a
Relief	Arboreal Quadruped	9	1.38	0.12	1.28–1.47
	Vertical Clinging and Leaping	11	1.35	0.09	1.29–1.41
	Slow-climbing	16	1.40	0.09	1.35–1.44
	Nail-climbing	2	1.36	0.15	0.03–2.70
	Semi-terrestrial Quadruped	0	n/a	n/a	n/a

		N	Mean	SD	95% CI
ID2					
Length	Arboreal Quadruped	47	0.46	0.13	0.42–0.50
	Vertical Clinging and Leaping	16	0.56	0.13	0.49–0.63
	Slow-climbing	16	0.55	0.12	0.49–0.62
	Nail-climbing	2	0.70	0.05	0.26–1.15
	Semi-terrestrial Quadruped	6	0.37	0.05	0.42–0.53
Width	Arboreal Quadruped	47	0.68	0.11	0.65–0.71
	Vertical Clinging and Leaping	16	0.62	0.08	0.57–0.66
	Slow-climbing	16	0.64	0.08	0.59–0.68
	Nail-climbing	2	0.91	0.09	0.19–1.63
	Semi-terrestrial Quadruped	6	0.74	0.11	0.65–0.84
Surface Area	Arboreal Quadruped	47	0.62	0.20	0.56–0.67
	Vertical Clinging and Leaping	16	0.62	0.18	0.52–0.72
	Slow-climbing	16	0.62	0.16	0.53–0.71
	Nail-climbing	2	1.26	0.13	0.05–2.46
	Semi-terrestrial Quadruped	6	0.52	0.07	0.45–0.59
Relief	Arboreal Quadruped	47	1.30	0.10	1.26–1.33
	Vertical Clinging and Leaping	16	1.36	0.10	1.30–1.42
	Slow-climbing	16	1.26	0.07	1.23–1.30
	Nail-climbing	2	1.30	0.10	0.83–1.77
	Semi-terrestrial Quadruped	6	1.25	0.10	1.17–1.32
ID3					
Length	Arboreal Quadruped	47	0.49	0.14	0.45–0.54
	Vertical Clinging and Leaping	16	0.49	0.08	0.44–0.53
	Slow-climbing	16	0.42	0.10	0.37–0.47
	Nail-climbing	2	0.66	0.20	-1.15–2.46
	Semi-terrestrial Quadruped	6	0.43	0.04	0.39–0.48
Width	Arboreal Quadruped	47	0.61	0.13	0.57–0.65
	Vertical Clinging and Leaping	16	0.54	0.12	0.47–0.60
	Slow-climbing	16	0.47	0.14	0.39–0.54
	Nail-climbing	2	0.88	0.01	0.83–0.92
	Semi-terrestrial Quadruped	6	0.67	0.09	0.58–0.76
Surface Area	Arboreal Quadruped	47	0.40	0.15	0.36–0.45
	Vertical Clinging and Leaping	16	0.33	0.09	0.29–0.39
	Slow-climbing	16	0.22	0.07	0.18–0.26
	Nail-climbing	2	0.72	0.06	0.18–1.27
	Semi-terrestrial Quadruped	6	0.32	0.05	0.27–0.38
Relief	Arboreal Quadruped	47	1.31	0.10	1.28–1.33
	Vertical Clinging and Leaping	16	1.31	0.11	1.25–1.36
	Slow-climbing	16	1.19	0.05	1.16–1.22
	Nail-climbing	2	1.31	0.08	0.19–1.33
	Semi-terrestrial Quadruped	6	1.23	0.08	1.19–1.28

		N	Mean	SD	95% CI
ID4					
Length	Arboreal Quadruped	47	0.82	0.20	0.76–0.87
	Vertical Clinging and Leaping	16	0.76	0.15	0.68–0.84
	Slow-climbing	16	0.68	0.10	0.63–0.74
	Nail-climbing	2	1.02	0.08	0.29–1.74
	Semi-terrestrial Quadruped	6	0.85	0.06	0.79–0.92
Width	Arboreal Quadruped	47	0.86	0.14	0.80–0.90
	Vertical Clinging and Leaping	16	0.80	0.17	0.71–0.89
	Slow-climbing	16	0.99	0.17	0.90–1.08
	Nail-climbing	2	1.33	0.34	-1.79–4.44
	Semi-terrestrial Quadruped	6	0.89	0.04	0.84–0.93
Surface Area	Arboreal Quadruped	47	0.44	0.12	0.40–0.47
	Vertical Clinging and Leaping	16	0.36	0.07	0.32–0.40
	Slow-climbing	16	0.47	0.12	0.41–0.53
	Nail-climbing	2	0.73	0.07	0.08–1.37
	Semi-terrestrial Quadruped	6	0.39	0.05	0.44–0.33
Relief	Arboreal Quadruped	47	1.31	0.08	1.29– 1.33
	Vertical Clinging and Leaping	16	1.29	0.08	1.24–1.33
	Slow-climbing	16	1.28	0.07	1.24–1.33
	Nail-climbing	2	1.26	0.05	1.26–1.32
	Semi-terrestrial Quadruped	6	1.26	0.05	1.27–1.31

Table 6.2. Results of discriminant function analysis of the forelimb volar pads. Structure matrix coefficients indicate loading of discriminating variables on functions; the highest loading values for each function are indicated in bold type.

		Function			
Descriptives		**1**	**2**	**3**	**4**
	Eigenvalue	2.56	0.64	0.52	0.20
	% of Variance	65.4	16.2	13.4	5.0
Structure Matrix		**1**	**2**	**3**	**4**
	Length	0.04	0.24	0.35	-0.48
Hypothenar	Width	-0.25	0.18	0.38	-0.20
	Surface Area	-0.11	**0.37**	0.42	-0.37
	Length	-0.19	-0.12	0.54	0.22
ID2	Width	0.16	**-0.54**	0.18	0.22
	Surface Area	0.00	**0.34**	0.72	0.14
	Length	0.12	0.04	0.37	-0.06
ID3	Width	**0.32**	**0.42**	0.25	0.13
	Surface Area	**0.34**	**0.28**	0.58	-0.23
	Length	0.24	0.27	0.21	0.24
ID4	Width	-0.18	**0.61**	0.33	0.19
	Surface Area	-0.09	**0.57**	0.39	-0.18
Test of Functions					
		Wilks' λ	**χ^2**	**df**	***p***
1 – 4		0.09	180.54	48	< 0.01
2 – 4		0.34	83.39	33	< 0.01
3 – 4		0.55	45.79	2	< 0.01
4		0.84	13.63	9	0.14

Table 6.3. Classification percentages for discriminant function analysis of the forelimb volar surfaces.

			Predicted Group Membership %				
		Total %	**AQ**	**VCL**	**SC**	**NC**	**TQ/AQ**
Arboreal Quadruped	Correct:	84.8	84.8	6.5	0	2.2	6.5
	Cross-val.	63.0	63.0	21.7	2.2	4.3	8.7
Vertical Clinging and Leaping	Correct:	68.8	18.8	68.8	6.3	0	6.3
	Cross-val.	50.0	18.8	50.0	12.5	6.3	12.5
Slow-climbing	Correct:	87.5	0	6.3	87.5	0	6.3
	Cross-val.	81.3	0	12.5	81.3	0	6.3
Nail-climbing	Correct:	100	0	0	0	100	0
	Cross-val.	0	100	0	0	0	0
Semi-terrestrial Quadruped	Correct:	83.3	16.7	0	0	0	83.3
	Cross-val.	66.7	33.3	0	0	0	66.7
Total	**Correct:**	**82.6**					
	Cross-val.	**62.8**					

Table 6.4. Analysis of variance results for forelimb pad dimensions and associated post-hoc comparisons. Post-hoc comparisons are nested below ANOVA statistics where applicable. Between-group differences are calculated from body-size standardized means.

		Sum of Squares	df	Mean Square	F	p
Hypothenar						
Length	Between Groups	0.07	4	0.02	1.67	0.17
	Within Groups	0.83	82	0.01		
	Total	0.90	86			
Width	Between Groups	0.15	4	0.04	5.41	**< 0.01***
	Within Groups	0.55	81	0.01		
	Total	0.70	85			
	Group A	**Group B**	**Difference (A – B)**	**SE**		**p**
	AQ	VCL	0.00	0.02		0.95
		SC	**-0.07**	**0.02**		**< 0.01***
		NC	-0.14	0.06		0.02
		ST	0.07	0.04		0.04
	VCL	**SC**	**-0.08**	**0.03**		**0.01***
		NC	-0.14	0.06		0.03
		ST	0.07	0.04		0.07
	SC	NC	-0.06	0.06		0.32
		ST	**0.15**	**0.04**		**< 0.01***
	NC	**ST**	**0.21**	**0.07**		**< 0.01***
Surface Area	Between Groups	0.32	4	0.08	4.18	**< 0.01***
	Within Groups	1.59	82	0.02		
	Total	1.91	86			
	Group A	**Group B**	**Difference (A – B)**	**SE**		**p**
	AQ	VCL	0.06	0.04		0.17
		SC	-0.53	0.04		0.19
		NC	**-0.28**	**0.10**		**< 0.01***
		ST	0.11	0.06		0.08
	VCL	**SC**	-0.11	0.05		0.03
		NC	**-0.34**	**0.10**		**< 0.01***
		ST	0.16	0.07		0.02
	SC	NC	-0.23	0.10		0.03
		ST	0.16	0.07		0.02
	NC	**ST**	**0.39**	**0.11**		**< 0.01***
		Sum of Squares	**df**	**Mean Square**	**F**	**p**
ID2						
Length	Between Groups	0.36	4	0.09	5.48	**< 0.01***
	Within Groups	1.33	82	0.02		
	Total	1.69	86			

		Sum of Squares	df	Mean Square	F	p
ID2 cont'd						
	Group A	**Group B**	**Difference (A – B)**	**SE**		**p**
	AQ	**VCL**	**-0.10**	**0.04**		**0.01***
		SC	-0.09	0.04		0.02
		NC	**-0.24**	**0.09**		**0.01***
		ST	0.20	0.06		0.08
	VCL	SC	0.01	0.05		0.89
		NC	-0.14	0.10		0.14
		ST	**0.20**	**0.06**		**< 0.01***
	SC	NC	-0.15	0.10		0.13
		ST	**0.19**	**0.06**		**< 0.01***
	NC	**ST**	**0.34**	**0.10**		**< 0.01***
Width	Between Groups	0.21	4	0.05	5.38	**< 0.01***
	Within Groups	0.82	82	0.10		
	Total	1.03	86			
	Group A	**Group B**	**Difference (A – B)**	**SE**		**p**
	AQ	VCL	0.06	0.03		0.04
		SC	0.04	0.03		0.14
		NC	**-0.23**	**0.07**		**< 0.01***
		ST	-0.07	0.04		0.13
	VCL	SC	-0.02	0.04		0.64
		NC	**-0.29**	**0.07**		**< 0.01***
		ST	**-0.13**	**0.04**		**0.01***
	SC	**NC**	**-0.28**	**0.07**		**< 0.01***
		ST	-0.11	0.05		0.03
	NC	**ST**	**0.17**	**0.08**		**< 0.01***
Surface Area	Between Groups	0.87	4	0.22	6.88	**< 0.01***
	Within Groups	2.60	82	0.03		
	Total	3.47	86			
	Group A	**Group B**	**Difference (A – B)**	**SE**		**p**
	AQ	VCL	0.00	0.05		0.95
		SC	0.00	0.05		0.98
		NC	**-0.64**	**0.13**		**< 0.01***
		ST	0.09	0.08		0.22
	VCL	SC	0.00	0.06		0.98
		NC	**-0.64**	**0.13**		**< 0.01***
		ST	0.10	0.09		0.26
	SC	**NC**	**-0.64**	**0.13**		**< 0.01***
		ST	0.10	0.09		0.26
	NC	**ST**	**0.74**	**0.15**		**< 0.01***

		Sum of Squares	df	Mean Square	F	p
ID3						
Length	Between Groups	0.14	4	0.04	2.33	0.06
	Within Groups	1.23	82	0.02		
	Total	1.37	86			
Width	Between Groups	0.51	4	0.13	8.08	< 0.01
	Within Groups	1.29	82	0.02		
	Total	1.80	86			
	Group A	**Group B**	**Difference (A – B)**	**SE**		**p**
	AQ	VCL	0.07	0.02		0.05
		SC	**0.14**	**0.02**		**< 0.01***
		NC	**-0.27**	**0.06**		**< 0.01***
		ST	-0.06	0.04		0.27
	VCL	SC	0.07	0.03		0.12
		NC	**-0.34**	**0.06**		**< 0.01***
		ST	-0.13	0.04		0.03
	SC	**NC**	**-0.41**	**0.06**		**< 0.01***
		ST	**-0.20**	**0.04**		**< 0.01***
	NC	ST	0.21	0.07		0.04
Surface Area	Between Groups	0.69	4	0.17	10.75	**< 0.01***
	Within Groups	1.32	82	0.02		
	Total	2.00	86			
	Group A	**Group B**	**Difference (A – B)**	**SE**		**p**
	AQ	VCL	0.07	0.04		0.06
		SC	**0.18**	**0.04**		**< 0.01***
		NC	**-0.32**	**0.09**		**< 0.01***
		ST	0.08	0.05		0.87
	VCL	**SC**	**0.12**	**0.04**		**0.01***
		NC	**-0.39**	**0.09**		**< 0.01***
		ST	0.01	0.06		0.87
	SC	**NC**	**-0.50**	**0.09**		**< 0.01***
		ST	-0.11	0.06		0.08
	NC	**ST**	**0.40**	**0.10**		**< 0.01***
		Sum of Squares	**df**	**Mean Square**	**F**	**p**
ID4						
Length	Between Groups	0.36	4	0.09	3.08	**0.02***
	Within Groups	2.36	82	0.03		
	Total	2.72	86			

		Sum of Squares	df	Mean Square	F	p
ID4 cont'd						
	Group A	**Group B**	**Difference (A – B)**	**SE**		**p**
	AQ	VCL	0.06	0.05		0.24
		SC	**0.13**	**0.05**		**< 0.01***
		NC	-0.20	0.12		0.10
		ST	-0.04	0.07		0.60
	VCL	SC	0.07	0.06		0.22
		NC	-0.26	0.13		0.04
		ST	-0.10	0.08		0.24
	SC	**NC**	**-0.33**	**0.13**		**0.01***
		ST	0.17	0.08		0.04
	NC	ST	0.16	0.14		0.24
Width	Between Groups	0.73	4	0.18	7.86	**< 0.01***
	Within Groups	1.89	82	0.02		
	Total	2.62	86			
	Group A	**Group B**	**Difference (A – B)**	**SE**		**p**
	AQ	VCL	0.07	0.04		0.14
		SC	**-0.13**	**0.04**		**< 0.01***
		NC	**-0.47**	**0.11**		**< 0.01***
		ST	-0.03	0.07		0.70
	VCL	**SC**	**-0.19**	**0.05**		**< 0.01***
		NC	**-0.53**	**0.11**		**< 0.01***
		ST	-0.09	0.07		0.22
	SC	**NC**	**-0.34**	**0.11**		**< 0.01***
		ST	0.10	0.07		0.16
	NC	**ST**	**0.44**	**0.12**		**< 0.01***
Surface Area	Between Groups	0.30	4	0.08	6.16	**< 0.01***
	Within Groups	0.99	82	0.01		
	Total	1.29	86			
	Group A	**Group B**	**Difference (A – B)**	**SE**		**p**
	AQ	VCL	0.08	0.03		0.02
		SC	-0.03	0.03		0.29
		NC	**-0.29**	**0.08**		**< 0.01***
		ST	0.05	0.04		0.32
	VCL	**SC**	**-0.11**	**0.04**		**< 0.01***
		NC	**-0.37**	**0.08**		**< 0.01***
		ST	-0.31	0.05		0.55
	SC	**NC**	**-0.26**	**0.08**		**< 0.01***
		ST	0.08	0.05		0.13
	NC	**ST**	**0.34**	**0.09**		**< 0.01***

Table 6.5. Descriptive statistics for pedal volar pad dimensions. Group means are calculated from body-size standardized measurements.

		N	Mean	SD	95% CI
Thenar					
Length	Arboreal Quadruped	28	0.55	0.13	0.50–0.61
	Vertical Clinging and Leaping	16	0.63	0.21	0.51–0.74
	Slow-climbing	13	0.58	0.10	0.52–0.64
	Nail-climbing	2	0.80	0.00	0.77–0.82
Width	Arboreal Quadruped	28	0.22	0.04	0.21–0.24
	Vertical Clinging and Leaping	16	0.26	0.05	0.23–0.28
	Slow-climbing	13	0.23	0.06	0.19–0.27
	Nail-climbing	2	0.39	0.03	0.08–0.70
Surface Area	Arboreal Quadruped	28	0.17	0.06	0.15–0.20
	Vertical Clinging and Leaping	16	0.23	0.06	0.20–0.27
	Slow-climbing	13	0.23	0.08	0.19–0.28
	Nail-climbing	2	0.41	0.02	0.20–0.62
Relief	Arboreal Quadruped	28	1.14	0.07	1.11–1.17
	Vertical Clinging and Leaping	16	1.15	0.06	1.12–1.19
	Slow-climbing	13	1.23	0.10	1.17–1.30
	Nail-climbing	2	1.15	0.04	0.83–1.46
Hypothenar					
Length	Arboreal Quadruped	29	0.52	0.11	0.47–0.56
	Vertical Clinging and Leaping	16	0.58	0.21	0.46–0.69
	Slow-climbing	13	0.37	0.07	0.37–0.41
	Nail-climbing	2	0.40	0.04	0.07–0.73
Width	Arboreal Quadruped	29	0.25	0.06	0.22–0.27
	Vertical Clinging and Leaping	16	0.27	0.04	0.25–0.29
	Slow-climbing	13	0.31	0.07	0.26–0.35
	Nail-climbing	2	0.36	0.11	-0.62–1.34
Surface Area	Arboreal Quadruped	29	0.11	0.03	0.10–0.12
	Vertical Clinging and Leaping	16	0.13	0.03	0.11–0.15
	Slow-climbing	13	0.09	0.03	0.08–0.11
	Nail-climbing	2	0.11	0.02	-0.04–0.26
Relief	Arboreal Quadruped	29	1.20	0.10	1.16–1.23
	Vertical Clinging and Leaping	16	1.21	0.08	1.16–1.25
	Slow-climbing	13	1.16	0.05	1.13–1.19
	Nail-climbing	2	1.14	0.03	0.83–1.44
ID1					
Length	Arboreal Quadruped	28	1.99	0.34	1.86 – 2.13
	Vertical Clinging and Leaping	16	2.17	0.39	1.96 – 2.39
	Slow-climbing	13	2.13	0.37	1.90 – 2.35
	Nail-climbing	2	2.32	0.15	0.94 – 3.71
Width	Arboreal Quadruped	28	1.13	0.18	1.06 – 1.20
	Vertical Clinging and Leaping	16	0.96	0.26	0.81 – 1.10
	Slow-climbing	13	1.16	0.23	1.02 – 1.29
	Nail-climbing	2	1.60	0.06	1.04 – 2.17

		N	Mean	SD	95% CI
ID1 con't					
Surface Area	Arboreal Quadruped	28	2.74	0.58	2.51 – 2.96
	Vertical Clinging and Leaping	16	2.38	0.85	1.93 – 2.84
	Slow-climbing	13	2.08	0.59	2.08 – 2.80
	Nail-climbing	2	3.17	0.17	1.68 – 4.66
Relief	Arboreal Quadruped	28	1.46	0.11	1.42 – 1.50
	Vertical Clinging and Leaping	16	1.42	0.07	1.38 – 1.46
	Slow-climbing	13	1.36	0.11	1.29 – 1.42
	Nail-climbing	2	1.36	0.10	0.30 – 1.40
ID2					
Length	Arboreal Quadruped	28	0.96	0.13	0.91–1.00
	Vertical Clinging and Leaping	16	1.09	0.10	1.03–1.15
	Slow-climbing	13	0.96	0.25	0.81–1.07
	Nail-climbing	2	1.25	0.02	1.11–1.39
Width	Arboreal Quadruped	28	0.69	0.28	0.58–0.80
	Vertical Clinging and Leaping	16	0.61	0.09	0.61–0.71
	Slow-climbing	13	0.92	0.15	0.83–1.01
	Nail-climbing	2	0.75	0.19	-0.95–2.44
Surface Area	Arboreal Quadruped	28	0.92	0.19	0.85–0.99
	Vertical Clinging and Leaping	16	1.04	0.14	0.97–1.12
	Slow-climbing	13	1.16	0.35	0.95–1.37
	Nail-climbing	2	1.39	0.26	-0.95–3.76
Relief	Arboreal Quadruped	28	1.31	0.10	1.27–1.34
	Vertical Clinging and Leaping	16	1.32	0.07	1.29–1.36
	Slow-climbing	13	1.27	0.09	1.22–1.32
	Nail-climbing	2	1.30	0.09	1.30 – 1.33
ID3					
Length	Arboreal Quadruped	28	0.77	0.11	0.72–0.81
	Vertical Clinging and Leaping	16	0.81	0.09	0.76–0.86
	Slow-climbing	13	0.74	0.71	0.70–0.78
	Nail-climbing	2	1.10	0.04	0.72–1.47
Width	Arboreal Quadruped	28	0.50	0.11	0.46–0.55
	Vertical Clinging and Leaping	16	0.48	0.11	0.42–0.53
	Slow-climbing	13	0.36	0.06	0.32–0.39
	Nail-climbing	2	0.61	0.17	-0.89–2.11
Surface Area	Arboreal Quadruped	28	0.38	0.08	0.34–0.41
	Vertical Clinging and Leaping	16	0.37	0.07	0.33–0.41
	Slow-climbing	13	0.23	0.05	0.20–0.26
	Nail-climbing	2	0.60	0.08	-0.10–1.29
Relief	Arboreal Quadruped	28	1.24	0.07	1.21–1.27
	Vertical Clinging and Leaping	16	1.29	0.11	1.23–1.35
	Slow-climbing	13	1.22	0.05	1.19–1.25
	Nail-climbing	2	1.25	0.10	1.23–1.27

		N	Mean	SD	95% CI
ID4					
Length	Arboreal Quadruped	28	0.84	0.15	0.78–0.90
	Vertical Clinging and Leaping	16	0.85	0.13	0.78–0.92
	Slow-climbing	13	0.93	0.19	0.82–1.05
	Nail-climbing	2	1.16	0.21	-0.76–3.08
Width	Arboreal Quadruped	28	0.52	0.13	0.47–0.57
	Vertical Clinging and Leaping	16	0.57	0.09	0.52–0.62
	Slow-climbing	13	0.56	0.09	0.51–0.62
	Nail-climbing	2	0.61	0.13	-0.54–1.75
Surface Area	Arboreal Quadruped	28	0.47	0.13	0.42–0.52
	Vertical Clinging and Leaping	16	0.46	0.09	0.41–0.51
	Slow-climbing	13	0.60	0.15	0.51–0.69
	Nail-climbing	2	0.61	0.00	0.60–0.62
Relief	Arboreal Quadruped	28	1.26	0.07	1.24–1.29
	Vertical Clinging and Leaping	16	1.29	0.09	1.25–1.34
	Slow-climbing	13	1.22	0.07	1.18–1.27
	Nail-climbing	2	1.26	0.05	1.24–1.28

Table 6.6. Results of discriminant function analysis of the pedal volar surface. Structure matrix coefficients indicate loading of discriminating variables on functions; the highest loading values for each function are indicated in bold type.

		Function		
Descriptives		**1**	**2**	**3**
	Eigenvalue:	7.50	2.59	1.99
	% of Variance:	62.1	21.4	16.4
Structure Matrix				
Thenar	Length	0.02	0.21	-0.03
	Width	0.04	**0.36**	-0.12
	Surface Area	-0.03	**0.45**	-0.12
Hypothenar	Length	0.18	-0.04	0.18
	Width	-0.10	0.23	-0.09
	Surface Area	0.12	0.09	0.15
ID1	Length	-0.02	0.17	0.05
	Width	-0.05	0.08	**-0.32**
	Surface Area	0.03	-0.01	-0.15
ID2	Length	0.08	**0.28**	0.03
	Width	-0.17	0.04	-0.06
	Surface Area	-0.09	0.24	-0.09
ID3	Length	0.12	**0.32**	-0.22
	Width	**0.21**	-0.03	-0.17
	Surface Area	**0.49**	0.05	**-0.27**
ID4	Length	-0.06	0.19	-0.18
	Width	-0.02	0.13	0.02
	Surface Area	-0.19	0.11	-0.09

Test of Functions	**Wilks' λ**	**χ^2**	**df**	***p***
1 – 3	0.01	216.53	54	**< 0.01**
2 – 3	0.09	113.83	34	**< 0.01**
3	0.34	52.50	16	**< 0.01**

Table 6.7. Classification percentages for discriminant function analysis of the pedal volar surface.

			Predicted Group Membership %			
		Total %	**AQ**	**VCL**	**SC**	**CC**
Arboreal Quadruped	Correct:	96.6	96.6	3.4	0	0
	Cross-val.	79.3	79.3	13.8	6.9	0
Vertical Clinging and Leaping	Correct:	100	0	100	0	0
	Cross-val.	68.8	31.3	68.8	0	0
Slow Climbing	Correct:	100	0	0	100	0
	Cross-val.	84.6	0	15.4	84.6	0
Nail-climbing	Correct:	100	0	0	0	100
	Cross-val.	100	0	0	0	100
Total	**Correct:**	**98.3**				
	Cross-val.	**78.3**				

Table 6.8. Analysis of variance results for hindlimb pad dimensions and associated post-hoc comparisons. Post-hoc comparisons are nested below ANOVA statistics where applicable. Between-group differences are calculated from body-size standardized means.

		Sum of Squares	df	Mean Square	F	p
Thenar						
Length	Between Groups	0.19	3	0.06	2.24	0.09
	Within Groups	1.57	56	0.03		
	Total	1.75	59			
Width	Between Groups	0.07	3	0.02	7.01	**< 0.01***
	Within Groups	0.19	56	0.00		
	Total	0.25	59			
	Group A	**Group B**	**Difference (A – B)**	**SE**		**p**
	AQ	VCL	-0.04	0.02		0.02
		SC	-0.02	0.02		0.29
		NC	**-0.17**	**0.04**		**< 0.01***
	VCL	SC	0.03	0.02		0.29
		NC	**-0.13**	**0.04**		**< 0.01***
	SC	NC	**-0.15**	**0.04**		**< 0.01***
Surface Area	Between Groups	0.15	3	0.05	10.45	**< 0.01***
	Within Groups	0.27	56	0.01		
	Total	0.42	59			
	Group A	**Group B**	**Difference (A – B)**	**SE**		**p**
	AQ	VCL	**-0.07**	**0.02**		**< 0.01***
		SC	**-0.07**	**0.02**		**< 0.01***
		NC	**-0.21**	**0.05**		**< 0.01***
	VCL	SC	0.00	0.03		0.97
		NC	**-0.18**	**0.05**		**< 0.01***
	SC	NC	**-0.18**	**0.05**		**< 0.01***
		Sum of Squares	**df**	**Mean Square**	**F**	**p**
Hypothenar						
Length	Between Groups	0.34	3	0.11	5.81	**< 0.01***
	Within Groups	1.10	56	0.02		
	Total	1.44	59			
	Group A	**Group B**	**Difference (A – B)**	**SE**		**p**
	AQ	VCL	-0.06	0.04		0.17
		SC	**0.15**	**0.05**		**< 0.01***
		NC	0.12	0.10		0.25
	VCL	SC	**0.21**	**0.05**		**< 0.01***
		NC	0.18	0.11		0.09
	SC	NC	-0.03	0.10		0.81

		Sum of Squares	df	Mean Square	F	p
Hypothenar cont'd						
Width	Between Groups	0.05	3	0.02	4.48	**< 0.01***
	Within Groups	0.20	56	0.00		
	Total	0.25	59			
	Group A	**Group B**	**Difference (A – B)**	**SE**		**p**
	AQ	VCL	-0.02	0.02		0.26
		SC	**-0.06**	**0.02**		**< 0.01***
		NC	**-0.11**	**0.04**		**0.02***
	VCL	SC	-0.04	0.02		0.09
		NC	-0.09	0.05		0.05
	SC	NC	-0.05	0.05		0.28
Surface Area	Between Groups	0.01	3	0.00		**0.02***
	Within Groups	0.05	56	0.00		
	Total	0.06	59			
	Group A	**Group B**	**Difference (A – B)**	**SE**		**p**
	AQ	VCL	-0.02	0.01		0.03
		SC	0.02	0.01		0.12
		NC	0.00	0.02		0.84
	VCL	SC	**0.04**	**0.01**		**< 0.01***
		NC	0.02	0.02		0.47
	SC	NC	-0.02	0.02		0.38
		Sum of Squares	**df**	**Mean Square**	**F**	**p**
ID1						
Length	Between Groups	0.91	3	0.30	1.52	0.22
	Within Groups	11.11	56	0.20		
	Total	12.02	59			
Width	Between Groups	0.88	3	0.29	4.38	**< 0.01***
	Within Groups	3.73	56	0.07		
	Total	4.61	59			
	Group A	**Group B**	**Difference (A – B)**	**SE**		**p**
	AQ	VCL	0.14	0.08		0.09
		SC	-0.06	0.09		0.46
		NC	**-0.51**	**0.19**		**< 0.01***
	VCL	SC	-0.20	0.09		0.04
		NC	**-0.65**	**0.19**		**< 0.01***
	SC	NC	-0.45	0.20		0.02
Surface Area	Between Groups	1.62	3	0.54	0.97	0.41
	Within Groups	31.27	56	0.56		
	Total	32.90	59			

		Sum of Squares	df	Mean Square	F	p
ID2						
Length	Between Groups	0.50	3	0.17	9.62	**< 0.01***
	Within Groups	0.96	56	0.02		
	Total	1.46	59			
	Group A	**Group B**	**Difference (A – B)**	**SE**		**p**
	AQ	VCL	**-0.14**	**0.04**		**< 0.01***
		SC	-0.01	0.04		0.88
		NC	**-0.30**	**0.10**		**0.01***
	VCL	SC	0.13	0.05		0.02
		NC	-0.16	0.10		0.19
	SC	NC	-0.29	0.10		0.02
Width	Between Groups	0.88	3	0.29	4.38	**< 0.01***
	Within Groups	3.73	56	0.07		
	Total	4.61	59			
	Group A	**Group B**	**Difference (A – B)**	**SE**		**p**
	AQ	VCL	0.04	0.06		0.56
		SC	**-0.22**	**0.07**		**< 0.01***
		NC	-0.05	0.15		0.75
	VCL	SC	**0.12**	**0.08**		**< 0.01***
		NC	-0.13	0.16		0.09
	SC	NC	**-0.25**	**0.16**		**< 0.01***
Surface Area	Between Groups	0.88	3	0.29	3.98	**0.01***
	Within Groups	4.12	56	0.07		
	Total	5.00	59			
	Group A	**Group B**	**Difference (A – B)**	**SE**		**p**
	AQ	VCL	-0.12	0.08		0.16
		SC	**-0.25**	**0.10**		**< 0.01***
		NC	-0.47	0.20		0.02
	VCL	SC	-0.13	0.10		0.19
		NC	-0.35	0.20		0.09
	SC	NC	-0.22	0.21		0.29
		Sum of Squares	**df**	**Mean Square**	**F**	**p**
ID3						
Length	Between Groups	0.27	3	0.09	6.52	**< 0.01***
	Within Groups	0.78	56	0.01		
	Total	1.05	59			

		Sum of Squares	df	Mean Square	F	p
ID3 cont'd						
	Group A	**Group B**	**Difference (A – B)**	**SE**		**p**
	AQ	VCL	-0.05	0.04		0.12
		SC	0.02	0.04		0.51
		NC	**-0.33**	**0.09**		**< 0.01***
	VCL	SC	0.07	0.04		0.06
		NC	**-0.29**	**0.09**		**< 0.01***
	SC	NC	**-0.36**	**0.09**		**< 0.01***
Width	Between Groups	1.05	3	0.35	20.82	**< 0.01***
	Within Groups	0.94	56	0.02		
	Total	1.99	59			
	Group A	**Group B**	**Difference (A – B)**	**SE**		**p**
	AQ	VCL	0.03	0.04		0.39
		SC	**0.14**	**0.04**		**< 0.01***
		NC	-0.10	0.09		0.18
	VCL	SC	**0.15**	**0.05**		**< 0.01***
		NC	-0.13	0.10		0.09
	SC	NC	**-0.25**	**0.10**		**< 0.01***
Surface Area	Between Groups	0.83	3	0.28	36.07	**< 0.01***
	Within Groups	0.43	56	0.01		
	Total	1.25	59			
	Group A	**Group B**	**Difference (A – B)**	**SE**		**p**
	AQ	VCL	0.00	0.03		0.92
		SC	**0.26**	**0.03**		**< 0.01***
		NC	**0.22**	**0.06**		**< 0.01***
	VCL	SC	**0.26**	**0.03**		**< 0.01***
		NC	**-0.22**	**0.07**		**< 0.01***
	SC	NC	**-0.48**	**0.07**		**< 0.01***
		Sum of Squares	**df**	**Mean Square**	**F**	**p**
ID4						
Length	Between Groups	0.22	3	0.08	3.52	**0.02***
	Within Groups	1.19	56	0.02		
	Total	1.41	59			
	Group A	**Group B**	**Difference (A – B)**	**SE**		**p**
	AQ	VCL	-0.01	0.05		0.79
		SC	-0.10	0.05		0.07
		NC	**-0.32**	**0.11**		**< 0.01***
	VCL	SC	-0.08	0.05		0.16
		NC	**-0.31**	**0.11**		**0.01***
	SC	NC	-0.23	0.11		0.06

		Sum of Squares	df	Mean Square	F	p
ID4 cont'd						
Width	Between Groups	0.15	3	0.05	1.29	0.29
	Within Groups	2.14	56	0.04		
	Total	2.29	59			
Surface Area	Between Groups	0.59	3	0.20	5.95	**< 0.01***
	Within Groups	1.85	56	0.03		
	Total	2.44	59			

	Group A	**Group B**	**Difference (A – B)**	**SE**	**p**
	AQ	VCL	0.01	0.06	0.84
		SC	**-0.23**	**0.06**	**< 0.01***
		NC	-0.14	0.13	0.29
	VCL	SC	**-0.26**	**0.07**	**< 0.01***
		NC	-0.15	0.14	0.27
	SC	NC	0.09	0.14	0.50

Table 6.9. Analysis of variance results for pad dimensions of arboreal quadruped and vertical clinging and leaping galagids. Means are calculated from body-size standardized measurements.

		Standardized Group Means (SD)		df	F	p
		AQ	VCL			
ANOVA: Manual Pads		**N = 8**	**N = 11**			
	Length	0.68 (0.12)	0.63 (0.09)	18	0.75	0.40
Thenar	Width	0.85 (0.12)	0.90 (0.14)	18	0.57	0.46
	Surface Area	0.55 (0.13)	0.52 (0.09)	18	0.47	0.50
	Length	**0.56 (0.08)**	**0.49 (0.04)**	**18**	**5.39**	**0.03***
Hypothenar	Width	0.58 (0.04)	0.56 (0.08)	18	0.48	0.50
	Surface Area	0.43 (0.08)	0.41 (0.07)	18	0.46	0.51
	Length	**1.11 (0.15)**	**1.30 (0.22)**	**18**	**4.30**	**0.05***
ID1	**Width**	**0.96 (0.11)**	**1.38 (0.12)**	**18**	**61.88**	**< 0.01***
	Surface Area	**1.78 (0.33)**	**2.16 (0.41)**	**18**	**4.53**	**0.04***
	Length	**0.46 (0.08)**	**0.63 (0.08)**	**18**	**6.38**	**< 0.01***
ID2	Width	0.65 (0.06)	0.62 (0.09)	18	1.12	0.31
	Surface Area	0.74 (0.06)	0.67 (0.19)	18	0.76	0.40
	Length	**0.61 (0.06)**	**0.52 (0.07)**	**18**	**7.55**	**0.01***
ID3	Width	0.56 (0.09)	0.53 (0.11)	18	0.52	0.48
	Surface Area	0.39 (0.04)	0.34 (0.09)	18	2.17	0.16
	Length	**0.86 (0.08)**	**0.73 (0.16)**	**18**	**4.31**	**0.05***
ID4	Width	0.90 (0.09)	0.81 (0.18)	18	1.83	0.19
	Surface Area	**0.47 (0.06)**	**0.35 (0.02)**	**18**	**14.91**	**< 0.01***
		Standardized Group Means		**df**	**F**	**p**
		AQ	VCL			
ANOVA: Pedal Pads		**N = 10**	**N = 10**			
	Length	0.44 (0.18)	0.50 (0.06)	19	1.14	0.30
Thenar	**Width**	**0.20 (0.07)**	**0.29 (0.03)**	**19**	**12.37**	**< 0.01***
	Surface Area	**0.13 (0.06)**	**0.22 (0.03)**	**19**	**16.32**	**< 0.01***
	Length	**0.50 (0.05)**	**0.44 (0.05)**	**19**	**6.82**	**0.02***
Hypothenar	Width	0.29 (0.03)	0.28 (0.03)	19	0.51	0.48
	Surface Area	**0.14 (0.02)**	**0.11 (0.02)**	**19**	**5.03**	**0.04***
	Length	**1.59 (0.59)**	**2.36 (0.30)**	**19**	**13.70**	**< 0.01***
ID1	Width	1.16 (0.41)	1.11 (0.20)	19	0.10	0.76
	Surface Area	2.60 (1.01)	2.88 (0.58)	19	0.57	0.50
	Length	**1.04 (0.13)**	**1.13 (0.08)**	**19**	**4.98**	**0.05***
ID2	**Width**	**0.77 (0.08)**	**0.68 (0.09)**	**19**	**5.39**	**0.03***
	Surface Area	1.07 (0.19)	1.08 (0.16)	19	0.00	0.98
	Length	0.79 (0.09)	0.79 (0.09)	19	0.00	0.99
ID3	Width	0.51 (0.09)	0.48 (0.10)	19	0.47	0.50
	Surface Area	0.37 (0.05)	0.36 (0.06)	19	0.02	0.90
	Length	**0.91 (0.11)**	**0.78 (0.09)**	**19**	**7.29**	**0.02***
ID4	Width	0.55 (0.09)	0.61 (0.08)	19	2.68	0.12
	Surface Area	**0.55 (0.09)**	**0.42 (0.08)**	**19**	**12.13**	**< 0.01***

Table 6.10. Analysis of variance results for pad dimensions of arboreal quadruped and vertical clinging and leaping lemuroid taxa. Means are calculated from body-size standardized measurements.

		Standardized Group Means		df	F	p
		AQ	VCL			
ANOVA: Manual Pads		**N = 38**	**N = 5**			
Thenar/ID1	Length	0.63 (0.16)	0.53 (0.02)	42	1.97	0.17
	Width	0.48 (0.13)	0.45 (0.09)	42	0.23	0.64
	Surface Area	0.41 (0.18)	0.32 (0.05)	42	1.25	0.27
Hypothenar	Length	0.53 (0.10)	0.49 (0.06)	42	0.81	0.37
	Width	0.56 (0.09)	0.52 (0.09)	42	1.17	0.29
	Surface Area	0.47 (0.15)	0.38 (0.08)	42	1.65	0.21
ID2	Length	0.43 (0.11)	0.40 (0.03)	42	0.31	0.58
	Width	0.69 (0.11)	0.63 (0.09)	42	1.34	0.25
	Surface Area	0.60 (0.20)	0.50 (0.07)	42	1.21	0.28
ID3	Length	0.42 (0.14)	0.47 (0.06)	42	0.57	0.45
	Width	0.62 (0.13)	0.55 (0.16)	42	1.22	0.28
	Surface Area	0.41 (0.17)	0.33 (0.11)	42	1.13	0.30
ID4	Length	0.78 (0.15)	0.82 (0.09)	42	0.36	0.55
	Width	0.85 (0.15)	0.77 (0.15)	42	1.46	0.23
	Surface Area	0.42 (0.13)	0.39 (0.06)	42	0.41	0.53
		Standardized Group Means		**df**	**F**	**p**
		AQ	VCL			
ANOVA: Pedal Pads		**N = 19**	**N = 6**			
Thenar	**Length**	**0.59 (0.14)**	**0.83 (0.21)**	**24**	**10.53**	**< 0.01***
	Width	0.22 (0.05)	0.22 (0.02)	24	0.43	0.52
	Surface Area	**0.19 (0.06)**	**0.26 (0.09)**	**24**	**4.95**	**0.04***
Hypothenar	**Length**	**0.53** (0.14)	**0.81 (0.16)**	**24**	**18.77**	**< 0.01***
	Width	0.22 (0.06)	0.24 (0.03)	24	0.67	0.42
	Surface Area	**0.16 (0.02)**	**0.11 (0.03)**	**24**	**33.74**	**< 0.01***
ID1	Length	2.10 (0.35)	1.86 (0.34)	24	2.20	0.15
	Width	**1.06 (0.16)**	**0.69 (0.08)**	**24**	**27.67**	**< 0.01***
	Surface Area	**2.67 (0.62)**	**1.56 (0.48)**	**24**	**15.69**	**< 0.01***
ID2	**Length**	**0.90 (0.10)**	**1.03 (0.10)**	**24**	**7.24**	**0.01***
	Width	0.66 (0.32)	0.62 (0.09)	24	0.06	0.81
	Surface Area	0.84 (0.12)	0.99 (0.08)	24	6.69	0.02
ID3	Length	0.75 (0.11)	0.84 (0.09)	24	3.33	0.08
	Width	0.50 (0.12)	0.46 (0.17)	24	0.40	0.53
	Surface Area	0.38 (0.09)	0.38 (0.06)	24	0.03	0.87
ID4	Length	0.80 (0.16)	0.96 (0.09)	24	5.34	0.03
	Width	0.51 (0.15)	0.49 (0.04)	24	0.07	0.79
	Surface Area	0.43 (0.13)	0.53 (0.08)	24	2.81	0.11

Table 6.11. Analysis of variance results for manual pad relief. Between-group differences are calculated from raw relief indices.

		Sum of Squares	df	Mean Square	F	p
Thenar						
Relief	Between Groups	0.07	3	0.02	3.94	**0.02***
	Within Groups	0.19	34	0.01		
	Total	0.26	37			
	Group A	**Group B**	**Difference (A – B)**	**SE**		**p**
	AQ	VCL	0.01	0.03		0.70
		SC	**-0.08**	**0.03**		**0.01***
		NC	-0.04	0.06		0.53
	VCL	**SC**	**0.03**	**0.03**		**< 0.01***
		NC	-0.05	0.06		0.39
	SC	NC	0.04	0.06		0.47
ThID1						
Relief	Between Groups	0.01	1	0.01	1.43	0.24
	Within Groups	0.30	47	0.01		
	Total	0.31	48			
Hypothenar						
Relief	Between Groups	0.00	3	0.00	0.10	0.96
	Within Groups	0.55	81	0.01		
	Total	0.55	84			
ID1						
Relief	Between Groups	0.01	3	0.01	0.46	0.72
	Within Groups	0.35	34	0.01		
	Total	0.36	37			
ID2						
Relief	Between Groups	0.07	3	0.02	2.86	0.06
	Within Groups	0.78	82	0.01		
	Total	0.86	85			
ID3						
Relief	Between Groups	0.16	3	0.54	6.73	**< 0.01***
	Within Groups	0.67	83	0.01		
	Total	0.83	86			

ID3 cont'd

	Group A	Group B	Difference (A – B)	SE		p
	AQ	VCL	0.00	0.03		0.99
		SC	**0.11**	**0.03**		**< 0.01**
		NC	-0.05	0.06		0.45
		ST	0.07	0.04		0.06
	VCL	**SC**	**0.11**	**0.03**		**< 0.01**
		NC	-0.05	0.07		0.46
		ST	0.07	0.04		0.09
	SC	NC	-0.16	0.07		0.02
		ST	-0.04	0.04		0.34
	NC	ST	0.12	0.07		0.09

ID4

		Sum of Squares	df	Mean Square	F	p
Relief	Between Groups	0.01	3	0.01	0.82	0.49
	Within Groups	0.48	83	0.01		
	Total	0.49	86			

Table 6.12. Analysis of variance results for pedal pad relief. Between-group differences are calculated from raw relief indices.

		Sum of Squares	df	Mean Square	F	p
Thenar						
Relief	Between Groups	0.78	2	0.04	6.87	**< 0.01***
	Within Groups	0.32	57	0.01		
	Total	0.40	59			
	Group A	**Group B**	**Difference (A – B)**	**SE**		**p**
	AQ	VCL	-0.01	0.02		0.66
		SC	**-0.09**	**0.02**		**< 0.01**
		NC	-0.01	0.06		0.98
	VCL	**SC**	**-0.08**	**0.03**		**<0.01**
		NC	0.01	0.06		0.88
	SC	NC	0.09	0.06		0.13
Hypothenar						
Relief	Between Groups	0.02	2	0.01	1.48	0.24
	Within Groups	0.42	57	0.01		
	Total	0.44	59			
ID1						
Relief	Between Groups	0.09	2	0.05	4.84	0.01
	Within Groups	0.54	56	0.01		
	Total	0.64	58			
	Group A	**Group B**	**Difference (A – B)**	**SE**		**p**
	AQ	VCL	0.05	0.03		0.12
		SC	**0.11**	**0.03**		**< 0.01**
		NC	0.14	0.07		0.06
	VCL	**SC**	0.06	0.03		0.07
		NC	0.11	0.07		0.13
	SC	NC	0.05	0.07		0.53
ID2						
Relief	Between Groups	0.02	2	0.01	1.56	0.22
	Within Groups	0.42	56	0.01		
	Total	0.43	58			
ID3						
Relief	Between Groups	0.03	2	0.02	2.45	0.10
	Within Groups	0.38	56	0.01		
	Total	0.41	58			
ID4						
Relief	Between Groups	0.03	2	0.17	3.03	0.06
	Within Groups	0.32	57	0.01		
	Total	0.35	59			

Table 6.13. Paired t-test results of manual and pedal relief index comparisons in vertical clinging and leaping species. Means are calculated from raw relief indices.

Pad (n = 21)	Mean (Hand-Foot)	SD	95% CI		t	*p*
Thenar	0.17	0.24	0.07	0.28	**3.40**	**< 0.01**
Hypothenar	0.13	0.27	0.01	0.26	**2.33**	**0.03**
ID1	-0.29	0.26	-0.41	-0.17	-0.33	0.80
ID2	0.09	0.29	-0.03	0.23	1.56	0.13
ID3	0.06	0.22	-0.05	0.16	1.16	0.26
ID4	-0.02	0.23	-0.12	0.09	-0.31	0.76

Table 6.14. Analysis of variance results and post-hoc comparisons for total volar surface area. Post-hoc comparisons are nested with associated ANOVA results. Means and between-group differences are calculated from body-size standardized measurements.

	Group Means	SD	95% CI	n	F	p
Manual	AQ: 2.68	1.03	2.87–4.10	47	27.66	**< 0.01***
	VCL: 3.65	1.37	2.78–3.73	16		
	SC: 5.30	1.58	1.69–5.47	16		
	NC: 8.71	0.07	2.06–9.93	2		
	ST: 3.07	0.12	1.29–4.56	6		
	Group A	**Group B**	**Difference (A – B)**	**SE**		**p**
	AQ	**VCL**	**-0.97**	**0.34**		**< 0.01***
		SC	**-2.62**	**0.34**		**< 0.01***
		NC	**-6.04**	**0.85**		**< 0.01***
		ST	0.87	0.51		0.09
	VCL	**SC**	**-1.65**	**0.41**		**< 0.01***
		NC	**-5.06**	**0.88**		**< 0.01***
		ST	**1.85**	**0.56**		**< 0.01***
	SC	**NC**	**-3.41**	**0.88**		**< 0.01***
		ST	**3.50**	**0.57**		**< 0.01***
	NC	**ST**	**6.91**	**0.96**		**< 0.01***
	Group Means	**SD**	**95% CI**	**n**	**F**	**p**
Pedal	AQ: 4.69	1.03	4.29–5.08	29	1.64	0.19
	VCL: 4.62	0.87	4.16–5.08	16		
	SC: 4.76	1.20	4.04–5.49	13		
	NC: 6.30	0.55	1.38–11.22	2		

Table 6.15. Analysis of variance results for association of fused thenar/ID1 pad and metatarsal length and comparison of fused and unfused pad areas. Means are calculated from body-size standardized measurements.

		Means	Std. Dev.	95% CI	n	F	p
Metacarpal Length	Thenar & ID1	1.76	0.19	1.59–1.93	7	25.81	< 0.01*
	Thenar/ID1	1.28	0.19	1.13–1.42	9		
Pad Area	Thenar & ID1	2.21	0.68	2.03–2.42	50	132.23	< 0.01*
	Thenar/ID1	4.97	1.51	4.53–5.53	37		

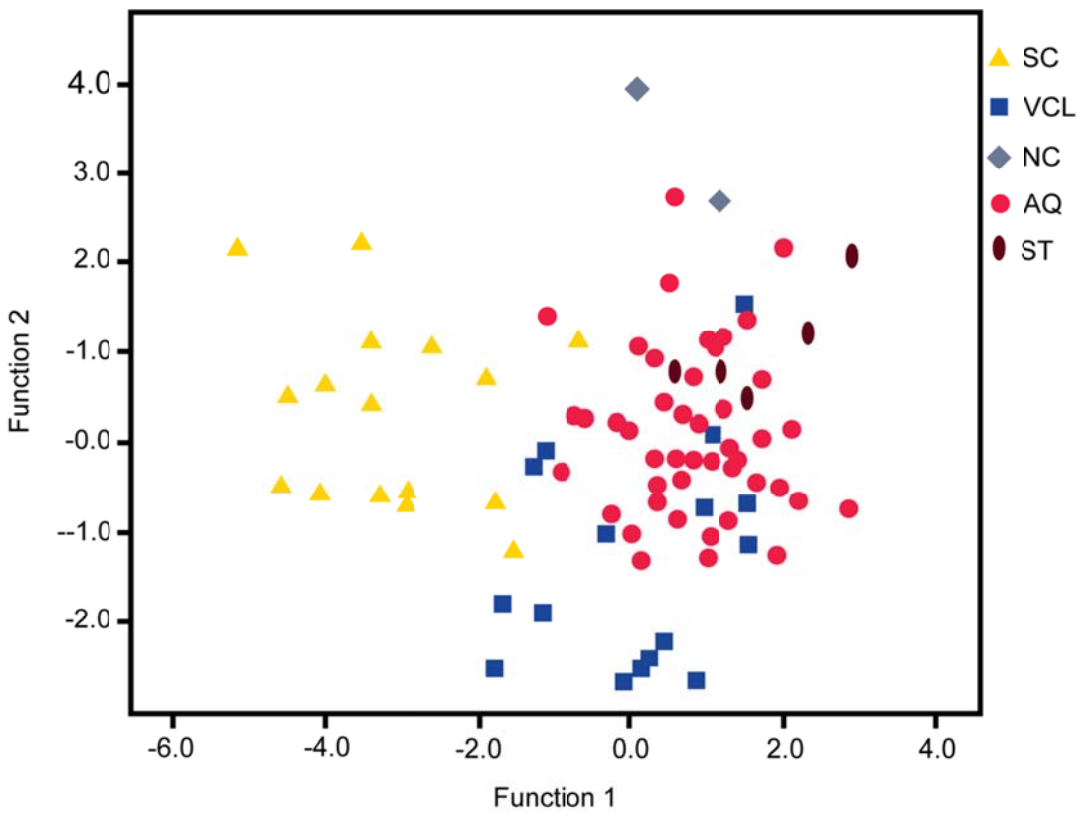

Figure 6.1. Plot of forelimb discriminant scores for functions one and two. Function one separates the slow-climbing lorises from the remaining species on the basis of their short, broad pads. The nail-climbing *Euoticus* is separated from the remaining species by function two on the basis of its large pads whereas the remaining taxa remain largely clustered on both functions.

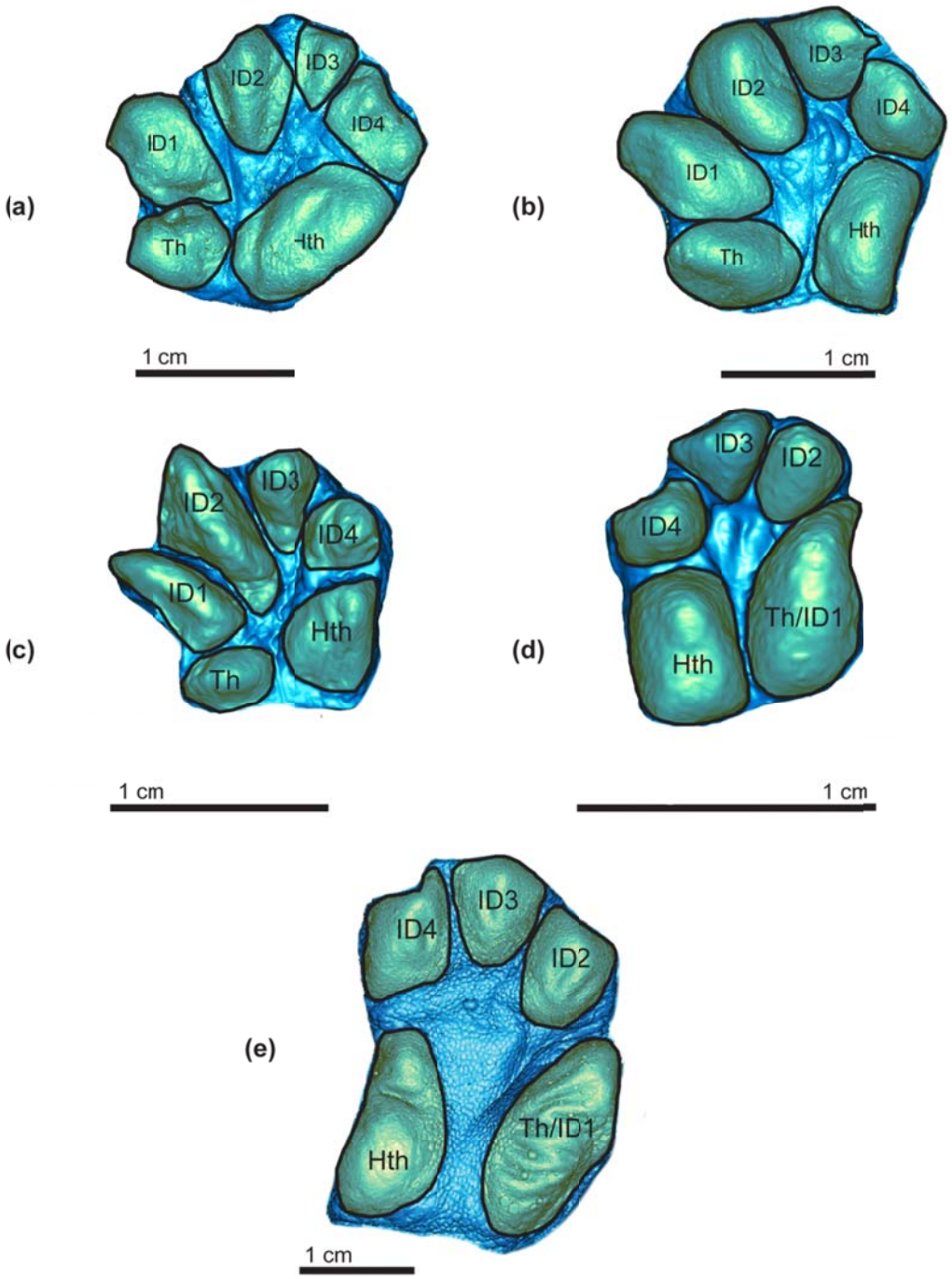

Figure 6.2. Illustration of manual volar pads representing each of the five locomotor categories examined in discriminant function analysis. (a) Slow-climbers (*Nycticebus coucang)* are distinct in having relatively short broad pads and a relatively small ID3. (b) Nail-climbers (*Euoticus elegantulus*) possess very large pads for their size. (c) Vertical clinging and leaping species (*Galago moholi*), (d) arboreal quadrupeds (*Microcebus murinus*), and (e) semi-terrestrial quadrupeds (*Lemur catta*) have pads with relatively similar dimensions.

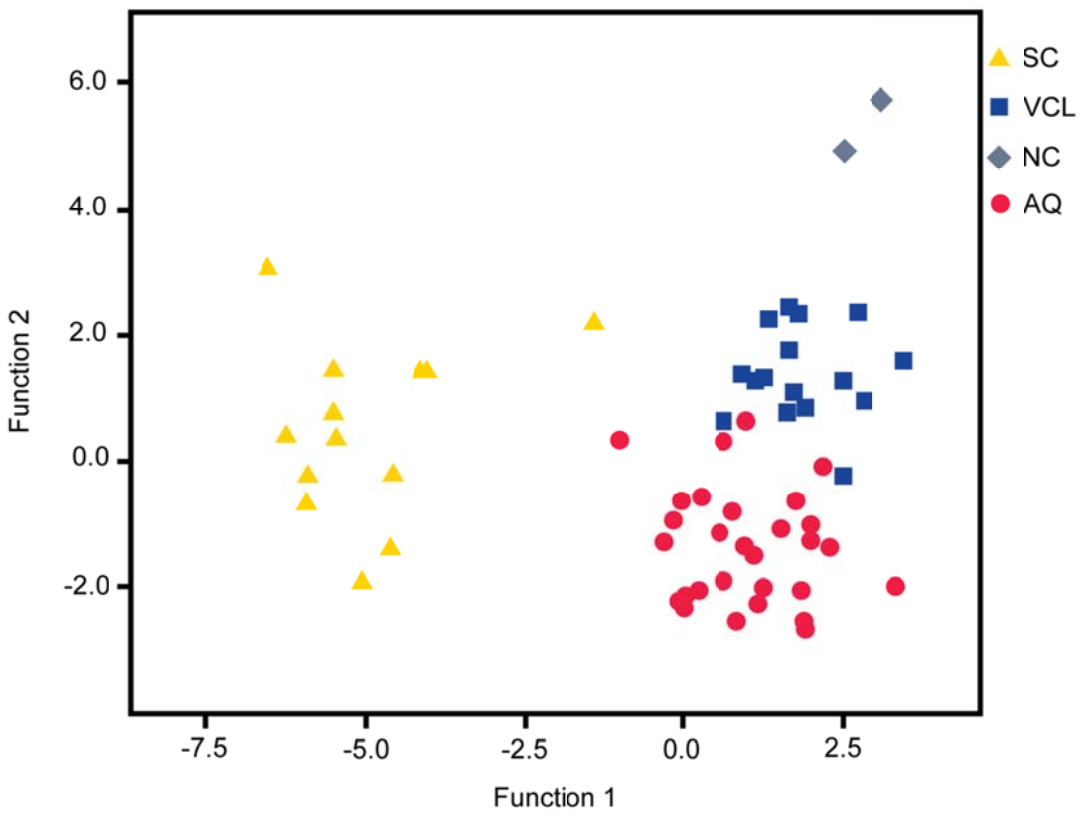

Figure 6.3. Plot of hindlimb discriminant scores for functions one and two. Function one separates the slow-climbing lorises from the remaining species on the basis of their short, broad pads and relatively small third interdigital pad. The remaining species separate on function two, which is heavily influenced by the size of the volar pads and the length of the second interdigital pad.

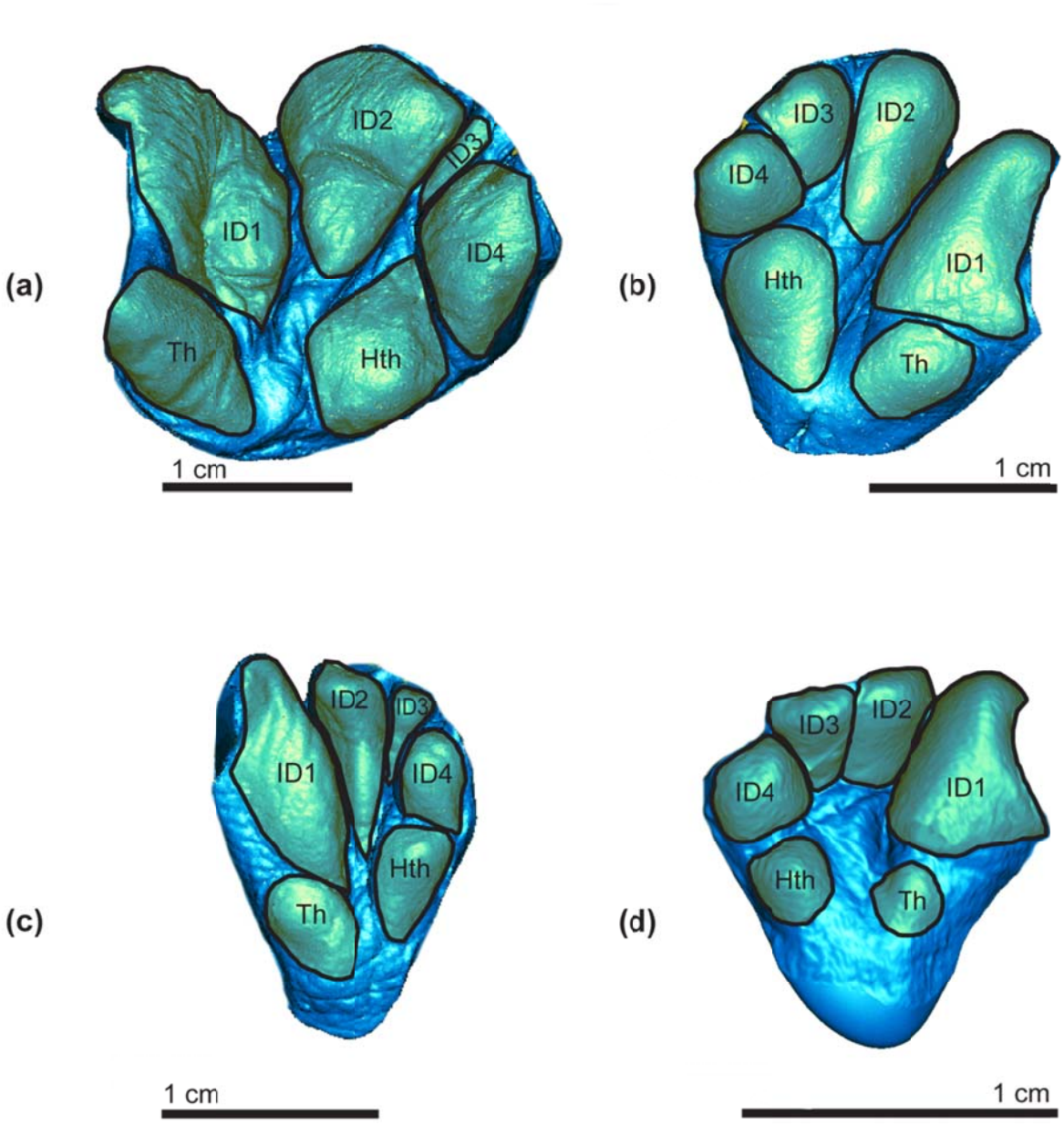

Figure 6.4. Illustration of pedal volar pads representing each of the four locomotor categories examined in the discriminant function analysis. (a) Slow climbers (*Nycticebus coucang)* are distinct in having relatively short, broad pads and a relatively small ID3. (b) Nail-climbers (*Euoticus elegantulus*) possess very large pads for their size. (c) Vertical clinging and leaping species (*Galago moholi*) are distinct from (d) arboreal quadrupeds (*Microcebus murinus*) in having a relatively long ID2 pad.

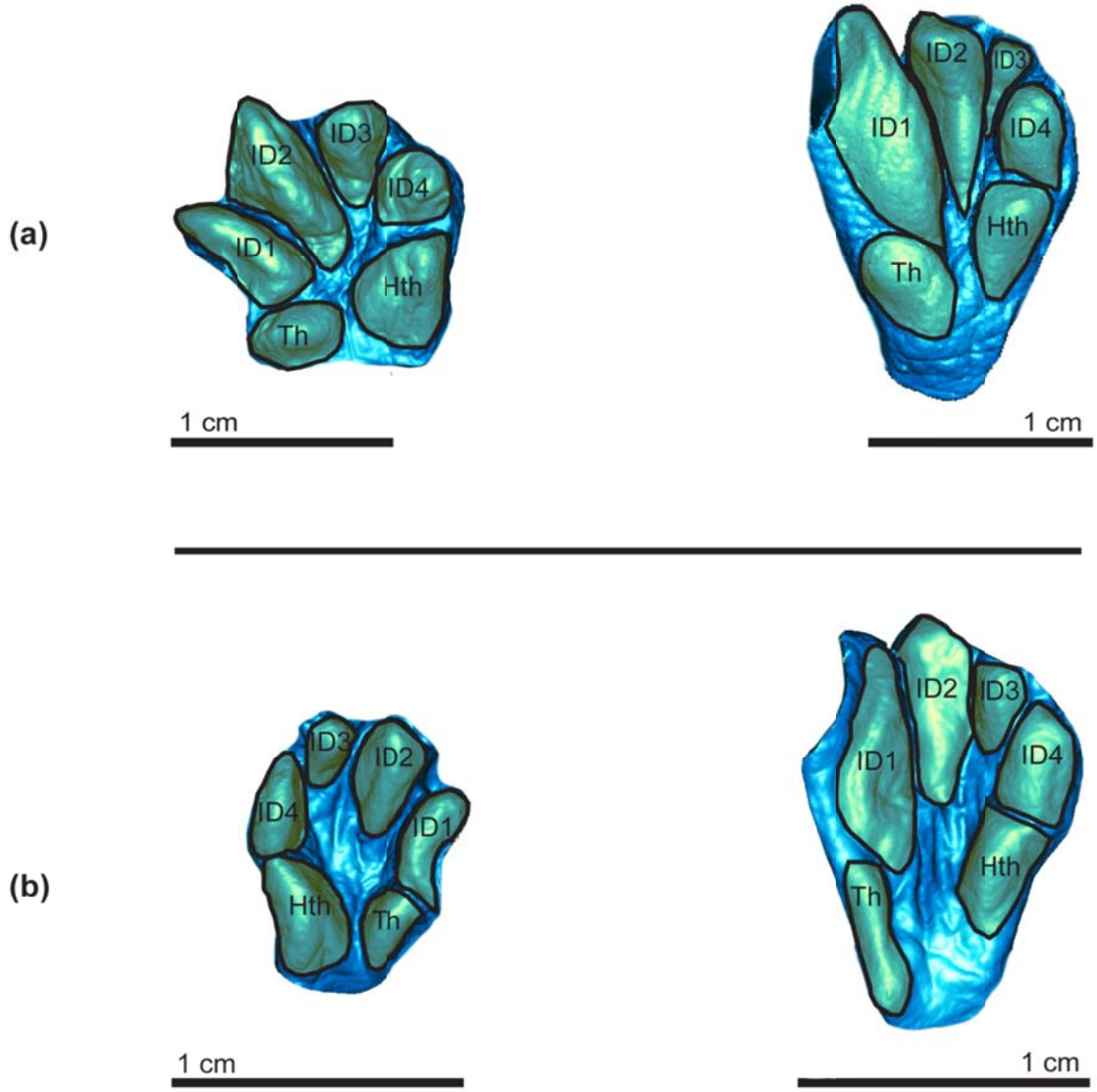

Figure 6.5. Illustration of volar pads of (a) a vertical clinging and leaping galagid (*Galago moholi*) and (b) an arboreal quadrupedal galagid (*Galagoides demidoff*). Manual volar surfaces are pictured to the left, pedal surfaces to the right; volar pads are abbreviated; Th: Thenar, Hth: Hypothenar, ID1: first interdigital, ID2: second interdigital; ID3: third interdigital; ID4: fourth interdigital. The vertical clinging and leaping *G. moholi* has significantly larger ID1 and ID2 pads; the arboreal quadrupedal *G. demidoff* has significantly larger Hth and ID4 pads.

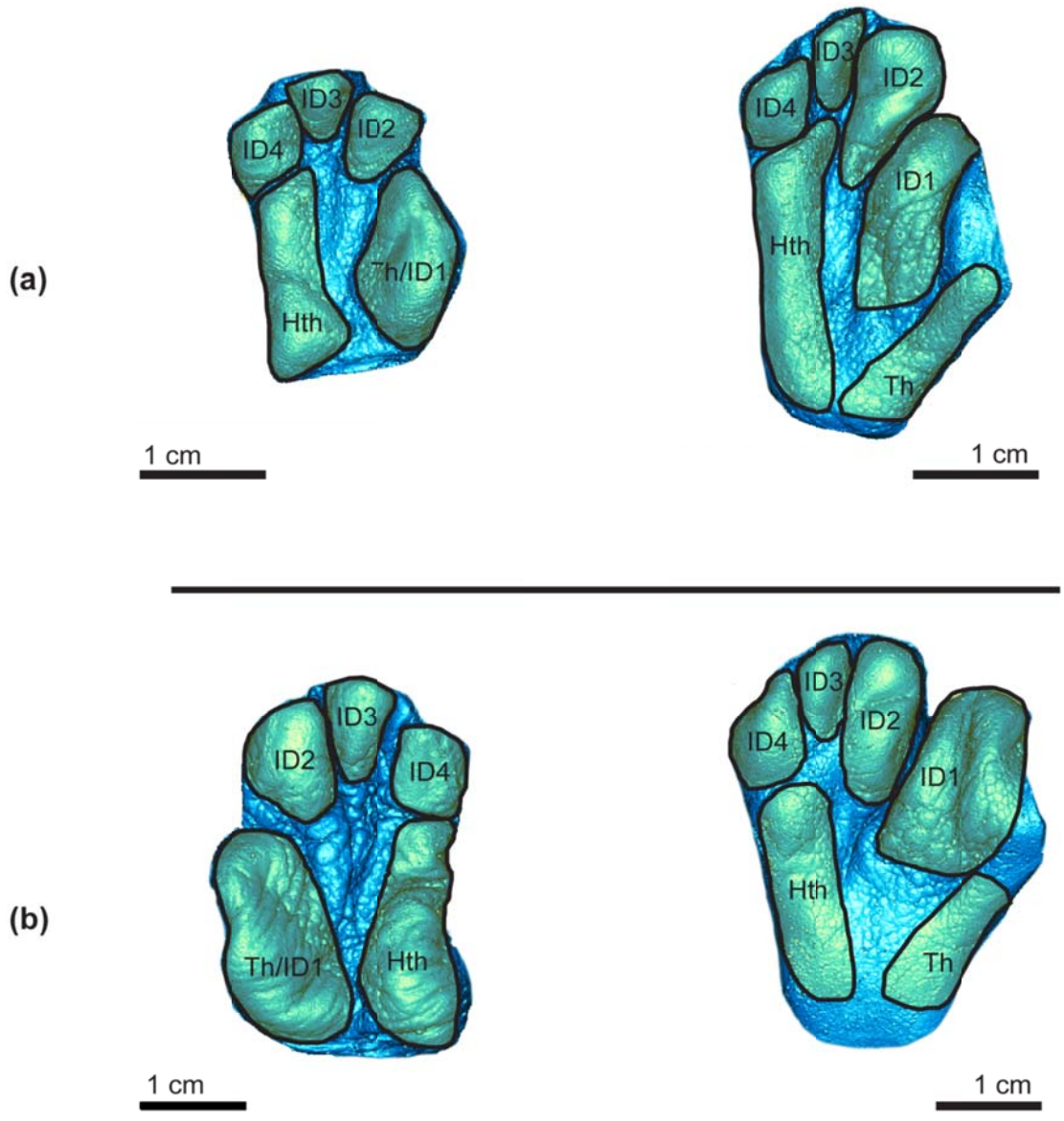

Figure 6.6. Illustration of volar pads of (a) a vertical clinging and leaping lemur (*Hapalemur griseus griseus*) and (b) an arboreal quadrupedal lemur (*Eulemur macaco macaco*). Manual volar surfaces are pictured to the left, pedal surfaces to the right; volar pads are abbreviated; Th: Thenar, Hth: Hypothenar, ID1: first interdigital, ID2: second interdigital; ID3: third interdigital; ID4: fourth interdigital. The manual volar pads of both locomotor categories are similar in lemur species. The pedal Th and Hth pads are significantly longer in vertical clinging and leaping taxa.

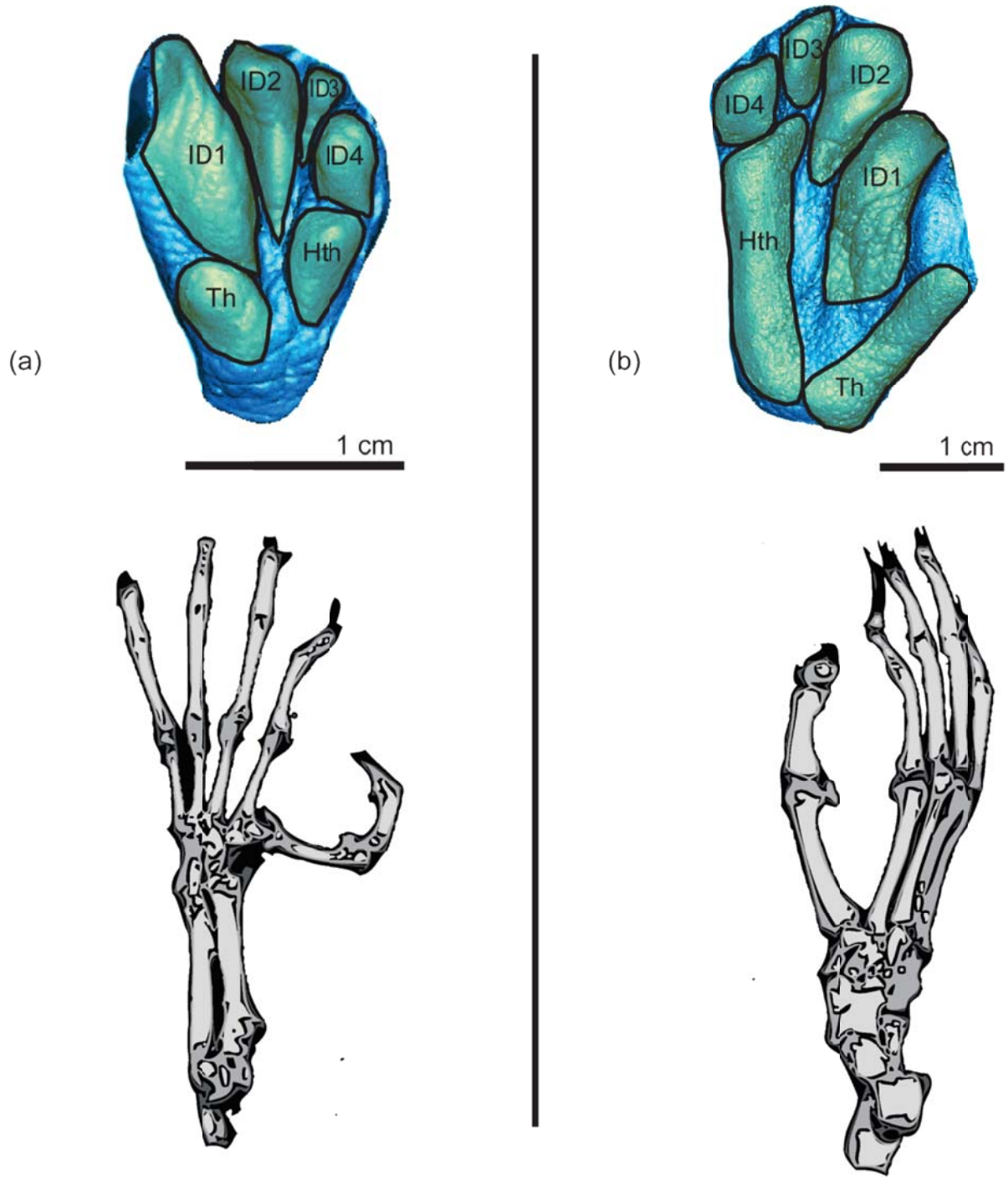

Figure 6.7. Illustration of differences in pedal pad and bony morphology for vertical clinging and leaping galagids and lemurs. (a) shows the galagid pedal morphology: the ID1 and ID2 pads are long with large surface areas and metatarsals 1-5 lie in the same plane (I-V grasp). (b) shows the lemuroid morphology: the Th and Hth pads are long with large surface areas and metatarsals 2-5 lie at a 45 degree angle to metatarsal I (I-II grasp). Volar pads are abbreviated; Th: Thenar, Hth: Hypothenar, ID1: first interdigital, ID2: second interdigital; ID3: third interdigital; ID4: fourth interdigital. Adapted from Gebo (1985).

Chapter 7:
Morphological Correlates of Locomotor Preference and Diet in the Dermatoglyphic Ridges

7.1: Summary

The dimensions of the dermatoglyphic ridges have been hypothesized to correlate with both locomotor mode and increased tactile acuity associated with frugivory in primates. Analyses of variance are conducted to examine each of these hypotheses. No significant association with locomotor mode or substrate preference is found for either the ridge widths or the intermediate ridge depths. An association between dietary habits and intermediate ridge depth is present, but contrary to predictions, the results here indicate that shallow intermediate ridge depth is strongly associated with an omnivorous diet. Descriptive statistics for raw measurments of dermatoglyphic dimensions are provided in Appendices E and F.

7.2 Results: Ridge Dimensions and Locomotion

A Kruskal-Wallis non-parametric analysis of variance was used to compare standardized dermatoglyphic ridge widths and intermediate ridge depths between locomotor groups as defined in Chapter Two. The widths of the dermatoglyphic ridges were hypothesized to decrease and the depth of the intermediate ridges to increase with dependence on friction grasping during arboreal locomotion; that is, species belonging to the slow-climbing and vertical clinging and leaping categories should have narrower dermatoglyphic ridges and deeper intermediate ridges than members of the arboreal quadruped group. Results of this analysis are presented in Table 7.1. No significant differences between locomotor groups were found for ridge width or intermediate ridge depths.

7.3 Results: Ridge Dimensions and Diet

The dimensions of the dermatoglyphic ridges were additionally hypothesized to vary with dietary categories as defined in Chapter Two due to their close association with the Meissner corpuscle tactile receptors. Dermatoglyphic ridge width was expected to decrease and intermediate ridge depth expected to increase with the amount of fruit in the diet category; exclusively faunivorous or folivorous species were expected to have wider, shallower ridges than frugivorous or omnivorous species. The results of this analysis are presented in Table 7.2. No significant differences between groups are evident for dermatoglyphic ridge width, but the

depths of the intermediate ridges of omnivores are significantly shallower than those seen in all other dietary groups. No significant differences between measurements taken from the thenar and hypothenar regions are evident (Width: t = -1.58, $p = 0.13$; Depth: t = -1.31, $p = 0.10$)

7.4 Discussion

Enhancement of frictional characteristics and tactile acuity have both been hypothesized to drive the adaptation and evolution of ridged volar skin. As discussed in previous chapters, the epidermal ridges are thought to provide a greater available contact area with irregular substrates, which in turn increases the frictional bonding capabilities of the semi-elastic volar skin (Cartmill, 1985; Hamrick, 1998, 2001; Lemelin, 2000). At the same time, the intermediate ridges are closely associated with Meissner corpuscles—rapidly adapting encapsulated tactile receptors—located in the dermal papillae of all examined primates (Winkelman, 1963). Movement against the dermatoglyphic ridges is thought to affect the orientation of the intermediate ridges, which in turn act as levers that move against the dermal papillae to deform and activate the Meissner corpuscles (Cauna, 1954; Martin, 1990). A longer lever-arm would increase the potential displacement of the intermediate ridges and magnify small movements occurring against the surface of the volar skin and result in better tactile discrimination while foraging (Martin, 1990; Kaas, 1993; Dominy, 2004; Hoffman et al., 2004; Verendeev et al., 2015). These hypotheses are not mutually exclusive; the use of the volar surfaces in both friction-generating and foraging activities are well documented across primate lineages, thus it seems likely that selection would favor adaptations to optimize both (Charles-Dominique & Bearder, 1979; Wrangham, 1977; Cartmill, 1979, 1985; Dominy, 2004). The findings in this chapter, coupled with those presented in Chapters Five and Six, indicate that multiple selective pressures may indeed differentially influence specific aspects of dermatoglyphic ridge morphology.

In Chapter Five, two distinct scaling relationships were identified for the dermatoglyphic ridge widths and the depths of the underlying intermediate ridges; the width of the ridges scale with negative allometry to body size, whereas the intermediate ridge depths scale isometrically. This discrepancy in scaling patterns suggests that these dimensions are not intrinsically linked and may appear in various combinations across species and groups. The negative allometric scaling of the dermatoglyphic ridges fits well with predictions of a friction-driven evolutionary model (see Chapter Six), but much of the variation present in the depth of the intermediate ridges remained unexplained. Here, no association between ridge dimensions and locomotor preferences is found, but evidence of a strong association between ridge depth and dietary habits is established. The finding that ridge width and depth exhibit associations with different selective forces is a departure from previous work, which has tended to look at the dermatoglyphic ridge components as a singular entity, rather than as a system wherein individual aspects may be adapted for different purposes (Hamrick, 1998, 2001; Lemelin, 2000).

The results here differ from previous work in several important ways. Hamrick (1998) reports substantial differences in ridge development across a group of callithricid primates with different locomotor habits and describes a morphocline wherein shallow limiting ridges are associated with heavy reliance on the derived tegulae (keeled, pointed nails possessed by callithricid primates) during gum foraging behaviors on large trunks. Deeper ridges are, conversely, associated with small-branch foraging. Here, there is no consistent pattern of ridge width or intermediate ridge depth among closely related species that are large- or small-substrate specialists. *Loris tardigradus*, a small substrate specialist, has significantly deeper ridges than its large-substrate preferring relative *Nycticebus coucang,* but the opposite relationship is true for *Cheirogaleus medius*, which prefers large substrates, and *Microcebus murinus*, who is reported to forage along fine terminal branches. Mean ridge width and depth for each species are provided in Table 7.3. (Species were included in the analysis based on availability and differ somewhat from those included in analysis of the volar pad morphology.) There are several reasons why this discrepancy may exist. First, the locomotor habits of the callitrichid primates examined in Hamrick's (1998) study are unique even among gum eating primates, and the mediolaterally compressed tegulae they employ to interlock with thick trunks while foraging and feeding are not seen in any other primate group (Maiolino et al., in press). It would not be surprising, then, for their volar skin morphology to possess correspondingly unique morphology. Second, it is worth highlighting that the associations described by Hamrick are based on gross morphological differences that have not been examined for scaling relationships or size-corrected before comparison. In Chapter Five of this dissertation, scaling relationships were found for both ridge width and depth. Although the precise scaling relationships of the ridges in platyrrhine primates remain unknown at present, that these features *do* scale in strepsirrhines indicates that some amount of the variation reported by Hamrick (1998) may be due to body size, especially as the callithricid species possessing the least-developed ridges (e.g., *Callithrix*, 275g) are significantly smaller than primates described as having deeper ridges (e.g., *Saguinus*, 485g; *Saimiri*, 825g).

The dietary correlations found here were also different than predicted. The depths of the intermediate ridges were expected to be highest among primarily frugivorous species, as these species are known to use their hands to identify and assess food items (Charles-Dominique & Bearder, 1979; Wrangham, 1977; Dominy, 2004). Here, no significant differences were found between frugivorous and faunivorous species, but species with omnivorous dietary habits were found to have significantly shallower intermediate ridges. This effect is strongly significant in both sampled regions and does not appear to be driven by any one species in particular (Table 7.2). This suggests that it may be dietary specialization and the associated foraging and tactile assessment that accompanies it, rather than fruit foraging in particular, that drives changes in the depth of the intermediate ridges. If a deeper intermediate ridge is associated with greater tactile sensitivity, this would indicate that greater sensitivity is required in foraging for specific food items than for opportunistic foraging. That is, a specialized diet requires mechanisms to identify the items one specializes on, whether these are ripe fruit or small animal prey. Although relatively little is known about the foraging behavior of nocturnal, faunivorous primates, use of

tactile cues in prey capture and processing has been documented for several faunivorous strepsirrhine species, thus this hypothesis seems worth pursuing (Charles-Dominique, 1974, 1977; Kumara et al., 2005; Nekaris, 2005; Siemers, 2013).

Although it would be premature to draw sweeping conclusions about tactile adaptations in the volar skin based on this finding alone, the significant association here between diet and intermediate ridge development indicates that a broader view of volar skin morphology is necessary to understand the evolutionary forces behind it. Recent work involving dietary and tactile adaptation in the volar skin has focused on evaluating the population densities of Meissner corpuscles, but has left the closely associated intermediate ridges unexamined. These studies have likewise focused narrowly on the association of the tactile endings and frugivory in haplorrhine primates. To date, no study has examined Meissner corpuscle density in faunivores or strepsirrhines. This bias is somewhat warranted, as haplorrhine primates tend to exhibit higher degrees of manual dexterity than strepsirrhines, which has been assumed to indicate a greater degree of tactile acuity (Heffner & Masterton, 1975; Iwaniuk et al., 1999; Dominy, 2004; Hoffman et al., 2004; Verendeev et al., 2015). However, this approach has resulted in only limited success in discriminating dietary groups; Hoffmann et al. (2004) reports slightly higher population densities of Meissner corpuscles in frugivores than folivores, but a subsequent study by Verendeev et al. (2015) fails to reproduce this result and, further, reports no significant differences in Meissner corpuscle population density between specific fingers or between right and left hands, challenging the view that precision grasping necessarily correlates with tactile acuity. An expanded, more inclusive sample is therefore vital to understanding the relationships of volar skin components.

The precise relationship between Meissner corpuscles, intermediate ridge depth, and tactile acuity is likewise poorly understood. The anatomical relationship between the skin ridges and the corpuscles is well-documented, but although the proposed mechanical model of the intermediate ridges acting as levers that activate the Meissner corpuscles is theoretically sound, there is no experimental evidence to confirm that a longer intermediate ridge results in greater tactile acuity. Similarly, it remains unclear as to how the morphologies of these structures may influence one another. Are the widths of the dermatoglyphic ridges constrained by the presence or size of the Meissner corpuscles? Do larger species with a relatively greater number of ridges on their volar surfaces have a correspondingly greater number of Meissner corpuscles? Exploring these questions will prove vital to establishing an evolutionary model explaining the development of this complex.

This study provides the first quantitative analysis of locomotion and diet's association with volar skin morphology. The findings here indicate that different selective pressures may be acting on individual aspects of the dermatoglyphic ridges. A novel link between diet and the depth of the intermediate ridges is indicated that should be further explored in relation to Meissner corpuscle density, tactile acuity, and foraging behavior as new data emerge.

Table 7.1. Kruskal-Wallis analysis of variance results for locomotor groups. Means and standard deviations are calculated from body-size standardized measurements.

	Standardized Group Means		Standard Deviation	95% Confidence Interval for Mean		X^2	*p*
Kruskal-Wallis Test							
Thenar Width	AQ:	55.31	8.76	50.81	59.81	4.46	0.11
	VCL:	62.26	7.03	55.75	68.76		
	SC:	58.36	3.35	50.03	66.70		
Thenar Depth	AQ:	15.25	4.87	12.75	17.75	3.41	0.18
	VCL:	17.72	2.82	15.12	20.33		
	SC:	16.87	3.09	9.18	24.55		
Hypothenar Width	AQ:	60.02	11.18	54.27	65.76	0.97	0.62
	VCL:	68.83	15.77	54.25	83.12		
	SC:	61.14	10.68	34.61	87.66		
Hypothenar Depth	AQ:	13.76	3.27	12.08	15.45	5.66	0.07
	VCL:	17.28	1.46	15.93	18.64		
	SC:	16.60	3.36	8.27	24.28		

Table 7.2 Kruskal-Wallis analysis of variance results for dietary groups. Means and standard deviations are calculated from body-size standardized measurements.

	Standardized Group Means		Standard Deviation	95% Confidence Interval for Mean	X^2	*p*
Kruskal-Wallis Test						
Thenar Width	Frugivore:	54.24	11.68	44.47–64.00	3.46	0.33
	Folivore:	61.34	9.94	48.99–73.67		
	Insectivore:	57.56	2.39	53.74–61.37		
	Omnivore:	58.04	5.38	54.19–61.89		
Thenar Depth	Frugivore:	18.31	5.07	14.07–22.55	**14.29**	**< 0.01**
	Folivore:	17.36	1.85	15.06–19.65		
	Insectivore:	19.48	1.16	17.64–21.33		
	Omnivore:	12.27	2.17	10.72–13.83		
Hypothenar Width	Frugivore:	57.77	14.55	45.60–69.93	2.77	0.43
	Folivore:	72.80	16.55	52.25–93.35		
	Insectivore:	59.36	11.71	40.73–77.99		
	Omnivore:	62.19	6.42	57.60–66.79		
Hypothenar Depth	Frugivore:	15.95	2.44	13.92–17.99	**13.45**	**< 0.01**
	Folivore:	16.29	1.91	13.92–18.67		
	Insectivore:	18.47	0.38	17.87–19.07		
	Omnivore:	12.18	2.92	10.09–14.27		

	Group A	Group B	Standard Error	Z	*p*
Dunn's Post Hoc Tests					
Thenar Depth	Frugivore	Folivore	4.53	-1.65	0.72
		Insectivore	4.86	-4.50	0.36
		Omnivore	**3.77**	**10.05**	**< 0.01**
	Folivore	Insectivore	5.32	-2.85	0.59
		Omnivore	**4.35**	**11.70**	**< 0.01**
	Insectivore	**Omnivore**	**4.70**	**14.55**	**< 0.01**
Hypothenar Depth	Frugivore	Folivore	4.53	-0.10	0.98
		Insectivore	4.86	-5.75	0.24
		Omnivore	**3.77**	**9.10**	**0.02**
	Folivore	Insectivore	5.32	-5.65	0.29
		Omnivore	**4.35**	**9.20**	**0.03**
	Insectivore	**Omnivore**	**4.70**	**14.85**	**< 0.01**

Table 7.3. Descriptive statistics for dermatoglyphic ridge width and intermediate ridge depth by species. Means and standard deviations are calculated from body-size standardized measurements.

Taxon	Diet Category	Thenar Width (SD)	Hypothenar Width (SD)	Thenar Depth (SD)	Hypothenar Depth (SD)
Cheirogaleus medius	Frugivore	44.95 (1.25)	44.43 (2.90)	24.31 (0.98)	24.31 (4.90)
Eulemur coronatus	Frugivore	52.56 (6.39)	59.11 (14.17)	14.49 (1.40)	13.34 (0.18)
Eulemur fulvus	Folivore	55.80 (5.28)	61.93 (9.01)	16.02 (0.33)	14.91 (0.37)
Eulemur macacao flavifrons	Frugivore	64.64 (12.69)	60.20 (12.85)	14.85 (1.25)	15.10 (0.99)
Galago moholi	Faunivore	58.68 (3.46)	56.46 (12.54)	20.31 (1.14)	18.42 (0.27)
Galago senegalensis	Omnivore	59.72 (3.27)	63.57 (6.19)	14.91 (1.39)	15.80 (0.79)
Hapalemur griseus griseus	Bamboo	69.64 (10.46)	74.10 (14.32)	19.35 (0.35)	18.37 (0.03)
Loris tardigradus	Faunivore	56.44 (0.54)	62.27 (14.84)	18.65 (0.04)	18.52 (0.59)
Mirza coquereli	Omnivore	56.45 (9.98)	56.80 (7.15)	10.15 (0.53)	8.31 (0.18)
Microcebus murinus	Omnivore	56.54 (0.27)	67.33 (2.19)	11.42 (0.44)	11.79 (0.45)
Nycticebus coucang	Omnivore	62.22	58.88	13.29	12.76
	Diet Category	**Thenar Width (SD)**	**Hypothenar Width (SD)**	**Thenar Depth (SD)**	**Hypothenar Depth (SD)**
	Frugivore	44.90 (11.88)	30.49 (5.83)	14.05 (1.07)	11.72 (0.18)
	Folivore	41.70 (23.63)	32.65 (12.84)	11.28 (3.47)	12.75 (2.90)
	Faunivore	53.99 (7.24)	31.04 (5.58)	14.37 (1.41)	13.63 (0.54)
	Omnivore	42.01 (13.43)	36.13 (14.17)	10.68 (2.41)	9.84 (2.51)

Chapter 8:
Conclusions

8.1 Summary

The volar surfaces of primates play important roles in generating friction during postural and locomotor activities, dampening impact forces, and facilitating tactile exploration. These roles are reflected in the morphology of the volar pads, skin, and metapodial bones to varying degrees. The volar pads and skin exhibit a wide range of adaptations within strepsirrhine primates to accommodate different functional demands and are strongly associated with different underlying bony morphology.

The volar surfaces are first and foremost friction-generating surfaces. This function is reflected in all aspects of their morphology, but most especially in the pads' surface area. Body size is tightly correlated with gross volar pad size and dermatoglyphic ridge width. The volar pads scale with positive allometry, which provides relatively expanded surface areas larger to larger taxa, which in turn facilitates adequate bonding with associated gravitational and shear forces. This scaling pattern is most apparent in the proximal volar pads. The widths of the dermatoglyphic ridges scale with negative allometry, which has the effect of providing larger taxa with a greater number of ridges on their volar surfaces and increasing the volar surface area. Individual pads are likewise adapted to optimize surface contact during different forms of locomotion.

The role of the volar pads in dissipating impact forces is well known. This function, however, is not reflected in the morphology of taxa experiencing differing impact forces as part of their habitual locomotor regime. All pads exhibit similar relief across taxa and the responsibility of diffusing higher impact forces falls to more proximal portions of the limbs and behavioral adaptations.

An association between diet and the morphology of the volar skin was present in this sample. The intermediate ridges of the epidermis are significantly deeper in the volar skin of frugivorous and faunivorous strepsirrhine species than in their omnivorous counterparts. This association may reflect an adaptation to increase tactile acuity for specialized foraging, but a great deal more work establishing the relationships between diet, tactile acuity, volar skin morphology, and associated nerve endings is required before this can be considered as more than an interesting association.

The volar surfaces of the hands and feet reflect different functional demands for each cheiridium. This follows a well-known pattern in primates wherein the roles of the upper and hindlimbs are differentiated during locomotion; the hindlimb is responsible for support and

propulsion, and the hand is freed for exploration and manipulation. Here, it was found that the metapodial bones of the feet scale with greater positive allometry than those of the hand, which provides a relatively longer platform for the pedal volar surfaces. The scaling of the manual and pedal volar pads mirror this trend; the pedal pads scale with greater positive allometry and provide a larger contact area for a secure pedal grasp. Interestingly, the total volar surface area of the pedal pads shows no significant differences between locomotor categories, even though differences are evident in the manual pads. This not only provides further evidence of different roles for the cheiridia, but also indicates that a consistent pedal surface area has been favored by selection across taxa. As all primates engage in some degree of arboreal locomotion, this stabilizing selection provides a functional baseline for friction grasping.

The volar surfaces are strongly associated with the underlying bony morphology. In addition to the scaling relationships of the volar pads and volar skin ridges discussed above, pad dimensions reflect the metapodial dimensions in individual taxa. This is especially evident in the relatively short, wide pads present in the loris clade, which sit superficial to correspondingly short metapodials. Additionally, in Malagasy taxa, the fusion of the manual thenar and first interdigital pads is closely associated with a reduction in the length of the first metacarpal. This close association indicates that the bony morphology and volar surface morphology function as a unit to provide adequate friction bonding and should be considered as such.

8.2 Future Directions

This work represents only the first steps in understanding the forces that shape primate (and mammalian) volar surfaces. Primates are a broad radiation with many adaptations for locomotor and positional behavior, yet members of this group all share a specific suite of derived manual and pedal traits for grasping arboreal substrates, including grasping cheiridia and long digits with nails on their apices. While differences are evident in volar pad morphology between groups engaging in different kinds of arboreal behavior, it is impossible to extrapolate how these morphologies might differ from those of animals adapted to different forms of terrestrial locomotion based on this sample. To better understand what influences arboreality itself has had on primate volar surfaces, a broader comparative sample comprising both terrestrial and arboreal taxa is necessary.

Comparative study of microscopic skin features across taxa remains in its infancy; very little is known about the adaptive morphology of mammalian skin outside of humans and rats. Again, a broad comparative sample will facilitate a more thorough understanding of how the volar skin and associated features are adapted to suit specific niches and, importantly, will also allow for a broader assessment of how different features are related to and influence the morphology of others, such as the intermediate ridges and Meissner corpuscles. Further experimental work is also necessary to confirm functional hypotheses concerning both frictional properties of the dermatoglyphic ridges and tactile acuity. While theoretically sound, it remains

to be demonstrated whether a greater number of ridges provides enhanced frictional bonding across multiple surfaces, or if this adaptation is limited in its usefulness to substrates with very specific surface characteristics. Likewise, tactile acuity has been rigorously examined in humans, but has not been assessed experimentally for most groups of primates. Hypotheses regarding the morphologies associated with tactile acuity are therefore necessarily extrapolated and lacking empirical support. Filling in the gaps in both our anatomical and functional understanding of the volar skin are therefore essential components of future study.

References

Adams MJ, Johnson SA, Lefevre P, Levesque V, Hayward V, Andre T, and Thonnard J-L. 2013. Finger pad friction and its role in grip and touch. Journal of the Royal Society Interface 10:20120467.

Aerts P, Ker RF, De Clercq D, and Ilsley DW. 1996. The effects of isolation on the mechanics of the human heel pad. Journal of Anatomy 188:417–423.

Aerts P, Ker RF, De Clercq D, Ilsley DW, and Alexander RM. 1995. The mechanical properties of the human heel pad: a paradox resolved. Journal of Biomechanics 28:1299–1308.

Anderson MJ. 1999. The use of hand morphology in the taxonomy of galagos. Primates 40:469–478.

Ankel-Simons F. 2007. Primate Anatomy, 3rd Edition. Cambridge: Academic Press.

Arnold C, Matthews LJ, and Nunn CL. 2010. The *10kTrees Website*: a new online resource for primate phylogeny. Evolutionary Anthropology 19:114–118.

Barr WA, and Scott RS. 2014. Phylogenetic comparative methods complement discriminant function analysis in ecomorphology. American Journal of Physical Anthropology 153:663–674.

Bearder SK, and Doyle GA. 1974. Ecology of bushbabies *Galago senegalensis* and *Galago crassicaudatus*, with some notes on their behaviour in the field. In: Martin RD, Doyle GA, and Walker AC, Eds. Prosimian Biology. Pittsburgh: University of Pittsburgh Press. p 109–130.

Bennett MB, and Ker RF. 1990. The mechanical properties of the human subcalcaneal fat pad in compression. Journal of Anatomy 171:131–138.

Benson DA, Karsch–Mizrachi I, Lipman DJ, Ostell J, and Wheeler DL. 2005. GenBank. Nucleic Acids Research 33:D34–D38.

Berbel-Filbo WM, Jacobina UP, and Martinez PA. 2013. Preservation effects in geometric morphometric approaches: freezing and alcohol in a freshwater fish. Ichthyology Research 60:268–271.

Biegert J. 1959. Die Ballen, Leisten, Furchen und Nägel von Hand und Fuss der Halbaffen Zeitschrift für Morphologie und Anthropologie 49:1959.

Biegert J. 1961. Volarhaut der Hände und Füsse. Basel: Karger Medical and Scientific Press. 316–409 p.

Biewener AA. 1989. Scaling body support in mammals: limb posture and muscle mechanics. Science 245:45–48.

Biewener AA. 2005. Biomechanical consequences of scaling. Journal of Experimental Biology 208:1665–1676.

Billy AJ. 1982. The effects of formalin and isopropyl alcohol on length and weight measurements of *Sarotherodon mossambicus* Trewavas. Journal of Fish Biology 21:107–112.

Bininda-Emonds ORP, and Russel AP. 1993. Effects of preservation on wing morphometry of the little brown bat (*Myotis lucifugus*). Journal of Zoology, London 230:141–158.

Bininda-Emonds ORP, and Russel AP. 1994. Flight style in bats as predicted from wing morphometry: the effects of specimen preservation. Journal of Zoology, London 234:275–287.

Bishop A. 1964. Use of the hand in lower primates. In: Buettner-Janusch J, Ed. Evolutionary and genetic biology of primates. New York: Academic press. p 133–225.

Bloch JI, and Boyer DM. 2002. Grasping primate origins. Science 298:1606–1610.

Blomberg SP, Garland TJ, and Ives AR. 2003. Testing for phylogenetic signal in comparative data: behavioral traits are more labile. Evolution 57(4):717–745.

Bolanowski SJ, and Pawson L. 2003. Organization of Meissner corpuscles in the glaborous skin of monkey and cat. Somatosensory and Motor Research 20:223–231.

Boyer DM, Patel BA, Larson SG, and Stern JTJ. 2007. Telemetered electromyography of peroneus longus in *Varecia variegata* and *Eulemur rubriventer*: Implications for the funcitonal significance of a large peroneal process. Journal of Human Evolution 53(2):119–134.

Buck C, and Baer H. 1993. Investigations on the biomechanical significance of dermatoglyphic ridges. In: Preuschoft H, and Chivers DJ, Eds. Hands of Primates. Vienna: Springer-Verlag. p 21–30.

Cartmill M. 1972. Arboreal adaptations and the origin of the order Primates. In: Tuttle R, Ed. The functional and evolutionary biology of primates. Chicago: Aldine-Atherton. p 97–122.

Cartmill M. 1974. Rethinking primate origins. Science(184):436–443.

Cartmill M. 1979. The volar skin of primates: its frictional characteristics and their functional significance. American Journal of Physical Anthropology 50:497–510.

Cartmill M. 1985. Climbing. In: Hildebrand M, Hildebrand H, Bramble DM, Liem KF, and Wake DB, Eds. Functional vertebrate morphology. Cambridge, MA: Harvard University Press. p 73–88.

Cartmill M. 1992. New views on primate origins. Evolutionary Anthropology 1:105–111.

Cartmill M, Lemelin P, and Schmitt D. 2002. Support polygons and symmetrical gaits in mammals. Zoological Journal of the Linnean Society 136:104–420.

Cauna N. 1954. Nature and functions of the papillary ridges of the digital skin. The Anatomical Record 119(4):449–468.

Cauna N. 1956. Nerve supply and nerve endings in Meissner corpuscles. American Journal of Anatomy 33:315.

Charles-Dominique P. 1974. Ecology and feeding behaviour of five sympatric lorisids in Gabon. In: Martin RD, Doyle GA, and Walker AC, Eds. Prosimian Biology. London: Duckworth. p 130–150.

Charles-Dominique P. 1975. Nocturnality and diurnality. An ecological interpretation of these two modes of life by an analysis of the higher vertebrate fauna in tropical forest ecosystems. In: Luckett WP, and Szalay FS, Eds. Phylogeny of the Primates: A Multidisciplinary Approach. New York: Plenum. p 69–88.

Charles-Dominique P. 1977. Ecology and Behaviour of Nocturnal Prosimians. New York: Columbia University Press.

Charles-Dominique P. 1990. Ecological adaptation related to locomotion in primates: an introduction. In: Jouffroy FK, Stack MH, and Niemitz C, Eds. Gravity, Posture and Locomotion in Primates. Florence: Il Sedicesimo. p 19–31.

Charles-Dominique P, and Bearder SK. 1979. Field studies of lorisid behavior; the lorisids of Gabon; the galagines of South Africa. In: Doyle GA, and Martin RD, Eds. The Study of Prosimian Behavior. p 567–629.

Chi K-J, and Schmitt D. 2005. Mechanical energy and effective foot mass during impact loading of walking and running. Journal of Biomechanics 38:1387–1395.

Clutton-Brock TH. 1985. Size, sexual dimorphism and polygyny in primates. In: Jungers WL, Ed. Size and Scaling in Primate Biology. New York: Springer. p 51–60.

Coleman MN. 2008. What does geometric mean, mean geometrically? Assessing the utility of geometric mean and other size variable in studies of skull allometry. American Journal of Physical Anthropology 135:404–415.

Corruccini RS. 1985. Incorrect size correction. American Journal of Physical Anthropology 66:91–92.

Coventry E, O'Connor KM, Hart BA, Earl JE, and Ebersole KT. 2006. The effect of lower extremity fatigue on shock attenuation during single-leg landing. Clinical Biomechanics 21:1090–1097.

Crompton RH. 1984. Foraging, habitat structure, and locomotion in two species of *Galago*. In: Rodman PS, and Cant JGH, Eds. Adaptations for Foraging in Nonhuman Primates: Contributions to an Organismal Biology of Prosimians, Monkeys, and Apes. New York: Columbia University Press. p 73–111.

Curtis DJ. 2004. Diet and nutrition in wild mongoose lemurs (*Eulemur mongoz*) and their implications for the evolution of female dominance and small group size in lemurs. American Journal of Physical Anthropology 124:234–-247.

Davies TG, Shaw CN, and Stock JT. 2012. A test of a new method and software for the rapid estimation of cross–sectional geometric properties of long bone diaphyses from 3D laser surface scans. Archaeological and Anthropological Sciences 4:277–290.

De Winter JCF. 2013. Using the Student's t-test with extremely small sample sizes. Practical Assessment, Research & Evaluation 18: http://pareonline.net/getvn.asp?v=18&n=10.

Demes B, Fleagle JG, and Jungers WL. 1999. Takeoff and landing forces of leaping strepsirhine primates. Journal of Human Evolution 37:279–292.

Demes B, Fleagle JG, and Lemelin P. 1998. Myological correlates of prosimian leaping. Journal of Human Evolution 34:385–399.

Demes B, Jungers WL, Fleagle JG, Wunderlich RR, Richmond BG, and Lemelin P. 1996. Body size and leaping kinematics in Malagasy vertical clingers and leapers. Journal of Human Evolution 31:367–388.

Demes B, Jungers WL, and Selpien K. 1991. Body size, locomotion, and long bone cross-sectional geometry in indriid primates. American Journal of Physical Anthropology 86:537–547.

Demes B, Larson SG, Stern JTJ, Jungers WL, Biknevicius AR, and Schmitt D. 1994. The kinetics of primate quadrupedalism: "Hindlimb drive" reconsidered. Journal of Human Evolution 26:353–374.

Demes B, Larson SG, Stern JTJ, Jungers WL, Biknevicius AR, and Schmitt D. 1995. Kinetics of leaping primates: influence of substrate orientation and compliance. American Journal of Physical Anthropology 96:419–429.

Derler S, Gerhardt L-C, Lentz A, and Hadad M. 2009. Friction of human skin against smooth and rough glass as a function of the contact pressure. Tribology International 42:1565–1574.

Derler S, Huber R, Feuz H-P, and Hadad M. 2009. Influence of surface microstructure on the sliding friction of plantar skin against hard substrates. Wear 267:1281–1288.

Diniz-Filho JAF, Santos T, Rangel TF, and Bini LM. 2012. A comparison of metrics for estimating phylogenetic signal under alternative evolutionary models. Genetics and Molecular Biology 35:673–679.

Dominy NJ. 2004. Fruits, fingers, and fermentation: the sensory cues available to foraging primates. Integrative & Comparative Biology 44:295–303.

Doyle GA. 1974. Behavior of prosimians. In: Schrier AM, and Stollnitz F, Eds. Behavior of Nonhuman Primates: Modern Research Trends. New York: Academic Press. p 155–338.

Dykyj D. 1980. Locomotion of the slow loris in a designed substrate context. American Journal of Physical Anthropology 52:577–586.

Edwards FK, Lauridsen RB, Armand L, Vincent HM, and Jones JI. 2009. The relationship between length, mass and preservation time for three species of freshwater leeches (*Hirudinea*). Fundamental and Applied Limnology 173:321–327.

Fawcett DW. 1994. Bloom and Fawcett: A Textbook of Histology (12th Ed.). New York: Chapman and Hall.

Felsenstein J. 1985. Phylogenies and the comparative method. The American Naturalist 125:1–15.

Fey DP. 1999. Effects of preservation technique on the length of larval fish: methods of correcting estimates and their implication for studying growth rates. Archive of Fishery and Marine Research 47:17–29.

Fleagle JG. 1985. Size and adaptation in primates. In: Jungers WL, Ed. Size and scaling in primate biology. New York: Plenum. p 1–19

Fleagle JG. 1999. Primate Adaptation and Evolution. Cambridge: Academic Press.

Gaston KA, Jacquemin SJ, and Lauer TE. 2013. The influence of preservation on fish morphology in museum collections based on two species of the genus *Lepomis* (*Actinopterygii: Perceiformes: Centrarchidae*). Acta Ichthyologica et Piscatoria 43:219–227.

Gebo DL. 1985. The nature of the primate grasping foot. American Journal of Physical Anthropology 67:269–277.

Gebo DL. 2014. Primate Comparative Anatomy. Baltimore: Johns Hopkins University Press.

Gebo DL, and Dagosto M. 1988. Foot anatomy, climbing, and the origin of the Indriidae. Journal of Human Evolution 17:135–154.

Gilbert CC. 2011. Phylogenetic analysis of the African papionin basicranium using 3-D geometric morphometric: the need for improved methods to account for allometric effects. American Journal of Physical Anthropology 144:60–71.

Gomez MI, Sanchez S, and Fuentes CM. 2014. Shrinkage of *Prochilodus lineatus* (Valenciennes, 1847) larvae preserved in either ethyl-alcohol or formalin in relation to their developmental stage and feeding condition. Journal of Applied Ichthyology 30:140–144.

Grand TI. 1967. The functional anatomy of the ankle and foot of the slow loris (*Nycticebus coucang*). American Journal of Physical Anthropology 26:207–218.

Haffner M. 1998. A comparison of the gross morphology and micro–anatomy of the foot pads in two fossorial and two climbing rodents (Mammalia). Journal of Zoology 244:287–294.

Haines RW. 1955. The anatomy of the hand of certain insectivores. Journal of Zoology 125:761–777.

Haines RW. 1958. Arboreal or terrestrial ancestry of placental mammals. The Quarterly Review of Biology 33:1–23.

Hamrick MW. 1998. Functional and adaptive significance of primate pads and claws: evidence from New World anthropoids. American Journal of Physical Anthropology 106:113–127.

Hamrick MW. 2001. Morphological diversity in digital skin microstructure of didelphid marsupials. Journal of Anatomy 198:683–688.

Hanna JB, John P, and Schmitt D. 2006. Forelimb and hindlimb forces in walking and galloping. American Journal of Physical Anthropology 130:529–535.

Harcourt CS, and Bearder SK. 1989. A comparison of Galago moholi in South Africa with Galago zanzibaricus in Kenya. International Journal of Primatology 10:35–45.

Harmon L, Weir J, Brock C, Glor R, Challenger W, Hunt G, FitzJohn R, Pennell M, Slater G, Brown J. 2008. GEIGER: investigating evolutionary radiations. Bioinformatics 24:129–131.

Harvey PH, and Pagel MD. 1991. The Comparative Method in Evolutionary Biology. Oxford: Oxford University Press.

Heffner R, and Masterton B. 1975. Variation in form of the pyramidal tract and its relationship to digital dexterity. Evolution 12:161–200.

Henriot AC. 2016. Piximetre.

Hladik CM. 1979. Diet and ecology of prosimians. In: Doyle GA, and Martin RD, Eds. The Study of Prosimian Behavior. New York: Academic Press. p 307–358.

Hoffman JN, Montag AG, and Dominy NJ. 2004. Meissner corpuscles and somatosensory acuity: the prehensile appendages of primates and elephants. The Anatomical Record 281:1138–1147.

Humason G. 1997. Animal Tissue Techniques, 5th ed. Baltimore: The Johns Hopkins University Press.

Iwaniuk AN, Pellis SM, and Whishaw IQ. 1999. Is digital dexterity really related to corticospinal projections? A reanalysis of the Heffner and Masterton data set using modern comparative statistics. Behavioral Brain Research 101:173–187.

Jindrich DL, Zhou Y, Becker T, and Dennerlein JT. 2003. Non-linear viscoelastic models predict fingertip pulp force-displacement characteristics during voluntary tapping. Journal of Biomechanics 36:497–503.

Johnson LE, Hanna JB, and Schmitt D. 2015. Single-limb force data for two lemur species while vertically clinging. American Journal of Physical Anthropology 158:463–474.

Jouffroy FK, Godinot M, and Nakano Y. 1991. Biometrical characteristics of primate hands. Human Evolution 6:1991.

Jouffroy FK, and Lessertisseur J. 1979. Relationships between limb morphology and locomotor adaptations among prosimians: an osteometric study. In: Morbeck ME, Preuschoft H, and Gomberg N, Eds. Environment, Behavior, and Morphology: Dynamic Interactions in Primates. New York: Gustav Fischer. p 143–181.

Jungers WL. 1977. Hindlimb and pelvic adaptations to vertical climbing and clinging in *Megaladapis*, a giant subfossil prosimian from Madagascar. Yearbook of Physical Anthropology 20:508–524.

Jungers WL. 1978. The functional significance of skeletal allometry in *Megaladapis* in comparison to living prosimians. American Journal of Physical Anthropology 49:303–314.

Jungers WL. 1979. Locomotion, limb proportions, and skeletal allometry in lemurs and lorises. Folia Primatologica 32:8–28

Jungers WL. 1984. Aspects of size and scaling in primate biology with special reference to the locomotor skeleton. Yearbook of Physical Anthropology 27:73–97.

Jungers WL. 1985. Body size and scaling of limb proportions in primates. In: Jungers WL, Ed. Size and scaling in primate biology. New York: Plenum. p 345–381.

Jungers WL. 1985. Size and Scaling in Primate Biology. New York: Springer.

Jungers WL, Falsetti A, and Wall CE. 1995. Shape, relative size and size-adjustments in morphometric. Yearbook of Physical Anthropology 38:137–161.

Kaas JH. 1993. The functional organization of somatosensory cortex in primates. Annals of Anatomy 175:509–518.

Kay RF. 1975. The functional adaptations of primate molar teeth. American Journal of Physical Anthropology 43:195–215.

Kay RF. 1984. On the use of anatomical features to infer foraging behavior in extinct primates. In: Rodman PS, and Cant JGH, Eds. Adaptations for Foraging in Nonhuman Primates: Contributions to an Organismal Biology of Prosimians, Monkeys, and Apes. New York: Colombia University Press. p 21–53.

Kembel SW, Cowan PD, Helmus MR, Cornwell WK, Morlon H, Ackerly DD, Blomberg SP, and Webb CO. 2010. Picante: R tools for integrating phylogenies and ecology. Bioinformatics 26:1463–1464.

Ker RF. 1990. The time-dependent mechanical properties of the human heel pad in the context of locomotion. The Journal of Experimental Biology 199:1501–1508.

Kingston AK, Boyer DM, Patel BA, Larson SG, and Stern JTJ. 2010. Hallucal grasping in *Nycticebus coucang*: further implications for the functional significance of a large peroneal process. Journal of Human Evolution 58:33–42.

Kirk EC, Lemelin P, Hamrick MW, Boyer DM, and Bloch JI. 2008. Intrinsic hand proportions of euarchontans and other mammals: implications for the locomotor behavior of plesiadapiforms. Journal of Human Evolution 55:278–299.

Klingenberg CP. 1996. Multivariate allometry. In: Marcus LF, Ed. Advances in Morphometrics. New York: Plenum Press. p 23–49.

Kumara HN, Kumar S, and Singh M. 2005. A novel foraging technique observed in slender loris (*Loris lydekkerianus malabaricus*) feeding on red ants in the western Ghats, India. Folia Primatologica 76:116–118.

Lammers AR. 2009. Mechanics of generating friction during locomotion on rough and smooth arboreal trackways. The Journal of Experimental Biology 212:1163–1169.

Larney E, and Larson SG. 2004. Compliant walking in primates: elbow and knee yield in primates compared to other mammals. American Journal of Physical Anthropology 125:42–50.

Larson SG. 1985. Organ weight scaling in primates. In: Jungers WL, Ed. Size and Scaling in Primate Biology. New York: Springer. p 91–113.

Larson SG. 1998. Unique aspects of quadrupedal locomotion in nonhuman primates. In: Strasser E, Fleagle JG, Rosenberger AL, and McHenry H, Eds. Primate Locomotion: Recent Advances. New York: Springer. p 157–173.

Larson SG, and Demes B. 2011. Weight support distribution during quadrupedal walking in *Ateles* and *Cebus*. American Journal of Physical Anthropology 144:633–642.

Larson SG, Schmitt D, Lemelin P, and Hamrick MW. 2001. Limb excursion during quadrupedal walking: how do primates compare to other mammals? Journal of Zoology, London 255:353–365.

Leeson CR, Leeson TS, and Paparo AA. 1985. Textbook of Histology. Philadelphia: W.B. Saunders.

Lemelin P. 1996. Relationships between hand morphology and feeding strategies in small-bodied prosimians. American Journal of Physical Anthropology S22:148.

Lemelin P. 1999. Morphological correlates of substrate use in didelphid marsupials: implications for primate origins. Journal of Zoology 247:165–175.

Lemelin P. 2000. Micro–anatomy of the volar skin and interordinal relationships of primates. Journal of Human Evolution 38:257–267.

Lemelin P, and Jungers WL. 2007. Body size and scaling of the hands and feet of prosimians. American Journal of Physical Anthropology 133:828–840.

Lemelin P, and Schmitt D. 2007. Origins of grasping and locomotor adaptations in primates: comparative and experimental approaches using and opossum model. In: Ravosa MJ, and Dagosto M, Eds. Primate Origins: Adaptations and Evolution. New York: Springer. p 329–380.

Lhota S, Junek T, and Bartos L. 2009. Patterns and laterality of hand use in free-ranging aye-ayes (*Daubentonia madagascariensis*) and a comparison with captive studies. Journal of Ethology 27:419–428.

Lleonart J, Salat J, and Torres GJ. 2000. Removing allometric effects of body size in morphological analysis. Journal of Theoretical Biology 205:85–93.

Maiolino S, Boyer DM, and Rosenberger A. 2011. Morphological correlates of the grooming claw in distal phalanges of platyrrhines and other primates: a preliminary study. The Anatomical Record 294:1975–1990.

Maiolino S, Huang S, and Boyer DM. 2015. Nail-like distal phalanges on postaxial digits is related to use of a terminal branch niche in non-primate mammals. American Journal of Physical Anthropology 156(SI 60):211.

Maiolino S, Kingston AK, and Lemelin P. *In Press*. Comparative and functional morphology of the primate hand integument In: Kivell TL, Lemelin P, Richmond BG, and Schmitt D, Eds. The Evolution of the Primate Hand: Perspectives from Anatomical, Developmental, Functional and Paleontological Evidence: Springer.

Maret D, Telmon N, Peters OA, Lepage B, Treil J, Inglese JM, Peyre A, Kahn JL, and Sixou M. 2012. Effect of voxel size on the accuracy of 3D reconstructions with cone beam CT. Dentomaxillofacial Radiology 41:649–655.

Martin RD. 1972. A preliminary field-study of the lesser mouse lemur (*Microcebus murinus*). Advances in Ethology 59:1–25.

Martin RD. 1985. Brain size allometry, ontogeny, and phylogeny. In: Jungers WL, Ed. Size and Scaling in Primate Biology. New York: Springer. p 147–173.

Martin RD. 1990. Primate Origins and Evolution: A Phylogenetic Reconstruction. Princeton: Princeton Univeristy Press.

McArdle JE. 1981. Functional morphology of the hip and thigh of the lorisiformes. Contributions to Primatology 17:1–132.

McCoy MW, Bolker BM, Osenberg CW, Miner BG, and Vonesh JR. 2006. Size correction: comparing morphological trait among populations and environments. Oecologia 148:547–554.

Meeuwig MH, and Bayer JM. 2005. Morphology and aging precision of statoliths from larvae of Columbia river basin lampreys. North American Journal of Fisheries Management 25:38–48.

Meldrum DJ. 1991. Kinematics of the cercopithecine foot on arboreal and terrestrial substrates with implications for the interpretation of hominid terrestrial adaptations. American Journal of Physical Anthropology 84:273–289.

Midlo C. 1939. Form of hand and foot in primates. American Journal of Physical Anthropology 19:337–389.

Moku M, Mori K, and Watanabe Y. 2004. Shrinkage in the body length of Myctophid fish (*Diaphus slender–type spp*.) larvae with various preservatives. Copeia 2004:647–651.

Motani R, and Schmitz L. 2001. Phylogenetic versus functional signals in the evolution of form-function relationships in terrestrial vision. Evolution 65:2245–2257.

Munger BL, and Pubols LM. 1972. The sesorineural organization of the digital skin of the raccoon. Brain, Behavior and Evolution 5:367–393.

Muñoz-Muñoz F, and Perpiñan D. 2010. Measurement error in morphometric studies: comparison between manual and computerized methods. Annales Zoologica Fennici 47:46–56.

Napier JR. 1993. Hands. Princeton: Princeton University Press.

Napier JR, and Walker AC. 1967. Vertical clinging and leaping—a newly recognized category of locomotor behaviour of primates. Folia Primatologica 6:204–219.

Nash LT. 1986. Dietary, behavioral, and morphological aspects of gummivory in primates. Yearbook of Physical Anthropology 29:113–137.

Nash LT, Bearder SK, and Olson TR. 1989. Synopsis of *Galago* species characteristics. International Journal of Primatology 10:57–80.

Neave FB, Mandrak NE, Dockers MF, and Noakes DL. 2006. Effects of preservation on pigmentation and length measurements in larval lampreys. Journal of Fish Biology 68:991–1001.

Nekaris KAI. 2005. Foraging behaviour of the slender loris (*Loris lydekkerianus lydekkerianus*): implications for theories of primate origins. Journal of Human Evolution 49:289–300.

Nekaris KAI, and Rasmussen DT. 2003. Diet and feeding behavior of Mysore slender lorises. International Journal of Primatology 24:33–46.

Nunn CL. 2011. The Comparative Approach in Anthropology and Biology. Chicago Univeristy of Chicago Press.

Nunn CL, and Barton RA. 2000. Allometric slopes and independent contrasts: a comparative test of Kleiber's law in primate ranging patterns. American Naturalist 156:519–533.

Nunn CL, and Barton RA. 2001. Comparative methods for studying primate adaptation and allometry. Evolutionary Anthropology 10:81–98.

Oates JF. 1984. The niche of the potto, *Perodicticus potto*. International Journal of Primatology 5:51–61.

Okajima M, and Asai Y. 1985. Anatomical and microscopic study of the volar dermal ridges of the rat (*Rattus norvegicus*). American Journal of Physical Anthropology 67:81–88.

Orkin JD, and Pontzer H. 2011. The narrow niche hypothesis: gray squirrels shed new light on primate origins. American Journal of Physical Anthropology 144:617–624.

Orme D, Freckleton R, Thomas G, Petzoldt T, Fritz S, Isaac N, and Pearse W. 2013. CAPER: comparative analysis of phylogenetics and evolution in R.

Oxnard, CE, et al., 1990. Animal life-styles and anatomies: the case of prosimian primates. Seattle: University of Washington Press.

Oxnard CE, German R, Jouffroy FK, and Lessertisseur J. 1981. A morphometric study of limb proportions in leaping prosimians. American Journal of Physical Anthropology 54:421–430.

Oxnard CE, German R, and McArdle JE. 1981. The functional morphology of the hip and thigh in leaping prosimians. American Journal of Physical Anthropology 54:481–498.

Pagel M. 1999. Inferring the historical patterns of biological evolution. Nature 401:877–884.

Pain MTG, and Challis JH. 2001. The role of the heel pad and shank soft tissue during impacts: a further resolution of a paradox. Journal of Biomechanics 34:327–333.

Pain MTG, and Challis JH. 2006. The influence of soft tissue movement on ground reaction forces, joint torque and joint reaction forces in drop landings. Journal of Biomechanics 39:119–124.

Panic R, Scott DW, Anderson WI, and Tennant BC. 1992. Microscopic anatomy of the skin of the woodchuck (*Marmota monax*)—comparison of woodchuck hepatitis virus-infected and non-infected animals. Cornell Veterinarian 82:387–404.

Paradis E, Claude J, and Strimmer K. 2004. APE: analyses of phylogenetics and evolution in R language. Bioinformatics 20:289–290.

Patel BA, Wallace IJ, Boyer DM, Granatosky MC, Larson SG, and Stern JTJ. 2015. Distinct functional roles of primate grasping hand and feet during arboreal quadrupedal locomotion. Journal of Human Evolution 88:79–84.

Paul IL, Munro MB, Abernethy PJ, Simon SR, Radin EL, and Rose RM. 1978. Musculo-skeletal shock absorption: relative contribution of bone and soft tissues at various frequencies. Journal of Biomechanics 11:237–239.

Pawluk DT, and Howe RD. 1999. Dynamic lumped element response of the human fingerpad. Journal of Biomechanical Engineering 121:178–183.

Pelabon C, Firmat C, Bolstad GH, Voje KL, Houle D, Cassara J, Le Rouzic A, and Hansen TF. 2014. Annals of the New York Academy of Sciences 1320:58–75.

Petter JJ, and Hladik CM. 1970. Observations sur le domaine vital et la densite de population de *Loris tardigradus* dans les forêts de Ceylan. Mammalia 34:394–409.

Preuschoft H, Witte H, Christian A, and Fischer M. 1996. Size influences on primate locomotion and body shape, with special emphasis on the locomotion of 'small mammals'. Folia Primatologica 66:93–112.

Rice FL, and Rassmusson DD. 2000. Innervation of the digit on the forepaw of the raccoon. Journal of Comparative Neurology 417:467–490.

Runestad Connour J, Glander K, and Vincent F. 2000. Postcranial adaptations for leaping in primates. Journal of Zoology 251:79–103.

Sargis EJ. 2001. The grasping behaviours, locomotion, and substrate use of the tree shrews *Tupaia minor* and *T. tana* (Mammalia, Scandentia). Journal of Zoology, London 253:485–490.

Scheumann M, Joly-Radko M, Leliveld L, and Zimmerman E. 2011. Does body posture influence hand preference in an ancestral primate model? BMC Evolutionary Biology 11:52.

Schmidt RF, and Thews G. 1983. Human Physiology. Berlin, Heidelberg, New York: Springer-Verlag.

Schmitt D. 1999. Compliant walking in primates. Journal of Zoology 248:149–160.

Schmitt D, and Hanna JB. 2004. Substrate alters forelimb to hindlimb peak force ratios in primates. Journal of Human Evolution 46:239–254.

Schmitt D, and Hanna JB. 2011. Locomotor energetics in primates: gait mechanics and their relationship to the energetics of vertical and horizontal locomotion. American Journal of Physical Anthropology 145:43–54.

Schmitt D, and Larson SG. 1995. Heel contact as a function of substrate type and speed in primates. American Journal of Physical Anthropology 96:39–50.

Schmitt D, and Lemelin P. 2004. Locomotor mechanics of the slender loris (*Loris tardigradus*). Journal of Human Evolution 47:85–94.

Shapiro LJ, Young JW, and VandeBerg JL. 2014. Body size and the small branch niche: using marsupial ontogeny to model primate locomotor behavior. Journal of Human Evolution 68:14–31.

Shields PA, and Carlson SR. 1996. Effects of formalin and alcohol preservation on lengths and weights of juvenile sockeye salmon. Alaska Fishery Research Bulletin 3:81–93.

Siemers BM. 2013. The sensory ecology of foraging for animal prey. In: Masters J, Ed. Leaping ahead: advances in prosimian biology, Developments in Primatology: Progress and Prospects. New York: Springer. p 257–263.

Siemers BM, Goerlitz HR, Robsomanitrandrasana E, Piep M, Ramanamanjato J-B, Rakotondravony D, Ramilijaona O, and Ganzhorn J, U. 2007. Sensory basis of food detection in wild *Microcebus murinus*. International Journal of Primatology 28:291–304.

Silcox MT, Sargis EJ, Bloch JI, and Boyer DM. 2007. Primate origins and supraordinal relationships: morphological evidence. In: Henke W, and Tattersall I, Eds. Handbook of Paleoanthropology: Primate Evolution and Human Origins. Berlin-Heidelberg: Springer-Verlag. p 831–859.

Smith JM, and Smith AC. 2013. An investigation of ecological correlates with hand and foot morphology in callitrichid primates. American Journal of Physical Anthropology 152:447–458.

Smith RJ, and Jungers WL. 1997. Body mass in comparative primatology. Journal of Human Evolution 32:523–559.

Soligo C, and Mueller AE. 1999. Nails and claws in primate evolution. Journal of Human Evolution 36:97–114.

Spears IR, and Miller-Young JE. 2006. The effect of heel-pad thickness and loading protocol on measured heel-pad stiffness and a standardized protocol for inter-subject comparability. Clinical Biomechanics 21:204–212.

Stephenson IR, Bearder SK, Donati G, and Karlsson J. 2010. A guide to *Galago* diversity: getting a grip on how best to chew gum. In: Burrows AM, and Nash LT, Eds. The evolution of exudativory in primates, Developments in Primatology: Progress and Prospects. New York: Springer. p 235–255.

Subramonian S. 1957. Some observations on the habits of the slender loris. Journal of Bombay Natural History Society 54:388–398.

Sussman RW. 1991. Primate origins and the evolution of angiosperms. American Journal of Primatology 23:209–223.

Sussman RW, and Raven RH. 1978. Pollination of flowering plants by lemurs and marsupials: a surviving archaic coevolutionary system. Science 200:731–736.

Suwa G, Wood BA, and White TD. 1994. Further analysis of mandibular molar crown and cusp areas in Pliocene and early Pleistocene hominids. American Journal of Physical Anthropology 93:407–406.

Terranova CJ. 1996. Variation in the leaping of lemurs. American Journal of Primatology 40:145–165.

Verendeev A, Thomas C, Mcfarlin SC, Hopkins WD, Phillips KA, and Sherwood CC. 2015. Comparative analysis of Meissner's corpuscles in the fingertips of primates. Journal of Anatomy 227:72–80.

Veron G. 1999. Pads morphology in the Viverridae (Carnivora). Acta Theria 44:363–376.

Vervus B, Van Dongen S, and Van Damme R. 2009. The effect of preservation on lizard morphometrics—an experimental study. Amphibia-Reptilia 30:321–329.

von Cramon–Taubadel N, Frazier BC, and Lahr MM. 2007. The problem of assessing landmark error in geometric morphometrics: theory, methods, and modifications. American Journal of Physical Anthropology 134:24–35.

Warman PH, and Ennos RA. 2009. Fingerprints are unlikely to increase the friction of primate fingerpads. Journal of Experimental Biology 212:2016–2022.

Wei X-F, Zhang X-Y, Yuan W, and Li Y-S. 2015. Accuracy of computer-aided geometric three-dimensional reconstruction of the human petrous bone based on serial unstained celloidin sections. Experimental and Theraputic Medicine 9:1113–1118.

Whipple IL. 1904. The ventral surface of the mammalian cheiridium. Zeitschrift für Morphologie und Anthropologie 7:261–368.

Whitehead P. 1993. Aspects of the wrist and hand. In: Gebo DL, Ed. Postcranial Adaptation in Nonhuman Primates. DeKalb: Northern Illinois University Press. p 96–120.

Winkelmann RK. 1963. Nerve endings in the skin of primates. In: Buettner-Janusch J, Ed. Evolutionary and Genetic Biology of Primates. New York: Academic Press. p 229–259.

Winkelmann RK. 1964. Nerve endings in the North American opossum (*Didelphis virginiana*): a comparison with nerve endings of primates. American Journal of Physical Anthropology 22:253–258.

Wood Jones R. 1916. Arboreal Man. London: Edward Arnold.

Wrangham R. 1977. Feeding behavior of chimpanzees in Gombe National Park in Tanzania. In: Clutton–Brock TH, Ed. Primate Ecology. London: Academic Press. p 504–538.

Yamashita N. 2003. Food procurement and tooth use in two sympatric lemur species. American Journal of Physical Anthropology 121:125–133.

Young JW. 2012. Ontogeny of limb force distribution in squirrel monkeys (*Saimiri boliviensis*): Insights into the mechanical bases of primate hind limb dominance. Journal of Human Evolution 62:473–485.

Appendix A. Descriptive statistics for raw measurements of manual volar pad dimensions.

		Length		Width		Projected Area		Surface Area	
Taxon	**Pad**	Mean	SD	Mean	SD	Mean	SD	Mean	SD
Daubentonia madagascariensis (1)	Thenar	11.73	-	5.83	-	52.87	-	68.22	-
	Hypothenar	-	-	-	-	-	-	-	-
	ID1	11.27	-	5.87	-	48.65	-	82.44	-
	ID2	13.70	-	7.22	-	59.46	-	90.51	-
	ID3	14.25	-	6.10	-	59.65	-	95.38	-
	ID4	20.16	-	9.20	-	131.81	-	198.01	-
Cheirogaleus major (2)	Th/ID1	895	0.23	5.27	0.82	34.43	4.84	56.19	4.40
	Hypothenar	6.48	0.53	5.58	0.43	28.09	1.50	45.76	5.31
	ID2	4.60	0.26	5.40	0.27	17.30	1.25	29.29	3.71
	ID3	4.55	0.49	4.43	0.14	14.38	1.30	28.69	1.93
	ID4	4.56	0.19	5.78	0.04	16.35	0.25	29.01	0.74
Eulemur fulvus collaris (4)	Th/ID1	20.54	2.55	9.46	1.40	156.82	21.93	261.67	23.46
	Hypothenar	21.52	1.64	9.45	1.31	164.04	24.83	261.40	17.91
	ID2	11.18	0.70	9.05	1.22	75.76	10.20	157.37	78.06
	ID3	8.36	0.82	8.37	1.31	44.48	4.19	70.81	6.93
	ID4	9.00	0.71	9.08	1.89	57.88	5.03	101.22	2.01
Eulemur fulvus fulvus (5)	Th/ID1	22.38	3.83	10.14	0.78	169.24	24.58	304.62	75.10
	Hypothenar	21.97	4.07	10.22	1.50	183.59	33.76	311.01	75.78
	ID2	10.75	1.75	9.09	1.88	69.87	12.56	123.88	23.22
	ID3	7.92	1.77	7.94	1.20	44.87	10.56	79.29	18.74
	ID4	8.74	1.82	9.63	1.44	67.67	20.65	151.65	25.39
Eulemur macaco macaco (8)	Th/ID1	19.80	2.21	9.68	1.25	148.76	34.83	248.76	48.25
	Hypothenar	18.36	2.73	9.65	1.25	118.30	26.50	191.85	56.35
	ID2	10.39	1.94	8.67	1.40	66.95	16.98	107.71	32.53
	ID3	7.76	1.40	6.99	1.08	35.51	8.56	60.24	13.92
	ID4	7.94	1.44	7.24	0.97	47.76	7.41	79.96	18.47

		Length		Width		Projected Area		Surface Area	
Taxon	**Pad**	Mean	SD	Mean	SD	Mean	SD	Mean	SD
Eulemur mongoz (2)	Th/ID1	17.75	0.13	6.66	0.56	101.41	8.40	196.86	35.65
	Hypothenar	17.03	0.64	7.33	1.03	101.30	11.49	177.64	22.37
	ID2	9.53	0.00	8.08	0.02	79.83	0.08	94.82	1.27
	ID3	7.97	0.66	6.74	0.07	34.56	4.95	58.58	8.29
	ID4	7.88	0.24	6.69	0.46	40.97	1.78	72.47	3.63
Hapalemur griseus griseus (3)	Th/ID1	13.76	0.12	6.82	0.80	78.95	8.21	126.33	13.16
	Hypothenar	12.95	2.30	6.08	0.56	62.37	11.38	99.36	17.81
	ID2	8.10	0.81	6.32	1.12	34.06	6.92	58.68	6.67
	ID3	5.88	0.75	5.18	1.72	22.60	6.22	36.10	11.02
	ID4	6.54	0.94	6.25	1.59	34.51	7.69	55.43	11.96
Lemur catta (6)	Th/ID1	19.10	2.43	8.68	1.15	126.27	20.16	207.81	22.06
	Hypothenar	18.47	2.01	9.15	0.84	117.08	53.19	205.87	47.43
	ID2	10.82	1.62	10.21	1.24	79.77	7.72	123.71	15.93
	ID3	9.39	0.94	9.17	1.19	54.57	6.03	83.03	12.85
	ID4	9.30	0.69	8.93	0.46	67.74	7.58	107.81	13.52
Lepilemur leucopus (2)	Th/ID1	11.78	0.75	7.99	0.13	76.35	9.79	110.87	8.19
	Hypothenar	10.74	0.80	7.08	0.30	58.12	4.19	90.78	12.50
	ID2	6.70	0.17	5.68	0.72	35.15	1.51	53.82	2.46
	ID3	6.15	0.20	5.54	1.37	26.75	1.63	42.53	2.13
	ID4	6.44	0.35	4.88	0.52	29.46	4.22	43.92	3.56
Microcebus murinus (11)	Th/ID1	6.06	0.34	3.42	0.32	15.06	1.03	24.90	3.89
	Hypothenar	4.47	0.57	2.96	0.31	11.54	1.92	18.59	3.78
	ID2	2.98	0.26	2.95	0.46	6.96	0.84	12.59	2.28
	ID3	2.96	0.43	2.98	0.54	6.22	1.09	11.07	1.45
	ID4	2.68	0.41	2.98	0.48	6.22	0.89	10.91	1.66
Mirza coquereli (3)	Th/ID1	10.92	0.56	6.99	0.20	56.82	4.71	80.37	3.45
	Hypothenar	8.39	0.95	5.65	0.53	41.33	1.04	59.75	4.37
	ID2	6.16	0.61	5.72	0.82	27.47	2.47	43.52	5.24
	ID3	5.00	0.24	5.01	0.35	18.57	1.33	33.33	1.05
	ID4	4.49	1.09	5.08	0.16	19.39	4.56	33.84	2.65

		Length		Width		Projected Area		Surface Area	
Taxon	**Pad**	Mean	SD	Mean	SD	Mean	SD	Mean	SD
Varecia variegata variegata (3)	Th/ID1	34.19	3.03	17.23	0.92	437.84	36.83	664.14	3.00
	Hypothenar	29.85	4.13	14.81	0.72	304.79	63.52	461.65	89.91
	ID2	24.89	5.21	12.08	2.20	200.19	56.44	295.57	57.70
	ID3	5.64	1.00	5.58	1.85	22.17	10.38	29.89	13.34
	ID4	13.61	0.99	10.84	0.60	129.65	19.68	204.91	20.32
Loris tardigradus (6)	Thenar	4.25	0.86	3.64	0.79	10.90	2.72	17.62	5.01
	Hypothenar	6.04	0.62	4.48	0.74	21.59	5.40	34.40	7.36
	ID1	6.36	1.89	3.56	0.98	14.56	4.48	30.74	11.33
	ID2	5.81	1.64	3.59	0.51	13.80	3.87	23.39	7.13
	ID3	3.55	0.78	2.24	0.44	5.89	3.08	8.26	3.45
	ID4	3.12	0.43	4.05	0.65	11.97	2.36	20.96	4.59
Nycticebus coucang (8)	Thenar	7.19	0.98	5.78	0.66	35.43	9.74	61.21	15.49
	Hypothenar	12.24	1.26	8.06	0.70	79.38	22.63	128.75	34.98
	ID1	11.44	1.78	6.13	1.03	50.79	12.51	97.48	23.77
	ID2	9.92	1.50	5.85	0.67	43.49	8.04	69.24	14.40
	ID3	5.86	1.49	4.76	1.49	18.98	5.94	56.99	7.81
	ID4	5.51	0.70	7.79	0.77	37.76	8.76	59.64	13.43
Perodicticus potto (2)	Thenar	7.94	0.46	7.54	1.67	48.05	9.19	70.92	14.78
	Hypothenar	13.33	1.01	8.10	0.68	88.42	10.81	133.36	8.61
	ID1	10.88	0.29	8.90	1.09	66.49	10.93	114.30	20.46
	ID2	9.70	0.07	7.91	0.79	56.46	11.02	76.80	11.61
	ID3	5.64	0.99	5.58	1.85	22.17	10.38	29.89	13.34
	ID4	6.18	1.01	7.99	1.07	39.02	11.90	56.81	14.47
Euoticus elegantulus (2)	Thenar	8.87	0.11	5.11	0.76	34.76	5.35	53.54	0.30
	Hypothenar	9.56	0.53	5.91	0.14	50.69	8.15	77.46	3.46
	ID1	9.39	0.85	5.80	0.87	39.86	7.58	73.17	1.94
	ID2	8.30	0.58	6.14	0.54	40.03	7.45	67.72	7.22
	ID3	6.19	1.90	5.92	0.03	22.60	3.39	41.15	3.47
	ID4	5.80	0.46	7.16	1.87	28.16	6.83	43.86	4.32

		Length		Width		Projected Area		Surface Area	
Taxon	**Pad**	Mean	SD	Mean	SD	Mean	SD	Mean	SD
Galagoides demidoff (7)	Thenar	3.02	0.52	2.54	0.38	5.37	1.13	7.94	1.72
	Hypothenar	4.14	0.48	2.66	0.19	8.35	1.29	13.00	2.50
	ID1	3.80	0.31	2.42	0.22	7.84	1.31	14.32	1.73
	ID2	4.05	0.38	2.70	0.23	8.29	2.61	13.68	1.17
	ID3	3.19	0.34	2.36	0.32	4.82	0.82	7.74	0.76
	ID4	3.04	0.30	3.21	0.14	5.79	0.75	9.79	1.19
Galago moholi (6)	Thenar	4.21	0.60	3.27	0.32	10.14	1.45	15.51	3.28
	Hypothenar	5.92	0.51	3.99	0.67	17.69	3.44	31.43	6.76
	ID1	5.83	0.97	4.38	0.37	16.59	3.31	32.86	7.96
	ID2	5.92	0.65	3.68	0.53	13.08	2.87	26.73	9.64
	ID3	4.52	0.51	2.67	0.51	7.82	1.50	14.44	5.74
	ID4	3.80	1.04	3.45	0.88	8.45	2.31	15.28	3.82
Galago senegalensis (5)	Thenar	5.30	0.82	4.62	0.63	16.89	4.36	22.15	3.23
	Hypothenar	7.37	0.56	5.25	0.57	30.50	4.78	41.34	3.82
	ID1	8.42	0.77	4.71	0.48	23.68	3.16	39.73	4.76
	ID2	8.07	1.02	4.08	0.60	19.76	1.56	37.45	7.33
	ID3	4.50	0.37	4.16	0.35	11.21	1.38	19.45	1.34
	ID4	3.97	0.49	4.93	0.69	13.59	1.42	21.40	4.53
Otolemur crassicaudatus (1)	Thenar	11.06	-	6.36	-	51.03	-	78.39	-
	Hypothenar	12.55	-	8.48	-	95.26	-	150.20	-
	ID1	12.87	-	3.72	-	38.35	-	97.45	-
	ID2	11.27	-	6.32	-	46.47	-	109.98	-
	ID3	9.38	-	4.54	-	27.45	-	56.07	-
	ID4	8.16	-	5.80	-	37.87	-	69.72	-

Appendix B. Descriptive statistics for raw measurements of pedal volar pad dimensions.

		Length		Width		Projected Area		Surface Area	
Taxon (n)	**Pad**	Mean	SD	Mean	SD	Mean	SD	Mean	SD
Eulemur fulvus collaris (1)	Thenar	18.78	-	8.29	-	122.91	-	150.18	-
	Hypothenar	29.77	-	9.13	-	182.23	-	268.29	-
	ID1	18.35	-	16.05	-	191.41	-	483.33	-
	ID2	17.57	-	8.70	-	89.10	-	187.96	-
	ID3	9.43	-	7.81	-	49.61	-	76.39	-
	ID4	11.14	-	9.51	-	72.67	-	121.68	-
Eulemur fulvus fulvus (1)	Thenar	19.15	-	8.32	-	118.81	-	158.37	-
	Hypothenar	26.89	-	8.94	-	172.52	-	285.95	-
	ID1	24.81	-	15.65	-	244.38	-	572.63	-
	ID2	21.53	-	9.54	-	101.65	-	196.21	-
	ID3	11.85	-	8.36	-	75.69	-	99.03	-
	ID4	7.19	-	13.69	-	67.48	-	123.08	-
Eulemur macaco macaco (6)	Thenar	15.69	1.05	9.01	1.39	112.85	22.90	137.02	26.68
	Hypothenar	24.89	1.45	7.73	1.12	156.76	13.68	229.63	22.32
	ID1	20.09	3.18	12.46	1.76	171.38	42.98	369.95	67.27
	ID2	16.67	2.01	13.11	1.04	111.95	26.72	188.80	47.45
	ID3	8.88	1.21	7.33	2.71	47.67	11.36	73.63	16.59
	ID4	8.34	2.50	7.74	1.09	55.55	14.40	88.04	16.07
Eulemur mongoz (2)	Thenar	15.69	0.19	8.33	0.41	97.63	9.95	118.15	5.27
	Hypothenar	24.93	1.91	6.73	0.80	128.76	11.48	201.11	14.14
	ID1	17.71	0.92	14.74	1.20	204.26	15.32	338.74	46.21
	ID2	15.28	0.23	7.46	0.85	83.62	10.26	147.99	21.03
	ID3	8.19	1.21	6.57	0.14	41.24	5.75	72.59	5.09
	ID4	8.05	0.60	6.92	0.27	44.94	1.10	77.75	0.12
Hapalemur griseus griseus (5)	Thenar	21.35	2.06	6.32	0.71	104.40	22.34	138.99	32.59
	Hypothenar	23.32	1.99	6.96	0.93	121.71	11.91	179.63	27.15
	ID1	13.55	1.53	6.37	0.51	60.58	9.76	125.87	13.09
	ID2	13.35	0.56	7.93	1.21	68.66	8.42	115.78	5.15
	ID3	7.77	0.38	5.50	1.66	32.69	7.98	48.85	9.53
	ID4	8.00	0.82	7.14	0.63	46.13	5.66	77.99	12.61

		Length		Width		Projected Area		Surface Area	
Taxon (n)	**Pad**	Mean	SD	Mean	SD	Mean	SD	Mean	SD
Lepilemur leucopus (1)	Thenar	7.98	-	5.60	-	35.98	-	39.67	-
	Hypothenar	11.38	-	5.69	-	61.46	-	80.66	-
	ID1	17.11	-	7.04	-	93.75	-	175.37	-
	ID2	14.06	-	6.51	-	65.29	-	102.87	-
	ID3	8.43	-	4.39	-	27.99	-	40.35	-
	ID4	7.14	-	6.07	-	36.50	-	57.62	-
Microcebus murinus (8)	Thenar	4.80	0.58	2.14	0.25	8.03	1.60	10.28	2.00
	Hypothenar	2.99	0.49	2.08	0.31	5.15	1.77	6.52	1.69
	ID1	7.89	1.27	4.02	0.54	19.57	3.27	44.41	10.05
	ID2	4.36	0.57	3.18	0.56	9.04	0.91	14.98	1.30
	ID3	3.06	0.50	2.51	0.42	5.38	0.76	8.39	1.47
	ID4	2.94	0.47	3.20	0.50	6.89	1.23	10.96	1.82
Mirza coquereli (1)	Thenar	8.67	-	3.56	-	23.56	-	31.13	-
	Hypothenar	5.54	-	3.79	-	15.94	-	21.45	-
	ID1	10.79	-	7.54	-	55.73	-	120.25	-
	ID2	7.90	-	5.00	-	29.71	-	57.54	-
	ID3	4.79	-	2.89	-	11.53	-	20.86	-
	ID4	5.25	-	4.13	-	19.37	-	32.83	-
Loris tardigradus (5)	Thenar	6.93	0.65	3.18	1.09	18.67	7.18	24.97	7.90
	Hypothenar	5.46	0.75	3.22	0.86	13.23	4.37	17.93	7.25
	ID1	10.62	2.17	6.74	1.73	44.40	16.93	79.95	22.63
	ID2	5.02	0.32	5.73	0.72	19.81	1.63	34.69	6.54
	ID3	3.90	0.45	2.04	0.39	5.56	1.21	7.98	1.14
	ID4	4.16	1.11	4.58	0.47	15.91	4.28	25.50	6.03
Nycticebus coucang (7)	Thenar	11.31	2.28	6.16	1.55	53.12	19.03	86.18	31.18
	Hypothenar	7.38	1.01	8.65	0.68	55.81	10.40	75.33	13.36
	ID1	15.02	2.26	9.89	1.53	100.63	15.02	183.57	31.69
	ID2	13.39	1.65	11.14	1.79	95.62	18.73	130.73	23.24
	ID3	6.10	0.46	3.98	0.61	20.41	2.26	25.38	2.30
	ID4	7.76	1.56	6.93	1.31	75.71	12.08	75.26	11.10

		Length		Width		Projected Area		Surface Area	
Taxon (n)	**Pad**	Mean	SD	Mean	SD	Mean	SD	Mean	SD
Perodicticus potto (1)	Thenar	12.34	-	7.57	-	80.36	-	114.46	-
	Hypothenar	10.12	-	7.81	-	71.00	-	86.97	-
	ID1	13.94	-	10.02	-	99.25	-	160.50	-
	ID2	16.01	-	10.88	-	93.01	-	133.51	-
	ID3	8.57	-	5.70	-	33.02	-	43.97	-
	ID4	6.91	-	8.25	-	49.19	-	79.41	-
Euoticus elegantulus (2)	Thenar	10.59	0.04	6.44	0.58	49.17	5.81	64.34	3.68
	Hypothenar	5.88	0.55	5.58	1.72	26.77	5.53	34.40	5.05
	ID1	12.51	0.83	10.22	0.40	74.98	3.74	128.89	6.73
	ID2	10.53	0.13	5.96	1.51	42.20	11.91	70.93	13.42
	ID3	6.98	0.26	4.57	1.26	21.22	6.09	32.04	4.15
	ID4	6.60	1.22	5.43	1.14	22.06	1.72	36.88	0.06
Galagoides demidoff (9)	Thenar	3.24	0.59	1.72	0.14	4.35	0.79	5.98	1.46
	Hypothenar	3.60	0.36	2.20	0.27	6.16	0.82	9.20	1.62
	ID1	6.09	0.67	5.01	0.30	20.74	3.42	43.73	7.45
	ID2	5.12	0.57	3.50	0.41	11.57	1.49	19.47	3.58
	ID3	3.14	0.30	2.27	0.40	4.86	0.54	6.99	0.89
	ID4	3.28	0.39	2.68	0.44	7.51	1.45	11.19	1.88
Galago moholi (5)	Thenar	5.58	0.50	3.85	0.61	18.18	2.14	22.98	3.84
	Hypothenar	5.66	0.58	3.66	0.50	17.59	2.46	26.07	4.47
	ID1	10.59	1.11	5.55	0.91	37.96	6.63	77.88	14.26
	ID2	8.50	0.42	4.78	0.67	24.95	2.41	43.38	5.38
	ID3	4.53	0.47	3.29	0.80	9.29	1.73	15.44	2.08
	ID4	4.00	0.44	4.81	0.65	12.11	0.73	19.85	2.37
Galago senegalensis (5)	Thenar	6.61	0.98	4.79	0.36	24.04	4.28	34.95	4.63
	Hypothenar	6.10	0.66	4.43	0.39	20.50	3.15	29.81	2.68
	ID1	13.57	1.79	7.88	1.16	68.76	11.63	133.94	21.32
	ID2	9.25	0.66	5.32	0.87	28.01	7.06	52.44	10.09
	ID3	4.91	0.61	3.51	0.61	10.52	2.78	18.70	4.40
	ID4	4.42	0.65	5.32	0.78	14.21	2.64	24.27	5.68

		Length		Width		Projected Area		Surface Area	
Taxon (n)	**Pad**	Mean	SD	Mean	SD	Mean	SD	Mean	SD
Otolemur crassicaudatus (1)	Thenar	-	-	-	-	-	-	-	-
	Hypothenar	13.95	-	9.33	-	109.55	-	166.81	-
	ID1	-	-	-	-	-	-	-	-
	ID2	11.70	-	11.82	-	78.67	-	129.31	-
	ID3	6.54	-	6.05	-	27.53	-	41.41	-
	ID4	7.29	-	9.87	-	53.92	-	87.40	-

Appendix C. Descriptive statistics for body-size standardized measurements of manual volar pad dimensions.

		Length		Width		Projected Area		Surface Area	
Taxon	**Pad**	Mean	SD	Mean	SD	Mean	SD	Mean	SD
Daubentonia madagascariensis (1)	Thenar	0.65	-	0.71	-	0.28	-	0.39	-
	Hypothenar	-	-	-	-	-	-	-	-
	ID1	1.00	-	1.05	-	0.77	-	1.41	-
	ID2	0.44	-	0.50	-	0.29	-	0.35	-
	ID3	0.62	-	0.43	-	0.27	-	0.34	-
	ID4	1.78	-	0.88	-	0.40	-	0.65	-
Cheirogaleus major (2)	Th/ID1	0.50	0.01	0.43	0.07	0.14	0.02	0.27	0.02
	Hypothenar	0.37	0.03	0.57	0.04	0.22	0.01	0.32	0.04
	ID2	0.33	0.02	0.70	0.04	0.29	0.02	0.42	0.05
	ID3	0.41	0.04	0.58	0.02	0.23	0.02	0.38	0.03
	ID4	0.71	0.03	0.96	0.01	0.19	0.00	0.37	0.01
Eulemur fulvus collaris (4)	Th/ID1	0.50	0.06	0.36	0.05	0.12	0.02	0.26	0.02
	Hypothenar	0.52	0.04	0.50	0.07	0.31	0.04	0.42	0.03
	ID2	0.37	0.02	0.65	0.09	0.39	0.05	0.64	0.32
	ID3	0.38	0.03	0.60	0.09	0.21	0.02	0.27	0.02
	ID4	0.81	0.06	0.89	0.18	0.19	0.01	0.35	0.01
Eulemur fulvus fulvus (5)	Th/ID1	0.56	0.10	0.40	0.03	0.14	0.02	0.32	0.08
	Hypothenar	0.55	0.10	0.55	0.08	0.36	0.06	0.52	0.13
	ID2	0.36	0.06	0.66	0.14	0.37	0.07	0.52	0.10
	ID3	0.36	0.08	0.58	0.09	0.22	.05	0.31	0.07
	ID4	0.80	0.17	0.96	0.14	0.23	0.07	0.42	0.09
Eulemur macaco macaco (8)	Th/ID1	0.47	0.05	0.36	0.05	0.11	0.03	0.24	0.04
	Hypothenar	0.43	0.06	0.50	0.07	0.21	0.05	0.29	0.08
	ID2	0.33	0.06	0.61	0.10	0.33	0.09	0.42	0.12
	ID3	0.34	0.06	0.49	0.08	0.16	0.04	0.22	0.05
	ID4	0.71	0.13	0.69	0.09	0.15	0.02	0.27	0.05
Eulemur mongoz (2)	Th/ID1	0.51	0.00	0.30	0.02	0.11	0.01	0.27	0.05
	Hypothenar	0.50	0.02	0.44	0.06	0.26	0.03	0.39	0.05
	ID2	0.37	0.00	0.65	0.00	0.52	0.00	0.50	0.00
	ID3	0.42	0.03	0.55	0.01	0.21	0.02	0.29	0.04
	ID4	0.80	0.02	0.73	0.04	0.17	0.01	0.33	0.01

		Length		Width		Projected Area		Surface Area	
Taxon	**Pad**	Mean	SD	Mean	SD	Mean	SD	Mean	SD
Hapalemur griseus griseus (3)	Th/ID1	0.51	0.00	0.38	0.04	0.14	0.02	0.28	0.03
	Hypothenar	0.48	0.09	0.45	0.04	0.24	0.04	0.34	0.06
	ID2	0.40	0.04	0.62	0.11	0.32	0.07	0.45	0.05
	ID3	0.38	0.05	0.50	0.17	0.2	0.05	0.26	0.07
	ID4	0.78	0.11	0.80	0.20	0.22	0.04	0.37	0.08
Lemur catta (6)	Th/ID1	0.47	0.06	0.34	0.05	0.11	0.02	0.22	0.02
	Hypothenar	0.46	0.05	0.49	0.05	0.23	0.10	0.34	0.08
	ID2	0.37	0.05	0.74	0.09	0.42	0.04	0.52	0.07
	ID3	0.43	0.04	0.67	0.09	0.27	0.03	0.32	0.05
	ID4	0.85	0.06	0.89	0.04	0.23	0.02	0.39	0.04
Lepilemur leucopus (2)	Th/ID1	0.54	0.03	0.54	0.00	0.21	0.02	0.37	0.02
	Hypothenar	0.50	0.03	0.62	0.32	0.32	0.02	0.45	0.07
	ID2	0.40	0.01	0.64	0.09	0.45	0.01	0.57	0.04
	ID3	0.47	0.02	0.63	0.16	0.32	0.02	0.42	0.03
	ID4	0.88	0.04	0.71	0.07	0.26	0.03	0.41	0.02
Microcebus murinus (11)	Th/ID1	0.84	0.04	0.61	0.06	0.34	0.02	0.64	0.10
	Hypothenar	0.62	0.08	0.62	0.06	0.41	0.07	0.61	0.12
	ID2	0.49	0.04	0.73	0.11	0.42	0.05	0.68	0.13
	ID3	0.57	0.08	0.74	0.13	0.36	0.06	0.57	0.07
	ID4	0.75	0.11	0.87	0.14	0.30	0.04	0.54	0.08
Mirza coquereli (3)	Th/ID1	0.69	0.03	0.62	0.02	0.29	0.02	0.48	0.02
	Hypothenar	0.53	0.06	0.64	0.06	0.39	0.01	0.50	0.04
	ID2	0.49	0.05	0.81	0.11	0.55	0.05	0.73	0.09
	ID3	0.50	0.02	0.71	0.04	0.35	0.02	0.53	0.01
	ID4	0.75	0.18	0.90	0.03	0.27	0.06	0.51	0.03
Varecia variegata variegata (3)	Th/ID1	0.68	0.06	0.56	0.03	0.24	0.02	0.47	0.00
	Hypothenar	0.59	0.08	0.67	0.03	0.41	0.09	0.53	0.10
	ID2	0.69	0.14	0.75	0.14	0.78	0.21	0.90	0.17
	ID3	0.75	0.15	0.67	0.07	0.50	0.07	0.64	0.07
	ID4	1.08	0.07	0.94	0.05	0.31	0.04	0.53	0.05

		Length		Width		Projected Area		Surface Area	
Taxon	**Pad**	Mean	SD	Mean	SD	Mean	SD	Mean	SD
Loris tardigradus (6)	Thenar	0.61	0.12	0.88	0.19	0.32	0.08	0.54	0.16
	Hypothenar	0.48	0.05	0.61	0.10	0.30	0.08	0.44	0.09
	ID1	1.25	0.37	1.12	0.31	0.90	0.28	1.99	0.74
	ID2	0.57	0.16	0.60	0.09	0.39	0.11	0.56	0.17
	ID3	0.43	0.08	0.37	0.07	0.16	0.07	0.19	0.07
	ID4	0.61	0.08	0.83	0.13	0.24	0.04	0.45	0.09
Nycticebus coucang (8)	Thenar	0.65	0.09	1.00	0.11	0.46	0.13	0.85	0.21
	Hypothenar	0.55	0.06	0.69	0.06	0.42	0.11	0.59	0.16
	ID1	1.53	0.24	1.47	0.25	1.64	0.40	3.35	0.82
	ID2	0.57	0.09	0.65	0.07	0.53	0.10	0.70	0.14
	ID3	0.44	0.10	0.53	0.15	0.22	0.06	0.25	0.06
	ID4	0.74	0.09	1.12	0.10	0.31	0.06	0.53	0.10
Perodicticus potto (2)	Thenar	0.57	0.03	1.10	0.24	0.41	0.08	0.65	0.14
	Hypothenar	0.44	0.03	0.54	0.05	0.28	0.03	0.36	0.02
	ID1	1.20	0.03	1.86	0.23	1.53	0.25	2.83	0.51
	ID2	0.42	0.00	0.70	0.07	0.45	0.08	0.49	0.07
	ID3	0.33	0.05	0.50	0.16	0.16	0.07	0.18	0.07
	ID4	0.68	0.11	0.95	0.13	0.20	0.06	0.32	0.08
Euoticus elegantulus (2)	Thenar	1.11	0.01	1.12	0.17	0.81	0.12	1.32	0.01
	Hypothenar	0.65	0.04	0.70	0.02	0.54	0.09	0.73	0.03
	ID1	1.65	0.15	1.69	0.25	2.03	0.39	3.95	0.10
	ID2	0.70	0.05	0.91	0.08	0.88	0.16	1.23	0.13
	ID3	0.66	0.02	0.88	0.01	0.47	0.07	0.72	0.06
	ID4	1.02	0.08	1.33	0.35	0.44	0.10	0.73	0.07
Galagoides demidoff (7)	Thenar	0.66	0.12	0.83	0.12	0.34	0.07	0.52	0.12
	Hypothenar	0.57	0.07	0.56	0.04	0.30	0.05	0.43	0.09
	ID1	1.06	0.09	0.98	0.09	0.88	0.15	1.68	0.19
	ID2	0.66	0.06	0.66	0.05	0.50	0.15	0.73	0.06
	ID3	0.61	0.06	0.58	0.07	0.28	0.04	0.40	0.04
	ID4	0.85	0.08	0.93	0.04	0.27	0.03	0.48	0.06

		Length		Width		Projected Area		Surface Area	
Taxon	**Pad**	Mean	SD	Mean	SD	Mean	SD	Mean	SD
Galago moholi (6)	Thenar	0.62	0.09	0.80	0.08	0.31	0.04	0.50	0.11
	Hypothenar	0.49	0.04	0.55	0.09	0.26	0.05	0.42	0.09
	ID1	1.17	0.19	1.40	0.12	1.06	0.21	2.21	0.53
	ID2	0.60	0.07	0.63	0.08	0.38	0.08	0.67	0.24
	ID3	0.57	0.06	0.46	0.08	0.22	0.04	0.34	0.13
	ID4	0.76	0.20	0.73	0.18	0.18	0.04	0.34	0.08
Galago senegalensis (5)	Thenar	0.66	0.10	1.01	0.14	0.38	0.09	0.53	0.08
	Hypothenar	0.49	0.04	0.61	0.07	0.32	0.05	0.38	0.04
	ID1	1.46	0.13	1.36	0.14	1.19	0.16	2.11	0.25
	ID2	0.67	0.08	0.60	0.09	0.43	0.03	0.68	0.13
	ID3	0.47	0.04	0.61	0.05	0.22	0.02	0.33	0.02
	ID4	0.69	0.08	0.91	0.12	0.21	0.02	0.35	0.07
Otolemur crassicaudatus (1)	Thenar	0.82	-	0.95	-	0.45	-	0.75	-
	Hypothenar	0.44	-	0.58	-	0.32	-	0.43	-
	ID1	1.15	-	0.79	-	0.92	-	2.50	-
	ID2	0.51	-	0.58	-	0.39	-	0.74	-
	ID3	0.56	-	0.41	-	0.21	-	0.35	-
	ID4	0.92	-	0.70	-	0.21	-	0.41	-

Appendix D. Descriptive statistics for body-size standardized measurements of pedal volar pad dimensions.

		Length		Width		Projected Area		Surface Area	
Taxon (n)	**Pad**	Mean	SD	Mean	SD	Mean	SD	Mean	SD
Eulemur fulvus collaris (1)	Thenar	0.53	-	0.17	-	0.13	-	0.14	-
	Hypothenar	0.72	-	0.20	-	0.07	-	0.10	-
	ID1	1.79	-	1.24	-	1.44	-	2.89	-
	ID2	0.92	-	0.49	-	0.39	-	0.82	-
	ID3	0.73	-	0.48	-	0.20	-	0.31	-
	ID4	1.01	-	0.46	-	0.25	-	0.42	-
Eulemur fulvus fulvus (1)	Thenar	0.56	-	0.18	-	0.14	-	0.16	-
	Hypothenar	0.67	-	0.21	-	0.07	-	0.11	-
	ID1	2.47	-	1.24	-	1.93	-	3.59	-
	ID2	1.01	-	0.51	-	0.41	-	0.95	-
	ID3	0.95	-	0.51	-	0.25	-	0.40	-
	ID4	0.66	-	0.68	-	0.25	-	0.45	-
Eulemur macaco macaco (6)	Thenar	0.43	0.03	0.18	0.03	0.12	0.02	0.12	0.02
	Hypothenar	0.59	0.03	0.17	0.03	0.05	0.01	0.08	0.01
	ID1	1.93	0.30	0.95	0.13	1.25	0.27	2.13	0.35
	ID2	0.86	0.10	0.73	0.58	0.47	0.11	0.80	0.20
	ID3	0.68	0.08	0.44	0.16	0.19	0.04	0.29	0.06
	ID4	0.74	0.22	0.37	0.05	0.19	0.05	0.29	0.05
Eulemur mongoz (2)	Thenar	0.52	0.01	0.21	0.01	0.15	0.01	0.15	0.01
	Hypothenar	0.72	0.05	0.18	0.02	0.07	0.01	0.11	0.01
	ID1	1.93	0.00	1.29	0.00	1.95	0.00	2.59	0.00
	ID2	0.92	0.00	0.49	0.00	0.48	0.00	0.84	0.00
	ID3	0.72	0.10	0.46	0.10	0.22	0.02	0.38	0.02
	ID4	0.82	0.05	0.39	0.01	0.20	0.00	0.35	0.00
Hapalemur griseus griseus (5)	Thenar	0.91	0.08	0.21	0.02	0.25	0.05	0.29	0.06
	Hypothenar	0.87	0.07	0.24	0.03	0.11	0.01	0.17	0.02
	ID1	1.74	0.17	0.66	0.05	0.81	0.11	1.37	0.12
	ID2	0.99	0.04	0.63	0.09	0.57	0.06	0.96	0.04
	ID3	0.81	0.04	0.47	0.14	0.25	0.06	0.38	0.07
	ID4	0.96	0.09	0.49	0.04	0.31	0.03	0.52	0.08

		Length		Width		Projected Area		Surface Area	
Taxon (n)	**Pad**	Mean	SD	Mean	SD	Mean	SD	Mean	SD
Lepilemur leucopus (1)	Thenar	0.42	-	0.23	-	0.13	-	0.12	-
	Hypothenar	0.52	-	0.24	-	0.09	-	0.11	-
	ID1	2.49	-	0.84	-	1.64	-	2.53	-
	ID2	1.22	-	0.60	-	0.73	-	1.15	-
	ID3	1.01	-	0.43	-	0.29	-	0.42	-
	ID4	0.97	-	0.50	-	0.34	-	0.53	-
Microcebus murinus (8)	Thenar	0.72	0.08	.27	0.02	0.21	0.04	0.25	0.04
	Hypothenar	0.41	0.07	0.28	0.04	0.08	0.02	0.10	0.02
	ID1	2.30	0.37	1.03	0.13	1.46	0.24	2.94	0.67
	ID2	0.91	0.11	0.69	0.12	0.51	0.04	0.84	0.07
	ID3	0.79	0.12	0.57	0.09	0.29	0.04	0.45	0.08
	ID4	0.82	0.13	0.64	0.10	0.34	0.06	0.54	0.09
Mirza coquereli (1)	Thenar	0.61	-	0.20	-	0.15	-	0.18	-
	Hypothenar	0.35	-	0.23	-	0.05	-	0.06	-
	ID1	1.92	-	1.13	-	1.49	-	2.70	-
	ID2	0.89	-	0.60	-	0.53	-	1.03	-
	ID3	0.72	-	0.36	-	0.19	-	0.35	-
	ID4	0.88	-	0.44	-	0.29	-	0.49	-
Loris tardigradus (5)	Thenar	0.62	0.05	0.23	0.07	0.18	0.07	0.22	0.06
	Hypothenar	0.44	0.06	0.24	0.06	0.06	0.02	0.08	0.03
	ID1	2.19	0.45	1.19	0.30	1.61	0.61	2.48	0.70
	ID2	0.68	0.03	0.82	0.08	0.50	0.03	0.87	0.14
	ID3	0.69	0.06	0.31	0.05	0.13	0.02	0.19	0.02
	ID4	0.81	0.18	0.59	0.05	0.34	0.07	0.55	0.11
Nycticebus coucang (7)	Thenar	0.57	0.11	0.24	0.06	0.18	0.06	0.25	0.09
	Hypothenar	0.33	0.04	0.36	0.02	0.08	0.01	0.10	0.01
	ID1	2.15	0.32	1.16	0.17	1.70	0.25	2.54	0.43
	ID2	1.14	0.13	1.01	0.13	1.40	0.29	1.43	0.53
	ID3	0.77	0.05	0.39	0.04	0.25	0.04	0.25	0.02
	ID4	1.04	0.13	0.55	0.11	0.66	0.15	0.86	0.37

Taxon (n)	Pad	Length		Width		Projected Area		Surface Area	
		Mean	SD	Mean	SD	Mean	SD	Mean	SD
Perodicticus potto (1)	Thenar	0.47	-	0.22	-	0.15	-	0.19	-
	Hypothenar	-	-	-	-	-	-	-	-
	ID1	1.65	-	0.96	-	1.12	-	1.47	-
	ID2	1.07	-	0.78	-	0.64	-	0.92	-
	ID3	0.82	-	0.44	-	0.21	-	0.28	-
	ID4	0.76	-	0.51	-	0.27	-	0.44	-
Euoticus elegantulus (2)	Thenar	0.80	0.00	0.39	0.03	0.35	0.04	0.41	0.02
	Hypothenar	0.40	0.03	0.36	0.10	0.09	0.01	0.11	0.01
	ID1	2.32	0.15	1.60	0.06	2.18	0.11	3.17	0.17
	ID2	1.25	0.01	0.75	0.18	0.83	0.23	1.39	0.26
	ID3	1.10	0.04	0.61	0.16	0.39	0.11	0.60	0.07
	ID4	1.16	0.21	0.61	0.12	0.37	0.02	0.61	0.00
Galagoides demidoff (9)	Thenar	0.49	0.09	0.22	0.01	0.12	0.02	0.15	0.03
	Hypothenar	0.50	0.05	0.29	0.03	0.09	0.01	0.14	0.02
	ID1	1.77	0.18	1.29	0.07	1.55	0.24	2.89	0.46
	ID2	1.07	0.10	0.76	0.08	0.65	0.07	1.09	0.19
	ID3	0.81	0.07	0.52	0.09	0.26	0.03	0.38	0.04
	ID4	0.92	0.10	0.54	0.08	0.37	0.07	0.55	0.09
Galago moholi (5)	Thenar	0.51	0.04	0.29	0.04	0.19	0.02	0.21	0.03
	Hypothenar	0.48	0.04	0.29	0.03	0.09	0.01	0.13	0.02
	ID1	2.23	0.23	1.00	0.16	1.44	0.25	2.53	0.46
	ID2	1.18	0.05	0.70	0.09	0.66	0.06	1.14	0.14
	ID3	0.82	0.08	0.51	0.12	0.23	0.04	0.39	0.05
	ID4	0.80	0.08	0.63	0.08	0.27	0.01	0.45	0.05
Galago senegalensis (5)	Thenar	0.49	0.07	0.28	0.02	0.17	0.03	0.22	0.02
	Hypothenar	0.41	0.04	0.28	0.02	0.06	0.01	0.09	0.01
	ID1	2.50	0.32	1.22	0.18	1.96	0.33	3.22	0.51
	ID2	1.08	0.06	0.66	0.09	0.54	0.11	1.01	0.16
	ID3	0.76	0.09	0.46	0.07	0.19	0.05	0.34	0.07
	ID4	0.77	0.11	0.59	0.08	0.23	0.04	0.39	0.09

Taxon (n)	Pad	Length		Width		Projected Area		Surface Area	
		Mean	SD	Mean	SD	Mean	SD	Mean	SD
Otolemur crassicaudatus (1)	Thenar	-	-	-	-	-	-	-	-
	Hypothenar	0.033	-	0.24	-	0.05	-	0.06	-
	ID1	-	-		-		-	-	-
	ID2	0.80	-	0.87	-	0.57	-	0.93	-
	ID3	0.82	-	0.44	-	0.21	-	0.28	-
	ID4	0.76	-	0.51	-	0.27	-	0.44	-

Appendix E. Descriptive statistics for raw measurements of manual dermatoglyphic dimensions (μm).

		Width		Depth	
Taxon (n)	**Pad**	Mean	SD	Mean	SD
Cheirogaleus medius (3)	Thenar	158.19	4.41	197.93	7.96
	Hypothenar	138.70	9.05	151.00	10.81
Eulemur coronatus (2)	Thenar	267.94	323.50	218.83	21.13
	Hypothenar	32.61	30.72	201.44	2.67
Euleumur fulvus (3)	Thenar	280.89	26.57	236.93	4.81
	Hypothenar	267.30	38.89	220.41	5.45
Eulemur macaco flavifrons (3)	Thenar	311.96	61.24	204.68	17.24
	Hypothenar	250.11	53.38	208.11	13.69
Galago moholi (2)	Thenar	174.61	10.29	125.06	6.99
	Hypothenar	151.44	33.62	113.39	1.65
Galago senegalensis (3)	Thenar	197.85	10.84	109.78	10.25
	Hypothenar	187.89	18.28	116.30	5.78
Hapalemur griseus griseus (2)	Thenar	293.89	44.15	213.27	3.84
	Hypothenar	327.83	25.38	202.44	0.31
Loris tardigradus (2)	Thenar	171.72	1.65	119.17	0.24
	Hypothenar	170.39	40.62	118.33	3.77
Mirza coquereli (3)	Thenar	189.59	33.52	76.44	4.07
	Hypothenar	169.96	21.40	65.96	1.36
Microcebus murinus (3)	Thenar	153.15	0.74	60.11	2.32
	Hypothenar	165.85	5.40	62.07	2.39
Nycticebus coucang (1)	Thenar	242.44	-	128.33	-
	Hypothenar	201.55	-	123.11	-

Appendix F. Descriptive statistics for raw measurements of pedal dermatoglyphic dimensions (μm).

		Width		Depth	
Taxon (n)	**Pad**	Mean	SD	Mean	SD
Cheirogaleus medius (1)	Thenar	153.72	-	153.22	-
	Hypothenar	159.14	-	137.33	-
Euleumur fulvus (2)	Thenar	185.15	84.88	266.27	22.41
	Hypothenar	254.41	21.09	240.99	10.19
Eulemur macaco flavifrons (1)	Thenar	322.11	-	247.25	-
	Hypothenar	327.99	-	237.60	-
Galago senegalensis (3)	Thenar	189.47	54.57	117.22	10.78
	Hypothenar	241.67	100.10	113.74	0.96
Hapalemur griseus griseus (1)	Thenar	345.79	-	106.83	-
	Hypothenar	370.59	-	249.63	-
Loris tardigradus (2)	Thenar	192.56	25.81	113.44	11.15
	Hypothenar	152.12	27.34	105.20	4.52
Mirza coquereli (1)	Thenar	145.00	-	84.13	-
	Hypothenar	146.94	-	71.44	-
Microcebus murinus (1)	Thenar	112.06	-	61.78	-
	Hypothenar	122.62	-	72.75	-
Nycticebus coucang (1)	Thenar	166.83	-	93.75	-
	Hypothenar	210.98	-	82.50	-